



DMP CO 2019

1st International Conference DESIGN AND MANAGEMENT OF PORT, COASTAL AND OFFSHORE WORKS

Organised by:



Laboratory
of Harbor
Works



Laboratory
for Floating
Structures and
Mooring Systems



Laboratory
of Maritime
Engineering and
Maritime works



Hydraulic
Engineering
Laboratory



8-11 MAY 2019
Eugenides Foundation
Athens, Greece

PROCEEDINGS Volume I



DMP CO 2019

1st International Conference DESIGN AND MANAGEMENT OF PORT, COASTAL AND OFFSHORE WORKS

8-11 May 2019 Eugenides Foundation, Athens, Greece

**Proceeding of the International Conference
Design and Management of Port,
Coastal and Offshore Works DMP CO 2019**

**Published by
Laboratory of Harbor Works**

**Editor
V. K. Tsoukala**

**Technical Support
M. Chondros
E. Belekou
C. Kouveli**

Year of Publication: 2019

Preface

“Blue Growth” initiative drives the society to the new era. The future for making reach and maintain the consuming way of living for the European citizens belongs to the seas and the oceans. Marine environment with its vast unexploitable resources promises socio-economic development, but simultaneously requires to cope with new technological challenges that inevitably arise. Ports and coastal facilities are the necessary hubs for the transit of people, goods and equipment between civilizations. Over 90% of global trade is conducted on the world’s oceans. To ensure that “Blue Growth” and “Blue Economy” are kept safe, commercial operators are increasingly looking to a whole range of maritime technologies. In the same context, coastal infrastructures are expected to play a crucial role to secure undisturbed transportation and storage of goods before being distributed to land convey equipment. The new era requires that ports, coastal, nearshore and offshore infrastructures should be further developed and modernized to satisfy the increased demands. In the same time, they should follow modern rules and regulations, which are associated with safety, security, risks mitigation and environmental sustainability.

Marine and maritime sectors allow nations the opportunity to generate economic growth, enhance the security of supplies, resilience and foster competitiveness through technological innovation. There is only a single, but challenging, way to exploit the practically infinite sustainable resources of the marine environment. And that comes from continuous research and development (R&D) efforts, which will find practical and economically efficient ways to make rich out of the sea for the benefit of the society. R&D is the inevitable mechanism to conceive and implement ideas and to rein the harsh marine environment. The sea is open, provides a variety of opportunities, is unexplored economically, aside only from the traditional activities. On the other hand, it is not friendly. Sea have to be respected, but in the same time it has to allow employment of tasks of innovation. Innovation through R&D may generates opportunities using breakthrough technologies and developing state-of-the-art knowledge for a flourish future. The ultimate goal is to support visions for maintaining industrial leadership. With public support, the blue economy sector may be able to play a crucial role in the future. In fact, it is more that certain that the future for economic growth belongs to seaborne activities.

The 1st International Conference on the Design and Management of Port, Coastal and Offshore Works has been particularly designed to address state-of-the-art topics, associated with “Blue Growth” and its pillars. The main goal, set by the organizers is to develop a forum for new ideas. Ambition of the organizing entities is to establish a long-lasting scientific environment, where novelty will prevail. Focus shall be given to the new generation and the ideas of the future. We sincerely hope that a new international scientific community will be generated by this effort, which aside from the pure scientific and engineering aspects, will address the most important for societal acceptance Science Practice Policy Interface. Our truthful aspiration is that DMPCO will stimulate discussions and intense scientific interactions between the participants about new trends and ideas in the design, construction, and operation of ports, coastal and offshore structures for the benefit of the engineering science and the society at large.

In terms of the core disciplines, the conference has been explicitly designed to update, to the major extend, the technical background of professionals involved in the production of port, coastal, and offshore projects, fostering the enhancement of the level of knowledge for engineers and scientists working in those subjects. Keynote speeches, special sessions and papers have been included in the program to address cutting-edge topics and state-of-the-art reviews in the current interdisciplinary professional environment that demands cooperation between specialties and acquaintance of the engineers with advanced techniques and good practices.

DMPCO 2019 International Conference which attracted 250 attendees from 8 Countries over the Europe discussing research and applications in port coastal and offshore engineering design and management.

The final program contained 103 presentations included submitted papers as well as, keynote invited speeches. In these 88 selected papers from the Scientific Committee are finally included. The papers have been listed within the ten main original conference topics, which included themes such as Sustainable Ports planning, construction and operation, design criteria guidelines and proposals for coastal structures adaptation in a changing climate, ecological issues monitoring and management under the framework and challenges of Marine Spatial Planning.

With the work of the secretariat, the Organizing, Scientific and External Advisory Committees, the persons who generously served as Chairmen of the technical sessions, the financial sponsors, this Conference has represented one of the premier technical meeting on Port, Coastal, and Offshore works. These e-proceedings amply reflect both the new scientific research results and the practical engineering achievements, fully in line with the concept of the DMPCO Conference.

This successful edition of e-proceedings gives more energy for organizing future DMPCO Conferences so that researchers and engineers from all countries will be able to participate in an exciting field with numerous intriguing problems to be solved.

See You in Thessaloniki in 2021.

On behalf of the DMPCO's Organizing Committee

Vicky Tsoukala,
Assoc. Professor, NTUA

ORGANIZING COMMITTEE

Chairwoman

Tsoukala Vicky - Assoc. Professor of Laboratory of Harbor Works, NTUA

Members

Memos Constantinos - Professor Em., NTUA
Chondros Michalis - Dr. Civil Engineer, Research Assoc., NTUA
Malliouri Dimitra - Dr. Civil Engineer, Research Assoc., NTUA
Martzikos Nikolaos - Phd Student, NTUA
Repousis Elpidoforos - Phd Student, NTUA
Spyropoulos Kyriakos - MSc Civil Marine Engineer

Conference Secretariat

Mastroianni Christina - Secretary of LHW, NTUA
Margaronis Panagiotis - Technical Assistant, NTUA
Belekou Eleni - Graduate Student, NTUA
Kouveli Kwnstantina - Graduate Student, NTUA

SCIENTIFIC COMMITTEE

Aggelidis D. - Professor Em., AUTH
Athanasoulis G. - Professor, NTUA
Chatjigeorgiou I. - Professor, NTUA
Chatzimpiros K. - Professor Em., NTUA
Chlomoudis K. - Professor, University of Pireus
Chondros M. - Dr. Civil Engineer, Research Assoc., NTUA
Coccosis Ch. - Professor, UTH
Dimakopoulos A. - Dr. Civil Engineer, HR Wallingford, UK
Dimas A. - Professor, University of Patras
Grigoropoulos G. - Professor, NTUA
Karambas Th. - Professor, AUTH
Karmpadakis I. - Research Assoc., Imperial College, UK
Katsardi V. - Assist. Professor, UTH
Klonaris G. - Dr. Civil Engineer, Research Assoc., NTUA
Kolokuthas G. - Dr. Civil Engineer, Flanders Hydraulics Research, Belgium
Koutitas Ch. - Professor Em., AUTH
Kupraios N. - Dr. Civil Engineer
Lozidou M. - Professor, NTUA
Loukogeorgaki E. - Assist. Professor, AUTH
Lyridis D. - Assoc. Professor, NTUA
Makris Ch. - Dr. Civil Engineer, Research Assoc., AUTH
Mavrakos S. - Professor, NTUA
Melissas D. - Professor, NTUA
Memos C. - Professor Em., NTUA
Metallinos A. - Dr. Civil Engineer, Research Assoc., NTUA
Mpardakis B. - Dr. Civil Engineer, President of HCCE
Pallis Ath. - Professor, University of the Aegean
Papadopoulou M. - Professor, NTUA
Prinos P. - Professor, AUTH
Soukissian Takvor - Dr. Naval Architecture and Marine Engineer, HCMR
Stamou A. - Professor, NTUA
Sylaios G. - Professor, DUT
Toumazis A. - Dr. Civil Engineer, University of Cyprus
Tsanis I. - Professor, University of Crete
Tsoukala V. - Assoc. Professor, NTUA
Vasilakis E. - Assist. Professor, UOA
Zacharias I. - Assoc. Professor, University of Patras, University of Patras

EXTERNAL ADVISORY COMMITTEE

Arcilla A. S. - Professor, Maritime Engineering Laboratory, UPC, Spain
Arena F. - Professor, University Mediterranea of Reggio Calabria, Italy
Benoit M. - Professor, IRPHE, France
Carevic D. - Professor, University of Zagreb, Croatia
Michailides C. - Professor, Cyprus University of Technology, Cyprus
Penchev V. - Professor, BDCA, Bulgaria
Sannasiraj S. - Professor, Head, Department of Ocean Engineering, IITM Chennai, India
Sundar V. - Professor Emeritus, IITM Chennai, India
Taveira Pinto F. - Professor, University of Porto, Portugal
Vicinanza D. - Professor, University Vanvitelli, Italy

CONTENTS Volume I

PREFACE

COMMITTEES

EXTENDED ABSTRACTS OF DMPCO 2019

Session I

Sub session 1

- 1. Accu-Waves: A decision support tool for navigation safety in ports** 5-9
C. Memos, C. Makris, A. Metallinos, Th. Karambas, D. Zissis, M. Chondros, G. Spiliopoulos, M. Emmanouilidou, A. Papadimitriou, V. Baltikas, Y. Kontos, G. Klonaris, Y. Androulidakis, V. Tsoukala
 - 2. HiReSS: Storm surge simulation model for the operational forecasting of sea level elevation and currents in marine areas with harbor works** 11-15
C. Makris, Y. Androulidakis, V. Baltikas, Y. Kontos, Th. Karambas, Y. Krestenitis
 - 3. WAVE-L: An integrated numerical model for wave propagation forecasting in harbor areas** 17-21
C. Makris, Th. Karambas, V. Baltikas, Y. Kontos, A. Metallinos, M. Chondros, A. Papadimitriou, V. Tsoukala, C. Memos
 - 4. Advanced numerical models for wave disturbance simulation in port basins** 23-27
A. Metallinos, M. Chondros, Th. Karambas, C. Memos, A. Papadimitriou
 - 5. Simulating wave transmission in the lee side of a breakwater in spectral wave models due to overtopping** 29-33
A. Papadimitriou, M. Chondros, A. Metallinos, C. Memos
 - 6. Ship approach and mooring design studies using advanced simulation software** 35-37
K. Spyropoulos, P. Sartampakos, A. Pritsivelis
- #### Sub session 2
- 1. Physical factors contributing to the selection of a port location. The case of the port of Alexandroupolis** 41-45
A. Karditsa, S.E. Poulos, P. Sartampakos
 - 2. Site investigation guidelines for planning, designing and constructing harbors: Experience gained from Greek harbor construction** 47-51
G. Ferentinos, G. Papatheodorou, D. Christodoulou, E. Fakiris, X. Dimas, N. Georgiou
 - 3. Design of an new marina design of a new marina in Paralimni Cyprus by implementing mathematical and Physical Modeling** 53-56
E. Rouchotas, I. G. Koutsourelakis, M. kalogirou, P. Aggelerou
 - 6. How can ports benefit from a holistic approach of fender system design?** 57-61
D. Polte
 - 7. Precast concrete floating pontoons** 63- 67
S. Apergis, K. Kampolis

Sub session 3

- 1. Comparative evaluation of learning curve models for large-scale infrastructure marine works productivity analysis: the case of caisson construction** 71-75
P. Ralli, A. Panas and J.P. Pantouvakis
- 2. Construction Environmental Management Plan (CEMP) for the installation of the 120 m floating dock ERENEOS, at Limassol Port** 77-82
M.I. Loizides, D. Petsa, D. L. Orthodoxou, X. I. Liozidou
- 3. Operational Environmental Management Plan (OEMP) for the 120m floating dry docks ERENEOS, mutimarine shipyards, Limassol port** 83-88
M.I. Loizides, D. Petsa, D. L. Orthodoxou, X. I. Liozidou
- 4. Small scale Infrastructure for the storage and regasification of LNG at the Port of Patras, within the context of European Project POSEIDON MED II.** 89-92
A.M. Boutatis, C. Solomonidis, P. Biniskos, M.N Kalpiri
- 5. Creation of a jetty for permanent berthing of a Floating Storage and Regasification Unit (FSR) for LNG Import in Vasilikos, Cyprus - Overcoming challenges** 93-97
C. Solomonidis, A. Toumazis, A. Boutatis, P. Biniskos, M. Kalpyri
- 6. An approach on the proecedure of selecting container handling systems in a container terminal** 99-103
A.-N. Papadopolis-Dezorzis, S. Theophanis, M. Boile
- 7. The Venetian Port of Heraklion. The unusual intertemporal intenventions in the development of this Historic Harbor** 105-106
S. Lyrintakis, X. Lytinaki, EM. Tsiplostefanakis, S. Perogiannaki, G. Fragomanolakis, M. Spyridakis

Session 2

- 1. Hydrodynamic performance of a floating wave energy converter system with multiple flaps** 109-113
G. Sismani, E. Loukogeorgaki
- 2. Hydrodynamic performance of a wave energy converter in front of a vertical wall** 115-119
E. Spanaki, E. Loukogeorgaki
- 3. Hydrodynamic interactions by arrays of vertical axisymmetric bodies in front of a wall for wave energy converter applications** 121-125
E. I. Anastasiou, I.K. Chatjigeorgiou, Th. D.
- 4. Experimental investigation of the oscillating properties response of a three-legged jacket tower** 127-131
V. Katsardi, I. Santic, I.K. Chatziionnou, A. Koukouselis, E. Mistakidis, V. Tsoukala, I.K. Chatjigeorgiou

Session 3

- 1. UAS-SfM as a cost-effective tool for coastal monitoring and management** 135-139
K. Lazogiannis, Emm. Vasilakis, S. Poulos, S. Kotsopoulos, J. Alexopoulos, N. Alamanis, G. Papageorgiou
- 2. Automated 2-D wave run-up detection from coastal video imagery. Examples from the islands of Santorini and Mykonos** 141-144
A. E. Chatzipavlis, V. Trygonis, A. Eleftheriou, O. Andreadis, I. Monioudi, A.F. Velegrakis

3. Trends in Coastal Erosion by combining Satellite Image Analysis and Copernicus wave data: Paggaion Coastline, Northern Greece	145-149
<i>K. Zachopoulos, N. Kokkos, M. Zidou, G. Sylaios</i>	
4. BIM application to high-end public realm design on waterfront reclamation areas	151-155
<i>Ch. Tzoumas</i>	
5. Combination of Very High Resolution (VHR) satellite imagery and side scan data for low cost seagrass mapping	157-161
<i>A. Tsokos, V. Tsoukala, Em. Vasilakis, C. Petropoulos, P. Sartampakos</i>	
6. Preliminary assessment of observing different regimes in the marine environment using SAR mode altimetry data	163-167
<i>N. Flokos, D. Delikaraoglou</i>	
7. Nearshore wave energy potential estimation using Sentinel-3 data	169-174
<i>M. Kaselimi, N. Doulamis, D. Delikaraoglou</i>	

CONTENTS Volume II

PREFACE

COMMITTEES

EXTENDED ABSTRACTS OF DMPCO 2019

Session 4

Sub Session 1

- 1. First key points concerning maritime spatial planning** 5-6
D. Melissas
- 2. Broadening the policy framework: from ICZM to MSP** 7-10
H. Coccoisis
- 3. The coasts at the front of the city of Attica Basin: Landforms coastal uses and management proposals under the principles of integrated coastal management** 11-15
Ch. Anagnostou, A. Petropoulos, A. Kikaki
- 4. Comparative analysis of six coastal urban industrial areas in Greece regarding their vulnerability to coastal flooding** 17-21
Ch. Giannakidou, D. Diakoulaki, C.D. Memos
- 5. A Spatial decision system for the city and port of Piraeus** 23-27
G. Koumparakis, A. Siolas, E. Bakogiannis, T. Hatzichristos
- 6. Coastal geomorphological changes in a semi- enclosed bay, induced by recreational interventions** 29-33
S. Petrakis, G. Alexandrakis, N. Rempis, N. Kampanis

Sub session 2

- 1. Improvement measures and prospects for the development of "Glyfada Marina", Attica, Greece** 37-41
N. Alamanis, Ch. Drimonas, E. Milozis, K. Lazogiannis, G. Papageorgiou, E. Vassilakis, J. Alexopoulos, S. Kotsopoulos I. Chouliaras
- 2. Development of the Metropolitan Area of Hellinikon - Agios Kosmas coastal front in Athens - Hellinikon Project** 43-47
A.M. Boutatis, X. Solomonidis, I.A. Rogan, M. Chondros
- 3. Design, Construction & Legal Framework of an Artificial Surfing Reef (ASR) in Marathon Bay, Attica** 49-53
V.I. Chalastani, V.K. Tsoukala
- 4. Multi-criteria ranking and assessment of alternative coastal defense schemes** 55-59
D. Charchousi, M.P. Papadopoulou, V.K. Tsoukala
- 5. Let's start with a million!** 61-64
I. Doulakis

Session 5

- 1. Advanced numerical model for the design of coastal protection structures** 67-72
A.-Ch. Tsiaras , Th. Karambas
- 2. Numerical modelling of coastal sediment transport with a Boussinesq-Type Model** 73-78
G. Klouaris, C. Memos
- 3. Morphodynamics of Vortex Ripples under Oscillatory Flow Conditions** 79-84
G. Leftheriotis, A. Dimas
- 4. Flow over Three-Dimensional Bed Formations** 85-89
I. Chalmoukis, A. Dimas
- 5. Numerical Approaches for the Evaluation of Sediment Transport Mechanisms on a Shallow Sloping Sea Bottom** 91-96
V. Afentoulis, A. Papadimitriou, V. Tsoukala, M. Benoit
- 6. Numerical simulation of berm and dune erosion, cross-shore profile evolution and scour in front of breakwaters using OpenFOAM** 97-101
N. Karagiannis, Th. Karambas., C. Koutitas
- 7. An investigation of the morphodynamic evolution of Oroklini beach in Cyprus via an innovative semi-analytical solution to the One-Line model** 103-107
A. Valsamidis, C. Michailides, G.C. Georgiou

Session 6

- 1. Evaluation of impacts in coastal morphology induced by different coastal structures using high-resolution coastal simulation software** 111-115
CH. Kapopoulos, F. Karathanasi
- 2. A numerical analysis method for addressing wave-structure interaction effects** 117-121
C. Michailides
- 3. Nearshore processes induced by oblique irregular waves in the vicinity of a segmented, detached, zero-freeboard breakwater** 123-127
M. Fotia, A. Dimas
- 4. Reliability analysis of rubble mound breakwaters. An easy-to-use methodology** 129-133
D. Malliouri, C. Memos, T. Soukissian, V. Tsoukala
- 5. Wave Transmission over a Narrow Crested Submerged Breakwater with Steep Slopes** 135-139
E. Repousis, C. Memos
- 6. Experimental Investigation of Sandbang Structures in the Swash Zone as a Mild Method of Coastal Protection** 141-146
I. Biliiani, A. Dimas
- 7. Experimental study of the wave generated current field in the vicinity of a segmented, detached rubble -mound, zero-freeboard breakwater** 147-151
K. Galani, A. Dimas
- 8. Assessing failure probabilities of rubble mound breakwaters for extreme conditions under climate change** 153-157
P. Galiatsatou, C. Makris, D. Kokkinos, P. Prinos

Session 7

Sub Session 1

- 1. Wave and Current Actions on Coastal Structures. The New Eurocode to-be** 163-167
C. Memos, Malliouri D.
- 2. Climate Change Effects on Extreme Total Water Levels of the Greek Coastal Zone** 169-173
P. Galiatsatou, X. Makris, D. Kokkinos, P. Prinos, Y. Krestenitis
- 3. Multivariate metocean design conditions in the Mediterranean and North Seas** 175-179
T. Soukissian, S.A. Mavrakos
- 4. A smart data selection tool for estimating design wave height** 181-185
M. Chondros, A. Metallinos, C. Memos, V. Tsoukala
- 5. Mediterranean coastal storms in a changing climate** 187-191
N. Martzikos, P. Prinos, C. Memos, V. Tsoukala

Sub session 2

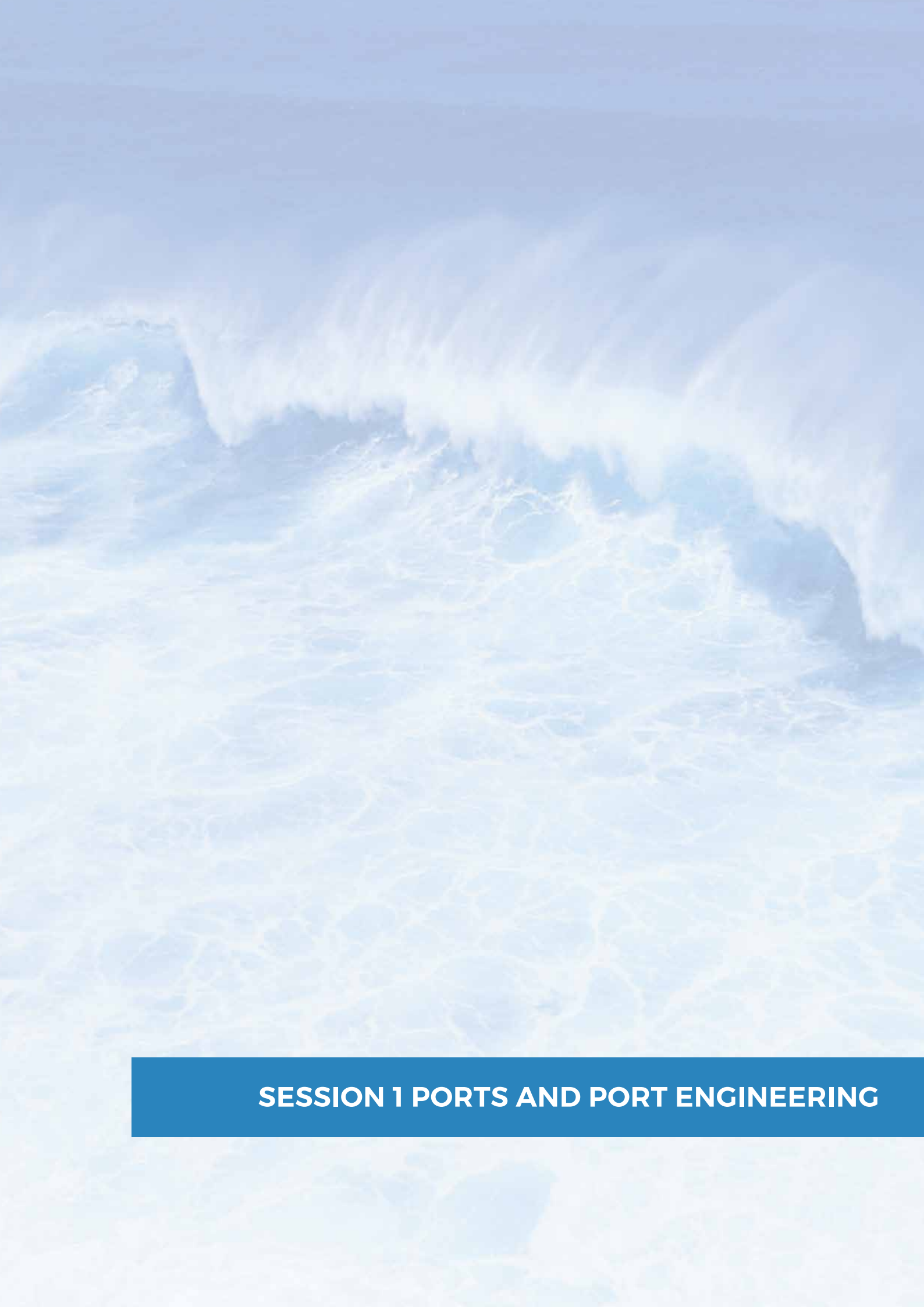
- 1. Hydrographic surveying methods and their contribution to harbor construction and coastal zone management** 195-199
A.K. Mavraeidopoulos
- 2. Climate change effect on extreme waves and wind-induced hydrodynamic circulation in the Corinthian Gulf** 201-205
E. Kypraiou, A. Dimas
- 3. Climate change adaptation strategies in developing countries - An exemplary coastal protection project in Beira, Mozambique** 207-210
H. Spekker , H. Krebs
- 4. Beach erosion hazard under Climate Variability and Change - The case of Saint Lucia (Eastern Caribbean)** 211-215
I.N. Monioudi, A. Nikolaou, R. Asariotis, M.I. Vousdoukas, A.F. Velegrakis
- 5. Protection of coastal monuments against climatic change under designing restrictions** 217-221
G. Alexandrakis, D. Rompogianakis, E. Papadakis, N. Kampanis, C. Liritzakis, X. Litinaki, E. Tsiplostefanakis, S. Perogiannaki, G. Fragkomanolaki
- 6. Master planning for the development or conversion of Port Areas: Two examples from the North of Germany** 223-228
H.G. Krebs, H. Spekker*

Session 8

- 1. Anthropogenic impacts on the geomorphological regime of Preveza straits (Amvrakikos Gulf)** 231-236
N. Georgiou, E. Fakiris, D. Christodoulou, X. Dimas, C. Koutsikopoulos, G. Papatheodorou
- 2. Protection of Agios Tychonas coastal front in Limassol-numerical simulation of coastal processes and monitoring initial response after construction** 237-241
X. Solomonidis, A. Toumazis, A. Boutatis, M. Chondros, E. Kypraiou

3. Sea bed evolution in the vicinity of longitudinal submerged discontinuous breakwaters - "Acripelagos"	243-247
<i>V. Afentoulis, N. Chini, P. Bardey, C. Raffourt</i>	
4. Integrated coastal management including detached breakwater system and artificial nourishment	249-253
<i>S. Kousoulos, I.G. Koutsourelakis, N. Panagopoulos, H. Tsekos</i>	
5. Proposed measures for the restoration of the coastal area under erosion in the Bay of Platis Gialos - Sifnos Isl. (Greece)	255-259
<i>A. Petropoulos, N. Evelpidou, V. Kapsimalis, Ch. Anagnostou</i>	
6. Coastal and architectural study of the fishing port on the estuarine of Liopetris's river "Potamos", Cyprus	261-265
<i>S. Gouloumis, V. Ieridis, A. Christou, Chr. Chatzigiagou, Cha. Jacovou</i>	
Session 9	
1. Advanced numerical models for simulation of nearshore processes	269-273
<i>M. Chondros, A. Metallinos, Th. Karambas, C. Memos, A. Papadimitriou</i>	
2. Adapting OpenFOAM® CFD numerical model, to the Simulation of significant coastal zone wave processes in full three dimensional (3D) applications	275-279
<i>I. Kazakis, T. Karambas</i>	
3. Nonlinear changes and energy dissipation in random water waves in finite water depths	281-285
<i>I. Karmpadakis, C. Swan, M. Christou</i>	
4. Prediction of extreme wind-generated waves offshore the Piraeus Port using a numerical model of wave growth in the SW Aegean Sea	287-291
<i>M. Sklia, A. Dimas</i>	
5. Numerical Simulation of Ship-Borne Waves Using a 2DH Post-Boussinesq Model	293-297
<i>A.G. Samaras, Th. Karambas</i>	
6. An Efficient Navier-Stokes based numerical Wave-Tank for complex wave hydrodynamics	299-303
<i>C. Frantzis, D.G.E. Grigoriadis</i>	
7. A three-dimensional approach for a spheroid water entry problem	305-309
<i>Th. D. Tsaousis, A. I. Chatzigeorgiou, E. I. Anastasiou</i>	
8. Simulation of a series of breakwaters with a series of elliptical cylinders	311-315
<i>E. Charisi, V. Katsardi, I.K. Chatjigergiou</i>	
Session 10	
1. Marine Corrosion of Steel with Aerobic and Anaerobic Biofilms under Changable Nutrient Concentration Conditions	317-321
<i>D.S. Sophianopoulos, V.S. Pantazi, M.I. Ntina</i>	
2. Modeling the "Agia Zoni II" Oil Spill Released in 2017 in the Gulf of Saronikos	323-327
<i>P.E. Makatounis, L. Tsiatsiou, A. Stamou</i>	
3. Geomorphology modification and its impact to coastal ecosystems	329-333
<i>I. Zacharias, A. Gianni</i>	

4. Improving the Water Renewal of Restricted Lagoons. Application to Pappas Lagoon (Western Greece)	335-339
<i>N.Th. Fourniotis, G.M. Horsch, G.A. Leftheriotis</i>	
5. Problems and Perspectives at the Market of Collection and Handling of Ship Waste and Cargo Residues in Greece	341-345
Special Session IV	
1. Environmentally friendly breakwater design	349-353
<i>D. Carevic, D. Bujak, G. Loncar</i>	
2. Evaluating the prospect of nearly Zero Energy Ports	355- 359
<i>N. Sifakis, O. Mavroudis, Th. Tsoutsos</i>	
3. Prospects of carbon capture and utilisation technologies in industrial complexes near Greek ports	361-365
<i>M. Kasidoni, N. Stylogiannis M. Loizidou M.</i>	
4. Achieving sustainable development of tourist ports, using environmental management models	367-370
<i>S. Manoglou, B. Tselentis</i>	



SESSION 1 PORTS AND PORT ENGINEERING



Sub session 1.1: Numerical Models

Accu-Waves: A decision support tool for navigation safety in ports

C. Memos^{1*}, Ch. Makris², A. Metallinos¹, Th. Karambas², D. Zissis³, M. Chondros¹, G. Spiliopoulos³,
M. Emmanouilidou¹, A. Papadimitriou¹, V. Baltikas², Y. Kontos², G. Klonaris¹, Y. Androurlidakis²,
V. Tsoukala¹

¹ Laboratory of Harbour Works, NTUA, Athens 15780, Greece

² Laboratory of Maritime Engineering, AUTH, Thessaloniki 54124, Greece

³ MarineTraffic, Katehaki 75, Athens 11525, Greece

*Corresponding author: cmemos@mail.ntua.gr

Abstract

The paper presents a decision support tool being developed to provide reliable forecasts on sea states prevailing at selected ports worldwide. The application will support approaching procedures of vessels to ports. It is based on co-operating, hydrodynamic models that derive data from global scale, open sea forecasts. The implementation of the project includes development and application of a hydrodynamic circulation model, a spectral wave propagation model and a phase-resolving wave model for port basins; model integration; and materialising a cloud-based forecast platform that will provide wind, wave, sea level and current data for a 3-day forecast every 3 hours. The laboratories of Harbour Works (NTUA) and Maritime Engineering (AUTH) will offer the research background while the third partner MarineTraffic will implement the on-line forecast platform for the end-users. The results of this applied research will lead to innovative products that will address significant needs such as increase of navigation safety at ports, facilitation of port pilotage operations, and improved port layouts.

Keywords Port navigation, Sea conditions, Navigation safety, Wave penetration.

1 INTRODUCTION AND SCOPE

Ports are vital links in the chain of maritime transportations and have a decisive impact on their quality. Recent reports of marine accidents show that 60% of them are due to the human factor. The majority of accidents could be avoided if appropriate means of support for navigation existed. The British Ministry for Transportation found that a 34% of ship accidents sailing in ports incur due to incompetent pilotage. Project Accu-Waves (<http://accuwaves.eu/>) will develop a tool to provide reliable data on prevailing sea states in port approaches and harbour basins in 3-day forecasts every 3 hours. The results will support navigation procedures of vessels calling to ports.

The project will build upon the cooperation of Marine Traffic, one of the world's leading platforms of intelligent services for ship tracking, with NTUA and AUTH as research partners through their Laboratories of Harbour Works and Maritime Engineering, respectively.

2 METHODOLOGY LAYOUT

The application will be based on high-resolution hydrodynamic models and will derive input data from global scale open sea forecasts. The implementation of the proposed project will be based on the following steps: (i) define and organize input data; (ii) develop three hydrodynamic numerical models, i.e. a spectral wave model for wind-induced irregular wave fields (model A), a mild-slope equation wave model (model B), and a barotropic hydrodynamic circulation model (model H); (iii) calibrate, test, and integrate the models into a single suite; (iv) apply the above suite to fifty ports worldwide; (v) develop an electronic operational forecast platform that will provide wind, wave, sea level and current data at 3-hourly 3-day forecast for the said ports.

Model A will simulate waves in the port approaches covering an area a few dozens of kilometres across, while model B will tackle wave propagation and transformation inside the harbour. Model A will provide input wave data to model B, while Model H will provide input data of sea levels and mean currents to both models A and B. Model H will incorporate storm surge and astronomical tide

effects. Models B and H will not be applied to all 50 ports; this will depend on the actual configuration of each harbour and the shape of the water body associated with its location.

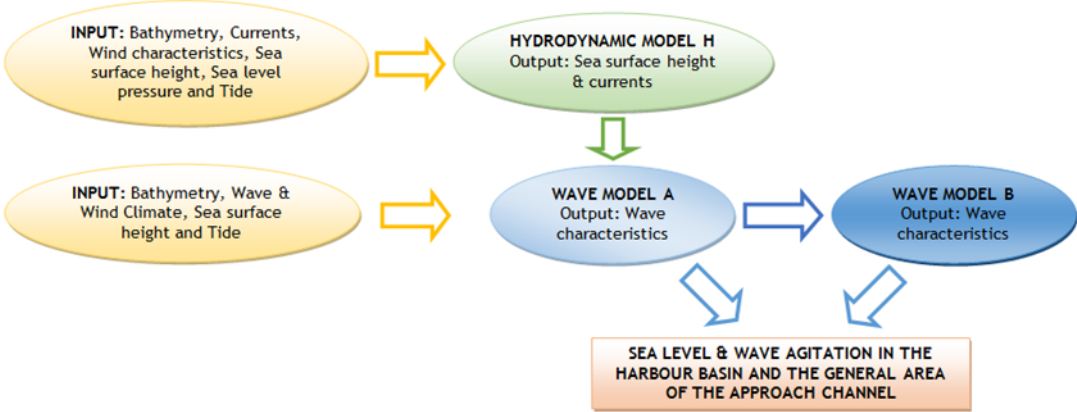
3 INPUT DATA AND THEIR ASSESSMENT

Missing bathymetric information in the relevant sea areas of the selected port sites (see §5) were obtained through National Hydrographic Services, British Admiralty, Navionics (www.navionics.com) and GEBCO (www.gebco.net). The environmental input data needed for implementing this project are forecast values of wave, sea level, tide, and wind characteristics. The wave data are focused on wind wave parameters (including swell), i.e. significant wave height, peak spectral period, and main direction; for tides, sea level, atmospheric pressure, current velocities and directions are collected; winds are represented by wind speed and direction. The sources used to obtain the above forecasts are the Copernicus Marine Environmental Monitoring Service (CMEMS), used for wave and tidal data; and the National Oceanic and Atmospheric Administration (NOAA), for atmospheric data.

Contingency plans have been set up in case any of the sources fails to function for a period longer than 3 days. These plans are required due to the on-line nature of the final product. Quality assessment of the above forecasts has been undertaken with satisfactory results.

4 NUMERICAL MODELS

The three numerical models mentioned earlier cover different needs in terms of area coverage and accuracy. These are set to interact efficiently in a way depicted in Figure 1.



1. **Figure 1** Workflow diagram between numerical models

HiReSS (Model H) is a high resolution storm surge numerical model simulating 2DH barotropic hydrodynamic circulation based on the shallow water equations (Androulidakis et al. 2015). It can predict the free surface elevation and the integrated over depth sea currents due to storm surge combined with wind and astronomical tide effects. HiReSS takes into account the astronomical tide through a static tide model (Schwidorski 1980). It has been developed, calibrated, verified and applied on a number of actual sites (see e.g. Makris et al. 2016, Krestenitis et al. 2017).

Tomawac (Model A) is a 3rd generation directional spectral wave model developed by Laboratoire National d’Hydraulique et Environnement (Benoit et al. 1996). It simulates the development in space and time of the spectrum of sea surface elevation in waters of any depth. The numerical calculations are executed by the finite elements method over an unstructured mesh. The model captures processes of wind wave generation and propagation, white-capping, energy dissipation due to bottom friction, wave refraction, shoaling and breaking, wave blocking due to opposing currents, wave-wave interactions, depth- or current- induced refraction, wave-current interaction, and, under certain conditions, wave diffraction.

WAVE-L (Model B) is a 2DH solver of the mild slope equation based on the hyperbolic approximation of Copeland (1985). It will be developed to cope with quasi-regular wave propagation in coastal waters of mildly sloping bed and capture wave modifications due to the presence of

currents; wave shoaling, refraction, diffraction; wave reflection at solid boundaries, energy dissipation due to bottom friction; depth-induced wave breaking (Karambas and Samaras 2017). The numerical solution of the equations is based on an explicit scheme applied on a grid staggered between the cell values of surface elevation and mean velocities. Along the open sea and lateral boundaries sponge layers are placed following the technique proposed by Larsen and Dancy (1983).

5 PORTS FOR APPLICATION

A number of 50 ports have been selected for application. The selection was based on criteria of world-wide coverage and traffic volume. The selected sites are shown in Figure 2.



2. **Figure 2** Location of ports selected for application

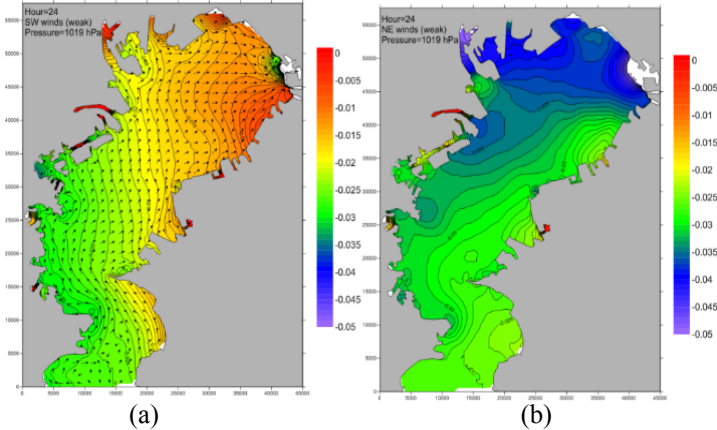
It is noted that input data for 34 out of the 50 port sites will be obtained from the Global package of CMEMS, whereas for eight of them data will be served by the relevant European NW and another eight by the MED regional packages of the Copernicus platform (<http://marine.copernicus.eu>).

A crucial parameter associated to the local conditions is the extent of the water body which models H and A should be applied upon taking into account the availability of input data over a grid much coarser than the model’s resolution. It was decided that model H will be applied to much larger water bodies than the vicinity of a single port in order to capture large scale meteorological processes present over such broader areas. Thus, 13 such areas were selected ranging in extend from the Mediterranean and Black Sea to the Halifax Gulf, Canada.

Regarding model A, to be run in all 50 sites, an ad hoc delineation of the sea area was performed, where environmental input data will be sought from the said sources. This expanse is defined as the water surface of a circular area centered at the port. The radius of those circles ranges in from 3 km to 45 km.

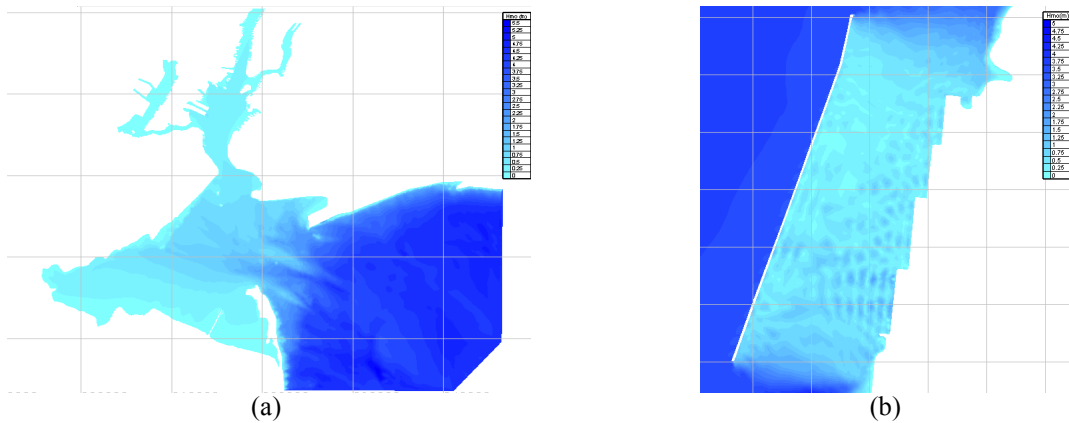
6 INITIAL MODEL RESULTS

Various tests were applied on the hydrodynamic models to check robustness and tackle a number of problems. A wide spectrum of numerical tools will be used to transfer appropriately the raw data to the required input format in models H and A. In the following, samples of first results are presented for models H (Figure 3), A (Figure 4a) and B (Figure 4b).



3. **Figure 3** Model H: Spatial distribution of the free surface elevation due to storm surge in Tokyo Bay,

Japan with (a) SW light winds (b) NE light winds



4. **Figure 4** Spatial distribution of significant wave height (a) Model A: for SE strong winds, NY port approaches, USA (b) Model B: inside the new Patras port, Greece, for strong NW winds

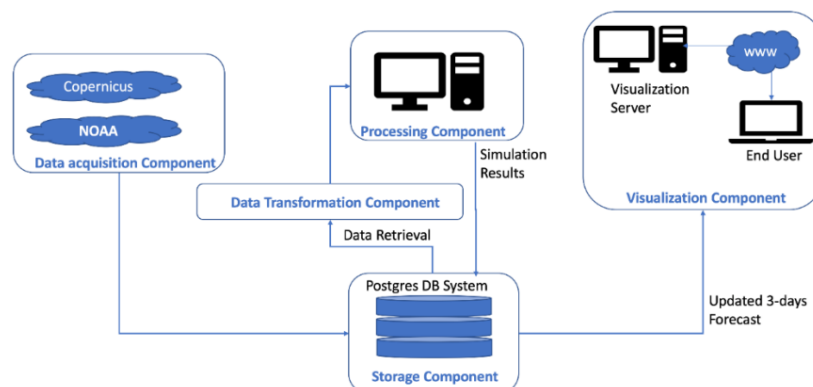
Synthesis of the results from models A and B is achieved by a technique of densification of the mesh inside the port ensuring compatibility with model's B grid.

7 MODEL VERIFICATION

All numerical models to be used have been in general verified adequately so far. However, since some advancements in particular to the mild-slope model are envisaged to take place in this project additional verification will be performed via measurements to be collected at two stations to be installed in Thessaloniki and Patras ports. A Seagauge Wave & Tide Recorder and a Directional Wave Buoy Station will be used to record significant wave height, peak spectral period, distribution of wave energy with direction, and sea surface elevation. Measurements will be compared with model predictions for the same input data and adjustments will eventually be imposed.

8 ARCHITECTURE OF THE IT SYSTEM

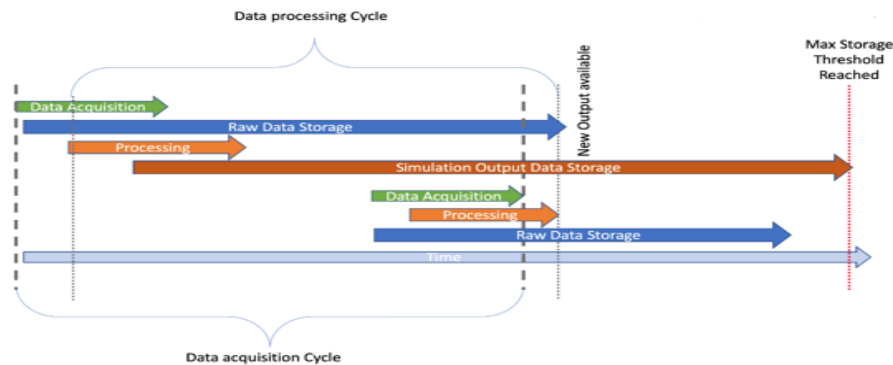
Managing the information flow from accessing the initial data to providing the final product to the end user is a critical element of this cloud-based automated forecasting system, considering the vast amount of data that should be continuously processed and accommodated. The co-ordination of the individual processes of the system will be implemented in the Python programming language on top of the LINUX operational system. A general layout of the IT system is shown in Figure 5.



5. **Figure 5** The operational system architecture of information flow

Data transformation is critical to our system, as it is responsible for all data handling required for the communication between the numerical process and the data storage units. To optimize resources management, i.e. the processing power and the vast amount of data generated during processing, the

co-ordination procedure parallelizes processing per port with respect to constraints risen from data and hardware availability, (shown by the Cycles of Figure 6). Finally, the database will be setup to support retrieving old data as part of contingency plans and facilitating data archiving and cleanup procedures.



6. Figure 6 Maintenance cycle of big data

9 IMPACT

The application will address significant needs such as safe spatial and temporal planning of navigation in the approaches and inside ports and mooring sites, while facilitating the captain–pilot interaction. This will allow more efficient management of the navigation and towage services. Indeed, the procedure by the European Space Agency to certify navigation paths in ports requires knowledge of operational conditions including sea state and related environmental data. The safety issue is underlined also in the e-Navigation strategy by the International Maritime Organization, where the aim is to analyse and provide quality data for limiting the human error in navigation. It will also be possible to better document dredging plans and manage more efficiently berth positions and moorings. Finally, the tool will prove particularly useful in modifying existing or designing new port layouts.

Acknowledgement

This three year project is co-financed by the European Union and Greek national funds through Programme “Competitiveness, Entrepreneurship, and Innovation” (code: T1EDK-05111).

References

- Androulidakis Y, Kombiadou K, Makris C, Baltikas V and Krestenitis Y (2015) Storm surges in the Mediterranean Sea: variability and trends under future climatic conditions. *Dynam Atmos Ocean* 71: 56–82. doi: 10.1016/j.dynatmoce.2015.06.001.
- Benoit M, Marcos F, Becq F (1996) Development of a third generation shallow-water wave model with unstructured spatial meshing. *Coastal Engineering Proceedings*, 1(25)
- Copeland G.J.M (1985) A Practical Alternative to the Mild-Slope Equation. *Coast Eng* 9: 125-149. doi: 10.1016/0378-3839(85)90002-X.
- Karambas T, Samaras A (2017) An Integrated Numerical Model for the Design of Coastal Protection Structures. *J Mar Sci Eng* 5(4). doi:10.3390/jmse5040050.
- Krestenitis Y, Pytharoulis I, Karacostas T, Androulidakis Y, Makris C, Kombiadou K, Tegoulis I, Baltikas V, Kotsopoulos S and Kartsios S (2017) Severe weather events and sea level variability over the Mediterranean Sea. Part of the Springer Atmospheric Sciences book series (Eds Karacostas T et al), *Perspec Atmos Sci*, 63-68. doi:10.1007/978-3-319-35095-0_9.
- Larsen J and Dancy H (1983) Open Boundaries in Short Wave Simulations – A New Approach. *Coastal Engineering* 7: 285-297. doi:10.1016/0378-3839(83)90022-4.
- Makris C, Galiatsatou P, Tolika K, Anagnostopoulou C, Kombiadou K, Prinos P, Velikou K, Kapelonis Z, Tragou E, Androulidakis Y, Athanassoulis G, Vagenas C, Tegoulis I, Baltikas V, Krestenitis Y, Gerostathis T, Belibassakis K, Rusu, E. (2016) Climate Change Effects on the Marine Characteristics of the Aegean and the Ionian Seas. *Ocean Dyn*, 66(12): 1603–1635. doi:10.1007/s10236-016-1008-1.
- Schwiderski E W (1980) On charting global ocean tides. *Rev of Geophys* 18(1): 243-268. doi: 10.1029/RG018i001p00243.

HiReSS: Storm surge simulation model for the operational forecasting of sea level elevation and currents in marine areas with harbor works

Ch. Makris*, Y. Androulidakis, V. Baltikas, Y. Kontos, Th. Karambas, Y. Krestenitis

Lab of Maritime Engineering, Department of Civil Engineering, Aristotle University of Thessaloniki,
Thessaloniki, 54124, Greece

*Corresponding author: cmakris@civil.auth.gr

Abstract

In this paper we present recent evolvments of a robust numerical model for the simulation of storm surges in gulfs and coastal areas, inside which large harbors and significant urban port facilities exist. HiReSS (High-Resolution Storm Surge) is a 2-DH barotropic model for the simulation of hydrodynamic circulation and sea level variations, based on the depth-averaged shallow water equations. It is applied in large enclosed water bodies or semi-enclosed marginal seas, gulfs, bays and shallow coastal areas over the continental shelf. HiReSS takes into account several processes, such as the inverse barometer effect, shear stresses of wind on the sea surface, Coriolis effects, astronomical tides, ocean bottom friction, turbulence of horizontal eddies, and impact of wave-driven circulation in open seas and nearshore zones. It is implemented in large computational fields, covering e.g. the entire Mediterranean Sea, led to dynamically downscaled simulations in nested high-resolution domains, e.g. Thermaikos Gulf in northern Greece. HiReSS model results refer to sea surface elevation and depth-averaged currents, used as input in irregular wave simulations with a spectral wave model at 3-hour time intervals for 3-day forecasts, producing 24 representations of storm surge impacts per daily prognostic model implementation. The model will be applied in 25 regions worldwide with complex bathymetries and diverse coastlines that contain in total 50 port facilities with high traffic load and commercial interest (project Accu-Waves). The produced data sets support mooring, navigation and towage procedures of vessels in commercial ports and harbors, reducing risk of vessel impact at the bottom.

Keywords Sea surface height, Ocean circulation, Ports, Navigation safety.

1 INTRODUCTION

1.1 Theme of research

In this paper we present recent evolvments of a robust numerical model for the simulation of storm surges (De Vries et al. 1995) in gulfs and coastal areas, inside which large harbors and urban port facilities exist. The model is named HiReSS (High-Resolution Storm Surge) and it is based on 2-DH formulations of the depth-integrated Navier-Stokes equations for the simulation of the barotropic mode of hydrodynamic circulation (Krestenitis et al. 2016). It can simulate the free surface elevation and the depth-integrated sea currents due to meteorological forcing (mostly severe weather conditions) combined with astronomical tide effects (Krestenitis et al. 2015a). Its newest version under development is intended to be part of a software suite for an operational tool that will provide reliable 3-hourly forecasts for 3 upcoming days about sea state conditions in coastal areas near ports and inside harbor basins (Memos et al. 2019; project Accu-Waves, <http://accuwaves.eu/>).

1.2 Scope of research

Main goal of this study is to develop new features of the HiReSS model in order to render it fully operational for robust forecasts of sea level and currents in engineered coastal regions. A second goal is to validate HiReSS against available sea level data from in situ observations by tide gauges of national hydrographic services (e.g. HNHS; <https://www.hnhs.gr/>). Moreover, the Fortran code of the storm surge model will be fitted in an integrated modeling system suite for automated operational forecasting of both surge-induced and tidal sea levels in the framework of high-resolution spectral wave modeling in and around fifty significant ports globally (Memos et al. 2019; project Accu-Waves,

<http://accuwaves.eu/>). Conclusively, the produced data sets of HiReSS results will support mooring, navigation and towage procedures of ships and boats in commercial ports and harbors, mostly reducing risk of vessel impact at the bottom.

2 METHODOLOGY

2.1 Numerical model

2.1.1 Basic attributes

HiReSS is a new version of the HRSS model (Krestenitis et al. 2015b); it is based on the depth-averaged shallow water equations of hydrodynamic circulation, and it is capable to simulate the response of the sea surface and consequent barotropic sea currents to atmospheric weather conditions (wind and pressure) in large regions of either enclosed water bodies or semi-enclosed marginal seas, gulfs and bays over the continental shelf (Krestenitis et al. 2015a).

HiReSS can take into account the combinatory effects of several processes, such as the inverse barometer (response of sea level to atmospheric pressure gradient of large barometric systems); shear stresses of wind applied on the air-water interface; geostrophic Coriolis forces on large water masses; astronomical tides; ocean bottom friction; turbulence of horizontal vortices through the eddy viscosity concept; impacts of the wave-induced mean flows (Stokes drift) on the wind-driven currents in open seas and nearshore coastal zones. It can predict the mean free surface elevation (termed herein as sea surface height) and the depth-integrated sea currents due to surges induced by wind-storms combined with the effect of low/high barometric systems and astronomical tides.

2.1.2 Main equations and assumptions

The extended continuity and momentum equations, in order to account for storm surge-driven and tidally affected circulation can be written as (Krestenitis et al. 2016):

$$\frac{\partial \zeta}{\partial t} + \frac{\partial}{\partial x} UH + \frac{\partial}{\partial y} VH = 0 \quad (1)$$

$$\frac{\partial U}{\partial t} + U \frac{\partial U}{\partial x} + V \frac{\partial U}{\partial y} - fV + Z_x = -\frac{1}{\rho_o} \frac{\partial P_A}{\partial x} + E_h \left(\frac{\partial^2 U}{\partial x^2} + \frac{\partial^2 U}{\partial y^2} \right) + \frac{C_s}{\rho_o} \frac{W_x \sqrt{W_x^2 + W_y^2}}{(h+\zeta)} - C_b \frac{U \sqrt{U^2 + V^2}}{\rho_o (h+\zeta)} \quad (2)$$

$$\frac{\partial V}{\partial t} + U \frac{\partial V}{\partial x} + V \frac{\partial V}{\partial y} + fU + Z_y = -\frac{1}{\rho_o} \frac{\partial P_A}{\partial y} + E_h \left(\frac{\partial^2 V}{\partial x^2} + \frac{\partial^2 V}{\partial y^2} \right) + \frac{C_s}{\rho_o} \frac{W_y \sqrt{W_x^2 + W_y^2}}{(h+\zeta)} - C_b \frac{V \sqrt{U^2 + V^2}}{\rho_o (h+\zeta)} \quad (3)$$

$$Z_x = 0.9g \frac{\partial \zeta}{\partial x} - 0.7g \frac{\partial \zeta_{tide}}{\partial x}, \quad Z_y = 0.9g \frac{\partial \zeta}{\partial y} - 0.7g \frac{\partial \zeta_{tide}}{\partial y} \quad (4)$$

where ζ is the free surface elevation, $H=h+\zeta$ is the total water depth of the sea, h is the local still water depth, U and V are the depth-integrated horizontal velocity components along the x and y axes of an ortho-regular staggered Cartesian grid of the Arakawa-C type for the finite difference method, t is the time, f is the Coriolis coefficient, g is the acceleration of gravity, P_A is the atmospheric sea level pressure (SLP), ρ_o is the water density, C_b is the bottom friction Manning-type coefficient, C_s is the air-water drag coefficient (Smith and Banke 1975), W_x and W_y are the wind velocity components at 10m above mean sea level, and E_h is the horizontal eddy viscosity coefficient.

HiReSS also takes into account the effects of astronomical tides on barotropic circulation through the static model parameterization by Schwidorski (1980), by initiating Z_x and Z_y terms (Eq. 4) in the momentum equations (Eqs. 2, 3). Tide forecasts are based on the solution of harmonic equation ζ_{tide} in all georeferenced grid cells with discrete longitudes and latitudes, concerning both semi-diurnal and diurnal tidal range signals (Krestenitis et al. 2015a). HiReSS model is implemented in the framework of dynamically downscaled simulations initiating from computational fields covering e.g. the entire Mediterranean Sea (discretization step of $\Delta x \approx 1/25^\circ$ or $\sim 4\text{Km}$) and led to nested domains of high spatial resolution ($\Delta x \approx 1/200^\circ$ or $\sim 500\text{m}$). These results are also used as input in TOMAWAC model runs.

2.2 Application study

General application of HiReSS model is intended for 25 coastal regions globally, indicatively covering among others the Red, Caribbean, Java, Yellow, Mediterranean and Black Seas, and Persian, Tokyo

and Halifax Gulfs. These areas have rather complex bathymetries with diverse coastlines and contain in total 50 port facilities with high traffic load and commercial interest. Herein we present specific implementations of HiReSS in the Mediterranean Sea with a special focus on the Thermaikos Gulf (northeastern Aegean Sea) and the port of Thessaloniki (Figure 1); ports of Patra and Piraeus in Greece are also checked together with the harbors in Barcelona, Algeciras, Haifa and Genova).

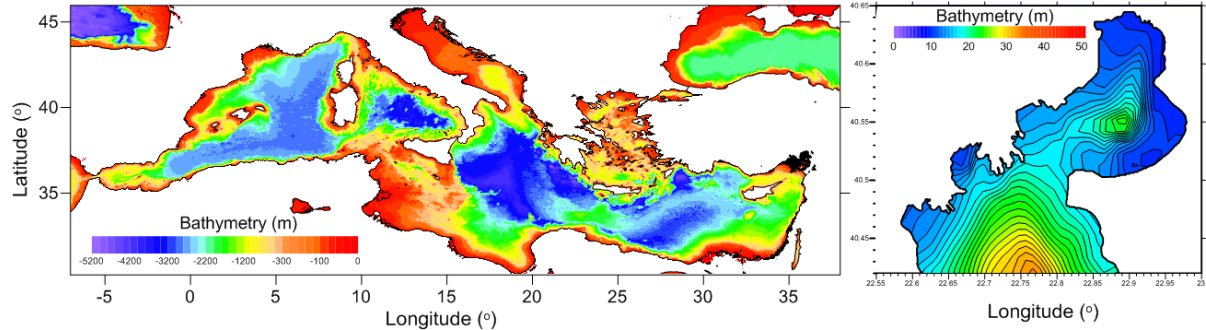


Figure 1 Bathymetry charts of Mediterranean Sea (left graph) and Thermaikos Gulf with the Thessaloniki Port basin (right graph); contours and color bars refer to depth d (m)

3 RESULTS

The results of pilot simulations with HiReSS concern maps of meteorologically induced sea surface heights (SSH) and current velocities (by zonal and meridional components, U and V) at 3-hourly time intervals for 3-day forecasts; 24 representations of storm surge impacts per day are produced. Preliminary results concern the entire Mediterranean basin with a focus on the Thermaikos, Patraikos and Saronikos Gulfs in Greece and other four Spanish, Italian and Israeli commercial ports.

3.1 Model validation

The model has been applied on a number of sites in the past, comprising large regions in open seas and coastal areas. It was calibrated and thoroughly validated via comparisons of hindcast modeling results against in situ observations for either short periods with intense weather events (Krestenitis et al. 2017) or large periods (>15yrs; for extreme events of annual maxima SSH) in the Mediterranean, Aegean and Ionian Seas, i.e. MeCSS (Androulidakis et al. 2015) and GreCSS (Makris et al. 2015, 2016) model versions. In Figure 2 characteristic comparisons of HiReSS hindcasting model results against tide-gauge measurements of SSH during 2012 in Thessaloniki and Genova ports are provided. Satisfactory accuracy of prediction is achieved with quite high Pearson product-moment correlations ($r > 0.7$) and acceptable errors reaching down to 15%. It is noted that the forecast skill of the storm surge model highly depends on the quality and resolution of the atmospheric weather input data, rather than its own parameterizations.

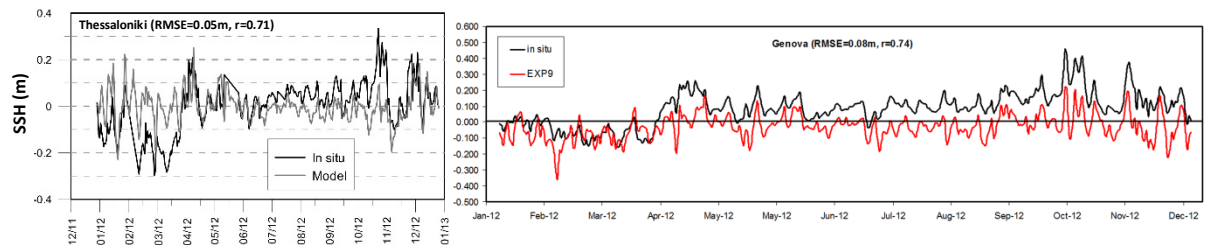


Figure 2 Comparisons of HiReSS hindcasting model results against in situ observations of SSH (m) by tide gauges during 2012 in Thessaloniki and Genova ports; $RMSE$: root-mean-square error; r : Pearson correlation

3.2 Case study

Figure 3 presents plots of HiReSS model forecast results concerning simulated fields of SSH and ocean current velocities in the entire Mediterranean Sea basin in conjunction with an atmospheric weather conditions field (SLP and wind vectors; upper graph). Negative SSH (sea surface below mean sea level) are observed in the Adriatic and Aegean Seas naturally due to the presence of a large

atmospheric high-pressure barometric system (“good weather”) and northerly winds (even if faint). On the contrary, large values of positive *SSH* are shown in the Gulf of Gabes (northcentral African coast) and near the Gibraltar straits, which are influenced by the low-pressure barometric system that prevailed south of the Iberian Peninsula on the northwestern African region. Strong easterly winds occurred between the two systems. It is concluded that HiReSS model may efficiently reproduce the inverse barometer effect together with wind-driven circulation.

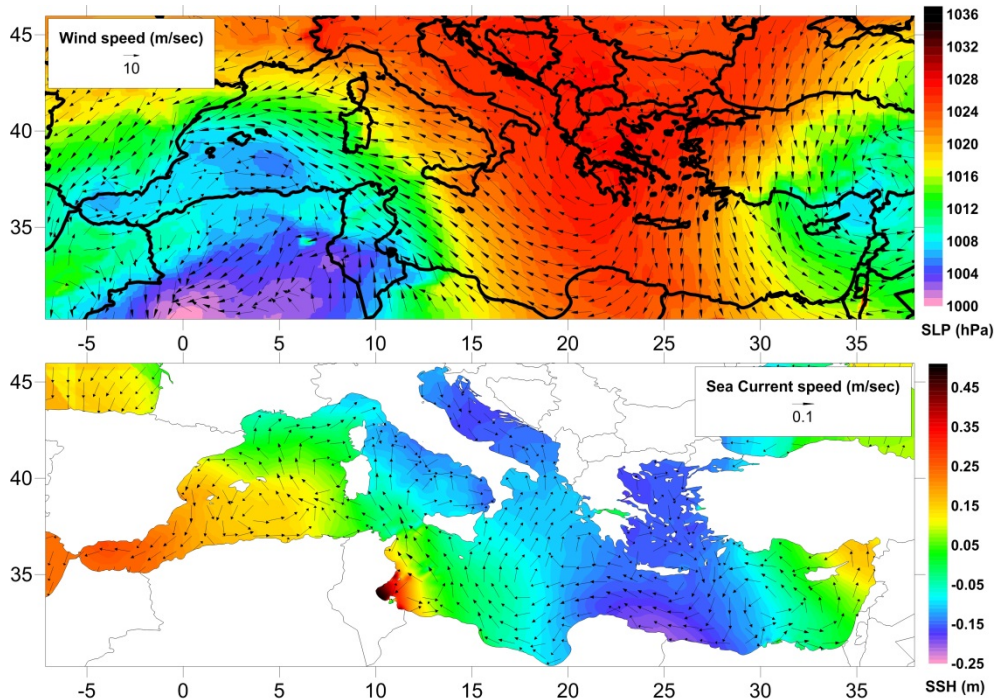


Figure 3 Upper graph: Atmospheric weather conditions (*SLP* in hPa and wind vectors in m/sec) chart over the Mediterranean Sea; Lower graph: HiReSS forecast results (*SSH* in m and current vectors in m/sec) chart of the Mediterranean basin on April 21st 2019, UTC 00:00.

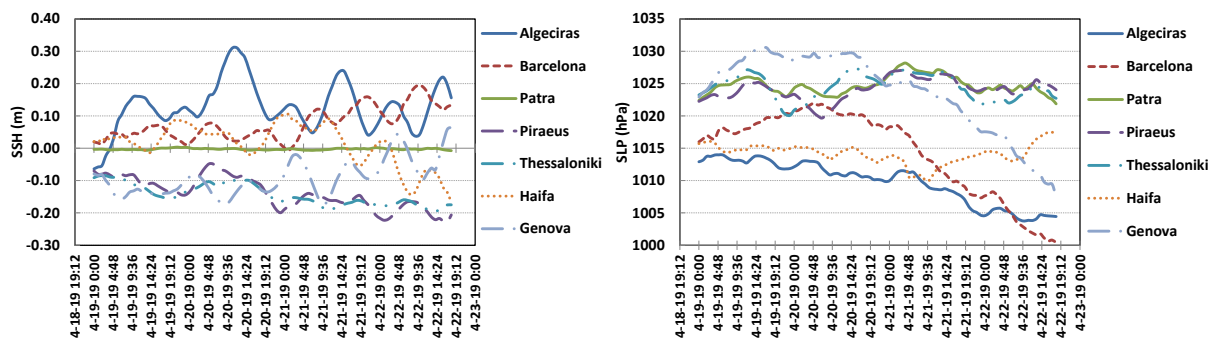


Figure 4 Graphs of HiReSS model results about surge- and tide-induced *SSH* (m) [left graph] and *SLP* (hPa) [right graph] in seven characteristic ports of the Mediterranean basin (Algeciras, Barcelona, Genova, Haifa, Patra, Piraeus, Thessaloniki ports); Forecasts refer to a 3-day period of April 19th-22nd 2019

Figure 4 presents characteristic *SSH* time-series (left panel) produced by HiReSS forecasts in seven ports of the Mediterranean basin. Sea levels in Greek ports and Genova are shown to range from zero (“dead calm” sea state in Patra port) to -20cm, whereas storm-induced sea surface elevation is evident in Algeciras and Barcelona up to 30cm. Reversed patterns are shown in *SLP* graph (right panel), corroborating the influence of the inverse barometer effect in these areas. Semi-diurnal undulating configurations are also clearly seen in the surge- and tide-driven *SSH* time-series, revealing the characteristic tidal patterns in the Mediterranean Sea; tidal effects are obvious even if astronomic tidal ranges are not significant in the specific region.

4 CONCLUSIONS

A robust operational forecast model for storm surges is built in the framework of an integrated tool for short-term marine weather and sea-state prognoses in broader areas around and inside port facilities with global commercial interest and high transportation loads. HiReSS has been validated by comparisons of model output against sea level observations from tide gauges in ports by official navy hydrographic services in southern Europe. It is proved to satisfactorily simulate the sea level variations inside harbor areas, providing also rough estimates of mean sea currents there. HiReSS results will hopefully address significant needs of port authorities, ship pilots and navigators towards battling problems of vessel impact on the harbor bed during mooring, towage and berth operations, according to reliable short-term sea-state forecasting. Presented cases in Mediterranean ports support that inference. Results are also judged to be crucial as input (local bathymetric changes) in irregular wave simulations with the TOMAWAC spectral wave model in the Accu-Waves modeling system.

Acknowledgements

This research is part of the Accu-Waves project (<http://accuwaves.eu>) co-financed by the European Union and Greek national funds through the Operational Program Competitiveness, Entrepreneurship and Innovation, under the call RESEARCH – CREATE – INNOVATE (project code: T1EDK-05111).

References

- Androulidakis Y et al. (2015) Storm surges in the Mediterranean Sea: variability and trends under future climatic conditions. *Dyn Atmos Ocean* 71: 56–82. doi:10.1016/j.dynatmoce.2015.06.001.
- De Vries H et al. (1995) A comparison of 2D storm surge models applied to three shallow European seas. *Environ Softw* 10(1): 23–42. doi:10.1016/0266-9838(95)00003-4.
- Krestenitis YN et al. (2011) Coastal inundation in the north-eastern Mediterranean coastal zone due to storm surge events. *J Coast Conserv* 15: 353–368. doi:10.1007/s11852-010-0090-7.
- Krestenitis Y et al. (2015a) Operational Oceanographic Platform In Thermaikos Gulf (Greece): Forecasting And Emergency Alert System For Public Use, Paper presented at 36th IAHR World Congress, The Hague, The Netherlands.
- Krestenitis Y et al. (2015b). Operational Forecast System of Storm Tides in the Aegean Sea (Greece), Paper presented at the 2015 ASLO Conference, Granada, Spain.
- Krestenitis YN et al. (2016) Coastal Engineering – Maritime Environmental Hydraulics. Kallipos Publications, NTUA, Athens, Greece. (in Greek) ISBN:978-960-603-253-0.
- Krestenitis Y et al. (2017) Severe weather events and sea level variability over the Mediterranean Sea: the WaveForUs operational platform. In: *Perspectives of Atmospheric Sciences* (Eds: Karacostas T et al.), Springer Atmospheric Sciences, 63-68. doi:10.1007/978-3-319-35095-0_9.
- Makris CV et al. (2015) Numerical Modeling of Storm Surges in the Mediterranean Sea under Climate Change. Paper presented at 36th IAHR World Congress, The Hague, The Netherlands.
- Makris C et al. (2016) Climate Change Effects on the Marine Characteristics of the Aegean and the Ionian Seas. *Ocean Dyn* 66(12): 1603–1635. doi:10.1007/s10236-016-008-1.
- Makris C et al. (2018) Climate change impacts on the coastal sea level extremes of the east-central Mediterranean Sea. Paper presented at XIV PRE Conference, 695-704. ISBN:978-960-99922-4-4.
- Memos CD et al. (2019) Accu-Waves: A decision Support Tool for Navigation Safety in Ports. Paper presented at the 1st International Scientific DMPCO Conference, Athens, Greece.
- Schwiderski EW (1980) On charting global ocean tides. *Rev Geophys*, 18(1): 243-268. doi:10.1029/RG018i001p00243.
- Smith SD, Banke EG (1975) Variation of the sea surface drag coefficient with wind speed. *Q J Roy Meteor Soc*, 101(429): 665-673. doi:10.1002/qj.49710142920.

WAVE-L: An integrated numerical model for wave propagation forecasting in harbor areas

Ch. Makris^{1*}, Th. Karambas¹, V. Baltikas¹, Y. Kontos¹, A. Metallinos², M. Chondros², A. Papadimitriou², V. Tsoukala², C. Memos²

¹Department of Civil Engineering, Aristotle University of Thessaloniki, Thessaloniki, 54124, Greece

²School of Civil Engineering, National Technical University of Athens, Zografos, Athens, 15773, Greece

*Corresponding author: cmakris@civil.auth.gr

Abstract

In this paper we present the evolution of an integrated numerical model (WAVE-L) for the simulation of wave propagation and transformation in areas around and inside ports and harbors. WAVE-L is a high-resolution phase-resolving wave model based on the hyperbolic mild-slope equations, capable of simulating the transformation of complex wave fields over varying bathymetries in harbors and coastal areas in the vicinity of ports. The modeled wave processes include shoaling, refraction, diffraction, total and partial reflection from structures, energy dissipation due to wave breaking and bottom friction in a combined way. The new version of WAVE-L incorporates wave generation simulated on any boundary (longitudinal, lateral or oblique) with corresponding expansion of peripheral sponge layers, providing potential to spatially restrict the computational field in areas adjacent to ports, thus reducing demand of computational time and resources. Moreover, the modified WAVE-L version is able to simulate quasi-irregular, multi-directional waves, whose generation and propagation may furthermore account for various angles and directions simultaneously. WAVE-L is one-way coupled to coarser implementations of an open-sea spectral wave model and a 2-DH hydrodynamic circulation model for storm surges that provide input and boundary conditions. WAVE-L model is thoroughly validated against experimental data on diffraction and multidirectional spectral wave propagation; pilot implementations of it are carried out at the Greek port basin of Thessaloniki. The ultimate goal is to create a tool for high-resolution operational forecasts of wave conditions around and inside significant ports with high traffic load and commercial value (project Accu-Waves).

Keywords Wave model, Wave propagation, Harbor areas, Ports.

1 INTRODUCTION

1.1 Theme of research

In this paper we present the evolution of a classic, integrated numerical model for the simulation of wave propagation and transformation in coastal areas around and inside ports and harbors. The model is called WAVE-L and it is based on the 2-DH depth-integrated harmonic hyperbolic formulation of the mild-slope equation for wave propagation. Its integrated version under development is intended as a crucial part of a computational tool that will provide reliable 3-day forecasts at 3-hour intervals on prevailing sea states in areas near the certified pathways of port approaches and in regions inside harbor basins (project Accu-Waves; <http://accuwaves.eu/>). WAVE-L's results will support safer navigation and maneuvering around harbor structures for ships and vessels accessing ports.

1.2 Scope of research

Main goal of this study is to formulate new features of the WAVE-L model in order to make it fully operational, quick and robust for high-resolution forecasts of both monochromatic and spectral wave fields around and inside port basins. A secondary aim is to thoroughly calibrate and validate the WAVE-L model against experimental data of wave propagation and transformation in the field and laboratory flume scales (Vincent and Briggs 1989; Yu et al. 2000). Furthermore, we intend to further manipulate the Fortran codes of the WAVE-L model in order to produce results integrated into a single-suite modeling system for automated operational forecasting of wave characteristics in and around fifty significant ports worldwide (project Accu-Waves; <http://accuwaves.eu/>). Ultimate goal of

research is to develop an operational ensemble of hydrodynamic numerical models (Memos et al. 2019), i.e. an open-seas spectral wave model for wind-induced irregular waves and a barotropic storm surge model for 2-DH hydrodynamic circulation that will provide input data and boundary conditions for the WAVE-L model to produce maps of high-resolution wave height, period and direction data at 3-hour/3-day forecasts for the said ports.

2 METHODOLOGY

2.1 Numerical model

The new version of the previously developed WAVE-L model (Karambas and Samaras 2017) is an evolved rendition of the HARBOUR-L model (Karambas et al. 2010). WAVE-L is a high-resolution phase-resolving wave model based on the hyperbolic mild-slope equations (Copeland 1985) and it is capable to simulate the transformation of complex wave fields in harbors and coastal areas in the vicinity of ports with varying bathymetries (Watanabe and Maruyama 1986). In these areas the modeled wave processes include propagation, transformation, shoaling, refraction, diffraction, total and partial reflection from structures, wave-current interaction, energy dissipation due to depth-limited wave breaking and bottom friction in a combined way (Christopoulos et al. 2012).

2.1.1 Basic equations and assumptions

The basic continuity and momentum equations (mass and quantity of motion conservation, respectively) can be derived by replacing both pressure and velocity distributions that correspond to linear theory (for small amplitude waves) in the linearized Navier-Stokes equations (valid for periodic wave propagation from deep to shallow waters), and thus for numerical simulations of wave transformation in 2-DH (depth-averaged) formulation they can be written as:

$$\frac{\partial \eta}{\partial t} + \frac{\partial(U_w d)}{\partial x} + \frac{\partial(V_w d)}{\partial y} = 0 \quad (1)$$

$$\frac{\partial U_w}{\partial t} + \frac{1}{d} \frac{\partial(c^2 \eta)}{\partial x} - \frac{1}{d} \frac{g \eta}{\cosh(kd)} \frac{\partial d}{\partial x} = v_h \frac{\partial^2 U_w}{\partial x^2} + v_h \frac{\partial^2 U_w}{\partial y^2} - f_b \sigma U_w \quad (2)$$

$$\frac{\partial V_w}{\partial t} + \frac{1}{d} \frac{\partial(c^2 \eta)}{\partial y} - \frac{1}{d} \frac{g \eta}{\cosh(kd)} \frac{\partial d}{\partial y} = v_h \frac{\partial^2 V_w}{\partial x^2} + v_h \frac{\partial^2 V_w}{\partial y^2} - f_b \sigma V_w \quad (3)$$

where η is the wave-induced free-surface elevation, d is the still water depth of the sea, U_w and V_w are the depth-integrated horizontal velocity components along the x and y axis, respectively, $k=2\pi/L$ is the wavenumber, L is the local wave length, c is the wave (phase) celerity, $\sigma=2\pi/T$ is the wave angular frequency, f_b is the normalized bed friction coefficient, v_h is the horizontal eddy viscosity coefficient.

Depth-limited wave breaking in shoal areas can be modeled by using the eddy viscosity concept for Reynolds stresses via a coefficient v_h in the r.h.s. of the momentum equations (Eqs. 2, 3), which is given by (Battjes, 1975), where D defines the energy dissipation due to wave breaking, and coefficient Q_b can be derived based on the assumption of a Rayleigh distribution for wave trains in nearshore areas from the following equations:

$$v_h = 2h \left(\frac{D}{\rho} \right)^{1/3} \quad (4)$$

$$D = \frac{1}{4} Q_b f_s \rho g H_m^2 \quad (5)$$

$$\frac{1-Q_b}{\ln Q_b} = \left(\frac{H_{rms}}{H_m} \right)^2 \quad (6)$$

where f_s is the mean spectral frequency ($f_s=1/T_m$, T_m mean spectral wave period), H_m is the maximum wave height with $H_m=\gamma d$, γ is the wave breaking parameter ($\gamma \approx 0.55-1.0$), Q_b is the percentage of breaking waves at a particular depth d , and H_{rms} is the root-mean-square wave height $H_{rms}=2(\langle 2\eta^2 \rangle)^{1/2}$ and brackets $\langle \rangle$ denote time-averaged values. It is inferred that for the total prevalence of breaking waves $Q_b=1$ whereas for non-breaking waves $H_{rms} \ll H_m$, i.e. $Q_b \ll 1$. This modeling approach can describe breaking of random waves in complex bathymetries, conforming to the requirements of operational random wave forecasts and consequent newly added features of WAVE-L (see §2.1.2). Bottom friction energy dissipation is modeled using the linearized (normalized by local depth d) terms

in the r.h.s. of the momentum equations (Eqs. 2, 3) in x - and y -directions of the Cartesian horizontal plane. The linearized bottom friction coefficient f_b is a function of the wave-induced velocity and the wave friction coefficient f_w , following the relationship:

$$f_b \sigma = \left(\frac{1}{2} f_w \sqrt{U_w^2 + V_w^2} \right) / d \quad (7)$$

2.1.2 Innovative features

In the new proposed version of the WAVE-L model, wave generation can be simulated both on lower-‘South’ and lateral boundary simultaneously, with corresponding expansion of the peripheral sponge layers (Larsen and Dancy 1983) by an exponential damping factor of wave energy content, $DF(x)$ as:

$$DF(x) = \exp\left[\left(b^{-x/\Delta x} - b^{x_s/\Delta x}\right) \ln 2\right] \quad (8)$$

where x_s is the width of the sponge layer, $b=1+r_s+\exp(-1/r_s)$ where $r_s=10/t_s$ (t_s is the number of grid points inside the sponge layer). In this way, we are now capable to spatially restrict the computational field in areas adjacent to harbors and thus reduce demand of computational time and resources.

Moreover, the existing version of the model is modified to simulate multi-directional, quasi-irregular waves (spectral waves propagating with single group celerity). The generation and propagation of spectral waves may furthermore account for several different angles and directions simultaneously, practically following the modeling approach of Lee and Suh (1998) that provides the directional spreading function $D(f, \theta)$ by the Fourier series representation for the wrapped normal spreading function (see also Vincent and Briggs 1989) as:

$$D(f, \theta) = \frac{1}{2\pi} + \frac{1}{\pi} \sum_{n=1}^N \exp\left[-\left(\frac{n\sigma_m}{2}\right)\right] \cos[n(\theta - \theta_m)] \quad (9)$$

where N is the number of terms in the series, θ_m is the mean wave direction (0° or 45° in our test cases), and for each case of θ_m , σ_m the directional spreading parameter (either 10° or 30° in our tests).

Partial and full reflection of incipient waves from harbor structures are modeled based on an updated version of the Karambas and Bowers (1996) modeling approach of an extra dissipation term in the momentum equations inserting a turbulent eddy viscosity coefficient, which is calculated via a system of complex equations (based on a complex wave number K) of the friction coefficient f_s , thus allowing to solve them iteratively for given values of the reflection coefficient R_s from literature.

2.2 Application study

Pilot implementation of the new WAVE-L model is carried out at the three largest Greek harbors, namely the ports of Patra, Piraeus and Thessaloniki (Figure 1). Fine resolution bathymetric depth charts are produced by digitizing 1:5000 maps of the Hellenic Navy Hydrographic Service (HNHS; <https://www.hnhs.gr/>) and interpolating by the Kriging method. The mild-slope equation model is one-way coupled to a coarser 3rd generation spectral wave model (TOMAWAC) for input boundary conditions; the port area of typically ≤ 10 Km² (Figure 1) is integrated in larger domains. It also receives input of local changes in bathymetry, viz. mean sea level elevation, from a barotropic 2-D hydrodynamic circulation model for storm surges (HiReSS; Makris et al. 2019).

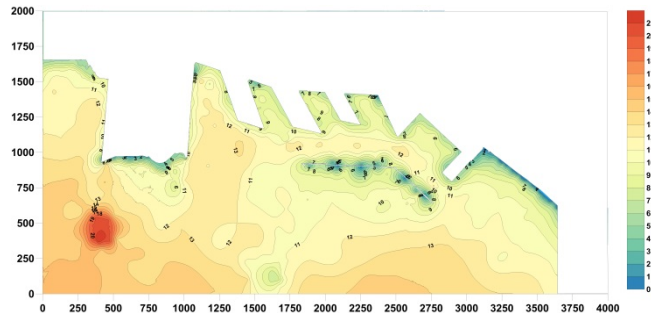


Figure 1 Bathymetry chart of Thessaloniki Port basin (six jetties and piers and one protective breakwater); contours and color bar refer to depth. X- and Y-axis refer to distances in m from arbitrary start point.

3 RESULTS

The results mainly concern gridded fields and relevant maps of wave characteristics (height, period and angle of propagation direction) for both regular and quasi-irregular wave fields of very high spatial resolution, i.e. discretization step of $dx \leq 2m$, at 3-hourly time intervals covering the needs of 3-day forecasts, leading to 24 representations of sea-states per daily model implementation. Model results support the approaching procedures of vessels to port and harbor basins.

3.1 Model validation

Evaluation of the WAVE-L model's performance is conducted by comparisons of simulation results with experimental data of multi-directional irregular wave diffraction around semi-infinite breakwaters and through breakwater gaps (Yu et al. 2000; Li et al. 2000). The elliptical shoal experimental setup by Vincent and Briggs (1989) with a directional spectral wave generator is also numerically reproduced with WAVE-L as a test. Figure 2 presents satisfactory comparisons of model results against experimental data of both implementations, in terms of normalized wave heights H/H_o , H_o is the offshore wave height (upper graphs), and diffraction coefficient K_D (lower graphs), respectively. All cases refer to new WAVE-L model implementations for spectral waves in several directions.

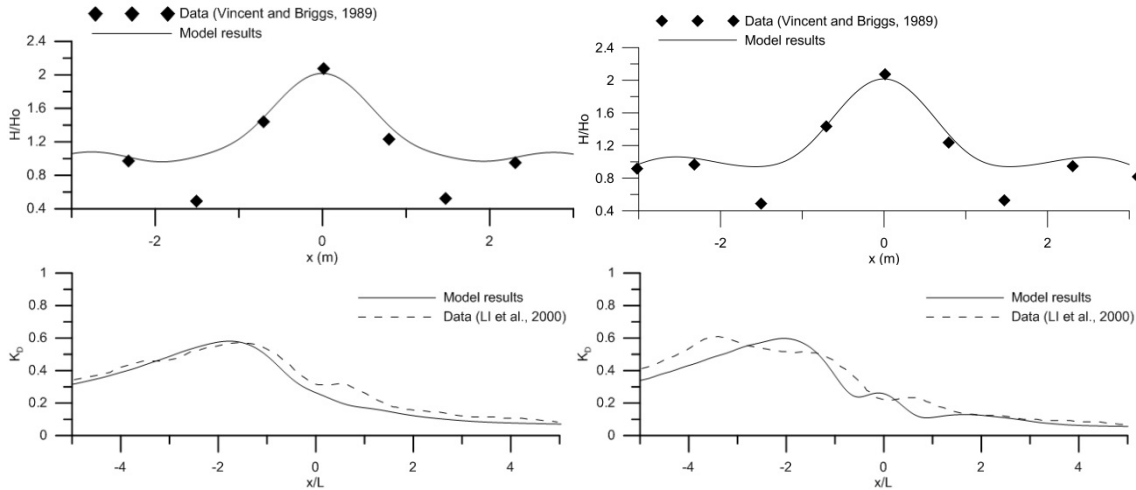


Figure 2 Comparisons of WAVE-L modeled results against experimental data of Vincent and Briggs (1989) and Li et al. (2000), in terms of normalized wave height H/H_o (upper graphs), for spectral waves in experimental cases U3 and B3 [left and right graphs, respectively], and diffraction coefficient K_D (lower graphs) for experimental data of unidirectional irregular waves (spreading parameter $s=\infty$ and initial angle of propagation $\theta_o=45^\circ$) and multi-directional irregular waves ($s=19$ and $\theta_o=45^\circ$) [left and right graphs, respectively].

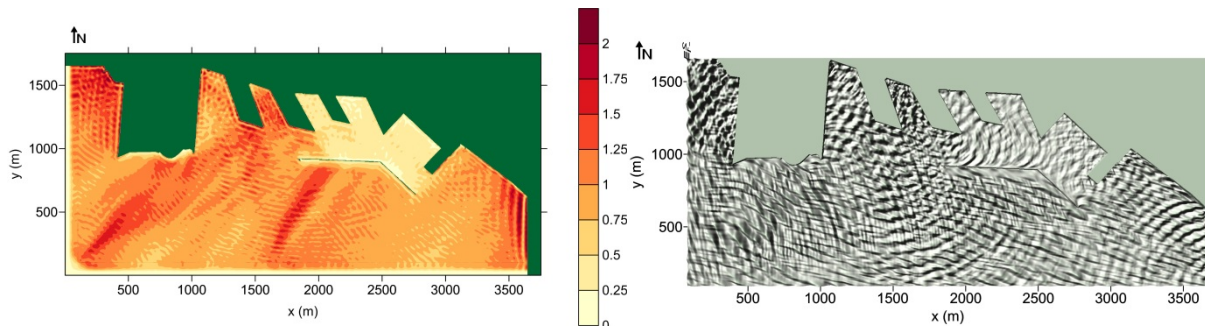


Figure 3 Results charts in the Thessaloniki Port basin for significant wave height H_s (color bar in m) [left graph] and surface elevation η [right graph] for quasi-irregular multi-directional wave fields, respectively.

3.2 Case study

Figure 3 presents plotted results concerning simulated fields of gridded data ($dx=2m$) for H_s (left panel) and η (right graph), depicting steady state conditions of extreme cases ($H_o=2m$) for southern seas as narrow spectral wave fields. The protection offered by the sub-aerial breakwater is obvious in the first case, as transmitted H_s is decreased by diffraction reaching hardly up to 1/4 of the offshore

wave height on the open boundary. Reflection patterns of quasi-irregular surface elevation are also visible in the port basin for the second case of spectral wave propagation, i.e. multidirectional harsh southern sea states.

4 CONCLUSIONS

WAVE-L is validated by comparisons of model output against experimental data by classic laboratory physical simulations for regular and spectral waves. It is proven to adequately simulate the wave propagation in nearshore areas over uneven bottoms and specifically inside harbors, around and on the leeward side of breakwaters, incorporating wave-structure interaction and plausible diffraction modeling. The new WAVE-L results will hopefully address significant needs such as safe spatial and temporal planning of navigation towards and inside ports, port operations to and from mooring sites, while facilitating the ship-pilot and port-navigator consultation. This should eventually allow for more efficient management of the navigation and towage services, such as berth positions assignment according to short-term weather forecasting. The presented Thessaloniki Port case corroborates that.

Acknowledgements

This research is part of the ACCU-WAVES project (<http://accuwaves.eu>) co-financed by the European Union and Greek national funds through the Operational Program Competitiveness, Entrepreneurship and Innovation, under the call RESEARCH – CREATE – INNOVATE (project code: T1EDK-05111).

References

- Battjes JA (1975) Modeling of turbulence in the surf zone. Paper presented at the Symposium of Modeling Techniques, California, ASCE, 1050-1061.
- Christopoulos S, Avgeris I, Karambas TV (2012) HMAR_HARBOURL: An Integrated Numerical Model For Harbour Layout Design. Paper presented at 22nd ISOPE Conference, Rhodes, Greece.
- Copeland GJM (1985) A Practical Alternative to the Mild-Slope Equation. *Coast Eng* 9: 125-149. doi:10.1016/0378-3839(85)90002-X.
- Goda Y (1999) A comparative review on the functional forms of directional wave spectrum. *Coast Eng J* 41(1): 1-20. doi:10.1142/S0578563499000024.
- Karambas TV, Bowers EC (1996) Representation of Partial Wave Reflection and Transmission for Rubble Mound Coastal Structures. *WIT Trans Ecol Environ* 18: 9. doi:10.2495/HY960421.
- Karambas T, Christopoulos S, Avgeris I (2010) HARBOUR_L: Integrated mathematical model for the design of harbor works. Paper presented at 5th Pan-Hellenic Conference on Harbor Works, Athens, Greece.
- Karambas TV, Samaras AG (2017) An Integrated Numerical Model for the Design of Coastal Protection Structures. *J Mar Sci Eng* 5(4): 50. doi:10.3390/jmse5040050.
- Makris C et al (2019) HiReSS: Storm Surge Simulation Model for the Operational Forecasting of Sea Level Elevation and Currents in Marine Areas with Harbor Works. Paper presented at 1st International Scientific DMPCO Conference, Athens, Greece.
- Memos CD et al (2019) Accu-Waves: A decision Support Tool for Navigation Safety in Ports. Paper presented at the 1st International Scientific DMPCO Conference, Athens, Greece.
- Larsen J, Dancy H (1983) Open Boundaries in Short Wave Simulations - A New Approach, *Coast Eng* 7: 285-297. doi:10.1016/0378-3839(83)90022-4.
- Li YS, Liu SX, Yu YX, Lai GZ (2000) Numerical modeling of multi-directional irregular waves through breakwaters. *Appl Math Mod* 24(8-9): 551-574. doi:10.1016/S0307-904X(00)00003-2.
- Vincent CL, Briggs MJ (1989) Refraction—diffraction of irregular waves over a mound. *J Waterw Port Coast Ocean Eng* 115(2): 269-284. doi:10.1061/(ASCE)0733-950X(1989)115:2(269).
- Watanabe A, Maruyama K (1986) Numerical modeling of nearshore wave field under combined refraction, diffraction and breaking. *Coast Eng Japan* 29(1): 19-39. doi:10.1080/05785634.1986.11924425.
- Yu YX, Liu SX, Li YS, Wai OW (2000) Refraction and diffraction of random waves through breakwater. *Ocean Eng* 27(5): 489-509. doi:10.1016/S0029-8018(99)00005-0.

Advanced numerical models for wave disturbance simulation in port basins

A.S. Metallinos^{1*}, M.K. Chondros¹, Th.V. Karambas^{1,2}, C.D. Memos^{1,3}, A.G. Papadimitriou¹

¹Scientia Maris, Agias Elenis 10, Zografos, 15772, Greece

²Department of Civil Engineering, Aristotle University of Thessaloniki, Thessaloniki 54124, Greece

³School of Civil Engineering, National Technical University of Athens, Zografos 15780, Greece

*Corresponding author: anast.metallinos@gmail.com

Abstract

In the present work, two advanced numerical models developed in-house by Scientia Maris to cover real-life applications, describing the wave agitation in a port basin, are presented. The first one, 2DH Maris-BW model, is a highly non-linear and fully dispersive Boussinesq-type model while the second one, 2DH Maris-HMS, is a non-linear hyperbolic-type mild slope model. Both models are capable of simulating the transformation of complex wave fields, mainly in harbors, but also in coastal areas, with varying bathymetries and steep slopes. The numerical models when compared with experimental data showed that a more than satisfactory agreement was achieved and in most cases a better behavior over other widely known models.

Keywords Advanced numerical models, Numerical simulation, Wave disturbance, Port basin.

1 INTRODUCTION

Harbors are vital links in the chain of maritime transportations having a crucial impact on the global economy. The function of a harbor is to provide safe anchorage for vessels and to facilitate smooth transfer of cargo and people between ships and hinterland. Assured surface tranquility inside the basin is not only essential for safe moorage, but it is also important for efficient port operations. Essentially, low wave agitation in harbors reduces the excitation of ships moored at anchorage or along a quay and optimizes the mooring forces.

Nowadays, numerical models are a major tool for engineers involved in the design of port and marine structures and have become increasingly important for many relevant applications. There are numerous models in the literature more or less advanced, covering various aspects of wave dynamics from deep water to the nearshore, at different scales and at varying levels of detail. However, port engineering practice requires robust models that are able to represent in an efficient as well as in a reliable way the full range of processes concerning the issue of wave disturbance inside port basins. They should be able to reproduce adequately the most important phenomena such as diffraction, depth shoaling/refraction, partial or total reflection, transmission and wave-wave interactions. At the same time, model versatility should also be considered as an essential requirement, since such models should be able to be adapted to a wide range of design layouts and applications.

In this paper, two advanced numerical models developed in-house by Scientia Maris able to cover real-life applications, with respect to the wave disturbance in a port basin, are presented. The first one, Maris-BW model, is a highly non-linear and fully dispersive Boussinesq-type model while the second one, Maris-HMS, is a non-linear hyperbolic-type mild slope model. Both models are capable of simulating the transformation of complex wave fields, mainly in harbors, but also in coastal areas, with varying bathymetries and steep slopes. The numerical models were also compared with numerous measurements and showed that a satisfactory agreement was achieved in all cases.

2 MODEL DESCRIPTION

2.1 *Maris-BW, Boussinesq-type Wave model*

This model is a sophisticated numerical model which was initially developed by Chondros and Memos (2014) based on the formulation of Madsen and Schäffer (1998). This model is able for simulating non-breaking and breaking long and short crested waves in a variety of bottom profiles and structures

of steep slopes, extending the applicability from very deep through to shallow waters and thus overcoming a shortcoming of most models of the same type. The applicability of that model was further extended by Metallinos et al. (2019), in order to tackle wave propagation over submerged porous breakwaters, as well as to estimate the velocity distribution inside the structure body, taking into account its porosity. The model's equations read in 2DH form :

$$\zeta_t + \nabla[(d + \varepsilon\zeta)\mathbf{U}] = 0 \quad (1)$$

$$\begin{aligned} \mathbf{U}_t + \nabla\zeta + \frac{1}{2}\varepsilon(\mathbf{U} \cdot \nabla)\mathbf{U} + \mu^2(\Lambda_{20}^{III} + \varepsilon\Lambda_{21}^{III} + \varepsilon^2\Lambda_{22}^{III} + \varepsilon^3\Lambda_{23}^{III}) + \mu^4(\Lambda_{40}^{III} + \varepsilon\Lambda_{41}^{III}) \\ + O(\mu^6, \varepsilon^2\mu^4) = 0 \end{aligned} \quad (2)$$

where ζ is the surface elevation, $\mathbf{U} \equiv (U, V)$ is the depth-averaged horizontal velocity vector, $\nabla \equiv (\partial/\partial x, \partial/\partial y)$ is the gradient operator, d is the water depth above the structure, ε is the nonlinearity parameter equal to H/d (where H is the local wave height) and μ is the frequency dispersion parameter equal to h/L (where L is the local wavelength). For the Λ^{III} terms the reader is referred to the original paper of Madsen and Schäffer (1998) and to that of Chondros and Memos (2014).

2.2 Maris-HMS, Hyperbolic-type Mild Slope model

Maris-HMS is an advanced version of a previous model initially developed by Karambas et al. (2010) and (2013). This model is a phase-resolving wave model based on the hyperbolic mild-slope equations as proposed by Copeland (1985) and it is capable to simulate the transformation of complex wave fields in harbors and coastal areas over uneven bottoms. It takes into account energy dissipation due to wave breaking and bottom friction as well as it incorporates the exact non-linearity in any depth. More specifically, the latter was achieved through an initial calculation of phase, group velocities and wave numbers by the linear dispersion relation and then by a recalculation of the nonlinear phase, group velocities and the wave numbers in accordance to any of Stokes second or fifth order, cnoidal or solitary wave theories. More details can be found in the companion paper of Chondros et al. (2019). The governing equations are:

$$\zeta_t + \frac{c}{c_g} \nabla \cdot \frac{c_g}{c} \mathbf{Q}_w = 0 \quad (1)$$

$$\mathbf{U}_{w,t} + \frac{c^2}{d} \nabla \zeta = \nu_{\square} \nabla^2 \mathbf{U}_w \quad (2)$$

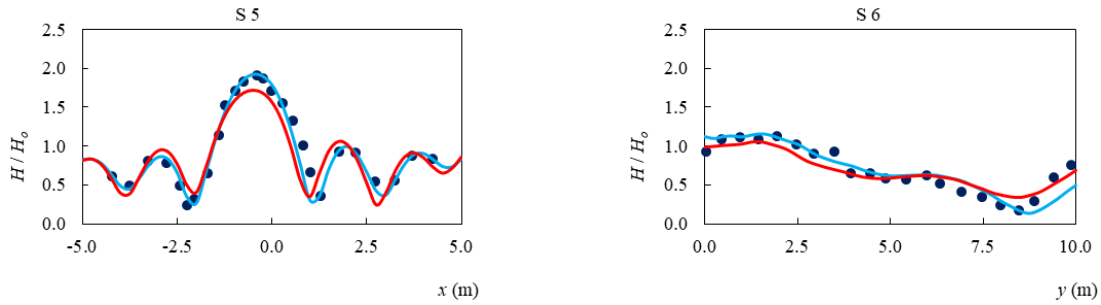
where ζ is the surface elevation, $\mathbf{U}_w \equiv (U_w, V_w)$ is the mean velocity vector, ∇ is the horizontal gradient operator, d is the depth, $\mathbf{Q}_w = \mathbf{U}_w h_w = (Q_w, P_w)$, h_w is the total depth ($h_w = d + \zeta$), c is the celerity, c_g is the group velocity ($c_g = (gd)^{0.5}$) and ν_{\square} is the horizontal eddy viscosity coefficient copying with wave breaking and (partial or total) wave reflection.

3 VERIFICATION WITH EXPERIMENTS

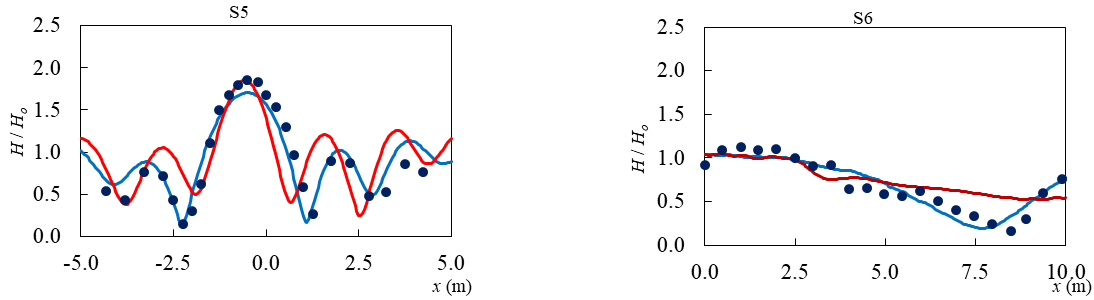
Numerical results of both models, comprising wave height, surface elevation and wave energy spectra, are compared against experimental data. The scenarios used for the comparison include the experimental layouts of Berkhoff et al. (1982), Vincent and Briggs (1989) and Metallinos et al. (2019). Further comparison has been made, with MIKE 21 models in some cases.

3.1 Experiment of Berkhoff et al. (1982)

In this section, the Maris-BW and Maris-HMS results were compared against test data of Berkhoff et al. (1982). The results of the widely known models MIKE21 BW and MIKE21 EMS were also compared against the same data. The bathymetry consisted of an elliptic shoal resting on a 1:50 plane sloping seabed, while the entire slope was turned at an angle of 20° to the wave paddles. The incident wave characteristic was $H_s=0.0464$ m and $T=1.0$ s. All models run for $t = 40$ s. The wave heights produced by the models were obtained by averaging over the last ten periods of simulation, since the wave field reached a stable state after 30 s. The results of all models are given in Figures 1 and 2.



7. Figure 1 Comparison of the Maris-BW (blue line) with MIKE21 BW (red line) against experimental data of Berkhoff et al. (1982) (dark blue circles).



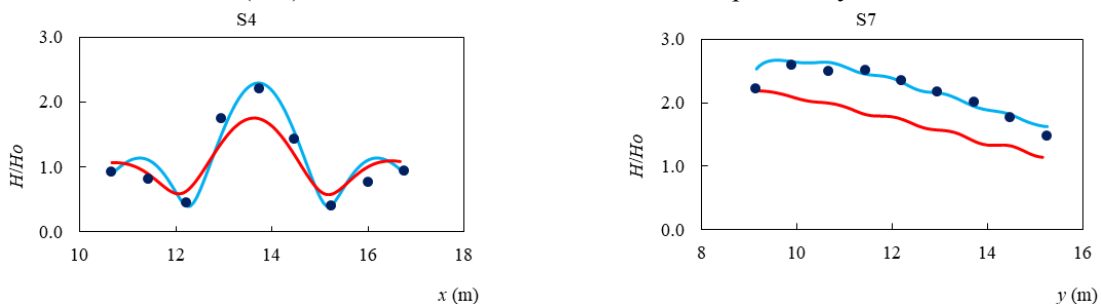
8. Figure 2 Comparison of the Maris-HMS (blue line) with MIKE21 EMS (red line) against experimental data of Berkhoff et al. (1982) (dark blue circles).

From the above results, we can state that all models behave well compared to the laboratory measurements of Berkhoff et al. (1982). However, in some cases, a slightly better performance from Maris-BW and Maris-HMS was achieved compared to MIKE21 BW and MIKE21 EMS respectively. The reason for the first case is the higher non-linearity embedded to the Maris-BW compared to MIKE21-BW, while in the second case the explanation is based on the fact that a calculation method of the non-linear amplitude dispersion velocities is incorporated in the Maris-HMS.

3.2 Experiment of Vincent and Briggs (1989)

Vincent and Briggs (1989) performed experiments with frequency-direction spreading which pass over a submerged elliptic shoal by using a directional spectral wave generator in a basin of the Coastal and Hydraulics Laboratory of the U.S. Army Engineer Research and Development Center. The wave conditions used for the simulation is a sinusoidal wave with $H_s = 0.0254$ m and $T = 1.3$ s. For the numerical simulations of this experiment, the bathymetry with a submerged elliptic shoal is reproduced. The computational grid was $\Delta x = \Delta y = 0.05$ m and the time steps $\Delta t = 0.01$ s. The model run for 30 s and the last 5 periods are used to extract the numerical results of wave heights.

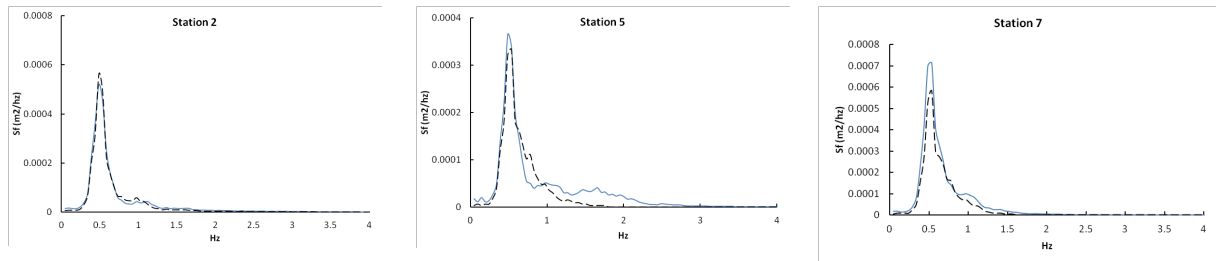
Below the comparison of Boussinesq models against the experimental data are shown at four transects. An overall satisfactory agreement of the Maris-BW results with the experimental measurements is again noted. This is true also in the most demanding domain of the experimental setup, i.e. just downstream of the shoal (#s7) where the MIKE21 BW results are quite away from the measurements.



9. Figure 3 Comparison of the Maris-BW (blue line) with MIKE21 BW (red line) against experimental data of Vincent and Briggs (1989) (dark blue circles).

3.3 Experiment of Metallinos et al. (2019)

In this section, results of Maris-BW compared to the measurements of Metallinos et al. (2019) are shown. The latter carried out 2DH laboratory experiments in a wave basin at the Hydraulic Engineering Laboratory, University of Patra. Part of these tests included measurements of free surface elevation over a permeable SB with steep slopes, under regular and irregular (Jonswap) wave attack, including breaking or non-breaking events. A permeable submerged breakwater (SB) with porosity $\varphi=0.50$ was constructed and placed on a mild sloping bottom at 1:15. The height of the structure was 0.2 m at the middle of the crest, while the crest width was 0.5 m. The SB was made of natural stones with $d_{50}=0.05$ m sloping 1:2 at both sides and downstream was placed sand in order to study the evolution of bed morphology. The water depth at the SB axis was 0.25 m, leaving a 0.05 m freeboard below S.W.L. The validation shown here, consists of one irregular wave with $H_s = 0.080$ m and $T_p=2.00$ s. The comparison between the measured and the computed wave energy spectra at three representative stations are given below.



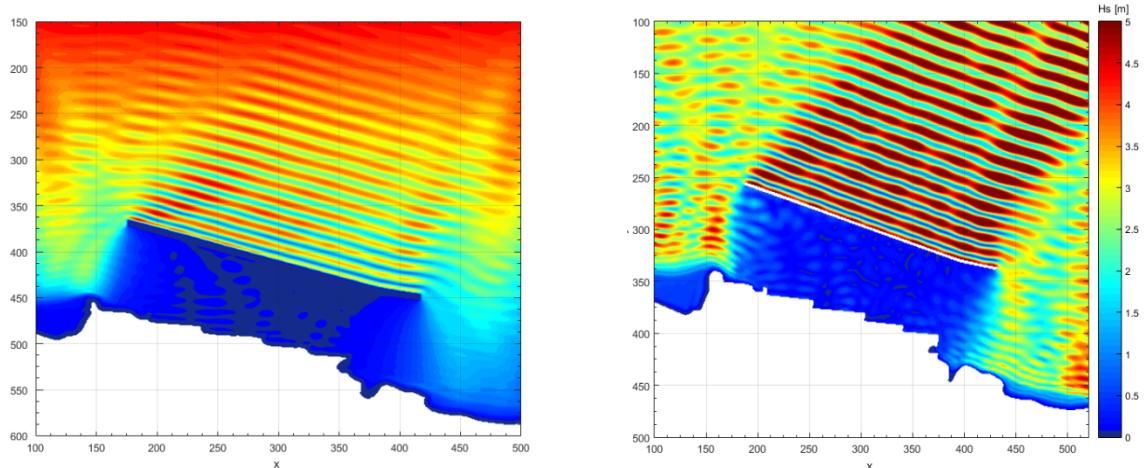
10. Figure 4 Spatial evolution of wave spectrum: (—) experiment, (- - -) Maris-BW.

From the above comparisons of the model's results with the measurements as well as the results of other cases not shown here, it can be deduced that the model was able to describe accurately the wave field over and around a porous SB with steep slopes capturing the nonlinear phenomena at the free surface, under regular or random wave attack. Also, it has to be noticed that those experiments could be also seen as a representation of a typical coastal defense project including a porous SB at a scale equal to 10÷15. Thus, the layout could represent a prototype SB constructed at a depth of about 2.5 – 3.75 m with armour stones of a mean diameter 0.5 – 0.75 m.

4 APPLICATION STUDY

Both models were also applied to a real case study regarding the wave disturbance in a port basin. More specifically, an implementation of Scientia Maris models was carried out for simulating the wave agitation at the new port of Patra. Incident extreme waves of characteristic height $H_s = 3.70$ m and $T_p=7.80$ s were considered referring to 9BF wind from western direction. The 2DH numerical domain in the BW model was discretized using a grid size of $\Delta x = \Delta y = 2.5$ m and a time step of $\Delta t = 0.01$ s while in the HMS model spatial and time step was 2.5 m and 0.005 s respectively. The simulation time was 600 s m for both models. The results are illustrated in maps below depicting wave heights and surface elevations.

It can be observed that both models can adequately simulate the wave processes of wave breaking, shoaling/refraction, diffraction and reflection. Regarding reflected wave trains, an increase in wave height is observed windward the breakwater in both models. These reflected waves are propagated in a large distance windward the structure's toe, seemingly without dissipation, which can be attributed to the linear nature of the propagated signal. However an important benefit of the BW model is that despite the regular waves considered, wave-wave interactions were taken into account due to the improved dispersion characteristics and high non-linearity embedded in the model. Consequently, the magnitude and propagation distance of the reflected waves is reduced and closer to the physical processes compared to the HMS model. The proper predicted reflected height is of paramount importance in wave agitation studies due to the reflected nature of a port basin. Nevertheless, the real time of the simulation of the BW model was around 6 hrs while in the HMS model was approximately 20 min. Indeed, given the nature of a mild slope model, the latter is much quicker, maintaining the needed computational resources at more reasonable levels, compared to the first one.



11. *Figure 5 Wave height results of Maris-BW model (left) and Maris-HMS model (right) in the new Port of Patra*

5 CONCLUSIONS

The presented Maris-BW and Maris-HMS numerical models when compared with test data showed that satisfactory agreement was achieved and in most cases show a better behavior over other widely known numerical models. Given the satisfactory agreement between models' results and laboratory measurements, both models were successfully applied to an application study in the new port of Patra. and were able to reproduce adequately phenomena related to the physical processes in a port basin. Hence they are deemed to constitute suitable models for the design and evaluation of the wave disturbance into a port basin addressing significant needs of the engineering community. In this paper the benefits as well as the drawbacks of each model were reported so that the engineer would be able to choose the appropriate model depending on his specific needs.

References

- Berkhoff JCW, Booij N, Radder, AC, (1982) Verification of numerical wave propagation models for simple harmonic linear water waves. *Coastal Engineering*, 6, 255–279. doi.org/10.1016/0378-3839(82)90022-9.
- Chondros et al. (2019) Advanced Numerical Models for Simulation of Nearshore Processes. 1st Int. Conf. on Design and Management of Harbor, Coastal and Offshore Works. Athens, Greece.
- Chondros MK, Memos CD (2014) A 2DH nonlinear Boussinesq-type wave model of improved dispersion, shoaling and wave generation characteristics. *Coastal Engineering*, 91, 99-122. doi.org/10.1016/j.coastaleng.2014.05.007.
- Copeland GJM (1985) A Practical Alternative to the Mild-Slope Equation. *Coastal Engineering*, 9, 125-149. doi.org/10.1016/0378-3839(85)90002-X.
- DHI, 2017a. MIKE21 Boussinesq Waves Module: Scientific doc. Danish Hydraulic Institute.
- DHI, 2017b. MIKE21 Elliptic Mild-Slope module: Scientific doc. Danish Hydraulic Institute.
- Karambas T, Christopoulos S, Avgeris . (2010) HARBOUR_L: Integrated mathematical model for the design of harbor works. 5th Pan-Hellenic Conf. of Harbour Works, Athens, Greece.
- Karambas Th, Koutandos E, Kampanis N (2013) Numerical simulation of wave induced morphology evolution. *Maritime Engineering Journal*, 166 (3), 113 –124. doi.org/10.1680/maen.07.00008.
- Madsen PA, Schäffer HA, (1998) Higher-order Boussinesq-type equations for surface gravity waves: derivation and analysis. *Phil. Trans. R. Soc. Lond. A*, 356 (1749), 3123-3184. doi.org/10.1098/rsta.1998.0309.
- Metallinos AS, Klonaris GTh, Memos C.D, Dimas, AA (2019) Hydrodynamic conditions in a submerged porous breakwater. *Ocean Engineering*, 172, 712-725. doi.org/10.1016/j.oceaneng.2018.12.038.
- Vincent CL, Briggs MJ (1989) Refraction-diffraction of irregular waves over a mound. *Journal of Waterway, Port, Coastal and Ocean Engineering*, 115(2), 269-284. doi:10.1061/(ASCE)0733-950X(1989)115:2(269).

Simulating wave transmission in the lee side of a breakwater in spectral wave models due to overtopping

A. Papadimitriou^{1*}, M. Chondros¹, A. Metallinos¹, C. Memos^{1,2}

¹Scientia Maris, Agias Elenis, 10, 15772 Zografos, Greece

²Laboratory of Harbor Works, NTUA, 15780 Zografos, Greece

*Corresponding author: andreas_papad@yahoo.com

Abstract

Spectral wave models have experienced constant development and vast improvements over the past decades. They are continuously extended in order to model the complex wave transformation processes that are present in the coastal zone. Nevertheless, wave transmission due to overtopping has not been included properly yet. In the present paper a new methodology to include wave overtopping in spectral wave models is presented. The methodology consists of executing sequential simulations at small time step intervals and whenever wave overtopping occurs in a breakwater, waves are generated and transmitted behind the structure. This is achieved by modifying the boundary condition at the lee of a coastal structure to account wave generation due to overtopping. The above methodology was implemented in the open source wave model TOMAWAC with satisfactory results, however it can be generalized and applied in any available third generation spectral wave models.

Keywords Wave overtopping, Spectral wave model, Overtopping in breakwaters, Wave generation.

1 INTRODUCTION

Over the last thirty years, models based on the spectral wave action balance equation (WAE) such as WAM (WAMDI Group 1988), TOMAWAC (Benoit et al. 1996), SWAN (Booij et al. 1999), and WAVEWATCH III® (Tolman 2002) have gained widespread usage, almost pushing out energy conserving methods based on ray tracing (O'Reilly and Guza 1993) or phase-resolving models based on the mild slope equation (Berkhoff 1972), the latter being now confined to harbor agitation applications. The biggest advantage of the spectral wave models concerns the low computational resources required for the model execution and the unconditional stability of the numerical schemes used to solve the WAE equation. Despite numerous advancements over the last decades, spectral wave models seem rather incapable of simulating the complex hydrodynamic processes that are dominant in the nearshore area, such as wave diffraction, reflection, wave overtopping etc. In the present paper a parametric methodology to incorporate wave transmission due to wave overtopping occurring in a rubble mound breakwater is proposed. The methodology is based on calculating the wave transmission coefficient and simulating the resulting wave generation and propagation at the lee side of the structure (i.e. breakwater), in case overtopping occurs.

2 WAVE TRANSMISSION DUE TO OVERTOPPING ON A SLOPING BREAKWATER

Breakwaters designed for coastal protection may have a reduced crest elevation that allows large overtopping volumes. This volume will plunge into the water that is present on the lee side of the structure and generate waves. However, in case the breakwater is designated to protect a harbor from wind waves, overtopping can cause agitations inside the basin and disturb the harbor tranquility. This process is called wave transmission and is defined by the wave transmission coefficient:

$$k_t = \frac{H_{m0,t}}{H_{m0,i}} \quad (1)$$

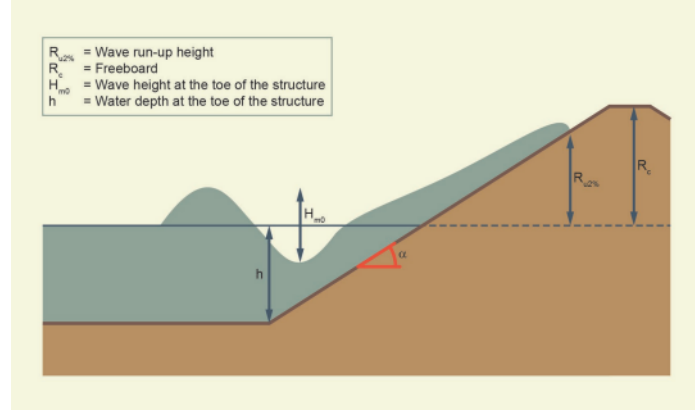
Where $H_{m0,i}$ is the incident significant wave height at the toe of the structure, and $H_{m0,t}$ is the transmitted significant wave height.

For smooth sloping structures, the following prediction formula was derived in the European DELOS project (EurOtop Manual 2018):

$$k_t = \left\{ -0.3 \frac{R_c}{H_{m0,i}} + 0.75 [1 - \exp(-\xi_{op})] \right\} (\cos\beta)^{2/3} \quad (2)$$

Where R_c is the crest freeboard height, ξ_{op} the breaker parameter in deep water and β the angle of wave attack.

Generally, for a low-crested sloping structure, overtopping occurs if the wave run-up height ($R_{u2\%}$), defined as the vertical difference between the highest point of wave run-up exceeded by only 2% of the waves, and the still water level (SWL) as shown in Figure 1 exceeds the crest freeboard height.



12. Figure 6 Definition of wave run up height and geometry of a smooth sloping structure

The wave run-up height for an assessment approach is given by the following formula (EurOtop Manual 2018):

$$\frac{R_{u2\%}}{H_{m0,i}} = 1.65 \gamma_b \gamma_f \gamma_\beta \xi_{m-1,0} \quad (3)$$

In the above equation γ_b is the influence factor for a berm, γ_f is the influence factor for roughness elements on a slope, γ_β is the influence factor for oblique wave attack and $\xi_{m-1,0}$ is the surf similarity parameter at the toe of the structure, based on the energy period.

Utilizing the above formulas, knowing the incident wave characteristics at the toe of the breakwater and the geometry of the structure one can calculate the transmitted wave height due to overtopping in the lee side of the breakwater.

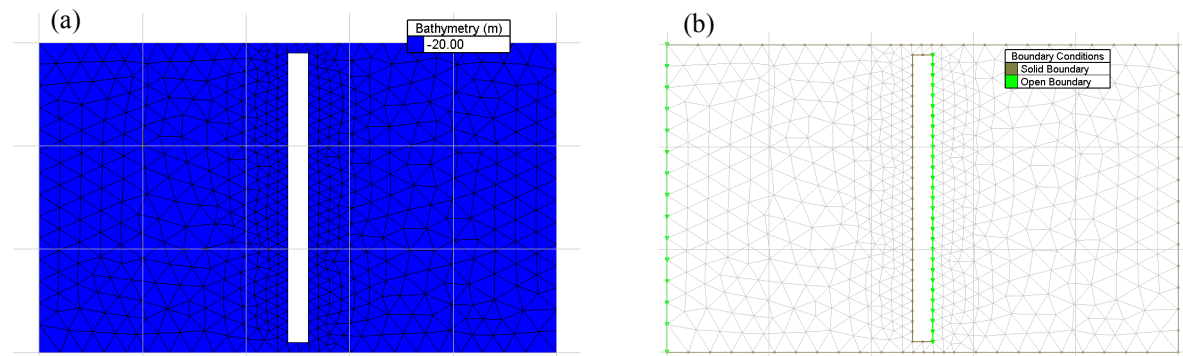
3 METHODOLOGY TO CALCULATE WAVE OVERTOPPING

A pilot implementation of the proposed methodology to calculate wave transmission due to overtopping in a rubble mound breakwater utilizing the TOMAWAC spectral wave model will be presented in this chapter. The methodology can be extended further and be implemented for various types of coastal structures, with simple modifications of the equations (2) and (3) to accommodate the different geometries of the coastal structures considered.

3.1 Model setup

A hypothetical wave basin, 100 m long and 60 m wide was constructed numerically to be used in the case study for the implementation of wave overtopping in the TOMAWAC wave model. About 48 m from the eastern boundary a breakwater 4 m wide and 56 m long is placed. The breakwater was sufficiently long in relation to the basin's width in order to minimize the diffraction effects. The breakwater therefore acts as a dam to the wave propagation and in such a case the only wave agitations behind the structure are expected to be caused by overtopping. The offshore wave generation boundary is located at the west side of the mesh. The novelty of the proposed approach is that the lee side of the breakwater is considered an open boundary as well, with wave generation only in the case overtopping occurs. The triangular mesh consists of elements with mean nominal length of 3.50 m. The mesh is more refined in the area around the structure to achieve a more accurate representation of the wave transmission behind the structure. The unstructured mesh, along with the applied boundary

conditions are shown in Figure 2.



13. Figure 7 (a) Unstructured bathymetric mesh (b) considered boundary conditions (green for open boundary, grey for solid wall)

3.2 Calculation procedure

The proposed methodology is based on the principle of executing sequential simulations with the TOMAWAC wave model, for a small time increment, and each time wave overtopping occurs, the boundary at the lee side of the structure (which was considered an open boundary with zero wave energy entering the domain until that time step) is modified, and wave generation occurs from this boundary with wave characteristics equal to those of the transmitted wave height due to overtopping. After each discrete simulation is completed, the wave energy spectrum is saved in order to be used to re-initialize the spectrum for the next simulation (hotstart).

The algorithm and methodology procedure is described below.

- 1) Creation of the unstructured mesh and the boundary conditions as shown in Figure 2
- 2) Extraction of the closest nodes' ID windward the breakwater and the wave generation nodes' ID at the lee side of the breakwater
- 3) Specification of geometrical parameters of the structure (such as crest freeboard height)
- 4) Specification of the maximum number of iterations (N_{max}) and the current iteration number (N), with $N=0$ initially
- 5) Increase of the number of iterations by one, $N=N+1$
- 6) Execution of the N th simulation of wave propagation with an adequately small time step to better capture the overtopping effect
- 7) Along with the simulation completion the wave energy spectrum is saved to reinitialize the simulation for the next time increment
- 8) Extraction of the values of H_{mo} , T_p , Mean Wave Direction at the windward nodes specified at step 2 for the end time step of the simulation
- 9) Calculation of wave run-up height at the windward side of the breakwater using equation (3)
- 10) In case wave run-up height exceeds the specified crest freeboard height, overtopping occurs and the transmission coefficient is calculated from equation (2), whereas transmitted wave height is calculated from equation (1) for the nodes at the lee side of the breakwater
- 11) Modification of the boundary conditions in order to assign the calculated wave characteristics at the nodes of the lee side of the breakwater
- 12) Generation of waves from the boundary described in step 11 in the case of wave overtopping.
- 13) In case $N < N_{max}$, return at step 5 using the previously saved spectrum at step 7 as initial conditions. If $N = N_{max}$ proceed at step 14
- 14) Concatenation of the 2-D results of the wave height distribution of the discrete simulations in one file. The total simulation time is $N_{max} * \Delta t$

The proposed methodology is generic and can be implemented in any spectral wave model, by modifying the boundary conditions in a similar manner and calculating the wave transmission coefficient due to wave overtopping.

For the hypothetical case presented in section 3.1 two different simulations were performed, the first one was the “do nothing” scenario, where no overtopping was considered, while the second

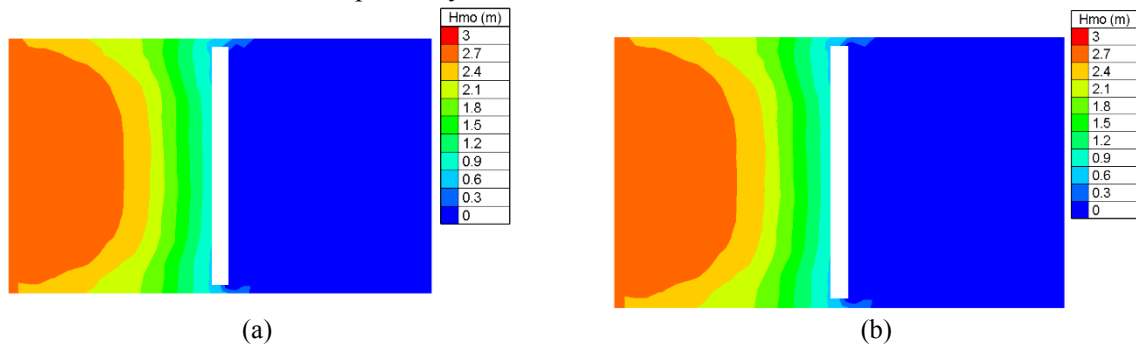
simulation was executed with the proposed methodology and the required modifications in the algorithm. General simulation parameters and incident wave characteristics are displayed in Table 1.

14. Table 1 Simulation parameters and wave characteristics at the offshore boundary for the idealized test case

	Overtopping	Δt (s)	Total time (s)	Crest freeboard height (m)	H_{mo} (m)	T_p (s)	MWD(from) ($^\circ$)
Simulation 0	NO	2.0	40.0	0.6	3.0	6.0	270.0
Simulation 1	YES	2.0	40.0	0.6	3.0	6.0	270.0

4 RESULTS AND DISCUSSION

The obtained results concern maps of the computed significant wave height for the whole computational domain. For the breakwater considered in the idealized test case and the incident wave characteristics at the offshore western boundary, all influence factors that are present in the calculation of wave run-up in equation 3 where set equal to 1. In Figures 3, 4, 5 and 6, snapshots of the calculated spatial distribution of wave height for both Simulation 0 and Simulation 1 are shown for a total time of 8.0 s, 14.0 s, 28.0 s and 40.0 s respectively.



15. Figure 8 Snapshots of computed significant wave height distribution at $T=8.0$ s a) for Simulation 0 b) for Simulation 1

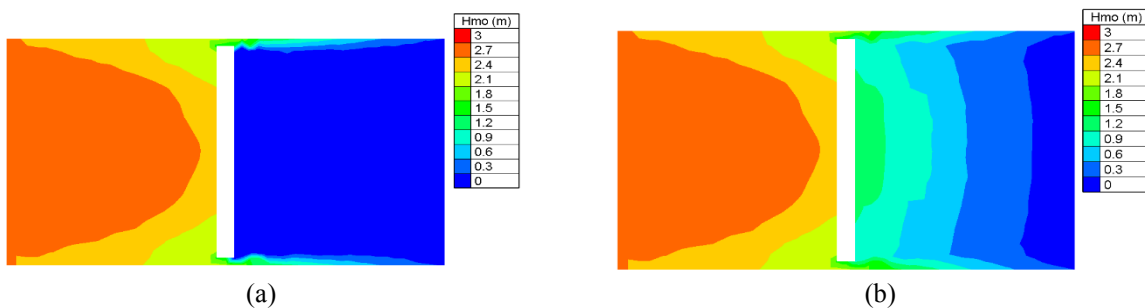


Figure 9 Snapshots of computed significant wave height distribution at $T=14.0$ s a) for Simulation 0 b) for Simulation 1

16. Observing the above snapshots, for the Simulation 0 case, no wave agitation is observed behind the structure since wave overtopping is not taken into account. The only computed significant wave height at the computational domain behind the breakwater can be attributed to the sheltering effect due to the structure's presence, which is minimal due to the relatively large length of the structure in relation to the basin's width. On the other hand, for the Simulation 1 case, excluding the distribution shown in Figure 3, wave transmission due to overtopping occurs at the lee side of the breakwater, since the computed wave run-up heights for the windward nodes exceed the relatively low crest elevation of the structure. Wave transmission coefficients for this test case range from 0.3 to 0.55 depending on the values of the incident significant wave height at the structure's toe. Additionally, wave run-up values are calculated at every time step, and in case wave run-up height is smaller than the crest freeboard height then the transmitted wave height is set to 0.0. This is the case shown in

Figure 3, where the incident wave height is not adequate to produce wave run-up height that exceeds the crest elevation of the structure, therefore no wave generation occurs at the lee boundary's nodes. Considering the above, the structure of the algorithm allows to use time and spatially non homogenous boundary conditions at the offshore boundary and calculate overtopping at each node independently.

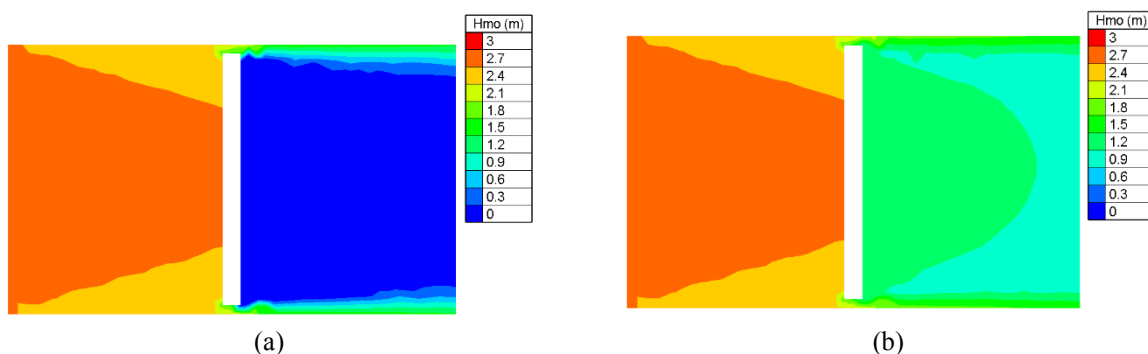
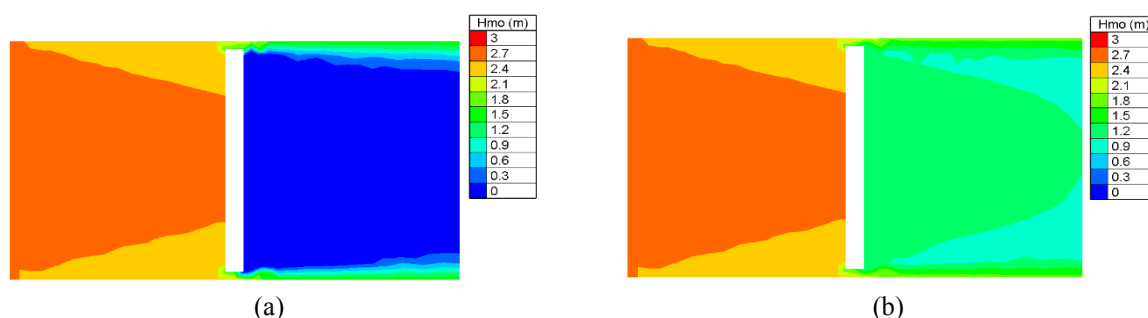


Figure 10 Snapshots of computed significant wave height distribution at $T=28.0$ s a) for Simulation 0 b) for Simulation 1



17. Figure 6 Snapshots of computed significant wave height distribution at $T=40.0$ s a) for Simulation 0 b) for Simulation 1

The methodology proposed in the present paper for the inclusion of wave overtopping in spectral wave models can be a valuable asset for engineers in order to simulate the effect of wave overtopping in various studies ranging from coastal protection or propagation of dam-break waves. This approach is not intended to push out the use of phase-resolving models for harbor agitation studies, but rather improve the performance and accuracy of phase-averaged models that are used for a large number of applications concerning wave propagation in the coastal zone.

References

- Benoit M, Marcos F, Becq F (1996) Development of a third generation shallow water wave model with unstructured spatial meshing. Paper presented at the 25th International Conference on Coastal Engineering, Orlando, USA.
- Berkhoff JCW (1972) Computation of combined refraction-diffraction. Paper presented at the 13th International Conference on Coastal Engineering, Vancouver, Canada.
- Booij N, Ris RC, Holthuijsen LH (1999) A third-generation wave model for coastal regions. 1. model description and validation. *J Geophys Res* 104(C4):7649–7666.
- EurOtop (2018) Manual on wave overtopping of sea defences and related structures. Van der Meer JW, Allsop NWH, Bruce T, De Rouck J, Kortenhaus A, Pullen T, Schüttrumpf H, Troch P, Zanuttigh B.
- O'Reilly WC, Guza RT (1991) Comparison of spectral refraction and diffraction wave models. *J of Waterway, Port Coast Ocean Eng* 117(3):199–215. doi: 10.1016/0378-3839(93)90032-4
- Tolman HL (2002) User manual and system documentation of WAVEWATCHIII version 2.22. Technical Note, U.S. Dept. of Commerce.
- WAMDI Group (1988) The WAM model - a third generation ocean wave prediction model. *J Phys Oceanogr* 18:1775–1810. doi:10.1175/1520-0485(1988)018.

Ship approach and mooring design studies using advanced simulation software

K. Spyropoulos^{1,*}, P. Sartampakos², A. Pritsivelis³

¹Maritime Civil Engineer, MSc, NIREAS Engineering, Athens, 176 73, Greece

²Senior Surveyor, NIREAS Engineering, Athens, 176 73, Greece

³Civil Engineer, MSc, NIREAS Engineering, Athens, 176 73, Greece

*Corresponding author: ksspyr@gmail.com

Abstract

The advance of simulation software provides useful tools for the analysis of the ship approach procedures and ship-infrastructure interaction. Hand calculation of the various applied methods described in several design recommendations, is difficult and time consuming. And the results of such hand calculations are only approximations. This paper refers to advantages provided by adopting the relevant software.

Keywords Navigation, Mooring, Simulation.

1 SHIP APPROACH

Available software is designed to simulate single or multiple ship dynamics in restricted water, taking into consideration wind, waves, currents, and possible obstacles. The user should input general topography, channel configuration, and environmental conditions. The software uses a simulator to generate probable ship tracks to evaluate harbor safety and estimate the likelihood of collision for various types of vessels, traffic densities, navigation channels geometries and environmental conditions. It is used by harbor designers and port managers for structures and waterway design, modification, improvement and implementation of safety measures.

The simulator is based on the knowledge of ship dynamics. Comprehensive models for ship dynamics under cruising and maneuvering conditions are implemented. It must incorporate a large variety of options to simulate vehicles (large ships and small boats), with different engine types, weather and sea conditions, and land and coastal configurations. Some of the navigation code rules have been implemented for allowing auto piloting of multiple ships in the computer-controlled mode.

The simulator employs modular mathematical models for the various components of the ship (hull, propeller(s), rudder(s), and thrusters) and environmental effects (wind, current, waves) and waterway (bottom, pier walls) to achieve a sophisticated mathematical model for the ship. The models are based on collective experience resulting from development of many simulators.

The simulator can be used for the following applications:

- Traffic safety evaluation in harbors
- Safety study of vessel types, traffic densities, waterway geometries
- Harbor structures design
- Navigation channels design
- Port traffic planning
- Marine/navigation regulation development
- Tug operation optimization

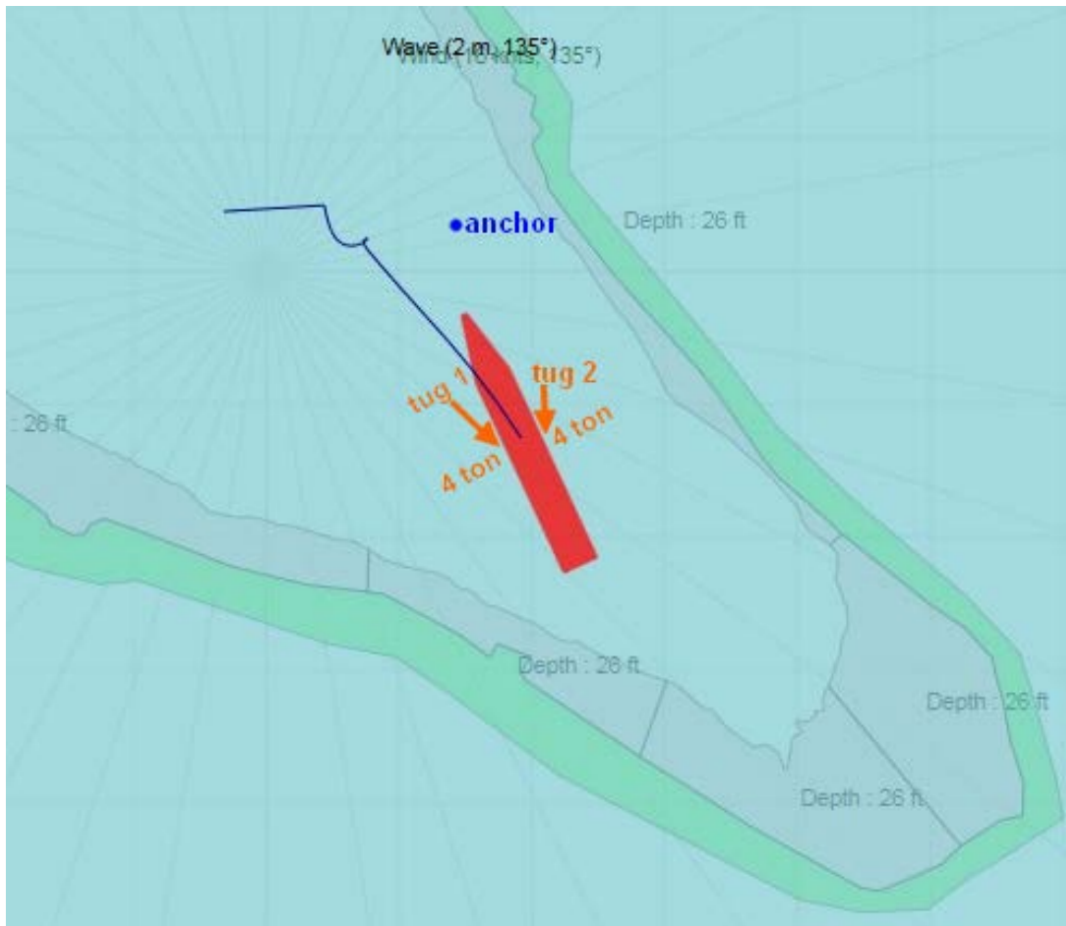


Figure 1 Tanker maneuvering within a narrow bay

2 MOORING DESIGN SOFTWARE

The software must be based on international recommendations and procedures such as OCIMF including wind and current coefficients for tanker moorings.

A port designer will be able to plan a vessel's mooring arrangement and to assess the adequacy of a terminal's mooring facilities and to manage the mooring while at the berth.

At terminals, available software can be used to assess the adequacy of vessel mooring equipment for the terminal mooring arrangement. The need for and effectiveness of auxiliary mooring lines can be judged. Wind or current limitations can otherwise be imposed. On vessel, it can be used to plan mooring arrangements in advance. Time will then be saved in deploying lines to the proper mooring points. At the mooring, it can be used in real- or fast-time mode to anticipate line tending requirements.

Key Features of available software should include

- All types of inshore and offshore ship moorings
- Shielding effect of piers
- In-built OCIMF methods and coefficients
- Time related analyses to account for vessel draft (loading) and tide level changes
- Auto generation of wind or wave capability rosette
- Fixed piers with catenary anchored buoys
- Side by side mooring

The basic simulator configuration should allow for quayside moorings at piers, jetties and sea islands

Additionally, the simulator may be built with added capability to include spread moorings with buoys and catenary chains (Catenary effects in chains included from both ship and anchor to buoy, catenary effects in wires included for CBM's, buoys allowed in pierside moorings.).

In case of a dynamic simulation vessel hydrodynamics with time varying wind and current can be used. The user can input other time dependent forces such as wave drift. The dynamic force and response of passing ships can also be calculated.

The Wave Response Module calculates the vessel response to first-order wave effects taking shallow water and solid wall effects into account. The changing line load due to vessel motion at each fairlead is calculated.

Finally a second ship can be added to any mooring type, pierside, turret, host at bow anchor, etc.

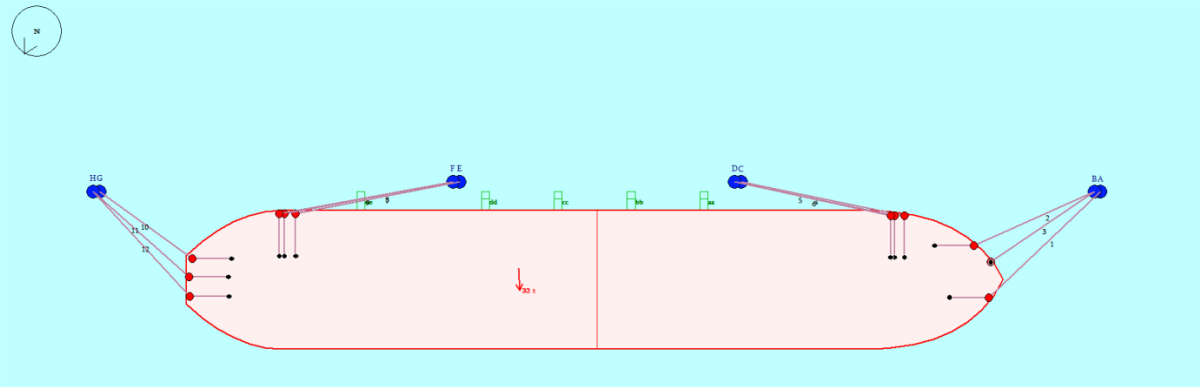


Figure 2 Mooring Simulation of LPG Carrier



Sub session 1.2: Port Planning

Physical factors contributing to the selection of a port location. The case of the port of Alexandroupolis.

A. Karditsa^{1*}, S.E. Poulos¹, P. Sartabakos²

¹Department of Geology & Geoenvironment, National & Kapodistrian University of Athens, Athens, Greece

²Nireas Engineering, Skra Str. 1-3, Kalithea, 17673, Athens, Greece

*Corresponding author: kkarditsa@geol.uoa.gr

Abstract

Physio-geographical factors play an important role in the selection of the appropriate site for a port location. The port of Alexandroupolis, started operating in the middle 1870s as a small fishing shelter, and is currently aspired to act as a major port in the Eastern Mediterranean region regarding tourism and commerce. The present contribution investigates the properness of its location, regarding physio-geographical setting, hydrodynamic and sedimentological features. The results show that the position of the port is rather problematic considering the shallow bathymetry and the hydrodynamic capability to rework seabed fine sediments, along with the supply of suspended material by the R.Evros; these factors constitute both the entrance of the port and the constructed navigation channel vulnerable to siltation and inappropriate for large vessel shipping.

Keywords Navigation channel, Dredging, Hydrodynamic activity, Resuspension.

1 INTRODUCTION

The selection of a port location is dependent on many factors which vary widely (e.g. social, commercial, geographic etc.) and are interconnected (Agerschou et al., 2004). Among all, the importance of the physical factors of the location is undoubtedly important and is related to the physical protection, land availability for infrastructure and services, the hydrographic network and the presence of river systems, coastal underwater geomorphology, sedimentology and hydrodynamics. These physical features are being examined in the case of the Port of Alexandroupolis to investigate the properness of its location.

2 THE PORT OF ALEXANDROUPOLIS

2.1 Geographic setting

The port of Alexandroupolis is situated at the western edge of the Evros River delta, in the shallow waters of the extensive open continental shelf of the North Aegean Sea, where the isobath of 10 m is located at a distance of 3 km offshore. The port started operating in the middle of 1870 as a small fishing shelter. Since 1924, continuous expansions started taking place (Figure 1) with simultaneous upgrade of the terrestrial installations aiming to increase port's capacity in the Eastern Mediterranean region regarding tourism (cruise ships, recreational craft) and commerce and, more importantly, the sector of combined transport.

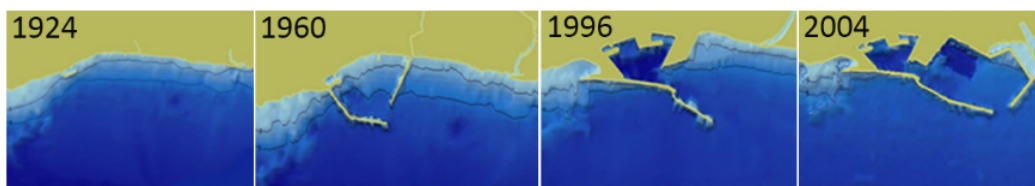


Figure 1 Map series of the Alexandroupolis port evolution

Reclamation works in the port are active up to date with excavation works at both the port basin and the navigational channel, which extend eventually at a distance of 4 km, in order to deepen the latter up to 14 m depth.

2.2 Hydrodynamic and sedimentological setting

The hydrodynamics of the area is mainly defined by the wave regime, as the astronomical tide is lower than 20 cm, whilst, sea level rise due to meteorological tide may reach 0.8 m (HNHS, 2005). Therefore, the port area is exposed to SW, S and SE wind-induced waves, with the SW waves being the most frequent (4.8%) on an annual basis, presenting the maximum wave conditions (Table 1).

Nearshore wave conditions (wave breaking height (H_b), wave direction (a_b), depth (d_b) and wave velocity (u_b) at breaking) induced by the aforementioned offshore wave regime, calculated with respect to the mean annual frequency of occurrence and the maximum wave conditions are presented in Table 2 (after Karditsa et al., 2013).

Table 1 Wave characteristics in the Alexandroupolis Gulf

	Wind Direction	f (%)	T_p (sec)	H_s (m)	L(m)	P (10^2 W/m)
MOST FREQUENT WAVES	SW	4.8	3.49	0.44	19.04	6.36
	S	1.8	3.78	0.53	22.32	3.71
	SE	0.8	1.82	0.12	5.16	0.40
MAXIMUM VALUES	SW	0.015	11.29	6.28	198.84	15.44
	S	0.005	7.86	4.83	96.38	1.80
	SE	0.002	6.87	3.22	73.63	0.28

Granulometrically, seabed sediments present a zonal distribution pattern, sub-parallel to the depth contouring. Thus, nearshore sediments (<10m depths) consist of sand (S, zS), while the zone extending from the 10 m to the 30 m isobaths is dominated by muddy (M, sM) sediment. A secondary zone enriched in silty material (Z, sZ) is extended within the muddy sediments, in water depths between 10 m and 20 m. The offshore sediments in water depths >30m, are classified as muddy sands (mS) (Karditsa et al., 2013), representing the transgression to the relict sandy deposits appeared in water depths > 40m (Pehlivanoglou et al., 2000) (Figure 2a). This zonal spatial distribution is closely related to wave induced hydrodynamic characteristics. Thus, seaward limit of nearshore sandy zone coincides with the breaking depth related to the highest incoming SW waves, whilst, closure depth (for maximum wave conditions) and the commencement of the intermediate zone of wave propagation (for the average wave conditions), generally, coincide with the shoreward limit of the silty zone lying in between 10 m and 20 m of water depth.

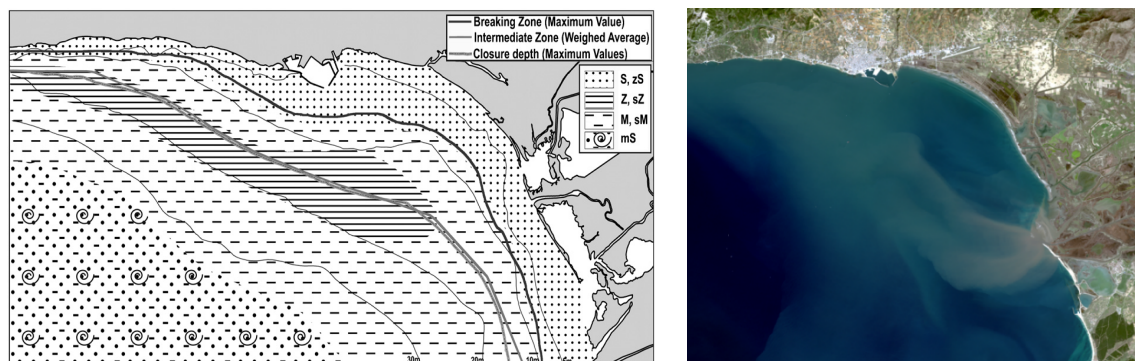


Figure 2 (a) Seabed sedimentology in the gulf of Alexandroupolis and (b) Evros plume dispersion under southerly directed winds

In addition, the gulf of Alexandroupolis receives suspended sediment provided by the westward dispersion of the Evros River plume, especially under the influence of SW and S directed winds (Figure 2b).

3 METHODOLOGICAL APPROACH

Wave data (offshore significant wave height (H_s) and wave period (T)) along with the nearshore hydrodynamic characteristics (wave breaking height (H_b), wave direction (a_b) at breaking, depth (d_b) and wave velocity (u_b) at breaking) were calculated with the use of the prognostic equations of CERC (1984) utilising the wind data obtained by the nearby airport's weather station, installed by the Hellenic National Meteorological Service (period 1951-2002).

The total wave energy flux (P) was calculated by the Eq. 1 (Komar, 1998): $P = E C_g$ (1)

where, $C_g = C_o/2$ (for deep water conditions) and C_o is wave velocity ($=1.56 T$) and E is the total wave energy given by the Eq. 2 (Komar, 1998): $E = 1/8 \rho g H_s^2$ (2)

where, ρ is sea water density, $g (=9.81 \text{ m/sec}^2)$ and H_s is significant wave height.

The seaward limit of wave impact upon the nearshore seabed sediment is given by the closure depth (h_c), during storm conditions (Hallermeier, 1981):

$$h_c = 2,28 H_e - 68,5 \left(\frac{H_e^2}{g T_e^2} \right) \quad (3)$$

where, H_e is the maximum (extreme) wave height before breaking and T_e is the extreme wave period.

The capability of near-bed flow to initiate resuspension of the bottom sediments was investigated with the use of the Shield's criterion of motion (θ), which is given mathematically by the Eq. 4:

$$\theta = \tau / [(\sigma - \rho) \cdot g \cdot d] \quad (4)$$

where, (τ) is the shear stress (see below), σ is the density of the sediment ($=2650 \text{ kgr/m}^3$), ρ is the density of sea water, $g (=9.81 \text{ m/sec}^2)$ and, d is the mean grain size of the sediment samples.

Shear stress (τ) induced by wave activity is calculated using the Eq 4: $\tau_w = 1/2 \rho f_w U_w^2$ (5)

where, f_w is wave friction factor and U_w is water orbital velocity. Wave friction (f_w) is given by Soulsby's (1997) Eq. 6: $f_w = 1.39 (A/z_o)^{-0.52}$ (6)

where, z_o is the hydraulic roughness length depending on two cases; (i) sediment skin friction (z_{osf}) calculated based on grain size (d_{50}) according to the Eq.7: $z_{osf} = k_s/30$, where $k_s = d_{50} 2.5$ (7)

and (ii) bedforms drag i.e. the presence of bed forms (ripples) which was set at $z_o = 0.01 \text{ m}$ (Sternberg, 1968). Near-bed orbital velocity is calculated using the Eq.8: $U_w = \pi H_s / T \sinh(k d)$ (8)

where, H and T are the significant wave height and period, respectively, k (wave number) $= 2\pi/L$; (L is the wave length) and d is the water depth.

4 THE IMPACT OF EXTREME EVENTS ON THE PORT OF ALEXANDROUPOLIS

During February 2015 extended dredging works had been taking place in the port of Alexandroupolis in order to deepen the navigation channel of the port up to 30% of its natural depth i.e. from 7-8 m natural depth to 12 m depth. The navigation channel following a SSE direction extends 4 km offshore. Dredging works started in October 2014 and in January 2015 had been completed up to 50% of the initial planning. Nevertheless, in February 2014 strong winds of South directions took place with velocities in the order of 15-33 knots (8-17 m/s), and bursts of 34-40 knots (17-20 m/s), lasting for more than 36 hours. The wind-induced south waves reached the 3.6 m height (H_s) and 7.2 s period (T_s). In Table 2, the calculated hydrodynamic – morphodynamic parameters (i.e. wave breaking height (H_b), depth (d_b) and wave velocity at breaking (u_b)) are presented. In addition, longshore transport induced by south waves is expected to follow a westward direction at both (west and east) sides of the

port, with respect to coastline orientation (Figure 3). Moreover, the result of the calculations regarding the capability of the incoming waves to initiate resuspension of the bottom sediments (Table 3) show that all shelf sediments could have been subjected to resuspension during this storm event.

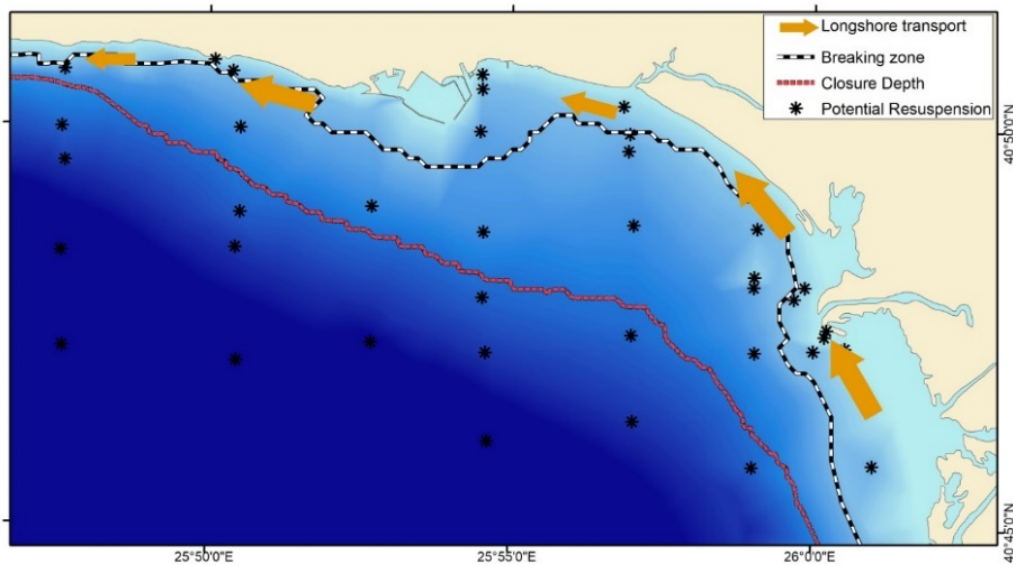


Figure 3 Schematic presentation of longshore transport direction, position of breaking zone and closure depth and positions of examined sediment's potential resuspension under extreme south wave activity

Table 2 Water depths of breaking (d_b) and depth of closure (d_c) together with the corresponding significant wave heights

Breaking Zone		Closure depth zone	
Depth (d_b , m)	Wave height (H_b , m)	Depth (d_c , m)	Wave height (H_s , m)
4.8	3.8	6.4	3.5

Table 3 Calculation of the capability of near-bed flow to initiate resuspension of the bottom sediments

		τ_w	θ	θ_{cr}
Sediment skin friction (z_{osf})	$d_{50}=0.019\text{mm}$	1.26	1.32	0.1
Bed forms drag (z_{osd})	$z_0=0.01\text{m}$	5.98	6.26	

Moreover, storm surge that exceeded +0,4 m (gauge station of Alexandroupolis port, HNHS), in combination with coastal geomorphology (i.e. shallow shelf, sheltered to the north and northeast) led to the initiation of a south-southwestward directed underflow which contributed not only to seabed sediment reworking but also to the removal and transfer of the resuspended sediments.

As a consequence, the storm event of February 2015 is related to the immediate filling of the dredged navigation channel during which channel depths turned from 13 m to 9 m, when the surrounding natural depths are ~ 7.5 m. Intersections in Figure 4 provide an indicative example of the sequence of dredging and infilling of the navigation channel close by to port entrance. More specifically, November 2014 corresponds to the initiation of dredging, January 2015 the completion of dredging actions in navigation channel in the area close to the port entrance and February 2015 the infilling after the storm event.

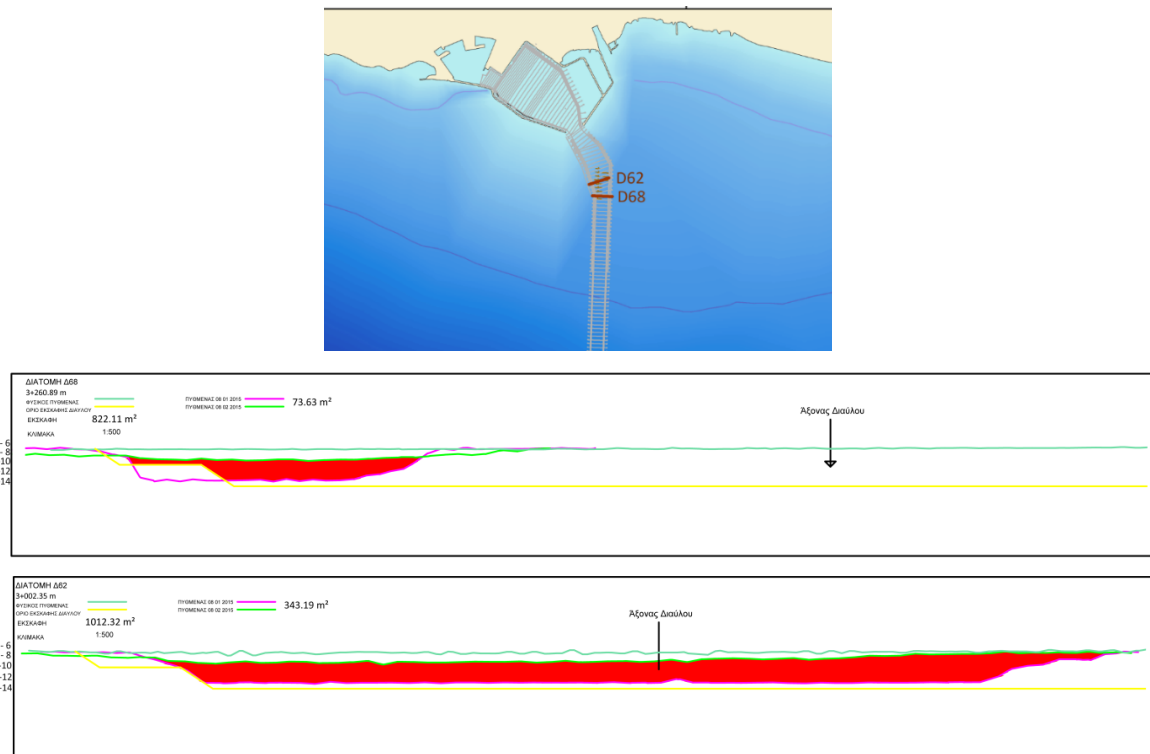


Figure 4 Indicative intersections in the navigation channels representing natural depths (green), and depths during January 2015 (pink) and February 2015 (light green)

5 CONCLUSION

The position of the port of Alexandroupolis is assessed to be problematic, based on the geomorphological, sedimentological and oceanographic characteristics of the area. The port is associated with a rather shallow, smooth and fine-grained seabed, with the 12 m isobath being at a distance of >3 km far from its entrance; the latter means that an artificially dredged navigational channel is required for large merchant shipping. However, the hydrodynamic (wave) ability to resuspend fine grained seabed material, along with the supply of suspended (fine grained) material by the Evros River, and the overall oceanographic setting, constitute both the area nearby to port entrance and the constructed navigation channel, vulnerable to siltation.

References

- Agerschou H, Dand I, Ernst T, Ghoo H, Jensen OJ, Korsgaard J, Land JM, McKay T, Oumeraci H, Petersen JB, Runge- Schmidt L, Svendsen HL (2004) Planning and Design of Ports and Marine Terminals.
- CERC (1984) Shore Protection Manual. Coastal Engineering Research Center, Waterway Experimental Station. U.S. Corp of Engineers.
- Hallermeier RJ (1981) A profile zonation for seasonal sand beaches from wave climate. *Journal of Coastal Engineering*, 4: 253-277.
- HNHS (Hellenic National Hydrographic Service) (2005) Tidal data from Greek Ports. Hydrographic Service, Hellenic Army Navy, Athens, 94 p.
- Karditsa A, Poulos SE (2013) Sedimentological investigations in a river-influenced tideless coastal embayment: The case of inner continental shelf of the Aegean Sea. *Cont. Shelf Res.* 55, 86–96.
- Komar PD (1998) *Beach Processes and Sedimentation*, Prentice Hall, New Jersey.
- Pehlivanoglou K, Tsirambides A, Trontsios G (2000) Origin and Distribution of Clay Minerals in the Alexandroupolis Gulf, Aegean Sea, Greece. *Estuar. Coast. Shelf Sci.* 51, 61-73.
- Stenberg RW (1968) Friction factors in tidal channels with differing bed roughness. *Marine Geology*, 6, 243-260.
- Soulsby RL (1997) *Dynamics of the marine sands*, Thomas Telford Publishing, 245pp.

Site investigation guidelines for planning, designing and constructing harbours: Experience gained from Greek harbour construction.

G. Ferentinos*, G. Papatheodorou, D. Christodoulou, E. Fakiris, X. Dimas, N. Georgiou

Laboratory of Marine Geology & Physical Oceanography, Geology Dept., Patras University.

*Corresponding author gferen@upatras.gr

Abstract

Experience gained over the years by harbour engineers has shown that the knowledge of the seafloor bathymetry and geology as well as the presence of geo-hazards on harbour project sites is a pre-requisite for the safe planning, design and construction of harbours. This paper focuses on and discusses case studies of maritime infrastructures in Greece, which were planned and designed without fully complying with worldwide adopted guidelines for site investigation studies. The lacking of knowledge in the prevailing seafloor bathymetry and geology as well as the presence of geo-hazards during the planning and design phase showed that the final cost of most of these constructions was much higher than originally estimated, some finished much later than the estimated date and others failed to meet the initial design. The above suggests that the study of the above mentioned using state of the art marine geophysical surveying technologies are necessary for the successful planning, design and construction of harbours.

Keywords Marine geophysical surveying, Seafloor bathymetry, Offshore geology, Geo-hazards.

1 INTRODUCTION

The frequent worldwide failure in foreseeing the effects of geological hazards on maritime infrastructures over the last century has put pressure on scientists and engineers to possess complete overview of the geological conditions and hazards prevailing on the site that may impose construction and/or operation constraints on the infrastructure. This paper focuses on and discusses case studies of maritime infrastructures in Greece (Fig 1), which were planned and designed without fully complying with worldwide adopted guidelines for site investigation studies, aiming at highlighting that the study of the geological conditions prevailing on the site, with state of the art strategies, is a pre-requisite for the efficient plan and design of maritime structures (Murphy et al., 2010; Kevin-Smith et al. 2010; Tarata et al., 2005). Furthermore, based on these case studies, the paper proposes a set of surveying strategies for acquiring an overview of the above-mentioned conditions, which may impose constraints on the construction and operation of such infrastructures.

Here, five cases of marine structures that were planned and designed in the late 1990's and constructed in the past two decades, are examined (Fig. 1). The New Patras Harbour, the New Aigion Harbour, the Katakolo Port and the Alexandroupolis Harbour and navigation channel dredging. In most of these cases the cost of construction was much higher than originally estimated and the infrastructure was completed much later than the planned schedule. The laboratory of Marine Geology and Physical Oceanography was involved in these projects after complains by the contractors to the public authorities supervising the projects, that there were discrepancies regarding the prevailing on the site conditions ie bathymetry, sediment composition, sediment thickness etc, given in the master plan and those, that the contractor meets in the site during the construction works.

2 CASE STUDIES

2.1 *New Patras Harbour*

Patras is the 3rd largest city in Greece with a population of around 200,000 and its harbour is the gateway to Italy and Western Europe (Fig. 1). The continuous increase in marine transport in the 80's led the central government to decide on the construction of a new harbour about 1km south of the existing one. The New Patras Harbour project started in 1993. According to the Master Plan the

harbour would have cost about 120.106 Euros, to be built in 3 phases and finished in 2004 (ADK. S.A. and Triton Inc., 1994). The harbour would have comprised a 2.8 km quay and a 2.5 km breakwater parallel to the coast and would have accommodated the simultaneous berthing of 12 ferries and Ro-Ro vessels. However, none of the above mentioned materialized. The first two harbour phases finished in 2011, that is 7 years later than scheduled, and the 3rd phase is pending with the cost almost doubled, the quay length is 1,000m with five docking stations and the breakwater length is 1,500m. All the above-mentioned changes to the master plan were the result of the poor master plan study. The site investigation, on which the planning and design of the New Harbour was based, was limited to bathymetric and geotechnical engineering studies but didn't include the use of worldwide high resolution bathymetric and marine geophysical surveys, which are pertinent to harbour engineering. These changes increased tremendously the original estimated cost of the harbor and delayed the schedule of the harbor operation starting time.

The data used in the master plan for the planning and design of the harbour was based on the study of bathymetry and of the physical and mechanical behavior of the sediments on the seabed under static and cyclic loading. The bathymetric map on the site was based on charts provided by the Hydrographic Department, which are suitable for navigation purposes, supplemented by lead sounding (ADK A.S. and Triton Inc., 1944). The geotechnical study of the sediments included bore-holes, sampling and laboratory tests as well as in-situ measurements (ADK A.S. and Triton Inc., 1944). The contractor (Christiani & Nilsen and EMPEDOS S.A.) during the construction phase, found that the depth along the site, where the breakwater was supposed to have been built, was by about 5m deeper than the depth given in the bathymetric map provided in the master plan. The bathymetric and marine geophysical survey that followed in order to check the contractor's claims, showed that the depth in the site where the breakwater was planned to be built was indeed 5 m. deeper. Furthermore, the survey showed, that the seafloor on the site was covered by craters seeping methane with an average diameter and depth of about 50m and 20m, respectively. The survey also showed the presence of active faults crossing the harbour site and the presence of methane in the pores of the sediments (Hasiotis et al. 1995; Christodoulou et al. 2003) (Fig.1b). These findings had a colossal impact on the harbour design. The breakwater was moved nearer to the coastline resulting in a smaller size harbour basin, the number of simultaneous ship berthings was reduced from 12 to 5 and the scheduled starting date of the harbour was delayed by 5.5 years to 2011 instead of 2004. Furthermore, significant design changes mainly in the ground improvement measures and in the sequence of construction operation were made, in relation to the initially recommended design to enhance the stability and safe construction of the quay and the breakwater (Loukakis and Yegian 1998). These changes increased tremendously the original estimated harbour cost.

2.2 The Aigio New Harbour

Aigio town is situated in the Corinth Gulf in Greece and its population is around 25,000 (Fig. 1). In 1997 the central government decided on the construction of a new harbour about 800m to the north of the existing one, to meet the demands of the increasing traffic. The new harbour was planned to service ferries, cruise liners and RO-RO vessels. The New Aigio Harbour consists of a rectangular quay built on reclaimed land with a length along the seafront of 265m and a width of 60m (Rogan and Associates, 1997). The site investigations carried out for the planning and design of the harbour were limited to bathymetric and geotechnical engineering studies but did not include high resolution bathymetric and marine geophysical surveying, used worldwide.

The on-site bathymetric map was based on an existing chart provided by the Hydrographic Department for navigation purposes and the seafloor was inspected by divers. The geotechnical study of the sediments included four bore-holes, sampling and laboratory tests as well as in-situ measurements for examining the mechanical behavior of the sediments on the seabed under static and cyclic loading (Gazetas, 1995). The contractor found during the construction, discrepancies in the bathymetry and in the geotechnical characterization of the surficial sediments given in the Master Plan. The high resolution bathymetry and marine geophysical survey which followed, was carried out after the excavation in the upper 2 m. of the surficial layer, the installation of 10 m. long stone columns and the construction of the first phase preloading embankment showed: (i) discrepancies in the bathymetry between the present high resolution bathymetric survey and the one carried out after

the excavation of the upper 2m in the surficial layer and the installation of the stone columns (ii) the presence of three parallel layers dipping downslope at an angle between 4 and 5% and the presence of methane in the sediments pores (Fig. 1c) and (iii) rotated slides affecting the upper layer in the seabed and the stability berm in the quay wall (Fig. 1c). Discrepancies of between 2 to 4m found in bathymetry along the zone, where the preloading embankment was placed, can be explained either by settlement of the seabed due to the consolidation effect caused by the construction of the preloading embankment and the pore water drainage through the stone columns or, at depth mistakes in the chart used. Furthermore, the marine geophysical surveying suggested that: (i) the Safety Factor determined for the slope stability of the proposed quay had to be recalculated because the slope gradient used for its calculation was different to that observed, (ii) the rate and magnitude of the expected sediment settlement had to be re-estimated and (iii) the stone column lengths had to be increased in order to penetrate the deeper layer.

2.3 Alexandroupolis Harbour and Navigation Channel Dredging

Alexandroupolis town is located in northwestern Greece and its population is around 50,000 (Fig. 1). The Alexandroupolis harbour is the 3rd largest in northern Greece and is considered the gateway to the Balkan and central Europe (Fig. 1d). The port comprises a small harbour about 280,000 m² in size, which is used as a marina and a larger outer one about 1x10 m², which can accommodate ferry-boats, general cargo and Ro-Ro vessels as well as tankers. At present the max. safe draft along the 1.7km quay varies from 4 to 10.5m whereas along the 3.5km navigation channel it is 7m. Since 2008 extensive dredging is going on to increase the safe draft in the harbour and in the entrance channel to 12 and 12.5m, respectively. The dredger type suggested for use in dredging the muddy sand sediments in the harbour basin was the suction dredger, in order to minimize the turbidity and confine the spread of the contaminant material within the basin. However, the dredger type chosen proved inefficient in dredging the muddy sand sediments in the harbour due to the presence of solid man-made debris in the sediments. Indeed, the marine geophysical survey, which was carried out detected a large number of solid man-made objects ranging from small size to ship anchors and chains lying on the seafloor and/or inter-bedded in the sediments.

2.4 Katakolo Port

The Katakolo Port lies on the western edge of the Peloponnesus peninsula in Greece. It is the gateway to Olympia, the birth place of the Olympic Games, and the Delphi Oracle, the Umbilicus of Earth. The port was built in 1857 for the transport of blackcurrants to Italy and Western Europe. The modern port was constructed in 1992 and about 250 cruise ships berth there every year. It is one of the busiest Greek ports for cruise ships. The port is comprised of a long and a short pier and a wharf in between with a total quay length of 700m. The long pier and the wharf can accommodate three cruise ships berthing alongside simultaneously. The maximum draft in the navigation channel is 6.1m and its width is 250m. The maximum draft along the cruise ships berths is 9.5 and 7m.

The site investigation for the port plan and design was based on existing bathymetric maps supplemented by lead soundings and the study of the geotechnical properties of the sediments on the seabed, together with a stability analysis of the seafloor-sediment interaction under static and cyclic loading. Local people witnessing in the past flames, emerging from the soil, (the most recent being in 1972) followed by an explosion in the vicinity of the port, (indicative of gas seepage from the soil) was not considered by the port authority as potential geological hazards, which could pose risk to the infrastructure, vessels or human life. Therefore, no further steps were taken to investigate gas seepage from the soil, nor were safety measures proposed.

Offshore geophysical and onshore geological/geochemical surveys which were carried out in 2003 and 2009 in and around the port within the ASSEM and HYPOX Project framework financed by E.U. (Etiopie et al. 2006) have shown that: (i) there are deep accumulations of natural gas migrating to the surface through fault zones, (ii) sediments in the port are gas charged, (iii) gas seeps from the seafloor and gas bubbles rise into the water column, (iv) gas seeps through vents on land causing cracks across the asphalt quay pavement beside the customs office, the duty free and the car park areas and (v) the gas is a mixture of methane and hydrosulfide, (vi) gas fluxes range from 5,600 to 165,000 mg.m⁻².d⁻¹ with the methane content in the air at about 50cm above the seeping vents being between 5 and 10%

and the hydrosulfide levels between 102 and 103 ppmv. These methane and hydrosulfide concentration levels in the air are considered as human hazards because they are potentially toxic when inhaled and inflammable, respectively (Etiopie et al., 2006). In addition, the presence of gas in the sediment pores reduces the shear strength of the sediments leading to loss in their bearing capacity. However, all these years the piers and the wharf have been affected by only minor damage.

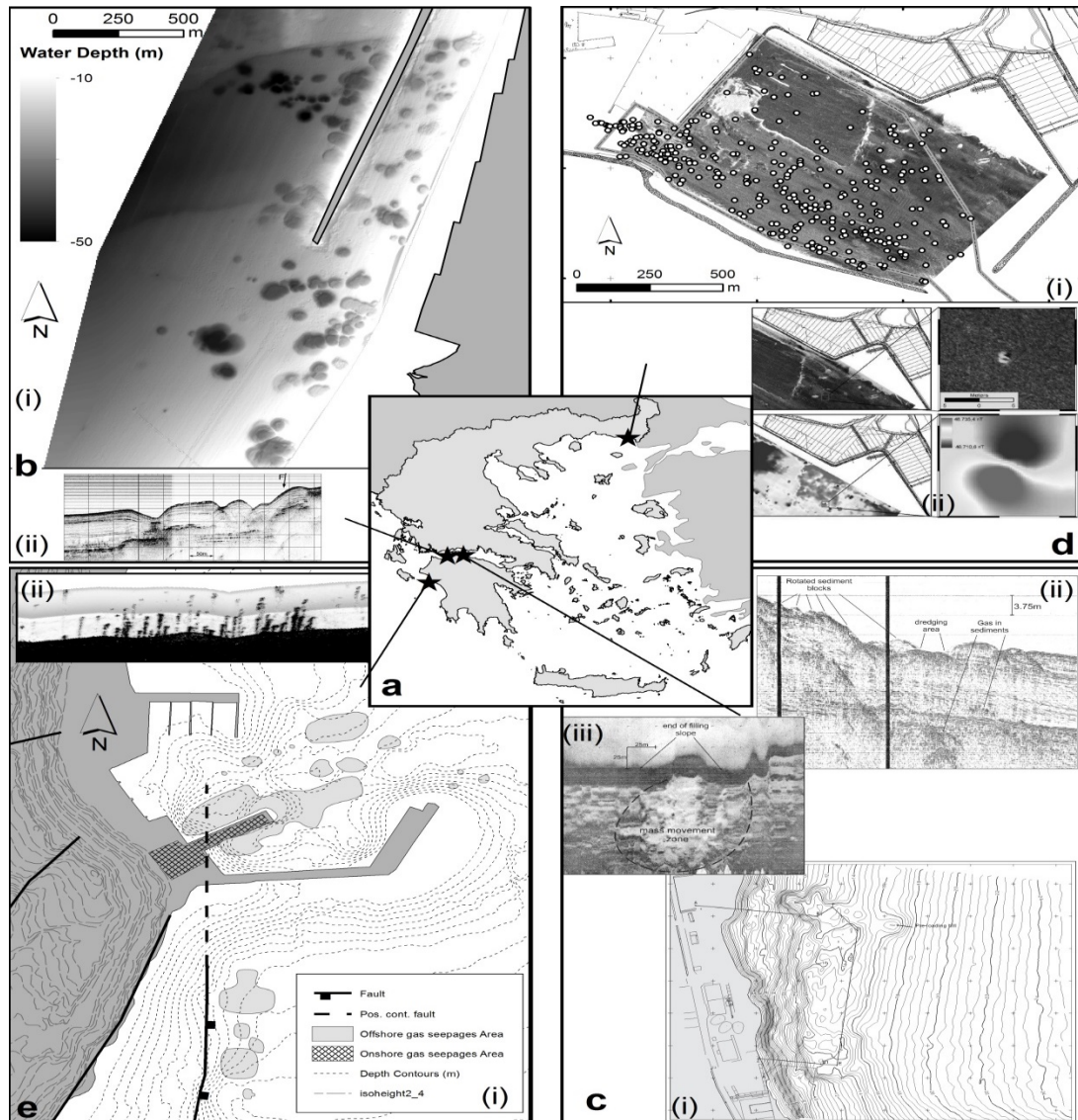


Figure 1 (a) Map showing the location of the surveyed harbours. (b) New Patras harbour (i) Bathymetrical map (DEM) showing the presence of a pockmark field where the breakwater was installed, (ii) seismic profile showing the presence of gas in the sediment pores of the surficial sedimentary layer, (c) New Aigion harbour, Seafloor images showing: (i) the bathymetry in the basin harbour, (ii) and (iii) slumped sediments on the seafloor over the dredged area and gas in the sediment pores, (d) Alexandroupolis harbour, Seafloor sonar image showing: (i) the presence of debris (dots) on the seafloor and (ii) a large solid debris on the seafloor with a strong magnetic signature and (e) Katakolo Harbour, (i) bathymetric map showing the presence of an active fault and the areal extend of gas seeping zones, and (ii) sonar image showing rising gas bubbles in the water column.

3 DISCUSSION

The above presented case studies have shown that the master plan study for the harbours construction that was drafted without taking into consideration the use of recently developed and worldwide accepted marine geophysical survey technologies has failed to fully assess the suitability of the seabed on which the infrastructure will be placed. On the contrary the supplementary marine geophysical surveys, which were carried out in a later stage during the construction, have shown that the purposed

planned high resolution geophysical surveys give solutions to the problems the engineers faced during the construction of the harbours.

Summarising, the lessons taken from the above discussed case studies, it can be suggested that the detailed knowledge of the bathymetry, the seabed geology including the thickness and stratigraphy of the subsurface sedimentary layers and the presence of geological hazards in the harbour site with the use of state of the art marine geophysical surveying technologies i.e multi-beam echo- sounders, side-scan –sonar, sub-bottom profilers, remote operated vehicles and magnetometers, is a pre-requisite for the safe construction and operation of a harbour. For more information about the state of the art of the seafloor mapping technologies please visit: www.oceanus.upatras.gr and www.ionian-acquarium.com

References

- ADK AS and Triton Inc, (1944) Final Design of Port of Patras, Ministry of Environment and Public Works (Greece), Dec. 1994.
- Ferentinos, G., (1991) Offshore geological Hazards in the Hellenic Arc. *Marine Geotechnology*, 9, pp 261-277.
- Christodoulou, D., Papatheodorou, G., Ferentinos, G. and Masson, M., (2003) Active seepage in two contrasting pockmark fields in the Patras and Corinth Gulfs, Greece. *Geo-Marine letters*, 23 pp194-199.
- Etiopie, G., Papatheodorou, G., Christodoulou, D., Ferentinos, G., Sokos, E. and Favali, P., (2006) Methane and hydrosulfide seepage in the N.W. Peloponnesus petroliferous basin (Greece): Origin and geo-hazard. *American Association of Petroleum Geologist Bulletin* 90, pp: 701-713.
- Hasiotis, T., Papatheodorou, G., Kastanos, N. and Ferentinos, G., (1995) A pockmark field in Patras Gulf (Greece) and its activation during the 14/7/1993 Seismic event. *Marine Geology*, 125, pp 131-152.
- Kevin-Smith, P., Pollard, M., Brotman, I., and Zdinak, A., (2010) Integrated site investigation for Cranex Island eastward expansion, Portsmouth, Virginia, *Ports 2010 ASCE*, pp 313-322.
- Loukakis, K. and Yegian, M., (1998) Quay wall and breakwater design and construction of the New Port of Patras, *Geotechnical Engineering for Transportation Projects*, ASCE pp 516-525.
- Murphy, W., Ward, W., Boyd, B., Fleming, G., Nolen-Hoeksema, R., Tetrant, I., Art, M., and Rosales-Roche, D., (2010) Geophysical and Geological Mapping for Infrastructures in New-York Harbor. *Ports*, ASCE pp 989-998.
- Tarata, S., Miele, M., Tyrata, L., and Michelsen, F., (2005) Cost Effective Geophysical Approaches for various geotechnical problems. *Geo-Frontiers, Site Characterization and modelling*, ASCE pp. 1-15.

Design of a new marina in Paralimni Cyprus by implementing mathematical and physical modeling

E. Rouchotas*, I. G. Koutsourelakis, M. Kalogirou P. Aggelerou

TRITON Consulting Engineers
*Corresponding author: triton@tritonsa.gr

Abstract

The aim of the current paper is the presentation of blank-sheet design of a new Marina foreseen at the Paralimni area in eastern Cyprus. The understudy coastal area consists of enclosed embayments and pocket beaches. The new Marina is foreseen in one of them. The knowledge of all the critical coastal and hydrodynamic processes was elaborated through studies that provided input for the geological factors, the surficial sediments and the wave climate. The optimization of the marina design was carried out through mathematical 2D modeling, by implementing the MIKE21 software suite. The calibration is based on extensive seabed sampling and a habitat mapping, along with current and wave measurements. Additional optimization regarding the design of the critical sections of the marine works was achieved through 2-D physical modelling executed in collaboration with the HR Wallingford laboratory. The scope of the current paper is the presentation of the design procedure implemented for the optimization of the various aspects of the new Marina in order to meet the high standards of safety and comfort for the Marina users along with minimization of environmental impacts.

Keywords Cyprus, Marina, Physical Modeling

1 LOCAL CONDITIONS

The Paralimni Marina site is located inside the greater Famagusta Bay of Cyprus, which occupies the eastern part of the island, and more specifically approximately 9 km to the north of cape Cavo Greco, as indicated on the aerial photo here below. The shore at the vicinity of the proposed marina's site runs in a general NW-SE direction following the general trend of the Cypriot eastern coast. The latter are stabilized by marine works, mainly small groynes and are widened by artificial nourishment.



18. Figure 11 Aerial view of the general project location in relation to the Island of Cyprus on the left and Aerial view of the project location on the right

2 FIELD STUDIES

Extensive field studies were required in order to accurately document the local conditions and factors that influence the hydrodynamic and sediment transport regime of the coastal area. These studies are listed here below:

- Topographic survey covering the coastal area and the bathymetry up to a depth of -27 m, extending for about 850 m to the NE from the proposed marina and about 1650 parallel to the coastline, covering as well the coastal land area around the project location.
- Seabed sampling of surficial sediments including more than 50 samples in sections spaced along 150 m-250 m intervals and covering the entire coastal profile.
- Seabed mapping, indicating the areas covered by rock boulders or continuous rock or by sand, the areas covered with *Posidonia Oceanica*.

- On-site wave and current measurement campaign.

3 DATA ANALYSIS AND MODELING

The analyses and modeling carried out, in order to investigate existing and developed conditions in the probe area, are presented in the following sections

3.1 MetOcean and Wave Climate Analysis Study

The available hindcast database which was used, provided by the MWM (Mediterranean Wave Model) covers 39 years of records. In order to establish the long-term wave climate of the area, this data was analyzed using the “Peaks-Over-Threshold” (or POT) approach employed for both wind and wave data. At the first stage, the MIKE 21 SW (Spectral Waves) module is applied to calculate the wave conditions caused by the examined wind and wave conditions. The regional model established from which the boundary conditions for the local wave model were extracted.

3.2 Sediment Transport Analysis

The scope of this study is to assess, both qualitatively and quantitatively, the wave induced hydrodynamic conditions and the relevant sediment circulation on the area of interest both in present day conditions and after the construction of the marina. The sediment transport analysis was carried out both for the annual average wave events but also took into account frequent storm events, i.e. those for 1-year return period.

3.3 Wave agitation Model

Wave agitation modelling was conducted in order to optimize the layout in terms of wave penetration, mainly focusing at the entrance and the inner marina works for the new Paralimni Marina in Cyprus. Several layouts were examined.

- Layout 1: The layout that originated from the Master Planning for the new marina
- Layout 2: The entrance width is increased and the roundhead section is lengthened compared with layout 1.
- Layout 3: Same as layout 2 including absorbing quays at the northern curved and at the northern side of the root of the Operations pier

The selected wave events’ simulation is carried out in two stages. The initial stage relates to the extreme wave conditions outside and inside the marina, namely arising from the 10-year and the 100-year return period wave events respectively. The second modeling stage, incorporates the finally selected option, i.e. Layout 3, by checking the most critical sectors by considering the 1 and 50 yrs return period wave events. These critical sectors are the NE, ESE and SE that owing to their orientation and wave characteristics result in higher wave energy penetration inside the basin.

3.4 Basin Water Circulation Modeling

The water quality is discussed in the water circulation Modeling. Different cases were selected regarding the number and the position of the culverts. The water circulation of the basin was examined under the influence of wind, tide and the combination of these two loads. The inspected cases are mentioned bellow.

- Case A: Present Marina Geometry without Culverts
- Case B: Marina with one (1) culvert at the main breakwater and one (1) at the operations Pier
- Case C: Marina with two (2) culverts at the main breakwater and one (1) at the Operations Pier
- Case D: Marina with two (2) culverts at the main breakwater and two (2) at the Operations Pier

Through the modelling, an estimation of the water renewal was possible as well as the pattern of the wave-, tide-induced current developed inside the basin.

3.5 Physical model

A 2D physical model was set up at scale of 1:31.37 which ensured the main aspects of wave/ structure interaction were reproduced accurately at a scale the avoided scale effects; particularly regarding Reynolds number considerations and for wave overtopping. The purpose of the physical model was to:

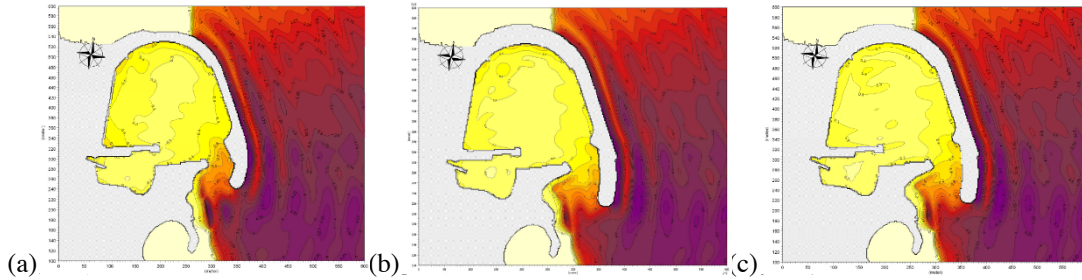
- Verify the stability of the breakwater armouring layers, namely the main layer (Accropode™), the filters and the toe protection mound.
- Measure wave overtopping discharges over the test section’s crest
- Optimize the above aspects by testing an optimized configuration of the typical section

4 RESULTS

In the present chapter, the results are presented in brief.

4.1 Wave penetration Model

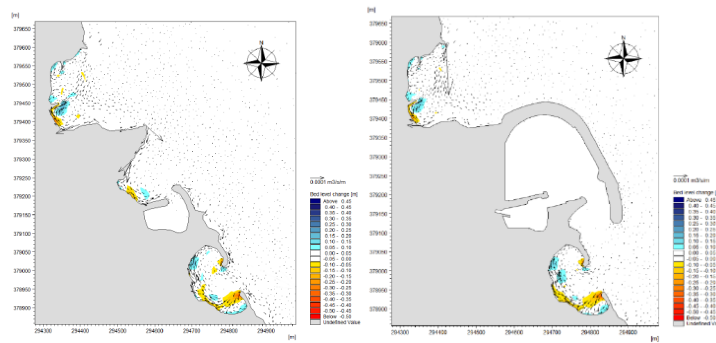
The results of the adverse wave conditions are presented below, ie the NE sector for the three examined layouts. The conditions occurring at the entrance are improved in layout 2 and 3 and the wave conditions inside the basin and specially in front of the quay walls became milder with the addition of absorbing quays at appropriate locations.



19. *Figure 12 Wave Height Distribution For the NE wave sector and the 10 years return period. a) layout 1, b) layout 2, c) layout 3*

4.2 Sediment Transport Analysis

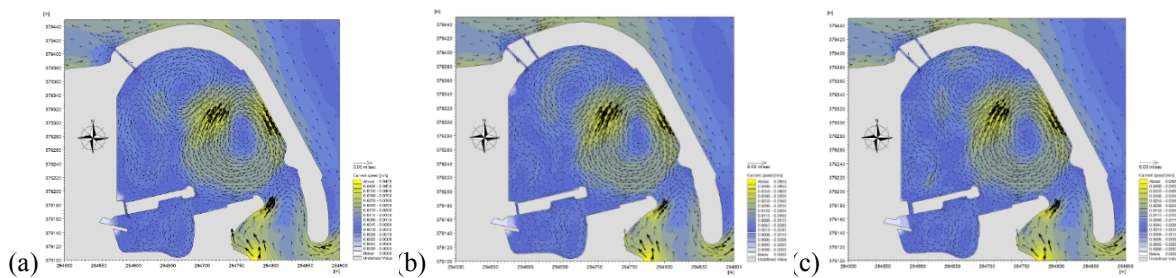
In the following figures the results of NE sector for the average wave conditions are presented, indicating that sediment transport regime remains almost unaffected by the presence of the marina works.



20. *Figure 13 Littoral transport of annual average events from the NE prior and after the inclusion of the Marina works*

4.3 Water Circulation Model

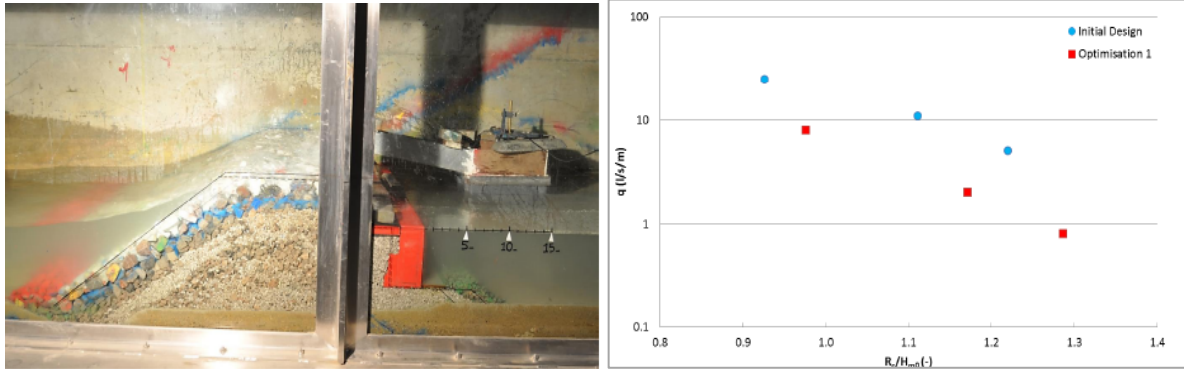
Under the combined effect of tide and wind, the wave circulation is shown below. The area of stagnant water (white color) is restrained in case C compared to the case D. At the case C the circulation in the large basin becomes more intense than in case B. In case D deterioration in flow pattern is noticed in both basins.



21. *Figure 14 A snapshot of hydrodynamic field (a) case B, (b) case C (c) case D*

4.4 Physical model

Physical Modeling indicated the excellent performance of the tested section against the most adverse wave conditions. Concerning wave overtopping, the discharges were recorded for the initial cross-section. In order to enhance the conditions at the lee side of breakwater for small craft, an optimized cross-section was proposed and tested. In the figure below the diagram of the wave overtopping discharges are shown for the initial and the optimized design.



22. *Figure 15 Overtopping event during 1 in 100yr wave condition on the left, comparison of wave overtopping discharges recorded during Test Series A and B for 1 in 50yr, 1 in 100yr and Overload wave conditions on the right*

5 CONCLUSIONS

A variety of design outputs arose from the aforementioned studies to determine basic design aspects of the preliminary stage design. The main conclusions emerged are summarized below:

- Modification of the marina works layout and type (tested Layout-3 option) resulted by the wave agitating model provides the higher tranquility levels within the marina.
- The hydrodynamic and sediment transport modeling process indicates that the inclusion of the Marina does not modify in the existing littoral regime for the embayments in the vicinity of the proposed works. Thus the inclusion of the new Marina is not expected to cause any morphological changes in the neighboring recreational coastal areas.
- Increase in the crest level and width of the most exposed part of the main breakwater in order to provide safe conditions even for the smallest of vessels moored there.
- Selection of location and dimensions for water circulation culverts both at the outer protective works and at the inner marina works. This works optimization will greatly facilitate water circulation and thus ameliorate water quality in the basin.

References

- Goda Y. (2000) Random Seas and Design of Maritime Structures, Advanced Series on Ocean Engineering: Volume 15, Third Edition.
- PIANC (2016) "PIANC Guidelines For Marina Design" Report n° 149/part I and II- 2016
- US Army Corps of Engineers (2006) Coastal Engineering Manual (CEM)
- Protecting Water Quality in Marinas (2008) PIANC Report No 98
- EPA-840-B-92-002, Chapter 5: Management Measures for Marinas and Recreational Boating, 1993
- Standards Australia TM (2000) – Guidelines for Marina Design

How can ports benefit from a holistic approach to fender system design?

D. Polte*

ShibataFenderTeam AG, Tarpen 40, 22419 Hamburg, Germany

*Corresponding author: d.polte@shibata-fender.team

Abstract

The aim is to share expertise and best practice examples of a durable and holistic approach to fender system design to increase productivity at marine terminals. Only when all components are designed in the correct balance and work together properly, the fender system will perform as expected. Users and engineers should be made aware of the fact that “what looks good in a drawings, might not work in the field”. Since the rubber units are mostly standardized in the industry, the main engineering and design challenge is with the steel panels, chains and the corresponding anchorage. The rubber unit is a crucial component of the system, but is only as good as the overall design of the system. Simple issues like incorrect chain angles or the positioning of the rubber unit on the steel panel and substructure could lead to premature failure of the fender system as a whole. When fenders fail or are not working properly due to low quality or incorrect designs, then there is a cost to the port in terms of repair, downtime, or even accidents which should not be underestimated.

Keywords Fender design, Maritime fenders, Rubber fenders, Holistic approach to fender systems.

1 AIM

The aim of the paper is to share expertise and best practice examples of a durable and holistic approach to fender system design to increase productivity at marine terminals. The paper starts by highlighting the importance of rubber fender materials, the compound mixing and manufacturing process. This is followed by important factors influencing the design of superior fender systems. An honest look on typical problems of poor fender system design and resulting consequences provides a unique insight to the industry. The paper closes with corrective measures to always ensure high-quality products.

2 INDUSTRY NEED AND IMPORTANCE

The road from designing the compound for a rubber fender with the desired properties to a mixing and manufacturing procedure that adheres to the highest quality standards is a complex one. It appertains to a holistic approach that a fender system is treated as one, starting from source materials over design to the manufacturing process. Only when all components are designed in the correct balance and work together properly, the fender system will perform as expected. When fender systems fail or do not work properly due to low quality or incorrect designs, then there is a cost to the port in terms of repair, downtime, or even accidents which should not be underestimated. In order to avoid increased maintenance and replacement cost or additional losses for downtime, a holistic approach to fender system design should be advocated throughout the marine industry. The entire project-specific process from calculations and design to creating and producing high-quality, durable fenders, fully committing to international standards and norms, and a clear sense of responsibility should be key to all manufacturers.

3 INTERACTION OF RUBBER FENDER MATERIAL AND FENDER SYSTEM DESIGN

Being a crucial component of the system, the rubber unit’s raw material, compounding and the mixing process is a very pivotal and sensitive part of rubber manufacturing. There is no international standard specifying the chemical composition of the rubber compound, it is rather based on practical knowledge and experience. Based on this, it is not the chemical composition but rather the physical properties of a fender being the only reliable indicator of the quality of a rubber compound. Adjusting the compound for every new fender project according to its requirements is the key to a customized

fender design, as the characteristics of rubber compounds greatly affect fender performance and durability. There are infinite combinations of rubber compositions and they all depend on the type and amount of raw rubber and compounding agents used in the formulation. The expertise in the fields of compound designing, mixing, production and testing that comes with long-standing know-how are the key to safety, reliability, and durability of fenders.



Figure 1 Raw rubber material

However, the best formulation of the compound and the highest quality raw materials may not result in a reliable rubber fender when inappropriate mixing techniques are involved, or the wrong equipment is used. Ultimately, the consistency of a multi-layered process such as customized rubber mixing depends to a great extent on the operational control over every production step, a solid concept of quality management and once again the manufacturer's experience.

Having produced a high-quality rubber unit is still not sufficient for a reliably operating fender system. The rubber unit is only as good as the overall design of the system.

4 IMPORTANT FACTORS INFLUENCING SUPERIOR FENDER SYSTEM DESIGNS

The overall philosophy of a fender is simple: the fender's capacity to absorb the berthing energy of a vessel needs to be more than the kinetic energy of the vessel. The engineering around fender designs has been described as "part science – part art" in that it requires comprehensive experience to fully understand how to provide a good balance between performance, functionality and cost.

4.1 Berthing Energy of Vessels

Calculating the berthing energy of vessels is the first and most important step in the fender design process. If something goes wrong here, the entire waterfront design could be at risk. The relevant parameters here are ship type, berthing mode or point of contact from bow. Several calculation tools are available on the market which support clients during the berthing energy calculation process. It is important to mention that the results should be seen as a guideline only. It is highly recommend to share your design approach with an experienced manufacturer to make sure that e.g. the substructure is sized correctly for the required fenders.

4.2 Factor of Safety

Another important topic is the factor of safety (FOS). It is applied to the normal berthing energy such that the fender system will be capable of absorbing reasonable abnormal impacts, which may be caused by mishandling, malfunction, adverse wind and current or a combination of all. It is important to know, however, that calculation of normal and abnormal berthing energy is based on experience, while the actual berthing energy can vary substantially each time the vessel berths.

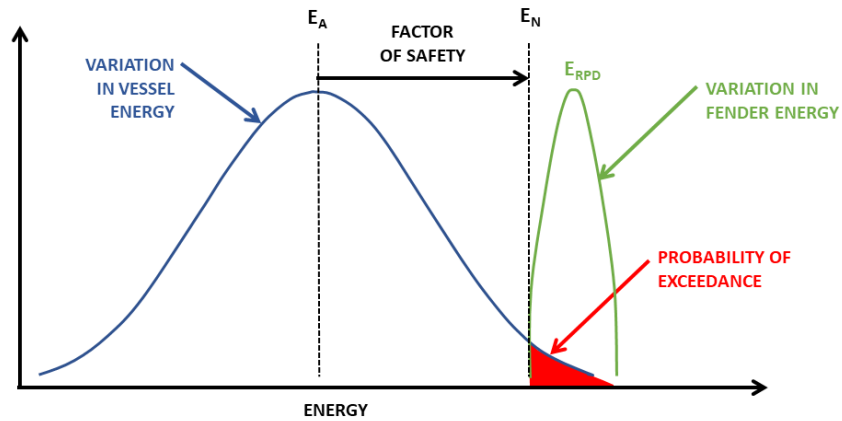


Figure 2 Factor of Safety

Even though all design principles are closely followed, there are several problems which can occur. Their severe consequences can be avoided if the corrective measures are followed from the beginning.

5 TYPICAL PROBLEMS OF POOR FENDER SYSTEM DESIGN, RESULTING CONSEQUENCES AND CORRECTIVE MEASURES

The typical problems of poor fender system design could be the rubber fender position on the panel and chain layout, the steel panel's internal structure, UHMW-PE protection pads, and coating system.

5.1 Fender Position on Panel

An unfavorable fender position on the panel exists if for example the rubber unit is installed too close to the top edge of the panel which can result in potential damage to vessel hull, damage to the rubber unit due to torsion and tension loads and a lower fender performance. A reduction of the life cycle of the fender system and the accompanying increase in maintenance and replacement cost negatively affects the efficiency of port operation.



Figure 3 Unfavorable panel position (P1), chains with incorrect angle (P2) and low rubber quality with incorrect design (P3)

A holistic approach positions the rubber unit so that it allows for an evenly distributed hull pressure. Well placed, with the right angled and tensioned chains, the rubber unit is protected against panel self-weight, tension and shear forces.



Figure 4 High-quality solution by SFT

5.2 Internal Structure of Steel Panels

A wrong structural calculation for the steel panels can result in the capacity of the steel beams being lower than required for the applicable load cases. The consequences are bent panels and a dramatic reduction of the life cycle of the system. A structural calculation following specified standards should be based on real load cases, vessels and berthing conditions. A robust steel fender panel needs to be designed to support loads over the complete life cycle.

5.3 UHMW-PE Protection Pads

If inappropriate FQ/100% virgin material is used, a quick deterioration of protection pads and a following damage to the steel panel and rubber unit is a severe consequence. High quality UHMW-PE material protects the steel panel from direct impact by vessels and the rubber fender from shear forces.

5.4 Coating System

Corrosion of steel components is a problem with major consequences. Several causes attribute to that, one of them being that the coating system for the panel is below the required minimum thickness.

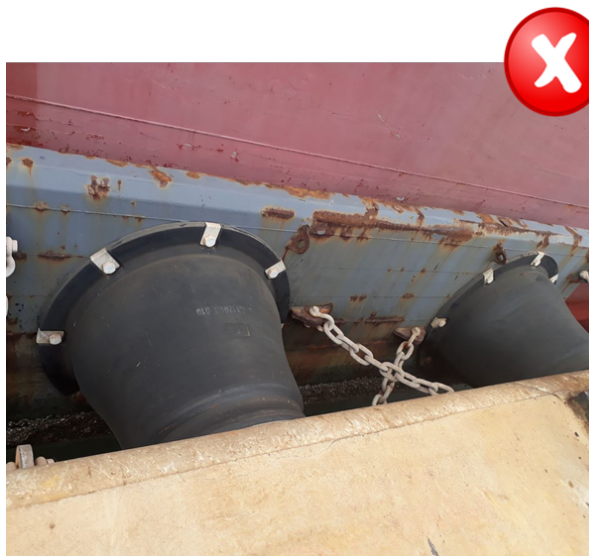


Figure 5 Incorrect steel protection

Another reason could be the missing hot-dip galvanization or not using stainless steel. Besides corrosion, the consequences are manifold: reduction of the steel panel load support capacity, damages to anchors and chains and a dramatic reduction of the fender system’s life cycle. The coating thickness should be applied according to specifications and the chains and hardware should be either hot dip galvanized or produced from stainless steel (hardware only).

Poor fender design has many faces with severe consequences for ports, ships and people. A holistic approach to fender manufacturing and design based on experience and expertise can minimize risks and failures.

6 HOLISTIC APPROACH OF FENDER SYSTEM DESIGN

Users and engineers should be made aware of the fact that “what looks good in a drawing, might not work in the field”. Since the rubber units are mostly standardized in the industry, the main engineering and design challenge is with the steel panels, chains and the corresponding anchorage. Simple issues like incorrect chain angles or the positioning of the rubber unit on the steel panel and substructure leads to premature failure of the fender system as a whole. If a rubber fender system does not perform as required, safety in marine operation and efficiency for marine terminals cannot be ensured.

For the ShibataFenderTeam Group, the approach to achieving a high-quality fender system has emerged through a long history of experience with the materials and the processes involved.

All steps of fender design go hand in hand and influence each other. This fact emphasizes the need for a holistic approach to fender system design in the industry and an experienced manufacturer to ensure reliable, safe and efficient operations for ports.



Figure 6 Holistic approach to fender system design

Πλωτές προβλήτες από οπλισμένο σκυρόδεμα

Α. Απέργης, Κ. Καμπόλης*

*Υπεύθυνος επικοινωνίας: (k.kampolis@asprokat.gr)

Περίληψη

Στην παρούσα ανακοίνωση παρουσιάζεται η θεωρητική προσέγγιση του φαινομένου της πλευσης και της ισορροπίας των επιπλέοντων προκατασκευασμένων στοιχείων από οπλισμένο σκυρόδεμα, η τεχνολογία και μέθοδοι εξασφάλισης στεγανότητας και αντοχής των πλωτών προκατασκευασμένων στοιχείων από οπλισμένο σκυρόδεμα. Επεξηγείται η αιφορία των κατασκευών αυτών σε δυσμενείς καιρικές συνθήκες και περιγράφονται οι δυνατότητες των εγκιβωτισμένων εξαρτημάτων που αφορούν την εξυπηρέτηση των σκαφών. Συγκρίνεται η οικονομική και δόκιμος μέθοδος χρήσης των πλωτών προκατασκευασμένων στοιχείων από οπλισμένο σκυρόδεμα, με αντίστοιχες πλωτές κατασκευές άλλων υλικών. Παρουσιάζεται η εθνική νομολογία καθώς και τεχνικές οδηγίες παραγωγών προκατασκευασμένων πλωτών στοιχείων. Τέλος παρουσιάζονται συγκεκριμένες εφαρμογές πλωτών, και σταθερών προκατασκευασμένων στοιχείων από οπλισμένο σκυρόδεμα, σε λιμένες και Μαρίνες.

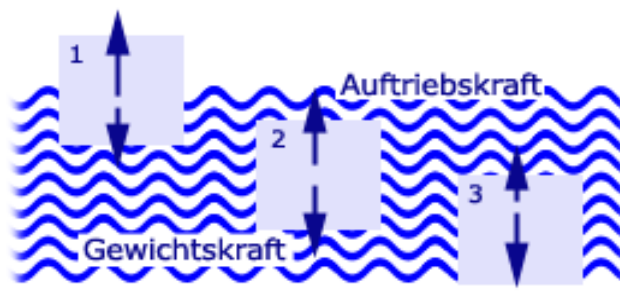
1 ΕΙΣΑΓΩΓΗ

Η μεγιστοποίηση του θαλάσσιου τουρισμού, δημιούργησε τους τουριστικούς λιμένες και ειδικότερα τις Μαρίνες. Για την ορθολογική αξιοποίηση της επιφάνειας των λιμένων εφαρμόστηκε η χρήση πλωτών προκατασκευασμένων κατασκευών. Ειδικότερα οι πλωτές προβλήτες από οπλισμένο σκυρόδεμα, με την χαρακτηριστική υψηλή αντοχή τους και την διαχρονικότητα τους αντιμετωπίζουν θετικά τα έντονα περιβαλλοντολογικά προβλήματα του θαλάσσιου περιβάλλοντος.

2 ΤΟ ΦΑΙΝΟΜΕΝΟ ΤΗΣ ΠΛΕΥΣΗΣ ΤΩΝ ΣΩΜΑΤΩΝ

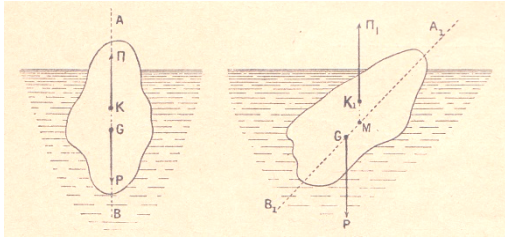
Η Αρχή του Αρχιμήδη: «Παν σώμα ευρισκόμενο εντός υγρού υφίσταται ώθηση κατακόρυφη (Άνωση) εκ των κάτω προς τα άνω και ίση προς το βάρος του υγρού που εκτοπίζεται από το σώμα»

- 1) Όταν το βάρος του σώματος < της Άνωσης → επιπλέει
- 2) Όταν το βάρος του σώματος = της Άνωσης → αιωρείται
- 3) Όταν το βάρος του σώματος > της Άνωσης → βυθίζεται

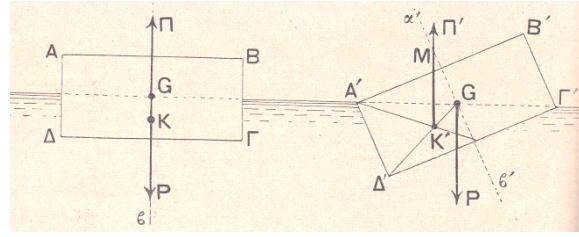


Σχήμα 1 Οι τρεις περιπτώσεις 1, 2, και 3

Η εξασφάλιση της ευστάθειας του σώματος κατά την πλευση, δηλαδή πότε η ισορροπία του επιπλέοντος σώματος είναι ευσταθής ισχύει όταν το ζεύγος των δύο δυνάμεων είναι σε τέτοια θέση ώστε το σώμα να τείνει να επανέλθει στην αρχική του θέση. Ειδικότερα όταν το Κέντρο Βάρους (KB) του σώματος είναι κάτω από το κέντρο του. (Σχήμα 3)



Σχήμα 2 Η εξασφάλιση της ευστάθειας του σώματος κατά την πλεύση



Σχήμα 3 Η εξασφάλιση της ισορροπίας του σώματος κατά την πλεύση

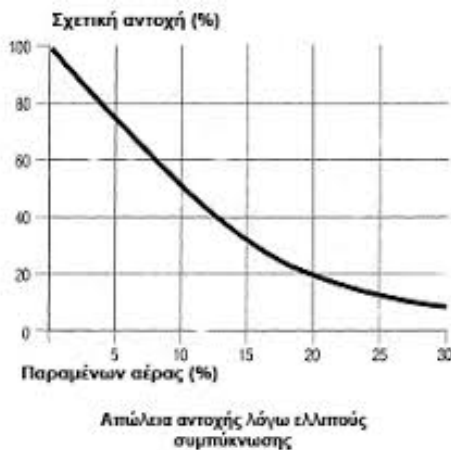
Η ισορροπία του σώματος κατά την πλεύση είναι ευσταθής ή ασταθής όταν το Μετάκεντρο (M) βρίσκεται πάνω ή κάτω από το Κέντρο Βάρους (G). (Σχ.3)

3 Η ΧΡΗΣΗ ΤΟΥ ΣΚΥΡΟΔΕΜΑΤΟΣ ΣΤΙΣ ΠΛΩΤΕΣ ΠΡΟΒΛΗΤΕΣ ΚΑΙ Η ΔΕΙΦΟΡΙΑ ΤΟΥ

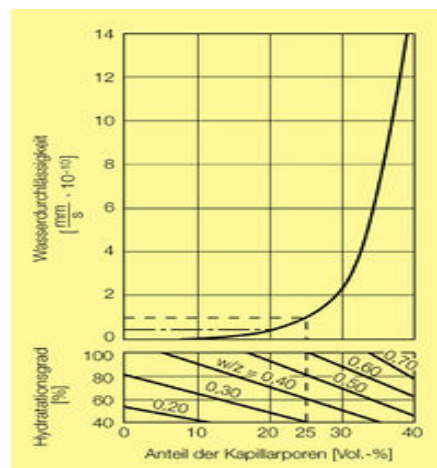
Συστηματικές μελέτες σχετικά για τη συμπεριφορά του σκυροδέματος στο θαλασσινό νερό έδειξαν ότι το συμπυκνωμένο σκυρόδεμα είναι υπό κανονικές συνθήκες ανθεκτικό στην επίδραση του θαλασσινού νερού.

Για την παραγωγή σκυροδέματος κατάλληλου για λιμενικά έργα γενικότερα, μπορούν να χρησιμοποιηθούν όλα τα είδη τσιμέντων σύμφωνα με το EN 197-1 (π.χ. Τσιμέντο τύπου Portland κλπ). Προϋπόθεση για την υψηλή αντοχή του σκυροδέματος είναι:

- Η επαρκώς υψηλή περιεκτικότητα του σε τσιμέντο. > 400 Kg./m³
- Η τιμή του λόγου Νερού / Τσιμέντου να είναι μικρότερη από 0,50. ($w/c < 0.50$)
- Η επικάλυψη του οπλισμού από το σκυρόδεμα να είναι αυξημένη, και κατά κανόνα μεγαλύτερη των 5 cm (Βλ. Κανονισμό Τεχνολογίας Σκυροδέματος ΚΤΣ 2016)
- Να εφαρμόζεται μια ευνοϊκή κοκκομετρία αδρανών.
- Το σκυρόδεμα να είναι σημαντικά συμπυκνωμένο, ώστε να έχει υψηλή μηχανική αντοχή και υδατοστεγανότητα. (Σχήμα 4 & 5)



Σχήμα 4 Διάγραμμα αντοχής



Σχήμα 5 Διάγραμμα υδατοστεγανότητας σε ποσοστό ο/ο πόρων αέρος συνάρτηση ποσοστού ο/ο πόρων αέρος και λόγου w / c

Ήδη ο Πλίνιος ο Πρεσβύτερος αναφέρει στο Naturalis Historia το 77 μ.Χ. ότι οι ρωμαϊκές αποβάθρες στο θαλασσινό νερό γίνονται "Μια ενιαία πέτρινη μάζα, ακατανόητη για τα κύματα και ισχυρότερη καθημερινά". Έκτοτε χρησιμοποιείται σχεδόν αποκλειστικά το σκυρόδεμα στα λιμενικά έργα.

Όσο αφορά πλωτά μέσα από σκυρόδεμα, το 1848 κατασκευάζεται το πρώτο πλεούμενο από οπλισμένο σκυρόδεμα από τον Joseph-Louis Lambot ως βάρκα, που παρουσιάστηκε το 1855 στην Παγκόσμια Έκθεση του Παρισιού. Ενώ κατά τον Α΄ Παγκόσμιο Πόλεμο εμφανίζονται ποταμόπλοια από οπλισμένο σκυρόδεμα στην κεντρική Ευρώπη, και κατά τον Β΄ Παγκόσμιο Πόλεμο,

κατασκευάζονται εν σειρά ακταιωροί κλπ πολεμικά πλοία από την γνωστή γερμανική εταιρεία DYWIDAG, ενώ τις επόμενες δεκαετίες κατασκευάζονται ποικίλα τουριστικά σκάφη από Ferocement.

5.1 4 ΣΧΕΔΙΑΣΜΟΣ ΚΑΙ ΤΕΧΝΟΛΟΓΙΑ ΠΑΡΑΓΩΓΗΣ

5.2 Ο σχεδιασμός πλωτής προκατασκευασμένης προβλήτας από οπλισμένο σκυρόδεμα λαμβάνει υπ' όψη κατ' αρχή την σωστή λειτουργία της:

- Μηχανική Αντοχή - Στεγανότητα
- Βάρος - Άνωση
- Πλεύση- Ισορροπία- Μετάκεντρο

Και όλες τις προϋποθέσεις του σχεδιασμού των λιμενικών έργων:

- Ανεμολόγιο
- Κυματισμός
- Χωροταξία – Κυκλοφορία σκαφών
- Πρόσδεση σκαφών
- Παροχές Νερού, Ηλεκτρικού ρεύματος, Τηλεφώνου, Αποχέτευσης, κλπ

Για την βιομηχανική τους παραγωγή πρέπει να εφαρμόζεται πρότυπο διαχείρισης ποιότητας (π.χ. ISO 9000). Ενώ είναι απαραίτητη η αντίστοιχη συμμόρφωση βάσει της σήμανσης CE για κάθε παραγόμενο προϊόν. Δεδομένου ότι αυτές οι κατασκευές υπόκεινται σε δυσμενείς καιρικές συνθήκες, απαιτούνται επί πλέον εργαστηριακές και in situ δοκιμές. (π.χ. Υδατοπερατότητα σκυροδέματος βάσει EN 12390.08).

Ιδιαίτερα τα εγκιβωτισμένα εξαρτήματα, για την εξυπηρέτηση των σκαφών, πρέπει να πληρούν τις αντίστοιχες προδιαγραφές της ναυσιπλοΐας και να είναι εγκεκριμένα από πιστοποιημένο νηογνώμονα. (Π.χ. ανοξείδωτα εξαρτήματα, κλπ). Οι δε εγκιβωτισμένες παροχές, νερού, ηλεκτρικού ρεύματος, τηλεφώνου, αποχέτευσης κλπ που συνήθως καταλήγουν σε συγκεντρικό κιβώτιο, πρέπει να πληρούν τις αντίστοιχες προδιαγραφές και διατάξεις των υδραυλικών και ηλεκτρολογικών εγκαταστάσεων. (Σχήμα. 6 & 7)



Σχήμα 6 Ανοξείδωτη δέστρα και Κιβώτιο Α' Βοηθειών + Σωσίβιο+Φωτιστικό σώμα.



Σχήμα 7 Συγκεντρικό κιβώτιο παροχών νερού & ηλεκτρικού ρεύματος

5 ΧΡΗΣΗ ΚΑΙ ΟΙΚΟΝΟΜΙΚΟΤΗΤΑ

Οι πλωτές προβλήτες από οπλισμένο σκυρόδεμα βρίσκουν εφαρμογή :

- Σε μαρίνες για να υποδιαιρέσουν την επιφάνεια του λιμένα και να αξιοποιήσουν όσο το δυνατόν περισσότερες θέσεις πρόσδεσης σκαφών.
- Σε ιχθυοτροφεία για εύκολη πρόσβαση προσωπικού και μικρών μεταφορικών μέσων .
- Σε λιμένες με παλιρροιακά φαινόμενα, όπου οι πλωτές προβλήτες λειτουργούν ανεξάρτητα από την εκάστοτε στάθμη των υδάτων
- Σε προστατευτικούς κυματοθραύστες σε λιμένες, μαρίνες κλπ

Οι πλωτές προβλήτες από σκυρόδεμα λόγω της διαχρονικότητας τους, είναι μακροβιότερες και οικονομικότερες από αντίστοιχες κατασκευασμένες από άλλα υλικά. Έτσι ο χρόνος απόσβεσης της αρχικής δαπάνης είναι μεγαλύτερος για τις προκατασκευασμένες προβλήτες από οπλισμένο σκυρόδεμα.

6 ΕΘΝΙΚΗ ΝΟΜΟΛΟΓΙΑ ΧΡΗΣΗΣ ΠΛΩΤΩΝ ΠΡΟΒΛΗΤΩΝ

Το ΦΕΚ 1651/23.06.2014 αφορά στην διαδικασία τοποθέτησης πλωτών εξεδρών, επιφάνειας μέχρι εκατό πενήντα (150) τ.μ., στη θάλασσα, χωρίς επέμβαση στον αιγιαλό, για εποχιακή χρήση. Ενώ το μεταγενέστερο ΦΕΚ 2252/20.07.2016, βελτιώνει τις σχετικές διαδικασίες έγκρισης.

Γενικότερα ισχύουν και οι εξής διατάξεις:

ΦΕΚ 674/Β`/17.4.2008 & ΦΕΚ 479/Β`/20.4.2010 που αφορούν την εκπόνηση μελετών αξιολόγησης ασφαλείας λιμενικών εγκαταστάσεων, καθώς και το Π.Δ. 190/1984_ (ΦΕΚ 64/Α`/15.5.1984) και Π.Δ. 70/1990 (ΦΕΚ 31/Α`/14.03.1990) που αφορούν την υγιεινή και ασφάλεια των εργαζόμενων σε ναυπηγικές και λιμενικές εργασίες.

7 ΣΤΟΙΧΕΙΑ ΑΠΑΡΑΙΤΗΤΑ ΓΙΑ ΧΡΗΣΗ ΠΛΩΤΩΝ ΠΡΟΒΛΗΤΩΝ

- Έγκριση τοποθέτησης
- Χωροταξία – Κυκλοφορία σκαφών
- Αντιμετώπιση ανέμου και κυματισμού
- Τρόποι πρόσδεσης, στερέωσης, και αγκύρωσης
- Συντήρηση
- Ολισθηρότητα επιφανείας
- Τεχνικά δεδομένα εγκιβωτισμένων εξαρτημάτων.
- Χρόνος λειτουργίας και αντίστοιχη απόσβεση κόστους αγοράς,
- Τεχνική και οικονομική σύγκριση με προβλήτες άλλων υλικών.

8 ΕΦΑΡΜΟΓΕΣ ΠΛΩΤΩΝ ΚΑΤΑΣΚΕΥΩΝ

Ανάλογα με την πρόσβαση απαιτείται θαλάσσια ή χερσαία μεταφορά και αντίστοιχη πόντιση των προκατασκευασμένων πλωτών στοιχείων. Όπου ανάλογα με το βάρος, την απόσταση κλπ χρησιμοποιούνται αντίστοιχα μεταφορικά και ανυψωτικά μέσα. (Σχήμα. 8 & 9). Κατασκευάζονται πλωτές προβλήτες σε ποικιλία διατομής, μήκους, και μορφής. Σημαντικός παράγοντας εκτός από τα αναφερθέντα είναι η σωστή συνδεσμολογία αναμεταξύ τους, η πρόσδεση τους στις σταθερές προβλήτες και η σταθερή αγκύρωση τους. (Σχήμα. 10 & 11).



Σχήμα 8 Πόντιση προκατασκευασμένου πλωτού κυματοθραύστη σε ιχθυοτροφείο



Σχήμα 9 Χερσαία πόντιση πλωτής προκατασκευασμένης προβλήτας



Σχήμα 10 Προκατασκευασμένες πλωτές προβλήτες από οπλισμένο σκυρόδεμα.

9 ΣΥΜΠΕΡΑΣΜΑΤΑ

Οι πλωτές προκατασκευασμένες προβλήτες από οπλισμένο σκυρόδεμα, όπως και όλα τα αντίστοιχα προκατασκευασμένα προϊόντα από οπλισμένο σκυρόδεμα για τα λιμενικά έργα, με την χαρακτηριστική υψηλή αντοχή τους την υδατοστεγανότητα τους και την διαχρονικότητα τους αντιμετωπίζοντας θετικά τα έντονα προβλήματα του θαλάσσιου περιβάλλοντος, έχουν καταστεί ένα δόκιμο στοιχείο στους τουριστικούς λιμένες, μαρίνες ιχθυοτροφεία κ.α. λιμενικές εγκαταστάσεις.

ΕΥΧΑΡΙΣΤΙΕΣ

ΑΣΠΡΟΚΑΤ ΑΕ – INGEMAR INGEGNERIA MARITTIMA - ΕΔΡΑΣΗ –Χ. Ψαλλίδας ΑΤΕ

Βιβλιογραφικές Αναφορές

Αιγινήτης Βασίλειος / Γενική Φυσική / Αθήναι 1930

Ρογκάν , Αδέλκης Ι. Μαθήματα θαλάσσιας υδραυλικής & λιμενικών έργων / Αθήνα 1973.

Jochen Stark, Bernd Wicht / Dauerhaftigkeit von Beton / Springer Verlag/ Hamburg 2005.

ΑΣΠΡΟΚΑΤ ΑΕ: Τεχνικό Φυλλάδιο προκατασκευασμένων πλωτών προβλητών.



Sub session 1.3: Construction and Operation

Συγκριτική αξιολόγηση μοντέλων μάθησης για τη διερεύνηση της παραγωγικότητας σε λιμενικά έργα υποδομής μεγάλης κλίμακας: η περίπτωση των κυψελωτών κιβωτίων οπλισμένου σκυροδέματος (caisson)

Π. Ράλλη¹, Α. Πανάς^{2,*}, Π. Παντουβάκης²

¹Κτιριακές Υποδομές Α.Ε., Αθήνα, Φαβιέρου 30, Τ.Κ. 10438, Ελλάδα

²Κέντρο Καινοτομίας Κατασκευών, Εθνικό Μετσόβιο Πολυτεχνείο, Αθήνα, Ζωγράφου, Τ.Κ. 15780, Ελλάδα

*Υπεύθυνος επικοινωνίας: antpanas@gmail.com

Περίληψη

Η θεωρία της καμπύλης μάθησης εφαρμόζεται, τόσο στο χρονικό προγραμματισμό όσο και στη κοστολόγηση σύνθετων κατασκευαστικών δραστηριοτήτων. Σκοπός της έρευνας είναι η αξιολόγηση δημοσιευμένων μοντέλων καμπύλης μάθησης ως προς την ανάλυση πολύπλοκων κατασκευαστικών συστημάτων υπό το πρίσμα του φαινομένου της μάθησης. Η διερεύνηση αφορά τα εξής πέντε (5) μοντέλα: (α) Ευθύγραμμο (ή Wright), (β) Stanford "B", (γ) Κυβικό, (δ) Βαθμωτό και (ε) Εκθετικό. Η ερευνητική μεθοδολογία περιλαμβάνει τη συγκριτική εφαρμογή κάθε μοντέλου, για την ανάλυση λιμενικού έργου υποδομής μεγάλης κλίμακας, με χρήση στοιχείων παραγωγικότητας. Η ανάλυση πραγματοποιείται σε δύο επίπεδα καθώς κάθε ένα από τα πέντε (5) μοντέλα χρησιμοποιείται για τον προσδιορισμό: i) του βέλτιστου μοντέλου για την προσαρμογή ιστορικών δεδομένων παραγωγικότητας και ii) του βέλτιστου μοντέλου για την πρόβλεψη του ρυθμού παραγωγικότητας. Κριτήριο αξιολόγησης είναι ο βαθμός απόκλισης των πραγματικών δεδομένων από τις εκτιμήσεις που δίνει το κάθε μοντέλο. Τα αποτελέσματα υποδεικνύουν ότι το Κυβικό μοντέλο υπερέχει ως προς την εκτίμηση ιστορικών δεδομένων, ενώ το μοντέλο Stanford "B" προβλέπει καλύτερα το ρυθμό παραγωγικότητας. Ως μελλοντική ερευνητική κατεύθυνση προτείνεται η επέκταση του πεδίου της έρευνας με την ενσωμάτωση περισσότερων μοντέλων καμπύλης μάθησης σε συνδυασμό με την ενίσχυση των δεδομένων πεδίου από άλλα, παρόμοιου τύπου, έργα.

Λέξεις κλειδιά Καμπύλη μάθησης, Επαναληπτική δραστηριότητα, Παραγωγικότητα, Στατιστική ανάλυση.

1 ΕΙΣΑΓΩΓΗ

Η εκτίμηση της παραγωγικότητας λαμβάνει υπόψη της διάφορους παράγοντες που αντικατοπτρίζουν τη φιλοσοφία της διοίκησης του έργου (Panas και Pantounakis 2010). Ένας από τους βασικούς παράγοντες παραγωγικότητας είναι η επαναληπτική φύση των κατασκευαστικών δραστηριοτήτων. Γι' αυτό το λόγο, η παρατηρούμενη βελτίωση της παραγωγικότητας σε επόμενους κύκλους παραγωγής για μία συγκεκριμένη επαναληπτική δραστηριότητα (π.χ. κατασκευή κτιρίου με πολλούς τυπικούς ορόφους) είναι συχνά απόρροια του φαινομένου της μάθησης που αναπτύσσεται μεταξύ των μέσων παραγωγής που απασχολούνται στο έργο (Pellegrino και Costantino 2018, Thomas κ.ά. 1986). Με άλλα λόγια, η παραγωγικότητα επαναληπτικών δραστηριοτήτων βελτιώνεται, όσο αυξάνεται η εμπειρία των απασχολούμενων συνεργείων.

Η θεωρία της καμπύλης μάθησης έχει δεχθεί κριτική κυρίως για την υπεραπλούστευση των συστημάτων που μελετούνται καθώς και για τη μονοδιάστατη εφαρμογή του ευθύγραμμου μοντέλου, που σχεδόν μονοπωλεί όλες τις σχετικές μελέτες παραγωγικότητας (Jarkas 2016, Jarkas και Horner 2011). Αυτό έχει ως αποτέλεσμα τον περιορισμό του πεδίου εφαρμογής των αποτελεσμάτων καθώς και των παραμέτρων που αποτυπώνονται στα άλλα μοντέλα μάθησης. Μέσα σε αυτό το πλαίσιο, γίνεται διερεύνηση και συγκριτική αξιολόγηση πέντε δημοσιευμένων και ευρέως αποδεκτών μοντέλων καμπύλης μάθησης για την ανάλυση λιμενικού έργου υποδομής μεγάλης κλίμακας, κάνοντας χρήση στοιχείων παραγωγικότητας με σκοπό τον προσδιορισμό: i) του βέλτιστου μοντέλου καμπύλης μάθησης για την προσαρμογή των ιστορικών δεδομένων παραγωγικότητας και ii) του βέλτιστου μοντέλου καμπύλης μάθησης για την πρόβλεψη του ρυθμού παραγωγικότητας. Είναι η πρώτη ερευνητική προσπάθεια που αναλύει με λεπτομέρεια την εφαρμογή μοντέλων καμπύλης μάθησης για την κατασκευή λιμενικών έργων υποδομής μέσα από το πρίσμα της παραγωγικότητας.

Η δομή της εργασίας είναι η εξής: Αρχικά, παρέχονται οι απαραίτητες πληροφορίες σχετικά με τον τύπο των μοντέλων καμπύλης μάθησης που επιλέχθηκαν. Στη συνέχεια, αναλύεται η ερευνητική μεθοδολογία, παρουσιάζονται τα αποτελέσματα της έρευνας και τέλος διατυπώνονται τα βασικά συμπεράσματα καθώς και οι προτάσεις για περαιτέρω διερεύνηση.

2 ΒΙΒΛΙΟΓΡΑΦΙΚΗ ΑΝΑΣΚΟΠΗΣΗ

2.1 Καμπύλη Μάθησης

Η θεωρία της καμπύλης μάθησης υποδεικνύει ότι ο απαιτούμενος χρόνος (εργατοώρες) για την παραγωγή μίας δομικής μονάδας μειώνεται ως ποσοστό του χρόνου που απαιτήθηκε για την παραγωγή της προηγούμενης μονάδας (Jarkas και Horner 2011). Το ποσοστό ονομάζεται ρυθμός μάθησης (learning rate) και χαρακτηρίζει την έκταση του φαινομένου της μάθησης για μία δραστηριότητα (Thomas κ.ά. 1986). Μαθηματικά, ο ρυθμός μάθησης ταυτίζεται με την κλίση της καμπύλης μάθησης. Όσο μικρότερη η τιμή του ρυθμού μάθησης, τόσο εντονότερο το φαινόμενο της μάθησης. Η θεωρία της καμπύλης μάθησης εφαρμόζεται για την εκτίμηση του απαιτούμενου χρόνου παραγωγής μίας μονάδας (π.χ. όροφος κτιρίου, χιλιόμετρο οδοποιίας) ή για τον υπολογισμό της αθροιστικής μέσης διάρκειας κατασκευής διαφορετικών ποσοτήτων μίας μονάδας (Everett και Farghal 1994). Η αθροιστική μέση διάρκεια υπολογίζεται ως το πηλίκο του συνολικού χρόνου που απαιτήθηκε για την κατασκευή ενός δεδομένου αριθμού μονάδων προς τον αριθμό των μονάδων που παρήχθησαν (Panas και Pantounakis 2014). Όταν χρησιμοποιείται η πρώτη κατηγορία δεδομένων, τότε η ανάλυση θεωρείται ότι εμπεριέχει μοναδιαία δεδομένα (unit data), ενώ όταν χρησιμοποιείται η δεύτερη κατηγορία δεδομένων, η ανάλυση εμπεριέχει αθροιστικά δεδομένα (cumulative data). Για λόγους περιορισμού χώρου, η παρούσα έρευνα περιορίζεται στη χρήση μοναδιαίων δεδομένων.

2.2 Μοντέλα Καμπύλης Μάθησης

Οι πέντε (5) τύποι μοντέλων καμπύλης μάθησης που εφαρμόστηκαν στην έρευνα είναι οι εξής (Everett και Farghal 1994, Srour κ.ά. 2016, Thomas κ.ά. 1986):

- Ευθύγραμμο μοντέλο (ή Wright): Είναι το πρώτο μοντέλο καμπύλης μάθησης και αναπτύχθηκε το 1936 από τον T. P. Wright για τον προσδιορισμό συντελεστών που επηρεάζουν το κόστος κατασκευής αεροσκαφών. Η ονομασία του προέρχεται από την ευθεία γραμμή που δημιουργείται όταν σχεδιαστεί σε λογαριθμική κλίμακα. Υποθέτει ότι ο ρυθμός μάθησης $L=2^n$, όπου n η κλίση της λογαριθμικής καμπύλης, είναι σταθερός σ' όλη τη διάρκεια της δραστηριότητας. Αποτελεί το πιο συχνά χρησιμοποιούμενο μοντέλο στις μελέτες παραγωγικότητας του κατασκευαστικού κλάδου λόγω της απλότητας του και της ικανότητάς του να παρέχει αποδεκτή ακρίβεια (Srour κ.ά. 2018).
- Μοντέλο Stanford "B": Είναι παραλλαγή του ευθύγραμμου μοντέλου με την προσθήκη ενός συντελεστή «B» ο οποίος εκφράζει την προηγούμενη εμπειρία του συνεργείου και κυμαίνεται μεταξύ 0-10. Για ένα άπειρο συνεργείο ισχύει ότι $B=0$, ενώ για ένα έμπειρο ισχύει ότι $4 < B < 10$.
- Κυβικό μοντέλο: Είναι ενίσχυση του ευθύγραμμου μοντέλου και υποθέτει ότι ο ρυθμός μάθησης μπορεί να αλλάξει με την πάροδο του χρόνου λόγω της επιρροής της προηγούμενης εμπειρίας και της εξισορρόπησης της παραγωγικότητας καθώς το έργο πλησιάζει στην ολοκλήρωσή του.
- Βαθμωτό μοντέλο: Αποτελεί γραμμική προσέγγιση του κυβικού μοντέλου με τρεις διακριτές φάσεις, κάθε μία με σταθερό ρυθμό μάθησης. Η πρώτη ονομάζεται φάση μάθησης όπου οι εργαζόμενοι αποκτούν γνώση του έργου και η παραγωγικότητα αυξάνεται με ταχείς ρυθμούς. Η δεύτερη αναφέρεται ως φάση ρουτίνας κατά την οποία επιτυγχάνεται σταδιακή βελτίωση της παραγωγικότητας, ενώ η τρίτη φάση ορίζεται ως η περίοδος της «τυπικής παραγωγικότητας» και συμβαίνει όταν ο ρυθμός παραγωγής σταματήσει να βελτιώνεται.
- Εκθετικό μοντέλο: Βασίζεται στην παραδοχή ότι μέρος του χρόνου ανά μονάδα είναι σταθερό ενώ το υπόλοιπο υπόκειται σε βελτίωση μέσω της επανάληψης. Το μέρος που

υπόκειται σε βελτίωση θα μειωθεί κατά το ήμισυ μετά από ένα σταθερό αριθμό μονάδων, που αναφέρεται ως "συντελεστής κατά το ήμισυ" και ο χρόνος ανά μονάδα θα προσεγγίσει σταδιακά μια τελική ή χαμηλότερη τιμή.

Οι μαθηματικές σχέσεις για την εκτίμηση της παραγωγικότητας με βάση τα προηγούμενα μοντέλα απεικονίζονται στον Πίνακα 1.

Πίνακας 1 Μαθηματικές σχέσεις εκτίμησης παραγωγικότητας για τα μοντέλα καμπύλης μάθησης

Μοντέλο	Μαθηματικές σχέσεις
Ευθύγραμμο	$Y = A * X^{-n}$ ή $\log Y = \log A - n * \log X$
Stanford "B"	$Y = A * (X + B)^{-n}$ ή $\log Y = \log A - n * \log (X + B)$
Κυβικό	$\log Y = \log A - b * \log X + C * (\log X)^2 + D * (\log X)^3$
Βαθμωτό	$\log Y = \log A - n_1 * \log X - n_2 * J_1 * (\log X - \log x_{p1}) - n_3 * J_2 * (\log X - \log x_{p2})$
Εκθετικό	$Y = Y_{ult} + \frac{A - Y_{ult}}{2 * X / H}$

Όπου (με σειρά εμφάνισης): Y=χρόνος ή ανθρωπόωρες ή κόστος μονάδας X; A=χρόνος ή ανθρωπόωρες ή κόστος πρώτης μονάδας; X=αριθμός μονάδων; n=κλίση της λογαριθμικής καμπύλης; B=προηγούμενη εμπειρία συνεργείου; b=κλίση της καμπύλης για την πρώτη μονάδα; C=τετραγωνικός παράγοντας; D=κυβικός παράγοντας; n₁=κλίση 1^{ης} φάσης; n₂,n₃=πρόσθετη κλίση 2^{ης} και 3^{ης} φάσης; x_{p1}=σημείο αλλαγής 1^{ης}-2^{ης} φάσης; x_{p2}= σημείο αλλαγής 2^{ης}-3^{ης} φάσης; J₁=1 όταν X>x_{p1}, αλλιώς 0 ; J₂=1 όταν X>x_{p2}, αλλιώς 0; Y_{ult}=τελικός χρόνος ανά μονάδα (ελάχιστη τιμή που μπορεί να φτάσει το Y); H=συντελεστής κατά το ήμισυ.

2.3 Διαδικασία κατασκευής κυβελωτών κιβωτίων οπλισμένου σκυροδέματος (caisson)

Τα caissons αναφέρονται στη βιβλιογραφία ως «πλωτά κιβώτια σκυροδέματος» (floating box caissons) και συνήθως κατασκευάζονται σε πλωτές αυτοβυθιζόμενες δεξαμενές. Επισημαίνεται ότι λόγω του τυποποιημένου σχήματος των caissons αλλά και της επαναληπτικής φύσης των εργασιών, αφού κατασκευάζονται συνήθως κατά ομάδες, η σκυροδέτησή τους γίνεται με χρήση ολισθαίνοντα μεταλλότυπου. Στη γενική περίπτωση, η σκυροδέτηση και η ολίσθηση του μεταλλότυπου περιλαμβάνει τρεις φάσεις (Εικόνα 1): i) συναρμολόγηση εξοπλισμού ολίσθησης, ii) ολίσθηση και iii) αποσυναρμολόγηση εξοπλισμού ολίσθησης. Για κάθε μία από αυτές τις φάσεις διαπιστώθηκε έντονη εκδήλωση του φαινομένου της μάθησης (Pantounakis και Panas 2013) του οποίου η περαιτέρω διερεύνηση ακολουθεί στις επόμενες παραγράφους.



Εικόνα 1 Κύκλος παραγωγής caisson

3 ΕΡΕΥΝΗΤΙΚΗ ΜΕΘΟΔΟΛΟΓΙΑ

Ένα λιμενικό έργο υποδομής μεγάλης κλίμακας αποτέλεσε τη μελέτη περίπτωσης για την έρευνα. Το έργο περιελάμβανε την κατασκευή 34 caissons και ολοκληρώθηκε το 2012 (Panas και Pantounakis 2018). Η μεθοδολογία είναι δισδιάστατη και γίνεται χρήση μοναδιαίων δεδομένων παραγωγικότητας. Πρώτον, για τον προσδιορισμό του βέλτιστου μοντέλου για την προσαρμογή των ιστορικών δεδομένων παραγωγικότητας, χρησιμοποιώντας το Solver του MS-Excel εφαρμόζεται η Μέθοδος των Ελαχίστων Τετραγώνων (MET), ώστε να προσδιοριστούν η βέλτιστη καμπύλη προσαρμογής και οι παράμετροι του κάθε μοντέλου. Το κριτήριο αξιολόγησης των μοντέλων για την προσαρμογή τους στα ιστορικά δεδομένα είναι ο συντελεστής προσδιορισμού του Pearson (R²) που κυμαίνεται στο

διάστημα [0,1], όπου το μηδέν υποδηλώνει καμία συσχέτιση και το ένα υποδηλώνει τέλεια συσχέτιση. Δεύτερον, για τον προσδιορισμό του βέλτιστου μοντέλου πρόβλεψης του ρυθμού παραγωγής, βάση της μεθόδου των Everett και Farghal (1994) τα δεδομένα χωρίζονται στη μέση. Τα πρώτα 17 caissons γίνονται τα ιστορικά δεδομένα, ενώ τα υπόλοιπα 17 είναι τα μελλοντικά. Η MET εφαρμόζεται για τα πρώτα 17 caissons και προσδιορίζεται η βέλτιστη καμπύλη προσαρμογής για κάθε μοντέλο. Στη συνέχεια, οι καμπύλες μάθησης επεκτείνονται, σύμφωνα με την εξίσωση της βέλτιστης καμπύλης, για τα δεδομένα από το 17^ο μέχρι το 34^ο caisson. Ο συντελεστής προσδιορισμού του Pearson (R^2) δεν ισχύει για τη συσχέτιση των σημείων της εκτεταμένης καμπύλης με τα πραγματικά δεδομένα και η ακρίβεια πρόβλεψης των μοντέλων αξιολογείται με βάση το στατιστικό δείκτη E_f που διατυπώθηκε από τους Everett και Farghal (1994) ειδικά για μοντέλα καμπύλης μάθησης (εξ. 1):

$$E_f = \frac{\sum_{i=1}^k \frac{|y'_{m+i} - y_{m+i}|}{y_{m+i}}}{k} * 100 \quad (1)$$

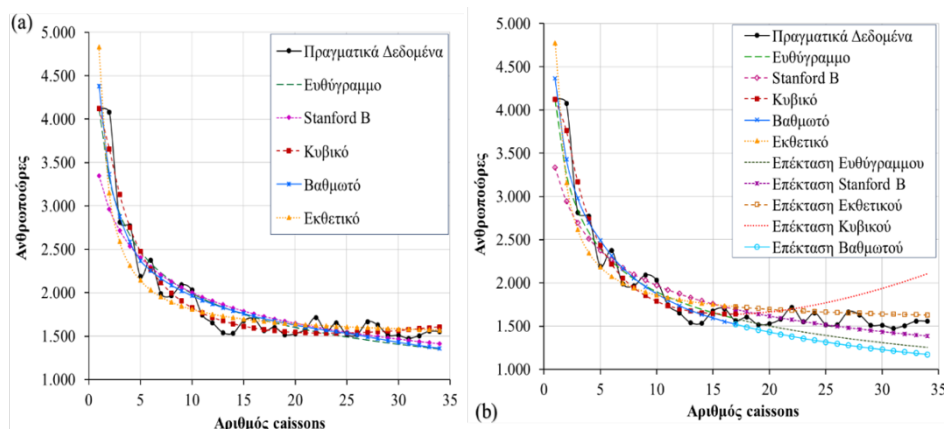
όπου: m = ο αριθμός των caissons που έχουν κατασκευαστεί, k = ο αριθμός των caissons που η παραγωγικότητα πρέπει να προβλεφθεί, y'_{m+i} = οι εκτιμώμενες τιμές παραγωγικότητας και y_{m+i} = οι πραγματικές τιμές παραγωγικότητας. Ο στατιστικός δείκτης E_f κυμαίνεται από 0%, που υποδεικνύει τέλεια συσχέτιση, σε μεγάλες θετικές τιμές που υποδεικνύουν καμία συσχέτιση.

4 ΑΠΟΤΕΛΕΣΜΑΤΑ

Ο Πίνακας 2 συνοψίζει την απόδοση κάθε μοντέλου για τις δύο περιπτώσεις και η Εικόνα 2 δίνει μια γραφική αναπαράσταση των αποτελεσμάτων. Όσον αφορά τον προσδιορισμό του βέλτιστου μοντέλου για την προσαρμογή ιστορικών δεδομένων παραγωγικότητας, διαπιστώνουμε ότι το κυβικό μοντέλο υπερέχει (Πίνακας 2). Το Εκθετικό μοντέλο δίνει τη λιγότερο ενοϊκή προσαρμογή, χωρίς όμως να είναι μη αποδεκτή, σε απόλυτες τιμές. Τα αποτελέσματα ενισχύουν την προγενέστερη έρευνα και υποδηλώνουν ότι το καλύτερο μοντέλο προσαρμογής εξαρτάται από τη θέση και τη φύση κάθε έργου. Συγκρίνοντας το Κυβικό και Βαθμωτό με το Ευθύγραμμο μοντέλο παρατηρούμε μια στατιστικά ασήμαντη διαφορά 2.51% και 0.43% αντίστοιχα ($p < 5\%$), γεγονός που επιβεβαιώνει την τάση του κατασκευαστικού κλάδου να χαρακτηρίζει το Ευθύγραμμο μοντέλο ως πιο "φιλικό προς το χρήστη" αφού δίνει αξιόπιστα αποτελέσματα απαιτώντας λιγότερες παραμέτρους και παραδοχές.

Πίνακας 2 Αποτελέσματα μοντέλων καμπύλης μάθησης για τα 34 caissons

Μοντέλο Καμπύλης Μάθησης	R^2	$R^2_{(0.17)}$	$E_f_{(0.34)} (\%)$
Ευθύγραμμο	0.9530	0.9629	11.33
Stanford "B"	0.9327	0.9626	5.75
Κυβικό	0.9781	0.9767	17.42
Βαθμωτό	0.9573	0.9628	16.21
Εκθετικό	0.9256	0.9096	6.87



Εικόνα 2 Καμπύλες μάθησης: α) Καμπύλες μάθησης για προσαρμογή ιστορικών δεδομένων, β) Καμπύλες μάθησης και εκτεταμένες καμπύλες μάθησης για πρόβλεψη ρυθμού παραγωγής

Όσον αφορά την ακρίβεια πρόβλεψης των μοντέλων για το ρυθμό παραγωγής (Πίνακας 2) το μοντέλο Stanford "B" έχει την καλύτερη απόδοση με δείκτη $E_{f(18-34)}=5.7\%$, που δεικνύει πολύ καλή συσχέτιση. Γενικά είναι αποδεκτό ότι το μοντέλο Stanford "B" προσομοιώνει με πολύπλοκες κατασκευαστικές διαδικασίες, ειδικά σε έργα μεγάλης κλίμακας. Το Κυβικό και Βαθμωτό μοντέλο έχουν τους μεγαλύτερους δείκτες $E_{f(18-34)}$. Παρόλο που οι τιμές είναι αποδεκτές, οι εκτεταμένες καμπύλες τους μετά το 25^ο caisson (Εικόνα 2b) υποδηλώνουν μία σημαντική τάση αύξησης για το Κυβικό και μία έντονη τάση «βύθισης» για το Βαθμωτό. Αμφότερες οι καμπύλες, σηματοδοτούν κίνδυνο παραγωγής μη ρεαλιστικών αποτελεσμάτων για επέκταση του πεδίου τιμών τους εκτός του δείγματος των 34 caissons. Το Κυβικό και Βαθμωτό μοντέλο επιβεβαιώνουν την άποψη των Everett και Farghal (1994) ότι είναι κακοί προγνωστικοί δείκτες, όπου διαπίστωσαν παρόμοιες αδυναμίες σε οικοδομικά έργα.

5 ΣΥΜΠΕΡΑΣΜΑΤΑ

Η έρευνα απέδειξε ότι το φαινόμενο της μάθησης ήταν έντονο κατά την κατασκευή των caissons, με αποτέλεσμα να εμφανιστεί σημαντική βελτίωση στην παραγωγικότητα. Από τις περίπου 4,000 εργατοώρες/caisson για τα πρώτα 2 caissons, το έργο ολοκληρώθηκε με μέση παραγωγικότητα περίπου 1,500 εργατοώρες/caisson. Τα πέντε μοντέλα καμπύλης μάθησης που αναλύθηκαν, όσο αφορά την περίπτωση της προσαρμογής τους στα ιστορικά δεδομένα παραγωγικότητας, είχαν συντελεστή προσδιορισμού $R^2>0.9$, που υποδηλώνει αρκετά υψηλό βαθμό συσχέτισης με τα πραγματικά δεδομένα πεδίου. Το Κυβικό μοντέλο αποδείχθηκε το καταλληλότερο, ενώ το Εκθετικό είχε τη μικρότερη ακρίβεια. Αντίστοιχα, στην περίπτωση της πρόβλεψης του ρυθμού παραγωγικότητας, το μοντέλο Stanford "B" βρέθηκε να είναι ο καλύτερος προγνωστικός δείκτης, με το Εκθετικό και Ευθύγραμμο μοντέλο να δίνουν επίσης πολύ καλές προβλέψεις. Σε κάθε περίπτωση, είναι αδιαμφισβήτητο γεγονός πως η εφαρμογή της θεωρίας της καμπύλης μάθησης σε λιμενικό έργο υποδομής μεγάλης κλίμακας αποτελεί ένα χρήσιμο εργαλείο, τόσο για την αποτίμηση όσο και για την εκτίμηση της παραγωγικότητας ιδιαίτερα σύνθετων και πολύπλοκων κατασκευαστικών δραστηριοτήτων, που συμβάλλει στη σωστή λήψη αποφάσεων που σχετίζονται με χρονικές και κοστολογικές παραμέτρους του έργου. Πιθανές επεκτάσεις της έρευνας θα μπορούσαν να αποτελέσουν η ενσωμάτωση και άλλων μοντέλων της βιβλιογραφίας και ο εμπλουτισμός της βάσης δεδομένων πεδίου με περισσότερες δραστηριότητες κατασκευής με έντονο το στοιχείο της μάθησης.

Βιβλιογραφικές Αναφορές

- Everett JG, Farghal S, (1994) Learning curve predictors for construction field operations. J Constr Eng M ASCE 120(3):603–616.
- Jarkas A (2016) Learning effect on labour productivity of repetitive concrete masonry blockwork: Fact or fable? International Journal of Productivity and Performance Management 65(8):1075-1090.
- Jarkas A, Horner M (2011) Revisiting the applicability of learning curve theory to formwork labour productivity. Constr Manage Econ 29(5):483-493.
- Panas A, Pantouvakis JP (2010) Evaluating research methodology in construction productivity studies. The Built and Human Environment Review 3(1):63-85.
- Panas A, Pantouvakis JP (2014) Simulation-based and statistical analysis of the learning effect in floating caisson construction operations. J Constr Eng M ASCE 140(1). doi:04013033
- Panas A, Pantouvakis JP (2018) On the use of learning curves for the estimation of construction productivity. International J Constr M doi: 10.1080/15623599.2017.1326302
- Pantouvakis JP, Panas A (2013) Computer simulation and analysis framework for floating caisson construction operations. Autom. Constr. 36:196-207.
- Pellegrino R, Costantino N (2018) An empirical investigation of the learning effect in concrete operations. Engineering, Construction and Architectural Management 25(3):342-357.
- Srouf FJ, Kiomjian D, Srouf IM (2016). Learning curves in construction: a critical review and new model. J Constr Eng M ASCE 142(4). doi: 10.1061/(ASCE)CO.1943-7862.0001515.
- Srouf FJ, Kiomjian D, Srouf IM (2018). Automating the Use of Learning Curve Models in Construction Task Duration Estimates. J Constr Eng M ASCE 144(7). doi:04018055
- Thomas HR, Mathews CT, Ward JG (1986) Learning curve models of construction productivity. J Constr Eng M ASCE 112(2):245-259.

Construction Environmental Management Plan (CEMP) for the installation of the 120 m floating dock ERENEOS, at Limassol Port

M.I. Loizides, D. Petsa, D.L. Orthodoxou, X.I. Loizidou *

ISOTECH LTD Environmental Research and Consultancy, P.O. Box 14161, Nicosia, 2154, Cyprus

*Corresponding author: xenia@isotech.com.cy

Abstract

Multimarine Shipyards Ltd has embarked upon a project to install a 120 m long floating dock at the Limassol Port. For the implementation of this project, a preparatory construction phase was mandatory and included: (1) the dredging of 25,000 m³ of material from the existing inclined sea-bed level to the level of -13.2 m from the Mean Low Water Still Sea Level (2) the construction of a 42 m long deck of a total area of 1,000 m² and the driving of two piles, to facilitate the mooring of the floating dock. This paper provides an overview of the development and implementation of a Construction Environmental Management Plan (CEMP) for the installation of the 120 m floating dock ERENEOS, at Limassol Port in Cyprus.

Keywords CEMP, Floating dock, Monitoring, Marine Good Environmental Status

1 INTRODUCTION

The Cyprus Ship Registry is one of the largest in the world and the third largest in the European Union. Cyprus is considered to be the largest Ship-management Centre in the EU and among the three largest globally (Cyprus Shipping Chamber, 2018). The wider shipping sector in Cyprus employs 4,500 employees ashore and 55,000 seafarers. Shipping constitutes one of the most active and profitable sectors of the economy, estimated at 7% of GOP (Cyprus Shipping Chamber, 2018). According to the International Convention for the Safety of Life at Sea (IMO, 1974) for all merchant vessels a minimum of two inspections of the ship's hull are required during any five year period, and the interval between any such two inspections should not be greater than 36 months. Although these inspections can happen while the vessel is in water, it is much easier, and more common, to perform them at dry docks.

In the last few years, hydrocarbon exploration activities in Cyprus's Exclusive Economic Zone have soared and several international energy companies are active in the area, including Noble Energy, ENI and Total (Deloitte, 2018). Massive discoveries of hydrocarbons in Egyptian and Israeli waters are also being investigated leading to a boom in the presence and growth of the oil and gas industry on the island. The exploration activities are supported by significant infrastructure, including vessels that require maintenance and repairs in nearby ports.

To better serve the needs of the Cypriot shipping industry and the growing oil and gas sector in the Eastern Mediterranean, Multimarine Ltd, a Cypriot company that operates at Limassol Port and specializes in mechanical and marine engineering services to the Marine, Power, and Oil and Gas industries, decided to invest in infrastructure that would provide dry docking services to vessels up to 7100 tonnes. A floating dock design was selected as it has several advantages over alternatives, which include inter alia the fact that (i) it does not require waterfront space, (ii) it can be constructed offsite anywhere in the world where there is expertise, and this makes its acquisition financially preferable as it can be constructed by the lowest bidder, (iii) it has a resale value as it can be sold anywhere in the world, and (iv) it can accommodate vessels that are longer than the dry dock itself (Heger, 2005).

The 'ERENEOS', as the Multimarine dry dock is called, was therefore constructed in the Ukraine by Pallada Ltd and delivered to Cyprus in January 2018. In accordance to relevant legislation (RoC, 2005), an Environmental Impact Assessment was implemented and a relevant Environmental Permit was received by the Department of Environment of the Cypriot Ministry of Agriculture. Additionally, and above the legislative requirements, Multimarine requested ISOTECH to prepare a Construction Environmental Management Plan (CEMP) to ensure that any environmental risks during the

construction of the necessary infrastructure for the installation of the floating dock would be minimized, and to put in place procedures to swiftly mitigate any environmental impacts. This paper provides an overview of the preparation and the implementation of the developed Construction Environmental Management Plan (CEMP).

2 METHOD: DEVELOPMENT OF THE CEMP

Prior to the installation of the ERENEOS Floating Dock several preparatory construction activities had to be implemented, specifically:

- Dredging of 25,000 m³ from the existing inclined sea-bed level to the level of -13.2 m from the Mean Low Water Still Sea Level (Figure 1).
- Construction of an underwater sheet pile wall to form a vertical retention front of the slopes of the excavations.
- Construction of a 42 m long deck and of a total area of 1,000 m².
- Installation of a gangway to provide access to the deck.
- Two exploratory drills and subsequent evaluation prior to the pile-driving.
- Driving of two piles to facilitate the mooring of the dock.

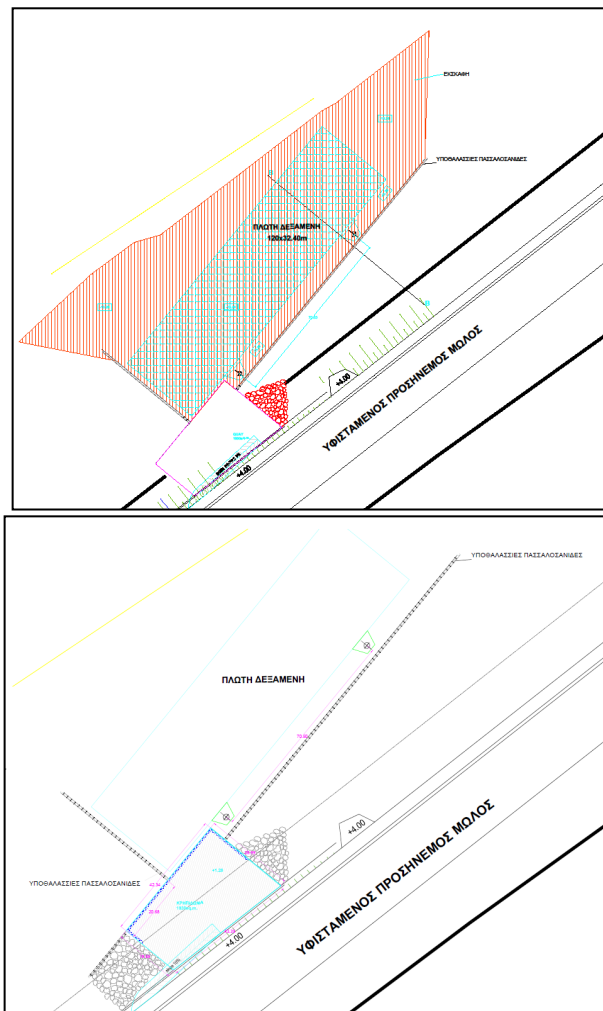


Figure 1 Left: Schematic of the planned dredging area (orange striped area). Right: Layout of the deck construction area (blue frame)

2.1 CEMP Scope of Work

This CEMP is a risk management tool, which has been developed to:

- Provide measures to avoid, minimize, and mitigate potential adverse environmental impacts associated with the proposed construction works.
- Identify roles and responsibilities of key personnel responsible for the implementation of the CEMP.
- Provide guidance for the monitoring, measuring, and reporting of environmental performance of all environmental aspects during the construction phase of the Project.

2.2 Environmental Control Plans

An evaluation of the foreseen construction activities, in combination with the environmental baseline at Limassol Port, the outcomes of the Environmental Impact Assessment (ISOTECH, 2017), and the terms of the Environmental Permit by the Cypriot Department of Environment (2017) identified that during the project's construction phase there was the potential for several activities to negatively impact the environment, for example by causing significant vibrations and noise, using limited natural resources, emitting dust etc. For each environmental aspect that could be impacted, an Environmental Control Plan (ECP) was developed. The ECPs are short (2-3 page), stand-alone documents that, for each of the potential environmental impacts, outline the mitigation/ prevention objectives and the relevant legal obligations, and assign roles and responsibilities for monitoring, reporting and the implementation of mitigation measures. The structure of each ECP appears in Table 1. The seven resulting ECPs were developed to facilitate the proper implementation of the CEMP by ensuring that busy staff are able to have a quick and clear reference document regarding concrete mitigation and, if necessary, corrective actions that they have to implement:

- ECP-001: Noise and Vibration
- ECP-002: Waste Management
- ECP-003: Air Quality- Dust Emission
- ECP-004: Use of Natural Resources
- ECP-005: Landscape and Visual
- ECP-006: Heavy Vehicles Requirements
- ECP-007: Emergency Response

Table 1 Structure of the Environmental Control Plans

ECP Section	Description of Content
Objectives	Goals for each ECP
Legal Limits	Deriving from EU/ National law and/or Environmental Approval
Relevant Literature	List of relevant laws and EIA referrals
Responsible Staff	Person responsible to identify potential impacts and non-conformances to undertake appropriate action
Monitoring	Monitoring requirements for the duration of the Project
Reporting	Responsibilities, format and frequency for reporting
Mitigation Measures	Provides a summary of how environmental objectives are to be achieved through practical actions
Corrective Action	Actions to be undertaken should limits and targets be exceeded
Equipment	Equipment needed to implement mitigation measures

2.3 CEMP Structure

The main sections of the CEMP document appear in Table 2. Two noteworthy aspects of the CEMP are the assignment of roles and responsibilities and the development of a communications procedure for all environmental issues during the project's construction phase. Roles and responsibilities were assigned to the Project Owner (i.e. Multimarine's Top Management), the Project Manager, the

Construction Manager, the site workers, general subcontractors and the Environmental Subcontractor (i.e. ISOTECH Ltd). Awareness-raising and training responsibilities for site workers and other key personnel were clearly defined within this section of the CEMP and an accompanying training schedule was drafted. The Communication Protocol included within the CEMP related particularly to communication of environmental issues arising during the construction phase, including the communication procedures in case of an environmental incident or emergency.

Table 2 CEMP Structure

Section Title	Description of Content
Project Description	Description of the Project.
Existing Environment and Construction Activities	Existing environment at the Project site and a description of the proposed construction works.
Legislative and Regulatory Requirements	Relevant legislative and regulatory requirements to the Project.
Potential Environmental Impacts	Potential impacts of construction on the existing environment.
Environmental Control Plans	Environmental Control Plans (ECP) on mitigation measures and monitoring requirements for every environmental impact.
Implementation of CEMP	How the CEMP will be implemented and specifies roles and responsibilities of concerned personnel.
Environmental Monitoring Procedure	The environmental monitoring programme to be followed.
Environmental Incident and Emergency Management Procedure	Details the protocol to be followed in the event of an incident or emergency.

3 CEMP IMPLEMENTATION: MONITORING AND REPORTING

The implementation of the CEMP consisted in the regular monitoring and reporting of the project’s environmental performance (Table 3). Specifically, the subcontractor responsible for the construction activities completed Daily Environmental Inspection Checklists (Figure 2), which were collected and reviewed on a weekly basis by Multimarine’s Project Manager. An external audit, including a site walkthrough, was carried out by ISOTECH Ltd on a monthly basis. The audit aimed to gather information on all the potential environmental aspects of the project, and specifically those relating to the Environmental Permit by the Department of Environment. The scope of the audit included, inter alia:

- Status of construction work and site activities.
- The environmental impacts and risks.
- Environmental monitoring programme and management plan; and the overall implementation status.
- Adequacy and effectiveness of the implementation of the proposed environmental controls (through Incident Reporting Form, Corrective Action Request etc.).
- Overall environmental monitoring results.
- Reporting of environmental incidents, complaints, accidents, and emergency.
- Status of closing out all non-conformances and corrective actions.
- Material usage, waste generation and disposal records.
- Environmental training records.
- Environmental complaints.
- Any other environmental issues arise from the implementation of this CEMP.

Question		Yes	No	Partial	Comments- Additional Information
Air and Dust					
1.	Is the site dusty?				
2.	Observation of any air polluting emissions from site relevant activities-sources?				
3.	Observation of any dust emissions from site relevant activities?				
4.	What is the Mean Air speed?				
5.	Presence of gusts or air speeds over 4 beaufort?				
6.	Formation of new piles?				
7.	Any action on piles and roads to minimize fugitive dust?				
8.	Presence of any uncovered vessel or container?				
9.	Any overfilling of vehicles during transportation of bulk materials?				
10.	Water reservoir full and water dispersion system operating properly?				
11.	Are all vehicles covered during transportation of aggregates?				
Noise					
12.	Any operation with excess noise?				
13.	Any noisy activity outside working hours (7:00am -5pm)?				
Waste Management					
14.	Bins and skips present for all waste streams?				
15.	All bins and skips covered, in good condition and with enough space for next day?				
16.	Any Wastes outside designated areas?				
Community Annoyance					
17.	Any environmental related complain from third party?				
Training					
18.	Any special need for training/informative note based on the work of the day?				
19.	Daily briefing for each phase of the project, regarding dust and noise emission, waste management, accident prevention and procedure?				

Figure 2 Daily Inspection Checklist

Table 3 Summary of CEMP Monitoring and Reporting Requirements

Report	Frequency	Responsibility
Daily Inspection Checklist	Daily	Construction Subcontractor
File with Daily Inspection Checklists	Weekly	Project Manager
External Audit	Monthly	ISOTECH Ltd
Waste Management Register (transfer notes)	Whenever waste leaves site	Project Manager
Induction and Training Log	Prior to personnel starting activities on site	Construction Subcontractor
Environmental Incident Report	When a significant incident occurs on site	Construction Subcontractor
Corrective Action Request	When a significant incident occurs on site	Construction Subcontractor

The development and implementation of the CEMP not only secured the environmentally responsible performance of the construction activities necessary for the installation of the ERENEOS floating dock, but also provided Multimarine with a proof of environmental performance, which could be provided to the relevant authorities at any time upon request. It could therefore act as a ‘best practice’ example to be replicated and applied in all construction activities that have the potential to significantly impact the environmental status of sensitive receivers.

References

- Cyprus Shipping Chamber (2018) Annual Report 2017. Limassol, Cyprus
- Deloitte (2018) Oil & Gas in Cyprus: Where Potential Lies. https://www2.deloitte.com/content/dam/Deloitte/cy/Documents/energy-resources/oil-and-gas/CY_EnergyAndResources_OilAndGas_Noexp.pdf
- Department of Environment (2017) Environmental Approval 167/8, 93A/16, 80/7, 154/2. [http://www.moa.gov.cy/moa/environment/environmentnew.nsf/All/DB2EDED0367B001FC22580F1003BED69/\\$file/GN20170560101.pdf?OpenElement](http://www.moa.gov.cy/moa/environment/environmentnew.nsf/All/DB2EDED0367B001FC22580F1003BED69/$file/GN20170560101.pdf?OpenElement)
- Heger R (2005) Dockmaster Training Manual. Heger Dry Dock, Inc. http://www.hegerdrydock.com/dockmaster_training_manual.pdf
- IMO (1974) International Convention for the Safety of Life at Sea (SOLAS), 1974. [http://www.imo.org/en/About/Conventions/ListOfConventions/Pages/International-Convention-for-the-Safety-of-Life-at-Sea-\(SOLAS\),-1974.aspx](http://www.imo.org/en/About/Conventions/ListOfConventions/Pages/International-Convention-for-the-Safety-of-Life-at-Sea-(SOLAS),-1974.aspx)
- ISOTECH (2017) EIA for the construction of a 42 m long deck and the installation and operation a floating dock at the Limassol Port, by Multimarine Shipyards Ltd. Nicosia, Cyprus. [http://www.moa.gov.cy/moa/environment/environmentnew.nsf/All/DB2EDED0367B001FC22580F1003BED69/\\$file/MP20170560101.pdf?OpenElement](http://www.moa.gov.cy/moa/environment/environmentnew.nsf/All/DB2EDED0367B001FC22580F1003BED69/$file/MP20170560101.pdf?OpenElement)
- Republic of Cyprus (2005) Law N(140(I)/2005-2014 of the Republic of Cyprus for the Environmental Impact Assessments of certain projects.

Acknowledgements

The authors would like to thank the Multimarine Group and especially Mr. Ereneos Phokas, Mr. Pavlos Phokas and Mr. Angelos Phokas.

Operational Environmental Management Plan (OEMP) for the 120m floating dry dock ERENEOS, Multimarine Shipyards, Limassol Port

M.I. Loizides, D. Petsa, D.L. Orthodoxou, X.I. Loizidou*

ISOTECH LTD Environmental Research and Consultancy, P.O. Box 14161, Nicosia, 2154, Cyprus

*Corresponding author: xenia@isotech.com.cy

Abstract

Multimarine Shipyards Ltd has successfully installed a 120m long Floating Dry Dock named 'ERENEOS' at Limassol Port in Cyprus. The Floating Dock, class ABS accredited, was constructed in the Ukraine in 2017 by the company Pallada Ltd and delivered to Cyprus in January 2018. The dock provides Multimarine with the ability to offer Vessel Dry docking Services. Several environment related studies (carried out by ISOTECH Ltd) have been completed prior to the installation of the dock at Limassol Port: Environmental Impact Assessment (EIA), an Environmental Permit, Construction Environmental Management Plan (CEMP) for the preparatory construction phase i.e. dredging, construction of a deck and of the two piles to facilitate the mooring of the floating dock. Multimarine Shipyards commissioned ISOTECH to prepare an Operational Environmental Management Plan (OEMP), a dynamic management system that identifies the environmental risks and legal obligations associated with the day to day operations of the Dock and specifies the management measures Multimarine will implement in order to prevent or minimise the environmental impacts associated with these operations, including guidance for the monitoring, measuring, and reporting of environmental performance during the operations. This is the first OEMP ever implemented in Cyprus. This paper provides an overview of the implementation of the OEMP for the day to day operating activities of the Floating Dry Dock 'ERENEOS' for the first year of its operation.

Keywords OEMP, Environmental risk, Shipyards, Mitigate environmental impacts

1 INTRODUCTION

In 2018, Multimarine Ltd, a Cypriot company that operates at Limassol Port and specializes in mechanical and marine engineering services to the Marine, Power, and Oil and Gas industries, decided to invest in infrastructure that would provide dry docking services to vessels up to 7100 tonnes. A floating dock design was selected as it has several advantages over alternatives, which include inter alia the fact that (i) it does not require waterfront space, (ii) it can be constructed offsite anywhere in the world where there is expertise, and this makes its acquisition financially preferable as it can be constructed by the lowest bidder, (iii) it has a resale value as it can be sold anywhere in the world, and (iv) it can accommodate vessels that are longer than the dry dock itself (Heger, 2005). This decision of Multimarine was based to better serve the needs of the Cypriot shipping industry and the growing oil and gas sector in the Eastern Mediterranean,

The 'ERENEOS', as the Multimarine dry dock is called, was therefore constructed in the Ukraine by Pallada Ltd and delivered to Cyprus in January 2018. In accordance to relevant legislation (RoC, 2005), an Environmental Impact Assessment was implemented and a relevant Environmental Permit was received by the Department of Environment of the Cypriot Ministry of Agriculture. Additionally, and above the legislative requirements, Multimarine requested ISOTECH to prepare a Construction Environmental Management Plan (CEMP) to ensure that any environmental risks during the construction of the necessary infrastructure for the installation of the floating dock would be minimized, and to put in place procedures to swiftly mitigate any environmental impacts. Once the construction/ installation phase was completed, Multimarine commissioned ISOTECH Ltd to prepare an Operations Environmental Management Plan, used to monitor and report on all relevant environmental parameters during the operation of 'ERENEOS' in order to prevent or minimise the environmental impacts associated with these operations, including guidance for the monitoring, measuring, and

reporting of environmental performance during the operations. This paper provides an overview of the implementation of the OEMP for the day to day operating activities of the Floating Dry Dock 'ERENEOS' for the first year of its operation.

2 METHOD: DEVELOPMENT OF THE OEMP

The 'ERENEOS' floating dock, which has been installed at the southeast basin of Limassol Port in Cyprus, is 120m long and 32m wide. It is U-shaped and made up of a reinforced concrete dock and two steel side walls (Figure 1).

The operating activities on the dock include the following:

- Tank Cleaning Works (Ballast Tanks, Fuel Oil Tanks, Diesel Oil Tanks, Lub Oil Tanks)
- Rudder, Propeller, Tailshaft Inspection and Maintenance
- Deck Machinery (Valves, Pumps, Winches) Overhaul and Repair
- Hull Blasting/Painting (Topsides, Vertical Sides/Boottop/Rudder Blade, Flat Bottom)
- High Pressure Water Cleaning/Washing
- Hand Scraping
- Paint Application by Rollers and/or Airless Spray
- Sea Chests Maintenance
- Anodes Renewal
- Anchor Chains Maintenance
- Chain Lockers Maintenance
- Cargo/Slop Tanks – Coating Repair
- Steel Plates and Pipes Renewal
- Welding Repairs
- Non-Destructive Testing
- Main Engine and Auxiliary Engines Overhaul



Figure 1 Floating Dock ERENEOS Installed at the Limassol Port

An evaluation of the foreseen activities, in combination with the environmental baseline at Limassol Port, the outcomes of the Environmental Impact Assessment (ISOTECH, 2017) and an extensive literature review on the main environmental impacts of the operation of floating docks and ship-repair activities in general (e.g. Hayman et al., 2000; Papaioannou, 2004) identified that the operation of ERENEOS could have the following environmental impacts:

- Noise emissions, particularly as it regards the operation of wet grit blasting for the cleaning of vessels hulls, steel/metal cutting operations and the operation of cranes.
- Increased water consumption due to hull cleaning operations taking place on the dock.
- Marine pollution by liquid wastes such as paints, solvents, oils, lubricants, fuel, and sludge.

- Marine pollution by solid wastes deriving from the various activities on the dock, such as empty paint cans, oily rags etc.
- Air pollution as it regards the emission of particles resulting from wet grit blasting operations, the emission of particles during painting activities and the emission of metals and gases during cutting and welding.
- Light pollution during night-time works.

2.1 OEMP Scope of Work

Following the identification of the main environmental impact risks from the operation of ERENEOS, the Operation Environmental Management Plan (OEMP) was developed as a dynamic management system that:

- Provides measures to avoid, minimize, and mitigate potential adverse environmental impacts associated with the operation of the Floating Dock, taking into consideration all permit terms and other legal requirements.
- Identifies roles and responsibilities of key personnel responsible for the implementation/application of the OEMP.
- Provides guidance for the monitoring, measuring, and reporting of environmental performance of all environmental aspects during operations.

2.2 Assignment of Responsibilities

A key aspect of the OEMP's development was the clear definition of roles and responsibilities as it regards the environmental performance of the 'ERENEOS', so that each key member of staff could know at any one time what they are responsible for. Specifically, roles and responsibilities were assigned to the Project Owner (i.e. Multimarine's Top Management), the Health, Safety and Environment Officer, the Dock Master, the site workers, general subcontractors and the Environmental Subcontractor (i.e. ISOTECH Ltd). Responsibilities for training of site workers and other key personnel were clearly defined within this section of the OEMP and an accompanying training schedule was drafted. Roles and procedures for responding to environmental incidents and emergencies were also developed at this stage.

2.3 Environmental Control Plans

A total of seven Environmental Control Plans (ECP) were developed, one for each of the main potential environmental impacts of the floating dock's operation:

- ECP-001: Noise
- ECP-002: Water Management
- ECP-003: Fluid Waste Management
- ECP-004: Solid Waste Management
- ECP-005: Air Quality
- ECP-006: Light Pollution
- ECP-007: Emergency Response.

The ECPs are short (2-3 page), stand-alone documents that, for each of the potential environmental impacts, outline the mitigation/ prevention objectives and the relevant legal obligations, and assign roles and responsibilities for monitoring, reporting and the implementation of mitigation measures. The structure of each ECP appears in Table 1. The ECPs were developed to facilitate the proper implementation of the OEMP by ensuring that busy staff are able to have a quick and clear reference document regarding concrete mitigation and, if necessary, corrective actions that they have to implement.

Table 1 Structure of the Environmental Control Plans

ECP Section	Description of Content
Objectives	Goals for each ECP
Legal Limits	Deriving from EU/ National law and/or Environmental Approval
Relevant Literature	List of relevant laws and EIA referrals
Responsible Staff	Person responsible to identify potential impacts and non-conformances to undertake appropriate action
Monitoring	Monitoring requirements for the duration of the Project
Reporting	Responsibilities, format and frequency for reporting
Mitigation Measures	Provides a summary of how environmental objectives are to be achieved through practical actions
Corrective Action	Actions to be undertaken should limits and targets be exceeded
Equipment	Equipment needed to implement mitigation measures

3 OEMP OUTPUTS: MONITORING AND REPORTING

The OEMP defines procedures for the regular and consistent monitoring of the operation of ERENEOS to ensure that any environmental risks are avoided or, if necessary, mitigated (Table 2). One of the main concerns of the Permitting Authority (i.e. Department of Environment), and in fact one of the points with the greatest environmental impact potential, is the submergence of the dock for the docking and undocking of vessels. If the floating dock is not properly cleaned before submergence hazardous wastes (e.g. metal grindings, paints, solvents or lubricants) could be released in the marine environment. The developed checklists, and specifically the 'Before Submergence' checklist (Figure 2), ensure that all the necessary steps are implemented prior to the submergence of the dock and thus all potential releases in the marine environment are avoided.

Table 2. OEMP Reporting Schedule

Report	Frequency	Form
Daily Inspection Checklists	Daily	Checklist
Other Inspection Checklists	As required	Checklist
File with all Inspection Checklists	Monthly	Report
Monthly External Audit	Monthly	Report
Waste Management Register	All waste leaving Dock	Waste waybill
Water Consumption Register	Monthly	Report
Induction and Training Log	Prior to start of activities	Log Book
Environmental Incident Report	When incident occurs	Incident report
Corrective Action Request	When CAR is issued	CAR Form

Further to the monitoring and reporting required by Multimarine staff, monthly external audits are implemented by ISOTECH's environmental experts, adding an additional level of control to the performance of the ERENEOS. The OEMP has also been seamlessly integrated in Multimarine's ISO14001:2015 certification.

Question	Yes	No	Partial	Comments- Additional Information	Environmental Approval Conditions Met
Optical observation along the platform					
1					EAC 1 (essential condition), EAC 3
2					EAC 1 (essential condition), EAC 3
3					EAC 1 (essential condition), EAC 3
4					EAC 1 (essential condition), EAC 3
5					EAC 1 (essential condition), EAC 3
6					
7					
8					
9					
10					
Additional Comments / Observations:					

Figure 2 Extract from the ‘Before Submergence’ Checklist used by Multimarine

The OEMP provides Multimarine with a proof of performance:

1. The OEMP secures the environmentally responsible performance of the dock, the monitoring and reporting requirements of the permitting authorities through a “real-time” monitoring structure
2. Through the OEMP, Multimarine can provide any documents/data to the relevant authorities at any time upon request.
3. The OEMP provides traceability of possible pollutants in a shared environment such as a harbour. In a harbour several activities take place and it is of high importance to identify who is responsible in case of environmental accidents. With a system such as the OEMP in place, the company can proof whether it is responsible or not for an accident.

The Operation Environmental Management Plan is a pro-active tool, a policy decision of any company that wants to secure proof of good environmental performance and at the same time boost its accountability to the competent authorities and the general public.

References

- Cyprus Shipping Chamber (2018) Annual Report 2017. Limassol, Cyprus
- Deloitte (2018) Oil & Gas in Cyprus: Where Potential Lies. https://www2.deloitte.com/content/dam/Deloitte/cy/Documents/energy-resources/oil-and-gas/CY_EnergyAndResources_OilAndGas_Noexp.pdf
- Hayman B, Dogliani M, Kvale I, Magerholm Fet A (2000) Technologies for reduced environmental impact from ships – Ship building, maintenance and dismantling aspects. <http://www.iot.ntnu.no/users/fet/Konferanser/2000-Treship-Newcastle.pdf>
- Heger R (2005) Dockmaster Training Manual. Heger Dry Dock, Inc. http://www.hegerdrydock.com/dockmaster_training_manual.pdf

- IMO (1974) International Convention for the Safety of Life at Sea (SOLAS), 1974.
[http://www.imo.org/en/About/Conventions/ListOfConventions/Pages/International-Convention-for-the-Safety-of-Life-at-Sea-\(SOLAS\),-1974.aspx](http://www.imo.org/en/About/Conventions/ListOfConventions/Pages/International-Convention-for-the-Safety-of-Life-at-Sea-(SOLAS),-1974.aspx)
- ISOTECH (2017) EIA for the construction of a 42 m long deck and the installation and operation a floating dock at the Limassol Port, by Multimarine Shipyards Ltd. Nicosia, Cyprus
- Papaioannou D (2004) Environmental implications, related to the shipbuilding and ship repairing activity in Greece. Pomorski zbornik 41(1): 241-252.
- Republic of Cyprus (2005) Law N(140(I)/2005-2014 of the Republic of Cyprus for the Environmental Impact Assessments of certain projects.

Acknowledgements

The authors would like to thank the Multimarine Group and especially Mr. Ereneos Phokas, Mr. Pavlos Phokas and Mr. Angelos Phokas.

Σχεδιασμός λιμενικών και χερσαίων υποδομών για την τροφοδοσία πλοίων με Υ.Φ.Α. (ING Bunkering) στο νότιο λιμένα Πατρών

Α.Μ. Μπουτάτης*, Χ.Δ. Σολομωνίδης, Π.Α. Μπινίσκος, Μ.Ν. Καλπύρη

Ρογκάν & Συνεργάτες, Βαλέττα 9, Τ.Κ. 15771 Αθήνα, Ελλάδα

*Υπεύθυνος επικοινωνίας: aboutatis@roganassoc.gr

Περίληψη

Η παρούσα μελέτη συντάχθηκε από την εταιρία ΡΟΓΚΑΝ ΚΑΙ ΣΥΝΕΡΓΑΤΕΣ Α.Ε. στα πλαίσια του προγράμματος «Poseidon Med II» και αφορά στο σχεδιασμό των απαραίτητων λιμενικών και χερσαίων υποδομών στο νότιο (Νέο) λιμένα Πατρών ώστε να φιλοξενήσει μικρής κλίμακας εγκαταστάσεις τροφοδοσίας και αποθήκευσης Υγροποιημένου Φυσικού Αερίου (Υ.Φ.Α.), την πρώτη που υλοποιείται στον ελλαδικό χώρο. Εκπονήθηκε, επιπλέον, η απαραίτητη για την περιβαλλοντική αδειοδότηση των έργων Μελέτη Προκαταρκτικού Προσδιορισμού Περιβαλλοντικών Απαιτήσεων (Π.Π.Π.Α.), κατά την οποία εξετάστηκαν οι επιπτώσεις των προτεινόμενων έργων, στο περιβάλλον τόσο κατά τη διάρκεια κατασκευής όσο και κατά τη διάρκεια λειτουργίας τους. Στα πλαίσια της μελέτης εκπονήθηκε πληθώρα υποστηρικτικών μελετών όπως η Κυματική και η Ακτομηχανική Μελέτη, η Μελέτη Πλοήγησης καθώς και η Προκαταρκτική Μελέτη Ασφάλειας των υπό μελέτη εγκαταστάσεων, σύμφωνα με τα όσα προβλέπονται στην οδηγία Seveso III. Τα έργα που προτείνονται είναι η κατασκευή καινούριας θέσης παραβολής και πρόσδεσης πλοίου μεταφοράς LNG (Liquified Natural Gas), νότια του Νέου Λιμένα, η κατασκευή εξέδρας εργασίας, γεφυρώματος πρόσβασης με την ακτή και συστήματος ναυδέτων παραβολής και πρόσδεσης του πλοίου μεταφοράς Υ.Φ.Α. Επιπρόσθετα, προτείνονται η δημιουργία μικρής κλίμακας χερσαίων εγκαταστάσεων αποθήκευσης και διανομής.

1 ΕΙΣΑΓΩΓΗ

Η δράση «Poseidon Med II» αποτελεί έναν πρακτικό οδικό χάρτη με στόχο την ευρεία υιοθέτηση του υγροποιημένου φυσικού αερίου (Υ.Φ.Α.) ως ένα ασφαλές, περιβαλλοντικά αποδοτικό και βιώσιμο εναλλακτικό καύσιμο για τη ναυτιλία.

Το πρόγραμμα, το οποίο συγχρηματοδοτείται από την Ευρωπαϊκή Ένωση υλοποιείται σε τρεις χώρες – Ελλάδα, Ιταλία και Κύπρο – και περιλαμβάνει έξι ευρωπαϊκούς λιμένες (Πειραιάς, Πάτρα, Ηράκλειο, Ηγουμενίτσα, Λεμεσός και Βενετία), καθώς και τον τερματικό σταθμό Υ.Φ.Α. στη Ρεβυθούσα. Περιλαμβάνει το σχεδιασμό μιας ολοκληρωμένης αλυσίδας ανεφοδιασμού με Υ.Φ.Α. στη ναυτιλία αποσκοπεί στη δημιουργία μιας βιώσιμης και εύρυθμης αγοράς Υ.Φ.Α.

2 ΠΡΟΤΕΙΝΟΜΕΝΑ ΛΙΜΕΝΙΚΑ ΚΑΙ ΧΕΡΣΑΙΑ ΕΡΓΑ

2.1 Χωροθέτηση των Έργων

Το λιμάνι της Πάτρας καταλαμβάνει τον θαλάσσιο χώρο και την δυτική παράκτια περιοχή της πόλης σε όλο σχεδόν το μήκος της ακτής της, δηλαδή τη χερσαία λιμενική ζώνη, όπως έχει καθοριστεί με τις σχετικές αποφάσεις. Οριοθετείται γενικά από τους ποταμούς Γλαύκο (νότια), Μείλιχο (βόρεια) και από τις γραμμές του τραίνου ή οδικές λεωφόρους /άξονες ανατολικά, προς την πλευρά της πόλης, που αποτελούν και τα φυσικά όρια της ζώνης του λιμένα με την πόλη.

Η εγκατάσταση μικρής κλίμακας Υ.Φ.Α. προτείνεται να χωροθετηθεί στην επιχωμένη περιοχή στο ΝΔ τμήμα του νέου λιμένα Πατρών, κοντά στην εκβολή του ποταμού Γλαύκου, εντός των ορίων του λιμένα. Η συγκεκριμένη κρίθηκε ως η βέλτιστη θέση για τη δημιουργία των απαραίτητων χερσαίων και λιμενικών εγκαταστάσεων αποθήκευσης Υ.Φ.Α. και αερίελευσης.

Η προτεινόμενη περιοχή έχει έκταση περίπου ίση με 38.000 τ.μ.. Η έκταση αυτή δύναται να φιλοξενήσει τις απαραίτητες χερσαίες εγκαταστάσεις της μονάδας Υ.Φ.Α. ενώ στο παράκτιο μέτωπό της θα αναπτυχθούν οι απαιτούμενες λιμενικές υποδομές.



Εικόνα 1: Θέση των Έργων, μικρής κλίμακας εγκατάσταση Υ.Φ.Α.

2.2 Περιγραφή των έργων

Τα προτεινόμενα λιμενικά έργα περιλαμβάνουν την δημιουργία λιμενικών υποδομών οι οποίες θα εξυπηρετούν

- α) την παραβολή του πλοίου τροφοδοσίας (LNG Carrier) με Υ.Φ.Α., χωρητικότητας έως 20.000 κ.μ..
- β) την μεταφορά του Υ.Φ.Α. από τη θέση ελλιμενισμού του πλοίου τροφοδοσίας στις δεξαμενές αποθήκευσης καθώς και
- γ) την παραβολή της φορτηγίδας τροφοδοσίας (μπάρτζας) που θα πραγματοποιεί την τροφοδοσία των πλοίων ακτοπλοΐας με Υ.Φ.Α. (ship to ship bunkering),
- δ) τη δημιουργία θέσεων τροφοδοσίας βυτιοφόρων οχημάτων με Υ.Φ.Α.
- ε) την κατασκευή μικρής κλίμακας μονάδας επανατροφοδοσίας Υ.Φ.Α.
- στ) τις απαραίτητες κτιριακές και Η/Μ υποδομές

Η λιμενική εγκατάσταση για την εξυπηρέτηση των πλοίων που μεταφέρουν Υ.Φ.Α. με σκοπό την τροφοδοσία των δεξαμενών στην χερσαία εγκατάσταση, αποτελείται από ευθύγραμμο γεφύρωμα πρόσβασης (jetty) επί βάθρων, το οποίο καταλήγει στην κεντρική πλατφόρμα φορτώσεως/εκφορτώσεως. Η θεμελίωση των βάθρων θα γίνει σε σωληνωτούς χαλυβδομασσάλους που εμπηγνύονται με αφαίρεση του εσωτερικού εδαφικού υλικού και πληρούνται με οπλισμένο σκυρόδεμα και τα ανοίγματα μεταξύ των βάθρων γεφυρώνονται με ελαφρά μεταλλική κατασκευή. Η κεντρική πλατφόρμα φορτώσεως κατασκευάζεται από προκατασκευασμένα στοιχεία οπλισμένου σκυροδέματος που χρησιμοποιούν ως ξυλότυπος για την επιτόπου έγχυση σκυροδέματος, και εδράζεται επί χαλυβδομασσάλων

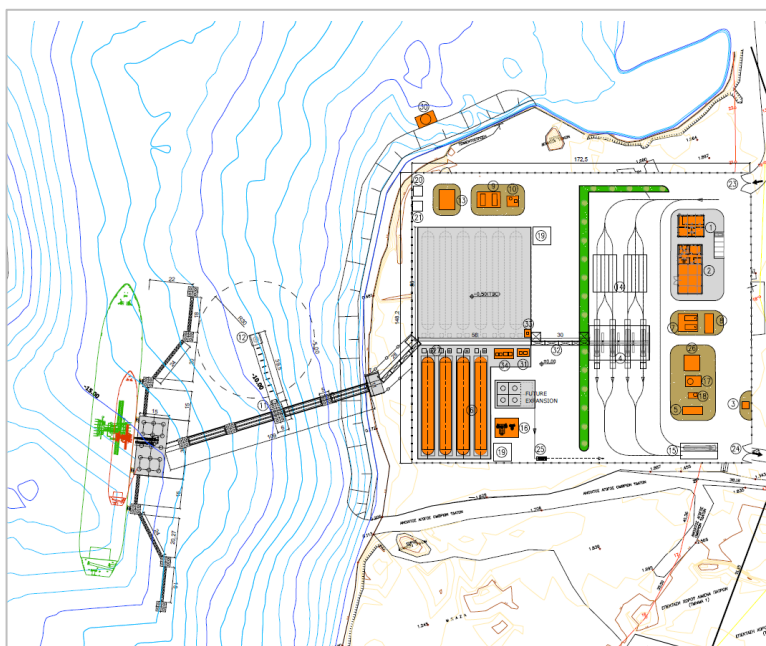
Εκατέρωθεν της κεντρικής πλατφόρμας προβλέπονται ναύδετα πρόσδεσης/ πλεύρισης τα οποία συνδέονται μεταξύ τους με διαδρόμους πρόσβασης, οι οποίοι είναι χαλύβδινα δικτυωτά γεφυρώματα χωρίς ενδιάμεσες στηρίξεις.

Επιπλέον, τοποθετούνται τέσσερα (4) πλωτά ναύδετα πρόσδεσης (mooring bouys).

Το ΥΦΑ μεταφέρεται από τα πλοία στις δεξαμενές, για αποθήκευση. Οι κρουγενικές δεξαμενές έχουν κυλινδρικό σχήμα με ονομαστική χωρητικότητα 1.000 κ.μ. ΥΦΑ, μήκους περίπου 50 μέτρων περίπου και διάμετρο / ύψος 5,80 μέτρο η κάθε μία.

Οι δεξαμενές τοποθετούνται στη σειρά. Έχει προβλεφθεί να εγκατασταθούν τέσσερις (4) δεξαμενές, τρεις (3) ενεργές και μία (1) κενή, οι οποίες καταλαμβάνουν έκταση περίπου 2.200 τ.μ.. Υπάρχει δυνατότητα και επαρκής χερσαίος χώρος, σε μελλοντικό χρόνο και εφόσον απαιτηθεί από τη ζήτηση, επέκτασης της εγκατάστασης.

Στη μελέτη συμπεριλήφθηκαν οι αναγκαίες Η/Μ και κτιριακές εγκαταστάσεις για την κατασκευή και λειτουργία των έργων, ενώ έγινε διεξοδική κυκλοφοριακή ανάλυση.



Εικόνα 2: Γενική Διάταξη Έργων, μικρής κλίμακας εγκατάσταση Υ.Φ.Α.

Η δημιουργία των απαραίτητων χερσαίων και λιμενικών εγκαταστάσεων αποθήκευσης Υ.Φ.Α. στο λιμάνι της Πάτρας είναι έργο με κόστος κατασκευής της τάξεως των 60.000.000 ευρώ και χρονικό ορίζοντα ολοκλήρωσης των έργων δύο (2) έτη.

3 ΘΕΜΑΤΑ ΑΣΦΑΛΕΙΑΣ

Η Προκαταρκτική Μελέτη Ασφαλείας για τις εγκαταστάσεις αποθήκευσης ΥΦΑ σε χώρο νότια του Λιμένα της Πάτρας συντάχθηκε με βάση την Ευρωπαϊκή Οδηγία 2012/18/ΕΕ και την Κοινή Υπουργική Απόφαση 172058/2016 (ΦΕΚ 354/Β/17.02.2016), για την αντιμετώπιση των κινδύνων ατυχημάτων μεγάλης κλίμακας σχετιζομένων με επικίνδυνες ουσίες. Αποτελεί βασικό γνώμονα για την αδειοδότηση των έργων και περιλαμβάνει την Πολιτική Πρόληψης Μεγάλων Ατυχημάτων του Διαχειριστή της εγκατάστασης, τη περιγραφή του Συστήματος Διαχείρισης της Ασφαλείας, ανάλυση των κινδύνων ατυχήματος από τις δραστηριότητες της εγκατάστασης, καθώς και τα εφαρμοζόμενα μέτρα πρόληψης ατυχημάτων.

Κατά την εκπόνηση της μελέτης, έγινε διερεύνηση όλων των πιθανών σεναρίων κινδύνου ατυχήματος (αίτια, συμβάντα και επιπτώσεις), συντάχθηκαν αντίστοιχα διαγράμματα και προτάθηκαν τα κατάλληλα μέτρα πρόληψης τέτοιων ατυχημάτων.

Κατά την ποσοτική ανάλυση κινδύνου (Quantitative Risk Analysis), το συμπέρασμα που προέκυψε είναι ότι ο κίνδυνος συνολικά χαρακτηρίζεται ως αμελητέος, ενώ προκύπτει ότι σε κανένα εξεταζόμενο σενάριο δεν θα προκληθούν επιπτώσεις εκτός των ορίων της εγκατάστασης.

Η λήψη μέτρων πρόληψης ατυχήματος αλλά και η οργάνωση αντιμετώπισης ατυχημάτων (Σχέδιο Έκτακτης Ανάγκης) είναι σε κάθε περίπτωση απαραίτητες προϋποθέσεις για την ασφαλή λειτουργία της εγκατάστασης.

Ακολουθεί ενδεικτικό σχέδιο αποτύπωσης των ζωνών επικινδυνότητας που συντάχθηκαν σύμφωνα με αποτελέσματα της Προκαταρκτικής Μελέτης Ασφαλείας και με τη χρήση κατάλληλου μαθηματικού ομοιώματος.



ΖΩΝΕΣ ΕΠΙΚΙΝΔΥΝΟΤΗΤΑΣ	
ΥΠΟΜΝΗΜΑ	
—	ΖΩΝΗ ΕΠΙΚΙΝΔΥΝΟΤΗΤΑΣ ΓΙΑ ΕΤΗΣΙΑ ΠΙΘΑΝΟΤΗΤΑ 1×10^{-4}
—	ΖΩΝΗ ΕΠΙΚΙΝΔΥΝΟΤΗΤΑΣ ΓΙΑ ΕΤΗΣΙΑ ΠΙΘΑΝΟΤΗΤΑ $4,2 \times 10^{-5}$
—	ΖΩΝΗ ΕΠΙΚΙΝΔΥΝΟΤΗΤΑΣ ΓΙΑ ΕΤΗΣΙΑ ΠΙΘΑΝΟΤΗΤΑ 1×10^{-5}
—	ΖΩΝΗ ΕΠΙΚΙΝΔΥΝΟΤΗΤΑΣ ΓΙΑ ΕΤΗΣΙΑ ΠΙΘΑΝΟΤΗΤΑ 1×10^{-6}
—	ΖΩΝΗ ΕΠΙΚΙΝΔΥΝΟΤΗΤΑΣ ΓΙΑ ΕΤΗΣΙΑ ΠΙΘΑΝΟΤΗΤΑ 1×10^{-7}

Εικόνα 3: Σχέδιο Επικινδυνότητας σύμφωνα με τα αποτελέσματα της Προκαταρκτικής Μελέτης Ασφαλείας

4 ΑΝΤΙΚΤΥΠΟ ΤΩΝ ΕΡΓΩΝ ΣΤΟ ΠΕΡΙΒΑΛΛΟΝ

Κατά τον Προκαταρκτικό Προσδιορισμό Περιβαλλοντικών Απαιτήσεων έγινε εκτίμηση και αξιολόγηση των Περιβαλλοντικών Επιπτώσεων που αναμένονται κατά την κατασκευή και λειτουργία των υπό εξέταση έργων.

Στον υπό εξέταση τερματικό σταθμό αποθήκευσης Υ.Φ.Α. μικρής κλίμακας, πέραν της διαδικασίας αποθήκευσης του Υ.Φ.Α. σε δεξαμενές, πρόκειται να λαμβάνουν χώρα επιμέρους υποστηρικτικές – συνοδές διεργασίες, όπως η εκφόρτωση του υγροποιημένου φυσικού αερίου από τα πλοία μεταφοράς μικρής δυναμικότητας στις δεξαμενές αποθήκευσης, η αεριοποίηση μέρους του υγροποιημένου φυσικού αερίου, η μεταφόρτωση του Υ.Φ.Α. σε φορτηγά πλοία καθώς και η χερσαία φόρτωση βυτιοφόρων οχημάτων με Υ.Φ.Α.

Σύμφωνα με την κείμενη νομοθεσία, λόγω των ανωτέρω δραστηριοτήτων και λαμβάνοντας υπ’ όψη ότι η αποθηκευτική ικανότητα του εν λόγω τερματικού σταθμού αποθήκευσης Υ.Φ.Α., εκτιμάται ότι θα ανέλθει αρχικά στα 3.000 κ.μ. περίπου, η υπό εξέταση δραστηριότητα κατατάσσεται στη μέση όχληση.

Επιπλέον, σύμφωνα με την κείμενη νομοθεσία, ο υπό εξέταση σταθμός αποθήκευσης Υγροποιημένου Φυσικού Αερίου κατατάσσεται περιβαλλοντικά στην Υποκατηγορία Α1 και συνεπώς η αρμοδιότητα ελέγχου και έγκρισης του φακέλου περιβαλλοντικής αδειοδότησης εμπίπτει στη Διεύθυνση Περιβαλλοντικής Αδειοδότησης του Υ.Π.Ε.Ν.

Τα προτεινόμενα έργα, πρόκειται να συνεισφέρουν στον περιορισμό των αερίων ρύπων, καθώς η χρήση Υ.Φ.Α. ως καύσιμο κίνησης των πλοίων, σε σύγκριση με τα συμβατικά καύσιμα πλοίων, θα έχει ως αποτέλεσμα τη μείωση των εκπομπών:

- οξειδίων του θείου (SOx) έως και 100%
- οξειδίων του αζώτου (NOx) κατά 90%
- αιωρούμενων σωματιδίων (PM) κατά περίπου 99%
- διοξειδίου του άνθρακα (CO2) έως και 20%

με συνολικά εξαιρετικά θετικό αντίκτυπο στην ανθρώπινη υγεία των κατοίκων της περιοχής.

Πέραν αυτού, αναμένονται σημαντικές θετικές επιπτώσεις στην οικονομία της περιοχής, τόσο κατά τη φάση της κατασκευής όσο και κατά τη φάση λειτουργίας της εγκατάστασης, ενώ θα πάψει η απομόνωση της Δυτικής Ελλάδας από τα δίκτυα διανομής του Υ.Φ.Α.

Creation of a jetty for permanent berthing of a Floating Storage and Regasification (FSR) unit for LNG Import in Vasilikos, Cyprus – Overcoming challenges

C.D. Solomonidis^{1*}, A.D. Toumazis², A.M. Boutatis¹, P. Biniskos¹, M.N. Kalpyri¹

¹ Rogan Associates, 9, Valetta Str, Athens 15771, Greece

² Dion. Toumazis Associates, 4 Romanos Str, 1070 Nicosia, Cyprus

*Corresponding author: csolomonidis@roganassoc.gr

Abstract

The present study contains a description of the Basic Design of the Offshore Marine Works foreseen for the Action of CYnergy project, namely the design of a Jetty for FSRU berthing and LNG transfer activities. The proposed works include the construction of a trestle/ jetty that will accommodate the permanent berthing, mooring and loading/ unloading operations, of an FSRU in the bay of Vasilikos, in Cyprus. An assessment of the Environmental and Social Impacts deriving from the construction and operation of the project is also given. The study identifies the existing site environmental conditions and presents the examined alternatives and the design considerations. A detailed technical description of the project as well as the supporting studies for the preparation of EIS are presented. Particular emphasis is also given in Hazard Identification Study and in Quantitative Risk Assessment Study where the impact of the project during the operational phase for various accidental or non-accidental disaster scenaria is examined.

Keywords Jetty, LNG import facility, Mooring Analysis, Environmental Monitoring.

1 INTRODUCTION

This work was implemented within the CYnergy Action. This Action contributes to the implementation of the energy PCI 7.3.2 "Removing internal bottlenecks in Cyprus to end isolation and to allow for the transmission of gas from the Eastern Mediterranean region", which aims at building the infrastructures and associated equipment intended to supply natural gas to Cyprus, remove internal bottlenecks and end energy isolation.

The Action of CYnergy project takes as a focal point a Liquefied Natural Gas (LNG) Storage Facility to be developed in Cyprus and aims at developing a comprehensive strategy for the use of Natural Gas (NG) in Cyprus, as well as an analysis of the financial structures for the implementation of infrastructure investments in the sectors of transport and energy. CYGAS and Lloyds Register are among the Partners of the Action, who contributed in the overall design of the Jetty.

2 SITE CONDITIONS

The planned location for the Natural Gas facilities in Cyprus is Vasilikos, about 25 km east of Limassol and about 30 km southwest of Larnaca. Some of the landside area is a brownfield site, previously occupied by the Hellenic Chemical Industries' fertilizer plant. This plant ceased operations in 1986 and was demolished and cleared in the 1990's. The area is characterized as a "phosphogypsum lagoon", and environmental requirements exist for it. Thus, no excavation will be allowed in this area.

Wave Conditions: There are no wave measurements in the area. Previous studies for the design of the Single Point Mooring (SPM) of the EAC and for the Ministry of Energy have reached to the conclusions that the predominant incident weather direction is SSW (195 to 225 degrees due North) and the significant wave height (Hs) offshore for 50 years return period is 6.45m.

Geotechnical Parameters: According to the Geotechnical Survey performed by Noble, Quaternary deposits and Pre-Quaternary Bedrock, local geologic units were encountered in the nearshore areas of the Site.

Sea Level: Sea level rise for the Eastern Mediterranean is estimated to be 4-5 mm/yr (HR Wallingford 2006).

Wind: Currently, wind rose data from Zygi is unavailable and wind data collected at Larnaca Airport are used (Table 1).

Table 1 Wind speed frequency table at Larnaca (1996-2012)

Total	3.2	3.27	3.12	2.04	3.58	2.57	1.95	3.48	10.17	15.29	6.54	3.26	5.52	12.86	14.61	8.54	100
17.50										0.02							0.02
15.00										0.02	0.2	0.08	0.01				0.05
12.50			0.01							0.02	0.2	0.08	0.01				0.33
10.00	0.04	0.08	0.06		0.01				0.12	1.26	0.24	0.04		0.02	0.03	0.06	2
7.50	0.2	0.36	0.31	0.08	0.1	0.02	0.01	0.05	0.8	3.8	0.66	0.11	0.04	0.11	0.17	0.25	7.06
5.00	0.89	1.08	0.97	0.36	0.51	0.28	0.32	0.95	4.92	4.73	1.48	0.29	0.21	0.45	1.03	1.3	19.76
2.50	1.42	1.29	1.25	0.93	1.84	1.78	1.24	2.01	3.23	3.76	2.54	1.2	1.93	7.55	6.39	4.66	45.05
0.00	0.83	0.46	0.52	0.68	1.11	0.49	0.37	0.45	1.07	1.51	1.56	1.61	3.33	4.73	4.98	2.25	25.73
	0.00	22.50	45.00	67.50	90.00	112.50	135.00	157.50	180.00	202.50	225.00	247.50	270.00	292.50	315.00	337.50	Total

Tidal Levels: The previously available information about tidal water levels was gathered from two sources The Admiralty Chart 849 “Ports in Western Cyprus” listed tidal datums for a few locations with Limassol being the closest location to Vasilikos Bay and the HR Wallingford (1995) report (Table 2).

Table 2 Tidal datum’s from Chart 849 and Wallingford (1995) report

Datum	Chart 849, Limassol, m CD	Wallingford (1995), m CD	Wallingford (1995), m LSDC
Extreme High Water		0.9	0.5
MHWS	0.6	0.5	0.1
MHWN	0.5	0.4	0.0
MLWN	0.3	0.3	-0.1
MLWS	0.2	0.2	-0.2
Extreme Low Water		-0.1	-0.5

3 DESIGN LOADS

The design life for all elements of the marine structures is 50 years. Adverse environmental loads are considered for the design of the marine infrastructure.

- The maximum design wave (from the prevailing wind direction) used was equal to max $H_s = 6.45m$
- The maximum fender thrust obtained through mooring analysis was equal to max $F_h = 9600 kN$.
- The ground acceleration factor used was equal to 0.25g.

The following loading categories are considered: Dead loads [DL], Live loads [LL], Operational loads [OL], Accidental loads [AL] and Earthquake loads [E]. Also, load combinations are considered: Ultimate Limit States [ULS] and Serviceability Limit States [SLS]. The allowable deflection of the superstructure is L/300 for operational maximum vertical deflections and 300mm for accidental maximum horizontal deflections.

4 TECHNICAL DESCRIPTION

The necessary infrastructure is expected to include the following:

- 1 Marine Works: Jetty for the permanent berthing of an FSRU and LNG transfer activities and revetment for the protection of the shoreline
- 2 Floating Storage and Regasification Unit (FSRU) – Gas export system and Loading Arm (inclusive of; meters, Gas compressors, filters, heaters, venting system, quick connection, export arm pipelines), permanently berthed in Vassilikos bay
- 3 Jetty borne Gas Pipeline (inclusive of; gas pipelines, valves) connecting the FSRU to the receiving point onshore

- 4 Onshore Gas Pipeline and Shoreside AGI (inclusive of; pipeline, inline valves, cathodic protection systems, PIG trap, civil works), connecting the receiving point onshore to the downstream delivery point
- 5 Pipeline Storage Array (inclusive of; inlet and outlet manifolds, inline valves, protection systems, civil works), able to store Natural Gas in gaseous form in the required operational pressure ranges adjacent to Vassilikos power station
- 6 Onshore Above Ground Installation (AGI) – Pressure Reduction, pre-Heating Filtering and Metering Station (inclusive of; inlet and outlet isolation valves, filtering metering, gas heating, pressure reduction, PIG trap, protection systems, civil works),

4.1 Technical Description of the Marine Works

4.1.1 Jetty

The jetty is located west of the main breakwater of Limassol Port – terminal 2 (Vasiliko), at a distance of about 1,3km. The trestle runs offshore in a north – south direction for about 750 meters before turning south-west 430 meters to form the FSRU berth. A future extension of the jetty by another 310m, in order to accommodate an LNG Carrier is foreseen.

The trestle is approximately 14 meters wide. The trestle pile cap is supported on vertical and raked steel pipe piles, at intervals of 20m. The pile caps, made of reinforced concrete, support a 5-meter-wide roadway and 9-meter-wide pipe rack, which is wide enough to accommodate both cryogenic (LNG) and natural gas pipes. Pipe expansion loop bends were assumed every 300 meters.

The orientation of the berth is about 220 degrees North, so that the ships are aligned into the prevailing direction of wind and waves. Thus, according to the proposed layout, the depth at the inner berth is between 15 and 18 meters while the outer (future) berth depth ends up being about 22 meters.

The berth will consist of a loading platform of dimensions 30 meters by 40 meters. The loading platform substructure and deck is supported by piles. Ships berth against four breasting dolphins. The breasting dolphins will be equipped with fenders and quick release mooring hooks to accommodate the LNGC's spring lines.

There are also eight (8) mooring dolphins for each berth, each mooring dolphin equipped with a quick release mooring hook.

Several models were used for the structural design of the structure. Geotechnical analysis was performed for the geotechnical design of the piles. Mooring analysis was also conducted and the outputs (loads on breasting and mooring dolphins) were used as input for the design of the Breasting and Mooring Dolphins.

The plan view of the jetty and a typical trestle section are presented in Figure 1.

4.1.2 Revetment

A rubble mound revetment will be constructed in order to protect the shore line in the area around the landing of the main access jetty, at both sides of abutment A1. The revetment will be designed to protect the slopes of the embankment and the regasification area from run-up and overtopping of waves as well as from scouring of the toe of the slopes. The revetment will protect an area of approximately 116m, 58m from each side of the axis of the longitudinal axis of the abutment A1.

4.2 Basic Calculations

4.2.1 Structural Analysis

Several models are used for the analysis of the jetty structure. The individual pile-heads for the jetty and the platform are analysed by respective individual models and also by a complete model of the jetty assembly. Similarly, the mooring and breasting dolphin structures are analysed by dedicated models. The pile embedment is modelled through corresponding elastic lateral bedding values along the depth of the pile, according to the recommendations of the geotechnical investigation report. The program RFEM (Dlubal Software GmbH, 2016) is used for the analysis.

The analysis and design of the deck is carried out separately for the 2 phases: construction phase with only single precast beams subject to erection loads and operation phase with the 4 beams rigidly connected by the concrete topping and under full-service loads. The construction phase loads considered are the following: self-weight of beam, prestress, self-weight of precast slabs, Weight of fresh concrete topping and Live load during concreting. The operational phase loads considered are the following: self-weight of beam & topping, prestress, self-weight of precast slabs, dead load from equipment and live load applied on the jetty surface deck not occupied by the piperacks.

For the design of the loading platform a finite element model is used representing the complete superstructure in the final stage, along with the support piles. The pile embedment is modelled through corresponding elastic lateral bedding values along the depth of the pile, according to the recommendations of the geotechnical investigation report.

4.2.2 Mooring Analysis

A static mooring analysis was carried out using the software OPTIMOOR (Version 6.3.8). OPTIMOOR (Tension Technology International, 2016) is a calculation tool that uses input data for a specified vessel, for a specified berth arrangement and calculates the wind-wave-current generated forces and other forces that relate to ship’s draft alterations and tide. Figure 2 presents the modeled vessel’s mooring arrangement. Note that there are two spring lines, two headlines and four breasting lines both at bow and at stern mooring arrangement. The following conclusions can be drawn by the analysis conducted:

- The maximum fender thrust is obtained when the wind and wave direction is 80o relative to the vessel’s longitudinal axis (120o N).
- The mooring lines of the ship were based on OCIMF’s guidelines (OCIMF, 2017).
- At this stage, and as the final design ship is not known yet, it is recommended to install triple quick release hook (QRH) in each mooring dolphin and double-quick release hook at each breasting dolphin.
-

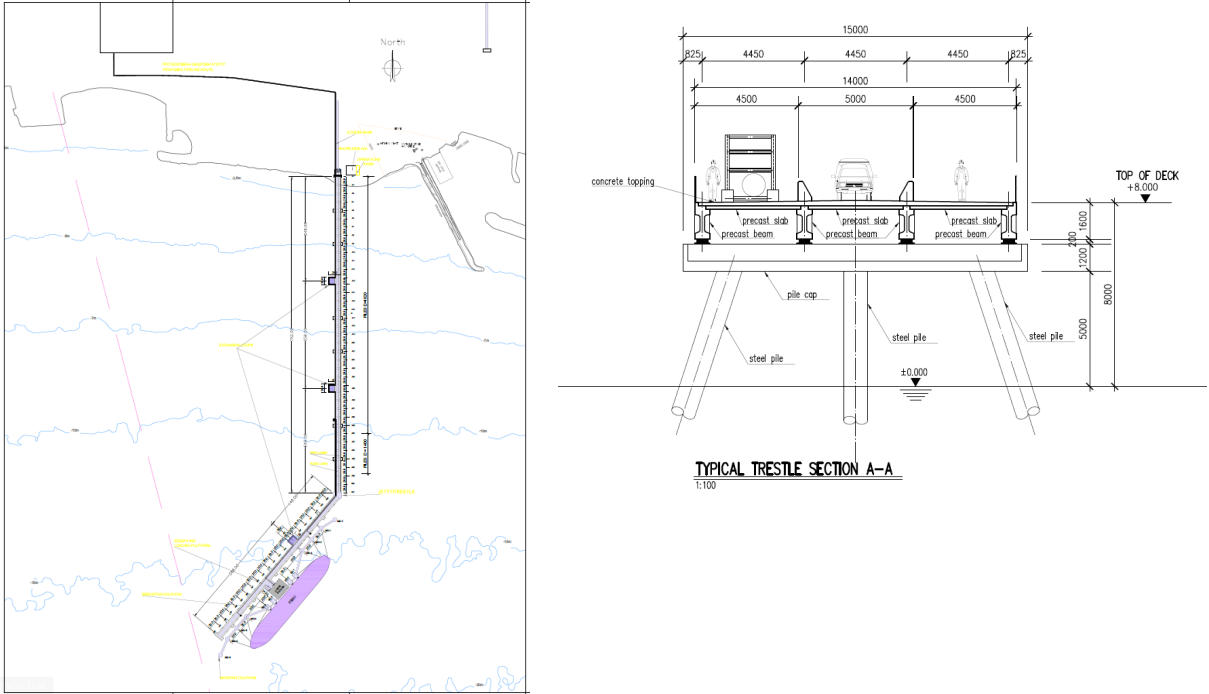


Figure 1 a) Plan view of jetty, b) Typical trestle section

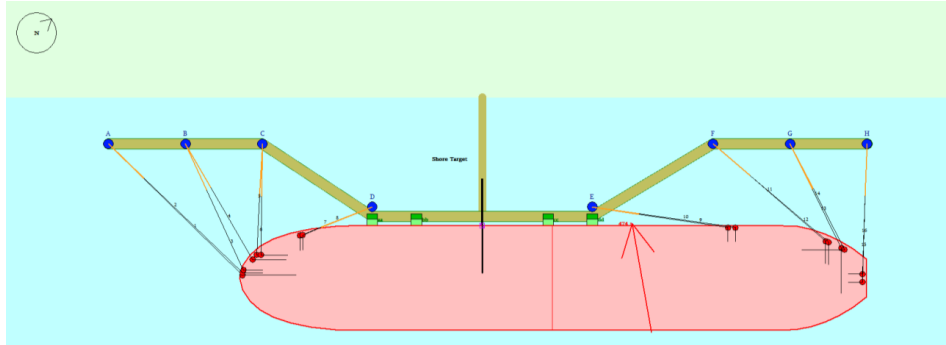


Figure 2 Modeled vessel's mooring arrangement

5 ENVIRONMENTAL STUDIES

The following specialized studies were conducted and served as an input to the of Environmental Impact Assessment (EIA):

- Basic Design – Offshore Marine Structures Structural Design Calculations
- FSRU Terminal Risk Assessment – Preliminary Site Evaluation Study (HAZID)
- FSRU Terminal Risk Assessment – Preliminary Quantitative Risk Analysis (QRA)
- Baseline Benthos Assessment and Impact on marine ecosystem
- Air Pollution Impact Study
- Noise Impact Study
- Temperature Modification Model Study

Two Natura 2000 Areas are located in the wider region of the Works: Periochi Asgatas (SCI , code: CY5000007) and Potamos Pentaschinos (SPA, code: CY6000008).

- The main outputs of EIA are listed below:
- The jetty is constructed on piles, therefore coastal hydraulics are not affected, thus no changes on the physical characteristics of the coastal area are expected.
- Small scale impacts might appear, concerning the water temperature, due to the seawater traffic during the operation of L.N.G. gasification, which is a negligible impact on seawater environment.
- Noise and vibrations because of construction works and ships traffic are expected to be of limited duration.
- No significant impact on the acoustic environment of the study area is expected from ships and the operation of FSRU
- Common Impact on marine ecosystem and fishes: Panic cause, change of routes, change of places to find food
- Implementation of an environmental monitoring program, on a regular bases for the basic environmental parameters (air pollution, noise pollution, solid and liquid waste, chemical analysis of liquid waste, monitoring of the aquatic environment, marine pollution control, soil pollution control, assessment of local economy, assessment of the road accidents/safety and quality control of the monitoring program) is proposed.

References

- Dlubal Software GmbH (2016) Program RFEM 5, Spatial Models Calculated According to Finite Element Method, Dieffenbach, Germany
- OCIMF (2017): Mooring Equipment Guidelines 3 (MEG3)
- Tension Technology International (2016) <https://www.tensiontech.com/software/optimoor>

An approach on the procedure of selecting container handling systems in a container terminal

A.-N. Papadopolis-Dezorzis^{1*}, S. Theofanis² and M. Boile.³

¹General Secretariat of Ports, Port Policy and Maritime Investments, Civil Engineer, GREECE

²Thessaloniki Port Authority S.A., Chairman of the BoD and C.E.O. GREECE; Senior Fellow, Rutgers University, USA.,

³Department of Maritime Studies, University of Piraeus, Associate Professor., GREECE

* Corresponding author email: anpd@live.com

Abstract

The present paper aims to describe the available equipment in the international market, for handling containers (Twenty-Foot Equivalent Unit or Forty-Foot Equivalent Unit) at a seaside container terminal. In addition, an initial approach is attempted in the procedure of selecting the suitable system of container-box handling equipment in a container terminal, based on the size of the berthing vessels and the estimated annual volume of containers. The procedure of designing a container terminal and the selection of the suitable equipment is a dynamic process, which can and should be modified in order to achieve increased container terminal productivity, especially in a field related to the very competitive area of international shipping. Finally, the most important Key Performance Indicators that should be used in order to evaluate the productivity and the effectiveness of the container handling process are mentioned.

Keywords Container terminal, TEU, STS crane, Container handling system.

1 DEFINITIONS

It is important to begin by giving some basic definitions:

Seaside container terminal is a port or a terminal in which almost exclusively container ships are being served.

The specialized equipment used for handling the container boxes at a container terminal is called **Container Handling Equipment**.

Containers are steel boxes with dimensions according to certain international standards, and with high resistance to mechanical stresses induced during a sea journey. The boxes are used to transport dry or liquid commodities all over the world.

Over the years waterborne transport is continuously increasing, mainly due to the increase of the standard of living on a global scale and the decrease of the sea-transportation cost, as a result of the use of containers.

Contemporary container ships are classified in various ways, including the one described below:

- Panamax and small size container ships
- Post Panamax and Super Post Panamax container ships
- New Panamax container ships
- Post New Panamax container ships
- Triple E class and Giga class container ships.

2 CONTAINER TERMINAL DESIGN & CONTAINER HANDLING SYSTEM

The most important issue in the design process of a container terminal and in the process of selecting the proper container handling system is the design vessel (maximum and average) and the estimated annually transported container volume (i.e. number of containers).

Due to the substantial increase in the size of new container ships, it is not technically or economically feasible for large container ships to berth in all ports. For this reason certain basic ship-routes have been formed by the so-called mainliner services, which are followed by the mega container ships (called mother ships), whilst the distribution on a local and regional level is achieved using smaller

container ships (called feeders). Thus, the essential criterion in the design of a container terminal is whether it will accommodate mega container ships (mother ships) or smaller feeder container ships (feeders) or both. It is easily understood that ports serving mainliner container vessels have considerable advantage.

Besides the above, the following information should be taken into account during the design procedure :

- Main & feeder lines served
- Imports, Exports, trans-shipment traffic and transit traffic, serviced by rail or road transport
- Loaded or Empty containers
- Container Size distribution between Twenty and Forty Foot Equivalent Units (T.E.U.) or (F.E.U.)
- Full Container Load (F.C.L.) or Less than Container Load (L.C.L.) containers.

A container terminal may be divided in two basic zones, the seaside operations zone and the landside operations zone.

The sea zone is divided in three areas:

- Anchoring area
- Approach channel area
- Berthing area.

The land zone is divided in three areas:

- Quay wall area
- Stacking area
- Land delivery/receipt area.

The typical cross section of the land zone can be seen in Fig. 1.

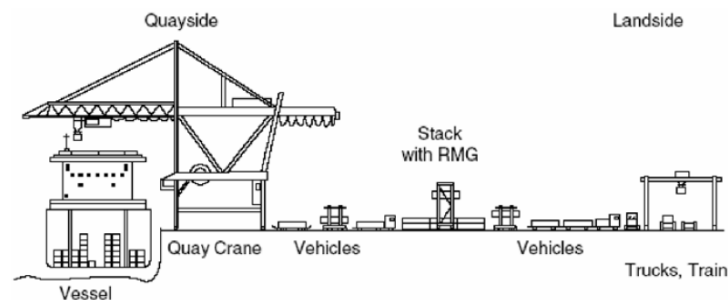


Figure 1 Cross Section of a land zone of a container terminal (source 4).

Specialized equipment is used in a container terminal for:

- Loading and unloading of container ships (Ship To Shore)
- Horizontal transportation of the boxes from quay wall area to the stacking yard and vice versa
- Stacking the container boxes in the stacking yard area
- Horizontal transportation of the boxes from the stacking yard area to the landside access area
- Loading and unloading trucks and trains on the landside receipt / delivery operations area

This specialized equipment comprises key part of the terminal's **Container Handling System**.

The equipment of the **Container Handling System** is divided into two main categories:

(a) Cranes or Gantry Cranes on Quay side or Loading and Unloading Cranes or Ship To Shore (STS) Cranes (Figure 2). The most important equipment of a container terminal is the Ship To Shore or Quay Gantry Cranes. They represent the equipment that determines the size of the maximum vessel that can

be served on the terminal, as well as the loading / unloading rate (TEU per hour). Besides the Quay Gantry Cranes (QGC) there are other types of smaller cranes that are described in subsequent sections. **(b)** Vehicles for intra-terminal horizontal transportation and vertical (stacking) movements. A wide variety of systems / equipment is available in the international market, for horizontal transportation and stacking in various stacking heights. The Container Handling Systems are divided in groups, detailed in subsequent sections, as shown in Figure 3.

For the intra-terminal horizontal transportation the following equipment alternatives may be used:

- Tractor – Trailer Units of various types. The trailer unit can be suitable for port use only or for street use, and may comprise single or multiple trailers (passive vehicle)
- Forklift truck (non-passive vehicle)
- Reach Stacker (non-passive vehicle)
- Straddle Carrier (SC) or Shuttle Carriers (ShC) (non-passive vehicle)
- Automated Guided Vehicle (passive vehicle)

The intra-terminal horizontal transport units may include passive vehicles and non-passive vehicles. The passive vehicles need assistance from another vehicle / crane for their loading / unloading, whilst the non-passive vehicles complete both the horizontal transportation and the loading / unloading procedure themselves without assistance from another vehicle / crane.

For stacking the following equipment can be used:

- Forklift truck (non-passive vehicle)
- Reach Stacker (non-passive vehicle)
- Straddle Carrier (SC) or Shuttle Carriers (ShC) (non-passive vehicle)
- Rubber Tyred Gantry Crane (RTGC)
- Rail Mounted Gantry Crane (RMGC)
- Over Head Crane (OHC) on concrete or steel frames

Two basic systems of intra-terminal transportation and stacking can be distinguished:

- ✓ Systems with **common equipment** for intra-terminal transportation and stacking (i.e., Forklift, Reach-stacker, Straddle Carriers)
- ✓ Systems with **different equipment for** intra-terminal transportation and stacking (i.e., Tractor – Trailer in combination with Rubber Tyred Gantry Cranes or Rail Mounted Gantry Cranes).

3 SELECTION AND EVALUATION OF THE PRODUCTIVITY OF CONTAINER HANDLING SYSTEMS

3a Selection of the container handling system

Selection of the Container Handling Systems in a container Terminal is carried out ad hoc, primarily as mentioned earlier, based on the maximum design vessel and the estimated number of container boxes to be handled. For this reason, a large variety of equipment types are available on the international market. In any case, it should be mentioned that acquisition / procurement cost and operation cost should be taken into account. In addition to the above and in order to improve / maximize the productivity of a container terminal, simulation models are being used for both the design and the handling system selection.

The most important piece of equipment in a container terminal is the vessel loading and unloading or Ship to Shore (STS) crane. The size of the STS crane is determined by the size of the design vessel and specifically on the number of container rows on the deck of the ship. Figure 2 shows the different sizes and relevant capabilities of the STS cranes.

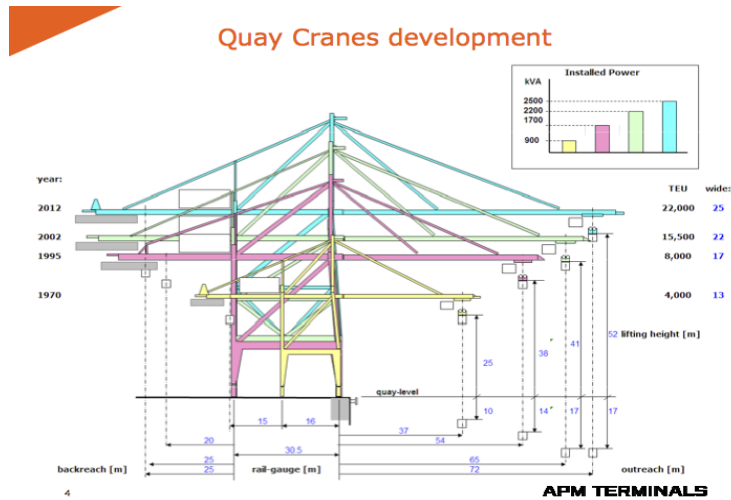


Figure 2 STS Crane Selection (Source : <http://notes.husk.org/image/122802778349>)

Figure 3 shows various types of stacking equipment and may be used to select the proper type of equipment on a container terminal based on the TEU density in the stacking area.

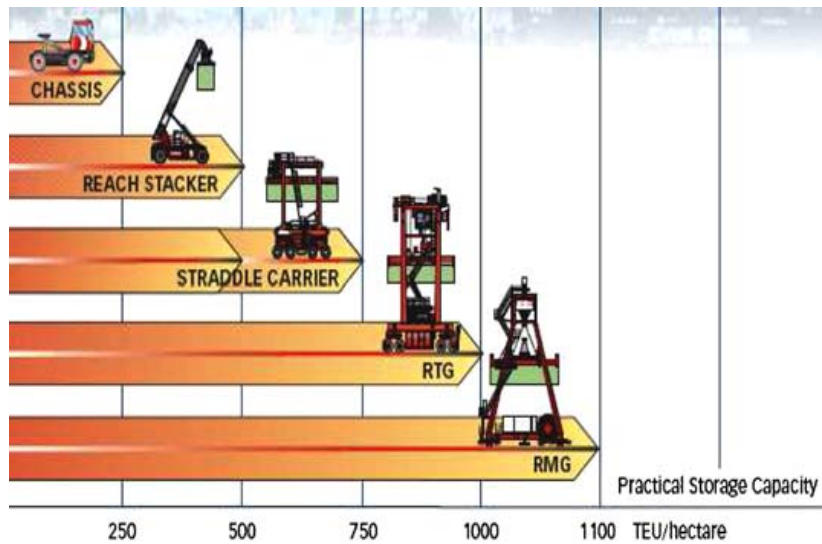


Figure 3 Selection of Stacking System based on the density of the stack area (source: KALMAR & 11)

Similarly, Figure4 may be used to select the proper stacking equipment on a container terminal based on the number of TEU's (import, export, transit) passing through the container terminal on an annual basis.

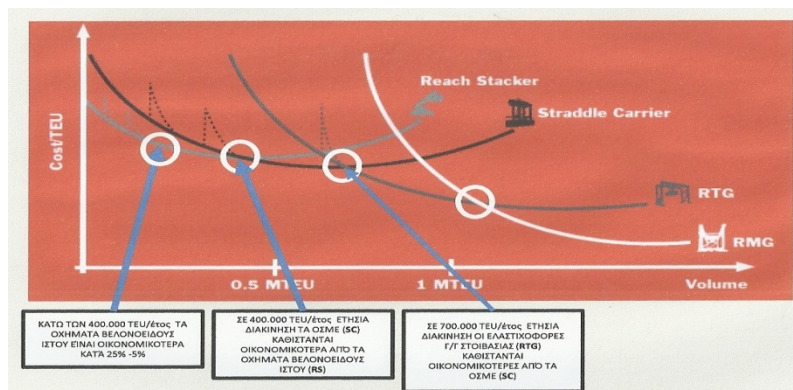


Figure 4 Selection of Stacking System annual throughput (Source: Konecranes & 11)

Various techniques and graphs have been produced to aid the design process and assist in the selection of the proper handling system in a container terminal. Recently, computer models have been produced using simulation techniques in order to improve the productivity and effectiveness of a container terminal, new or even an existing one.

3b Key Performance Indicators

For the evaluation of the productivity and the effectiveness of a container terminal, the following Key Performance Indicators should be counted:

- Waiting time of a ship at anchor
- Time of a ship on quay
- Number of container moves per STS in a certain period of time
- Traffic & Throughput indicators

For the evaluation of the Container Handling System in the case of high stacking the following should be taken into account:

- Acquisition / procurement cost and operation cost
- Compatibility with labor standards
- Flexibility / layout modification
- Response to peak demands
- Delays response / interaction

4 SUMMARY

An overview of the different types of equipment used in container terminals to load / unload vessels, horizontally move containers within the terminal area and vertically move (or stack) containers within the terminal yard was given. Metrics used to select the proper type of equipment based on the operations of a specific terminal were discussed. The container handling system in place affects the productivity of a terminal. Key performance indicators used to evaluate terminal productivity were presented.

References

- UNITED NATIONS CONFERENCE ON TRADE AND DEVELOPMENT, "Port Development, A handbook for planners in developing countries, UNITED NATIONS.
- Agershou H., Dand I., Ernst T., Ghos H., Jensen O.J., et al, "Planning and Design of Ports and Marine Terminals" Thomas Telford, 2004.
- Gunter H-O., Kim K.H., Editors "Container Terminal and Automated Transport Systems" Springer, 2005.
- Kim K.H., Gunter H-O., Editors, "Container Terminal and Cargo Systems" Springer, 2007.
- Frunk Meisel, "Seaside Operations Planning in Container Terminal" Physica – Verlag, November 2008.
- Bose Jurgen W., Editor "Handbook of Terminal Planning" Springer, ORCS Interfaces Series, October 2010.
- Masterclass on Crane Procurement, Modernization, and Maintenance
<http://www.liftech.net/wp-content/uploads/2014/12/Masterclass-on-Crane-Procurement-Modernization-and-Maintenance.pdf>
- Mohseni N.S., "Developing a Tool for Designing a Container Terminal Yard", Master Thesis Project, TU Delft, November 2011,
- Thessaloniki Port Master Plan, ADK Consulting Engineers, TRITON Consulting Engineers et al. March 2016 (Greek language).
- Psaraftis C.N., Economics of Sea Transportation I, Lecture Notes, School of Naval Architects NTUA, Athens, December 2005(Greek language).
- Theofanis S. Boile M., Lecture Notes from the Postgraduate Port Management Course NTUA year 2017-18, Types and Operation of Container Terminal, 2018 (in Greek).

Ενετικός λιμένας Ηρακλείου Κρήτης: Οι αδόκιμες διαχρονικές επεμβάσεις σε ένα ιστορικό λιμενικό έργο

Σ. Λυριντζάκης^{1*}, Χ. Λυτινάκη¹, Εμμ. Τσιπλοστεφανάκης¹, Σ. Περογιαννάκη¹,
Γ. Φραγκομανωλάκη¹, Μ. Σπυριδάκης^{2*},

¹Οργανισμός Λιμένος Ηρακλείου Α.Ε.Τ.Θ. 1068-71110 Ηράκλειο

²Ρογκάν & Συνεργάτες, Σύμβουλοι Μηχανικοί – Αρχιτέκτονες, Βαλέττα 9, 15771 Ζωγράφος Αθήνα - ΕΛΛΑΔΑ

*Υπεύθυνος επικοινωνίας: slirintz@yahoo.gr, spirmich@otenet.gr

Περίληψη

Η ανάπλαση ενός υπάρχοντος λιμένα, με επισκευές αστοχιών, ανακατασκευές και βελτιώσεις των συνθηκών ελλιμενισμού είναι μία διαδικασία που παρουσιάζει μεγάλες δυσκολίες. Ιδιαίτερα, όταν ο λιμένας είναι παλαιός, όπως στην παρούσα περίπτωση, οι δυσχέρειες και τα απρόβλεπτα είναι πραγματικότητα. Η έλλειψη πληροφοριών (σχέδια, μελέτες, μαρτυρίες), αλλά και η χρήση διαφόρων παλαιών τεχνικών, ασύμβατων με την σύγχρονη πρακτική, δυσχεραίνουν τη σύνταξη μελετών και την εφαρμογή κατάλληλων μεθόδων. Μεγάλο ενδιαφέρον παρουσιάζει η καθαίρεση προβόλου από οπλισμένο σκυρόδεμα (!), ο οποίος είχε χρησιμοποιηθεί σαν κρηπίδωμα, καθώς και η αντικατάστασή του από πλωτά στοιχεία βαρέως τύπου.

Λέξεις κλειδιά: Ανάπλαση λιμένα, Επισκευές στοιχείων λιμένα, Παλιός λιμένας.

1 ΕΙΣΑΓΩΓΗ

Ο Ενετικός Λιμένας, ο οποίος λειτουργεί σήμερα σαν Μαρίνα και Αλιευτικό Καταφύγιο, καταλαμβάνει το Δυτικό τμήμα του Λιμενικού Συγκροτήματος του Ηρακλείου και αποτελεί συνέχεια του Κεντρικού – Επιβατικού και του Ανατολικού – Εμπορευματικού.

Σύμφωνα με ιστορικές μαρτυρίες, στην θέση του Ενετικού Λιμένα προϋπήρχε Μινωϊκός Λιμένας ο οποίος λειτούργησε από το 1100 π.Χ. έως το 1210 μ.Χ., οπότε κατασκευάστηκε ο Ενετικός Λιμένας, ο οποίος λειτουργεί μέχρι σήμερα.

Όπως είναι φυσικό, ο Λιμένας αναμορφώθηκε σταδιακά παρακολουθώντας τις εξελίξεις της τεχνολογίας κατασκευής των Λιμενικών Έργων, σε συνάρτηση με τις κατά καιρούς απαιτήσεις ελλιμενισμού, τα χαρακτηριστικά των σκαφών και την πρόοδο μεθόδων, μέσων και υλικών κατασκευής.

Η ανάπλαση του Ενετικού Λιμένα περιλαμβάνει την αποδόμηση του δυτικού κρηπιδώματος (Δ. Κ.), το οποίο παρουσιάζει θλιβερό θέαμα στην περιοχή του Κούλε και εγκυμονεί σοβαρούς κινδύνους για την ασφάλεια των διερχομένων, την βυθοκόρηση της λιμενολεκάνης, την ανανέωση και συμπλήρωση του εξοπλισμού, καθώς και επεμβάσεις αισθητικού και λειτουργικού χαρακτήρα.

Το Δ.Κ., μήκους 100μ και πλάτους 3.50μ, που αποτελείται από πλάκα Ο.Σ., πάχους 0.45μ σε μορφή προβόλου, αντικαθίσταται από κιβωτιόσχημα πλωτά στοιχεία βαρέως τύπου.

2 ΕΠΙΤΟΠΙΕΣ ΕΡΕΥΝΕΣ

Προκειμένου οι εγκαταστάσεις του Ενετικού Λιμένα να ανταποκριθούν στις σημερινές απαιτήσεις, έγινε λεπτομερής καταγραφή των υπάρχοντων έργων και έγιναν ερευνητικές γεωτρήσεις στην περιοχή του Δ. Κ. καθώς και στο μέσον της λιμενολεκάνης.

Οι ερευνητικές γεωτρήσεις στην περιοχή του Δ. Κ. κατέδειξαν ότι σε βάθος από τον πυθμένα μέχρι τα 15m, δεν υπάρχει σταθερό υπόβαθρο. Η χαλαρή αμμοιλύδης σύσταση του υπεδάφους δεν επιτρέπει την θεμελίωση έργου βαρύτητας, ενώ η λύση με έγχυτους πασσάλους Ο.Σ. καθίσταται προβληματική και ιδιαίτερα αντικοινωνική.

3 ΕΠΙΣΚΕΥΕΣ ΚΑΙ ΑΝΑΠΛΑΣΕΙΣ

Προτού εγκατασταθούν τα πλωτά στοιχεία βαρέως τύπου μπροστά στο Δ. Κ., προηγείται η καθαίρεση του υπάρχοντος διαβρωμένου προβόλου. Η διαδικασία αυτή απαιτεί ιδιαίτερη προσοχή και επιμέλεια. Εκτελείται σταδιακά με αδιατάρακτη κοπή. Η εκκίνηση της εργασίας γίνεται πάντα με εγκάρσιες τομές ανά 0.50m, ενώ ακολουθούν διαμήκεις εγκοπές ανά 1.00μ , ξεκινώντας από το άκρο του προβόλου και προχωρώντας σταδιακά μέχρι την ρίζα αυτού. Τα αποτεμνόμενα τεμάχια απομακρύνονται ενώ συνεχίζεται η διαδικασία καθαίρεσης του προβόλου.

Επάνω στο κρηπίδωμα του Ενετικού Λιμένα κατασκευάζεται ξύλινο κατάστρωμα, το οποίο αποτελείται από δοκούς, τεγίδες και σανίδες (πέτσωμα). Χρησιμοποιείται ξυλεία ανθεκτική σε θαλάσσιο περιβάλλον και με ικανοποιητική αντοχή σε κρούση και τριβή (τύπου IROKO, ή αναλόγου). Η στήριξη της ξυλοκατασκευής επάνω στο κρηπίδωμα γίνεται με ανξείδωτα μεταλλικά ελάσματα και κοχλίες. Μεταξύ των σανίδων του πετσώματος αφήνονται κενά πλάτους 10mm.

Στις θέσεις των δεσμών και των άλλων στοιχείων εξοπλισμού του κρηπιδώματος αφαιρείται έντεχνα τμήμα του πετσώματος. Η τελική επιφάνεια του καταστρώματος εμφανίζει ομοιογένεια και καλαισθησία.

Η βυθοκόρηση προβλέπεται να ξεκινήσει από την κεντρική περιοχή της λιμενολεκάνης και να επεκταθεί σταδιακά προς τα περιφερειακά κρηπιδώματα και να σταματά σε απόσταση 10m από αυτά. Η αποκομιδή των βυθοκορημάτων θα γίνεται με φορηγίδες ανοιγομένου πυθμένα (κλαπέτα) και η απόρριψή τους σε θαλάσσια περιοχή όπου τα βάθη θα ξεπερνούν τα 50m.

Κατά τον σχεδιασμό της ανακατασκευής και διαμόρφωσης των κρηπιδωμάτων του Ενετικού Λιμένα ελήφθη μέριμνα, ώστε η πρόσβαση των ατόμων με ειδικές ανάγκες (πάντα συνοδευομένων) στην περιοχή, να γίνεται απρόσκοπτα και με απόλυτη ασφάλεια.

Συγκεκριμένα, τα διαμορφωμένα με ξυλοκατασκευή καταστρώματα των κρηπιδωμάτων δεν θα παρουσιάζουν κλίσεις μεγαλύτερες του 10% σε όλη την έκτασή τους. Σε όλη την διαδρομή του καταστρώματος δεν παρουσιάζονται εμπόδια ή φραγμοί. Προβλέπεται επίσης κατάλληλο σύστημα πυρόσβεσης και άνετες και ασφαλείς έξοδοι διαφυγής.

Σε περίπτωση δυσμενών καιρικών συνθηκών, ή εκτάκτων καταστάσεων, θα απαγορεύεται η επίσκεψη του λιμένα από ΑΜΕΑ

Βιβλιογραφικές Αναφορές

Chapon J (1974) Travaux Maritimes I, II, Paris, EYROLLES.

Herbich J (1999) Handbook of coastal engineering. McGraw-Hill, New York, ISBN 0-07-134402-0.

Tsinker G (1995) Marine structures engineering specialized applications, Chapman & Hall. New York, ISBN 0-412-98571-3.

Spiridakis M, Azorakos S, Mavrakos S, Papazoglou V, Trezos G (1988) Compilation of a set of rules concerning floating pontoons. MARTEDEC Greece.



**SESSION 2 ENERGY EXTRACTION FROM
THE OCEANIC ENVIRONMENT**

Hydrodynamic performance of a floating wave energy converter system with multiple flaps

G. Sismani*, E. Loukogeorgaki

Department of Civil Engineering, Aristotle University of Thessaloniki, Thessaloniki, 54124, Greece

*Corresponding author: gsismani@civil.auth.gr

Abstract

In the present paper, a new Floating Wave Energy Converter System (FloWECS), consisting of a floating platform and multiple rotating flaps, is proposed and is preliminary investigated. The numerical analysis is implemented in the frequency domain under the action of regular head incident waves and it is based on a “dry” mode superposition approach. In this approach, the generalized modes concept is utilized for describing the relative to the platform rotation of the flaps, additionally to the six rigid-body modes. The required mode shapes of the generalized modes are determined through appropriate vector shape functions, which are derived in the present paper. The diffraction/radiation problem is solved using a numerical model based on the conventional boundary integral equation method. Initially, the hydrodynamic forcing of the “isolated” platform is assessed. Next, the hydrodynamic behaviour and the energy absorption of the FloWECS are investigated.

Keywords Wave energy converters, Rotating flaps, Generalized modes, Hydrodynamic response.

1 INTRODUCTION

In the last decades, the global demand for energy security enhancement has led to a growing interest towards wave energy exploitation, as waves offer an abundant renewable energy source. As a result, various configurations/types of offshore Wave Energy Converters (WECs) have been proposed and developed by many researchers. However, up to now there is not a generally “approved” type of WEC, which has managed to overcome existing technological barriers, such as long-term reliability and survivability in the sea, while being at the same time financially viable (Magagna and Uihlein 2015). Therefore, wave energy technology still advances targeting to the development of new, energy-effective, cost-efficient and reliable WEC systems and, therefore, to the establishment of competitiveness with other renewable energy sources. Motivated by this, in the present paper, a new FloWECS is proposed and is preliminary investigated.

2 DESCRIPTION OF THE PROPOSED SYSTEM

The proposed FloWECS (Figure 1) of total draft, h , and of total radius, r_1 , consists of: (a) a floating platform, which has a central, semi-submerged, floating cylinder of large radius, r_2 , and four submerged pontoons of height, h_p , attached in the cylinder’s circumference and (b) four, submerged, rotating flaps hinged at the pontoons with two rigid structural arms, along with linear Power Take-Off (PTO) mechanisms for wave energy absorption. Elliptical flaps (maximum width, b_f , maximum height, h_f , and length, l_f , Figure 1) are selected for the FloWECS as, according to Kurniawan and Moan (2013), they achieve higher energy absorption compared to other flap configurations. Similar flaps have been combined with a Semi-Submersible Wind Turbine and were investigated by Luan et al. (2014). Due to its circular configuration and the placing of several flaps in its circumference, the proposed FloWECS has the main advantage of wave energy absorption independently of the incident wave direction, through the concurrent operation of two or more flaps. Moreover, the large diameter of the FloWECS’ central cylinder offers the potential to install a wind turbine or PV panels on the cylinder’s deck towards the combined exploitation of wave energy with offshore wind or solar energy.

In the present paper, a FloWECS of $r_1 = 50$ m and $h = 24$ m is examined, with a central cylinder of $r_2 = 25$ m and four submerged pontoons of $h_p = 6$ m. Each of the four elliptical flaps has $b_f = 3.5$ m, $h_f = 7$ m and $l_f = 20$ m and it is hinged to a pontoon with two supporting arms of length, l_s , equal to

12.5 m. All flaps are fully submerged and are placed below the Mean Water Level (MWL) at a distance $d_f = 2$ m from it (Figure 1).

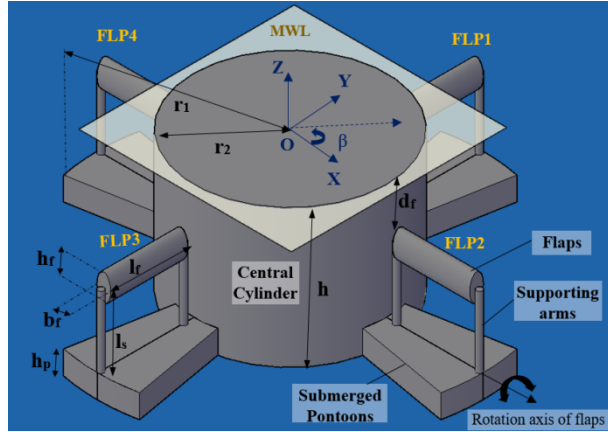


Figure 1 General view of the proposed FloWECS

3 NUMERICAL MODELLING

The FloWECS' hydrodynamic analysis is implemented in the frequency domain under the action of regular incident waves and it relies on the boundary integral equation method, which is numerically realized using the WAMIT© software (Lee 1995). The analysis is based on a three-dimensional linear potential theory, where the whole system is assumed to undergo small oscillations of complex amplitude $\xi_j, j = 1, \dots, 6$, in its six Degrees Of Freedom (DOFs) corresponding to rigid-body modes. Moreover, the relative to the platform motion (rotation) of the four flaps is taken into account through the inclusion of $N = 4$ additional DOFs, which correspond to generalized modes of body motion with amplitude $\xi_j, j = 7, \dots, (6 + N)$. The required mode shapes of the generalized modes are determined in this paper in vacuum ("dry" mode superposition approach), through the derivation of appropriate 3D vector shape functions, $\mathbf{S}_j, j = 7, \dots, (6 + N)$, as described below, based on the approach introduced by Newman (1994). The 1st order boundary value problem is solved based on a three dimensional low-order panel method, utilizing Green's theorem and imposing the appropriate boundary conditions on the free surface, the sea bottom, and on the floating body (Lee and Newman 2005). The radiation potentials, φ_j , for $j = 7, \dots, (6 + N)$, are subjected to the following boundary condition on the body boundary (Newman 1994):

$$\frac{\partial \varphi_j}{\partial n} = n_j = \mathbf{S}_j \mathbf{n} \quad (1)$$

where $\mathbf{n} = (n_x, n_y, n_z)$ is the unit normal vector.

Coming back to the vector shape functions, $\mathbf{S}_j, j = 7, \dots, (6 + N)$, is calculated at the middle of each panel of the FloWECS' discretized wetted surface, considering a unit rotation for each $(j - 6)$ th flap. Thus, assuming that the FloWECS' wetted surface has been discretized using NP panels, while each of the flaps has been discretized using NF panels, $\mathbf{S}_j, j = 7, \dots, (6 + N)$, has dimensions $(NP \times 3)$ and is defined as:

$$\mathbf{S}_j = \begin{bmatrix} \mathbf{S}_j^{\text{FLP}(j-6)} \\ \mathbf{S}_j^{\text{RM}(j-6)} \end{bmatrix} = \begin{bmatrix} \mathbf{u}_j^{\text{FLP}(j-6)} & \mathbf{v}_j^{\text{FLP}(j-6)} & \mathbf{w}_j^{\text{FLP}(j-6)} \\ \mathbf{0} & \mathbf{0} & \mathbf{0} \end{bmatrix} \quad (2)$$

where $\mathbf{S}_j^{\text{FLP}(j-6)}$ ($NF \times 3$) is the sub-matrix of \mathbf{S}_j corresponding to the panels of the $(j - 6)$ th flap, while $\mathbf{S}_j^{\text{RM}(j-6)}$ $[(NP - NF) \times 3]$ is the sub-matrix of \mathbf{S}_j related to the panels of the whole body except

for the $(j - 6)^{\text{th}}$ flap's panels. Moreover, $\mathbf{u}_j^{\text{FLP}(j-6)}$ ($NF \times 1$), $\mathbf{v}_j^{\text{FLP}(j-6)}$ ($NF \times 1$) and $\mathbf{w}_j^{\text{FLP}(j-6)}$ ($NF \times 1$) are the components vectors of $\mathbf{S}_j^{\text{FLP}(j-6)}$ along X, Y and Z directions respectively.

Based on the above, $\mathbf{S}_j^{\text{FLP}(j-6)}$, $j = 7, \dots, 10$, for the case of $N = 4$ flaps, are determined using Eq. 3, where θ is the unit rotation angle of each flap, \mathbf{X}_{j-6} ($NF \times 1$), \mathbf{Y}_{j-6} ($NF \times 1$) and \mathbf{Z}_{j-6} ($NF \times 1$), $j = 7, \dots, 10$, include the X, Y, Z coordinates of the middle of the panels of the $(j - 6)^{\text{th}}$ flap in the global coordinate system $OXYZ$. The corresponding mode shapes are schematically shown in Figure 2.

$$\begin{bmatrix} \mathbf{S}_7^{\text{FLP1}} \\ \mathbf{S}_8^{\text{FLP2}} \\ \mathbf{S}_9^{\text{FLP3}} \\ \mathbf{S}_{10}^{\text{FLP4}} \end{bmatrix} = \begin{bmatrix} \mathbf{X}_1 \cos \theta + \mathbf{Z}_1 \sin \theta + l_s \sin \theta & \mathbf{Y}_1 & -\mathbf{X}_1 \sin \theta + \mathbf{Z}_1 \cos \theta - l_s (1 - \cos \theta) \\ \mathbf{X}_2 & \mathbf{Y}_2 \cos \theta - \mathbf{Z}_2 \sin \theta - l_s \sin \theta & \mathbf{Y}_2 \sin \theta + \mathbf{Z}_2 \cos \theta - l_s (1 - \cos \theta) \\ \mathbf{X}_3 \cos \theta + \mathbf{Z}_3 \sin \theta + l_s \sin \theta & \mathbf{Y}_3 & -\mathbf{X}_3 \sin \theta + \mathbf{Z}_3 \cos \theta - l_s (1 - \cos \theta) \\ \mathbf{X}_4 & \mathbf{Y}_4 \cos \theta - \mathbf{Z}_4 \sin \theta - l_s \sin \theta & \mathbf{Y}_4 \sin \theta + \mathbf{Z}_4 \cos \theta - l_s (1 - \cos \theta) \end{bmatrix} \quad (3)$$

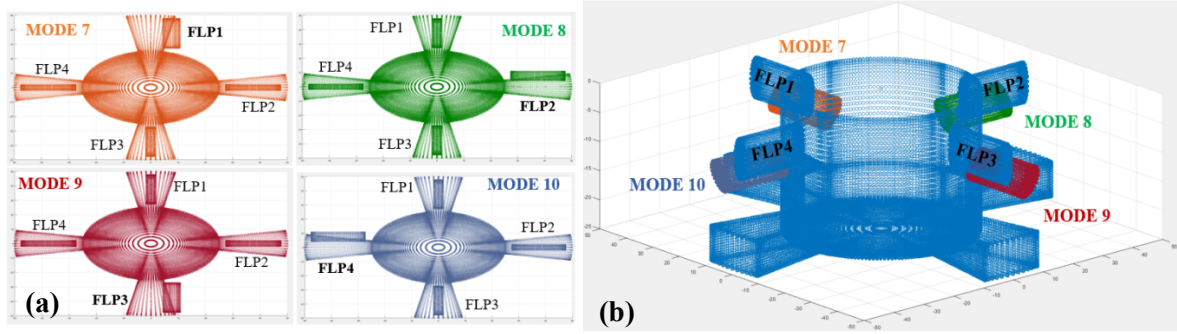


Figure 2 Mode shapes of the four generalized modes ($j = 7, \dots, 10$): a) Top view, b) 3D view

Having calculated 1st order hydrodynamic quantities, the amplitudes of the body's motions ξ_j , $j = 7, \dots, (6 + N)$, are obtained from the solution of the equation of motion (Eq. 4).

$$\sum_{j=1}^{6+N} [-\omega^2 (M_{ij} + A_{ij}) + i\omega (B_{ij} + B_{ij}^E) + C_{ij}] \xi_j = F_j \quad (4)$$

where, ω is the incident wave frequency, F_j are the generalized exciting forces, M_{ij} and C_{ij} are the coefficients of the generalized mass matrix and hydrostatic-gravitational stiffness matrix respectively, while A_{ij} and B_{ij} are the coefficients of the generalized added mass matrix and radiation damping matrix respectively. Finally, B_{ij}^E are the coefficients of the damping matrix caused by the PTO mechanisms. The PTO of each flap is modeled as a linear damping system, with b_{PTOi} , $i = 7, \dots, (6 + N)$, actuated from the rotational motion of the corresponding $(i - 6)^{\text{th}}$ flap. Therefore, $B_{ij}^E = b_{PTOi}$ for $i = j = 7, \dots, (6 + N)$, while $B_{ij}^E = 0$ for $i \neq j = 7, \dots, (6 + N)$. In the present paper, b_{PTOi} , $i = j = 7, \dots, (6 + N)$, is taken equal to the radiation damping of the i^{th} mode at its natural frequency, ω_{ni} , i.e. $b_{PTOi} = B_{ii}(\omega = \omega_{ni})$.

Finally, the total absorbed power of the FloWECS as a function of ω is calculated as follows:

$$P_{tot}(\omega) = \sum_{j=7}^{(6+N)} 0.5 b_{PTOj} \omega^2 |\xi_j|^2 \quad (5)$$

4 RESULTS AND DISCUSSION

The hydrodynamic analysis is implemented for regular head ($\beta = 0$ deg, Figure 1) waves with ω varying between 0.1 and 1.3 rad/s. Initially, the exciting force and the response of the "isolated" (without the flaps) platform of the proposed FloWECS is assessed, since this kind of structure presents a new configuration that has not been previously examined. For this purpose, the examined platform (referred hereinafter as "PLT3") is compared with two different platform configurations: a) a platform consisting of a single floating cylinder, i.e. without pontoons ("PLT1") and b) a platform consisting of a central cylinder and a continuous submerged pontoon attached at the lower part of the cylinder

(“PLT2”). In both PLT1 and PLT2 cases, the dimensions are defined in accordance with the dimensions of PLT3. Figure 3 shows indicatively the variation of the non-dimensional (in terms of $\rho g A r_2^2$) heave exciting force, F_3 , and of the heave response, expressed in terms of the Response Amplitude Operator, RAO_3 , as a function of ω . Based on Figure 3a, it can be easily concluded that F_3 for PLT3 has, contrary to PLT2, a quite smooth variation pattern, which is also very similar with the one obtained in the case of PLT1. Moreover, the values of F_3 for PLT3 are smaller compared to both PLT1 and PLT2 cases for most of the examined frequencies. As for RAO_3 (Figure 3b), the peak values of RAO_3 for the three examined platform cases occur at different frequencies, as a result of the existence of different heave natural frequencies, ω_{n3} ($\omega_{n3} = 0.849$ rad/s, 0.239 rad/s and 0.625 rad/s for PLT1, PLT2 and PLT3 respectively). It is interesting also to note that the existence of the pontoons (PLT2 and PLT3 cases) leads to a great reduction of the RAO_3 peak values compared to PLT1.

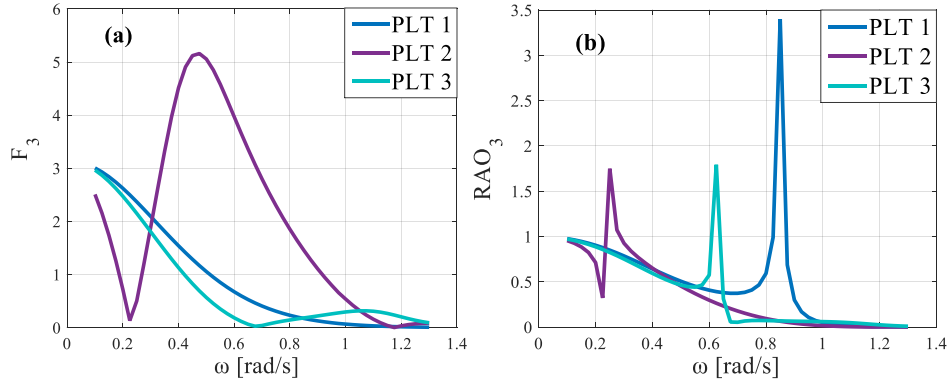


Figure 3 Effect of the platform's geometry on: a) F_3 , b) RAO_3

Next, the hydrodynamic behaviour and the energy absorption of the proposed FloWECS is assessed and investigated for head incident waves. In this case, the system is allowed to move freely only in heave, while for the examined β value, two of the four flaps (FLP1 and FLP3), corresponding to modes 7 and 9 (Figure 2a), are activated, since the other two flaps (FLP2 and FLP4) are parallel to the incident wave direction. Based on the hydrodynamic analysis of the examined FloWECS, the natural frequency of both the 7th and the 9th mode has been calculated equal to 0.225 rad/s, leading to b_{PTO_i} , $i = 7, 9$, values equal to $72,467.11$ Ns/m. In the following, r_2 has been considered as the characteristic length scale for non-dimensionalization.

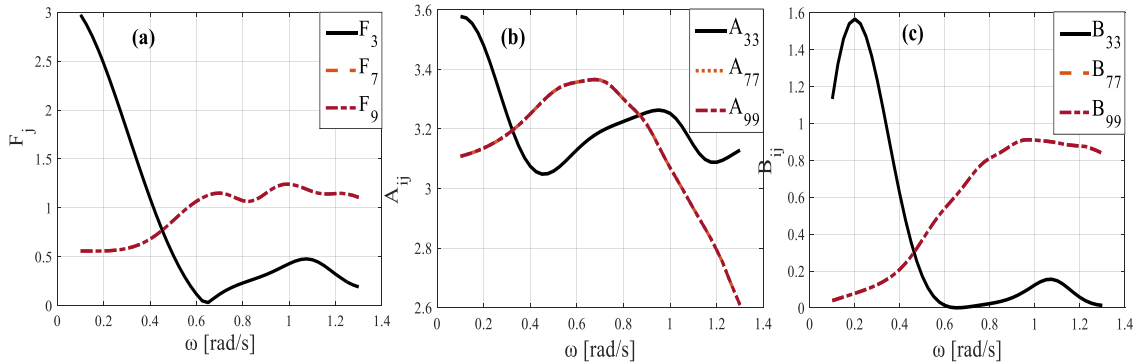


Figure 4 Variation of: a) F_j , $j = 3, 7, 9$, b) A_{ij} , $i = j = 3, 7, 9$, c) B_{ij} , $i = j = 3, 7, 9$ as a function of ω

Figure 4 shows the variation of the non-dimensional exciting force, F_j , $j = 3, 7, 9$, and of the non-dimensional added mass, A_{ij} , and radiation damping, B_{ij} , coefficients for $i = j = 3, 7, 9$, as a function of ω . As expected, the exciting forces and the hydrodynamic coefficients of the 7th and the 9th modes have exactly the same variation pattern and values. On the other hand, F_3 varies similarly with the case of the “isolated” platform (PLT3, Figure 3a), presented above. With regard to RAO_j , $j = 3, 7, 9$ (Figure 5a), RAO_j , $j = 7, 9$, have exactly the same values and the same variation pattern, which is characterized by the existence of two distinctive peaks. The first one is observed at $\omega = 0.2$ rad/s and

is attributed to the resonance of the 7th and the 9th modes at this frequency range ($\omega_{n7} = \omega_{n9} = 0.225$ rad/s). The second peak occurs at $\omega = 0.45$ rad/s and is related to the strong coupling of the 7th and 9th modes with heave along with the occurrence of heave resonance at this frequency range ($\omega_{n3} = 0.45$ rad/s). In an analogous manner, RAO_3 is characterized by the existence of two successive peaks, one at $\omega = 0.2$ rad/s and one at $\omega = 0.45$ rad/s, due to coupling effects with the 7th and the 9th modes and due to heave resonance respectively. It is noted that the peak values of RAO_j , $j = 3, 7, 9$, at $\omega = 0.2$ rad/s are very large. This fact is attributed to the values of the $bpto_i$, $i = 7, 9$, considered in the present paper, that may lead to very large responses close to resonance, as it has been also reported by Gunawardane et al. (2019). Finally, Figure 5b shows the variation pattern of P_{tot} as a function of ω , which has been calculated by applying Eq. 5 for $j = 7, 9$, considering the concurrent operation of FLP1 and FLP3 for the examined incident wave direction. The maximum absorbed power approximately equal to 200 kW/m² occurs at $\omega = 0.2$ rad/s, while a second peak with value equal to 70.76 kW/m² is observed at $\omega = 0.45$ rad/s. All the above are in absolute accordance with the discussion made above regarding RAO_j , $j = 7, 9$.

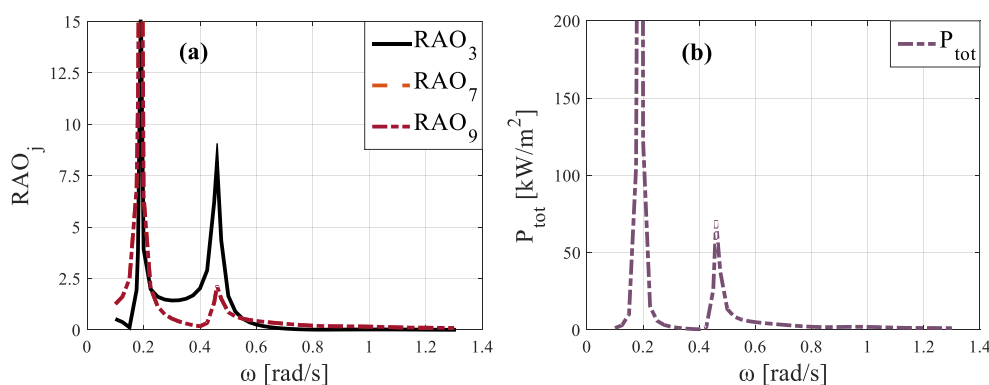


Figure 5 Variation of: a) RAO_j , $j = 3, 7, 9$, b) P_{tot} as a function of ω

5 CONCLUSIONS

In this paper, the generalized modes concept is utilized for the analysis of a new FloWECS, consisting of multiple rotating flaps. The required mode shapes are, initially, extracted, while, next, the FloWECS' hydrodynamic performance is preliminary assessed. The generalized modes' response is characterized by the existence of distinctive peaks at different ω values, attributed to resonance effects and to the strong coupling of these modes with heave. Consequently, the proposed FloWECS shows large power absorption at two frequency ranges. Further investigation is required towards the selection of appropriate damping values for the PTO, based on predefined maximum allowable rotations.

References

- Gunawardane SDGSP, Folley M, Kankanamge CJ (2019) Analysis of the hydrodynamics of four different oscillating wave surge converter concepts. *Renew Energ* 130:843-852. doi:10.1016/j.renene.2018.06.115.
- Kurniawan A, Moan T (2013) Optimal geometries for wave absorbers oscillating about a fixed axis. *IEEE J of Oceanic Eng* 38(1):117-130. doi: 10.1109/JOE.2012.2208666.
- Lee CH (1995) WAMIT theory manual. MIT report, Dept of Ocean Eng, MIT, p 95-2.
- Lee CH, Newman, JN (2005) Computation of wave effects using the panel method. In: Chakrabarti S (ed) *Numerical models in fluid-structure interaction*, WIT Press, Southampton, UK, p 211–251.
- Luan C, Michailides C, Gao Zh, Moan T (2014) Modeling and Analysis of a 5 MW Semi-Submersible Wind Turbine Combined With Three Flap-Type Wave Energy Converters. Paper presented at the 33rd International Conference on Ocean, Offshore and Arctic Engineering, San Francisco, California, USA. Paper No. OMAE2014-24215.
- Magagna D, Uihlein A (2015) Ocean energy development in Europe: Current status and future perspectives. *Int J Marine Energ* 11:84-104. doi: 10.1016/j.ijome.2015.05.001.
- Newman JN (1994) Wave effects on deformable bodies. *Appl Ocean Res* 16:47-59.

Hydrodynamic performance of a wave energy converter in front of a vertical wall

E. Spanaki^{1*}, E. Loukogeorgaki¹

¹ Department of Civil Engineering, Aristotle University of Thessaloniki, Thessaloniki, 54124, Greece

*Corresponding author: elespanaki@gmail.com

Abstract

The present paper focuses on the numerical investigation of the performance of a heaving Wave Energy Converter (WEC) placed in front of a bottom-mounted vertical wall. The analysis is implemented in the frequency domain under the action of regular and irregular waves, while emphasis is given on the effect of the WEC's dimensions, of the incident wave direction and of the distance between the WEC and the wall on the WEC's response and its power absorption. The results demonstrate that the device with the largest examined radius and draft is more effective in terms of power absorption for the examined installation site, while for given WEC's dimensions, the distance between the WEC and the wall affects significantly the power absorption of the WEC.

Keywords Heaving wave energy converter, Vertical wall, TMA spectrum, Absorbed power.

1 INTRODUCTION

Wave energy presents an abundant renewable energy source and, nowadays, the wave energy sector is rapidly growing, aiming at achieving competitiveness with other renewable energy sources. Various types of Wave Energy Converters (WECs) have been developed so far, which can be installed and operate either in offshore areas or at near-shore locations. At the latter locations, within the framework of integrating WEC technologies with other marine facilities (Mustapa et al. 2017) towards the realization of cost-efficient solutions, an oscillating-body device can be installed in front of existing coastal structures, such as vertical (wall-type) breakwaters. In those cases, hydrodynamic interactions between the WEC and the breakwater are introduced, which may have a direct impact on the absorbed power and, generally, on the overall performance of the WEC. Considering the well-known category of heaving WECs (point absorbers), there are a few studies dealing so far with the performance of this kind of device in front of a vertical wall. Specifically, Schay et al. (2013) assessed in the frequency domain the power absorption of a single heaving WEC (cone and hemispherical cylinder) in front of a bottom-mounted, vertical wall of infinite length, while the power absorption of an array of five heaving WECs placed in front of the aforementioned bottom-mounted structure has been investigated in both frequency and time domain by Mavrakos et al. (2004).

In the present paper, the performance (hydrodynamic behavior and energy absorption) of a free-floating, heaving, cylindrical WEC placed in front of a bottom-mounted vertical wall is investigated in the frequency domain. The WEC is selected to be installed at the North coast of Crete island, Greece, while energy is produced through a linear Power Take Off (PTO) mechanism, actuated from the heave motion of the WEC. The diffraction/radiation problem, assuming a wall of infinite length, is solved by utilizing the conventional boundary integral equation method. Two different geometries of the WEC are examined by modifying the radius and the draft of the device. The action of regular and irregular waves is taken into account, while focus is given on the effect of the WEC's dimensions, of the incident wave direction and of the distance between the WEC and the wall on the response and the power absorption of the WEC.

2 NUMERICAL MODELLING

A free-floating heaving cylindrical WEC of radius r and draft d is placed in an area of finite and constant water depth h in front of a bottom-mounted vertical wall at a distance b from it, as shown in Figure 1a, where the PTO mechanism is schematically represented as a linear damping system, with damping coefficient b_{pto} . The WEC and the wall are subjected to the action of regular incident waves of linear amplitude A and of circular frequency ω that propagate with angle β with respect to the

global horizontal X axis (Figure 1b). The WEC's hydrodynamic analysis, including hydrodynamic interaction effects between the WEC and the wall, is performed in the frequency domain under the action of regular waves. It is based on a 3D linear potential theory, where the WEC is also considered to oscillate freely only along its working direction, i.e. along the z direction (Figure 1a). For taking into account the wall, the method of images is applied (e.g. Mavrakos et al. 2004), assuming, therefore, the existence of a “pure” wave reflecting wall of infinite length.

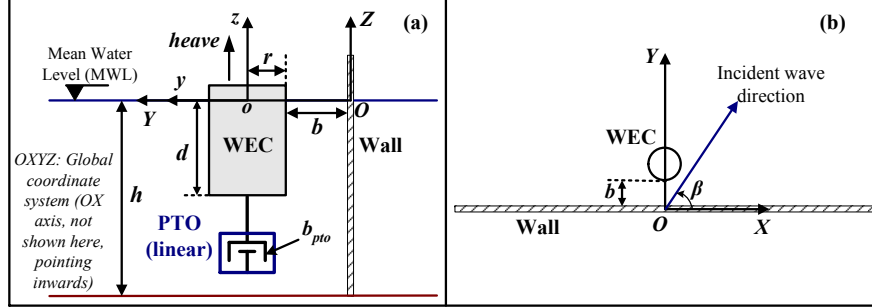


Figure 1 Geometry of the examined problem: a) $Y - Z$ plane, b) $X - Y$ plane

The 1st order boundary-value problem is formed and solved based on the boundary integral equation method (Lee and Newman 2005). The calculation of 1st order hydrodynamic quantities follows, while, finally, the WEC's response is obtained by solving the equation of motion, which is formed as follows:

$$[-\omega^2(m + A_{33}) + i\omega(B_{33} + b_{PTO}) + C_{33}]\xi_3 = F_3 \quad (1)$$

In Eq. 1, the subscript 3 denotes heave motion, $i^2 = -1$, F_3 is the heave exciting force, ξ_3 is the complex amplitude of heave, m is the mass of the WEC, A_{33} and B_{33} are the heave added mass and radiation damping coefficients respectively, while C_{33} presents the heave hydrostatic stiffness coefficient. b_{PTO} corresponds to the damping coefficient caused by the PTO mechanism, which is taken equal to the WEC's heave radiation damping at its heave natural frequency, ω_{n3} .

The heave response of the WEC is expressed in terms of the Response Amplitude Operator (Eq. 2), where $|\xi_3|$ denotes the amplitude of the complex quantity ξ_3 :

$$RAO_3 = \frac{|\xi_3|}{A} \quad (2)$$

For regular waves, the mean power, $p(\omega)$, absorbed by the WEC at a specific ω is given by:

$$p(\omega) = 0.5b_{PTO}\omega^2RAO_3^2 \quad (3)$$

For irregular incident waves, the absorbed power, $p(H_s, T_p)$, for a given sea state described by a spectrum with significant wave height, H_s , and peak period, T_p , is calculated as follows:

$$p(H_s, T_p) = \int_0^\infty S_{TMA}(\omega|H_s, T_p)p(\omega)d\omega \quad (4)$$

In Eq. 4, $S_{TMA}(\omega|H_s, T_p)$ is the spectral density of the TMA spectrum (e.g. Bergdahl 2009), which is deployed in the present paper as the incident wave spectrum in order to take into account limited water depth conditions. More specifically, the TMA spectrum has a finite depth spectral formulation and corresponds to a modified Jonswap spectrum in shallow waters. For a given sea state with H_s and T_p , $S_{TMA}(\omega|H_s, T_p)$ can be obtained by multiplying the corresponding spectral density of the Jonswap spectrum with the so-called “limited depth” function, $\Phi(h, \omega)$, given by Eq. 5 below (e.g. Bergdahl 2009). The spectral density of the Jonswap spectrum is obtained using the well-known relevant formulation (e.g. DNV-GL 2017).

$$\Phi(h, \omega) = \begin{cases} 0.5 \left(\omega \sqrt{h/g} \right)^2 & \text{for } \omega \sqrt{h/g} < 1 \\ 1 - 0.5(2 - \omega \sqrt{h/g})^2 & \text{for } 1 \leq \omega \sqrt{h/g} < 2 \\ 1 & \text{for } \omega \sqrt{h/g} \geq 2 \end{cases} \quad (5)$$

3 CHARACTERISTICS OF THE PHYSICAL PROBLEM EXAMINED

In the present paper, the WEC is selected to be installed in front of a vertical (wall-type) breakwater ($h = 12$ m) at the North coast of Crete island, Greece. The installation area is mainly affected by wind-generated waves of North (N), North-East (NE) and North-West (NW) directions corresponding to $\beta = 270^\circ$, 225° and 315° respectively (Figure 1b). Eight different sea states are taken into account, with characteristics shown in Table 1. The sea state No. 4 corresponds to the most frequent one having annual frequency of occurrence equal to 16.26%. All the above characteristics correspond to irregular waves. In the case of regular waves, the numerical analysis is implemented for the aforementioned β values and for ω varying between 0.4 and 3.5 rad/s.

Table 1 Examined sea states

No. of Sea State	N direction ($\beta = 270^\circ$)		NE direction ($\beta = 225^\circ$)		NW direction ($\beta = 315^\circ$)	
	H_s (m)	T_p (s)	H_s (m)	T_p (s)	H_s (m)	T_p (s)
1	0.010	0.517	0.010	0.517	0.010	0.517
2	0.113	1.772	0.113	1.772	0.113	1.772
3	0.478	3.640	0.478	3.640	0.478	3.640
4	1.345	6.106	1.345	6.106	1.345	6.106
5	2.216	7.214	2.239	7.262	2.064	6.883
6	3.105	8.090	3.137	8.145	2.892	7.720
7	4.127	8.912	4.169	8.972	3.844	8.503
8	5.284	9.693	5.338	9.759	4.921	9.249

As for the WECs, two different WEC geometries (WEC1 and WEC2) are examined. WEC1 has small d and r ($d/h = 0.06$ and $r/h = 0.08$), while WEC2 is a deep draft cylinder ($d/h = 0.5$) of larger radius ($r/h = 0.33$). For each WEC, we examine three different values of b equal to 0.5 m, 1 m and 4 m. The heave natural period of both WECs, $T_{n3} = 2\pi/\omega_{n3}$, along with the corresponding values of $b_{PTO} \equiv B_{33}(\omega = \omega_{n3})$ are shown in Table 2 for all three examined b values. It is emphasized that T_{n3} and b_{PTO} have been calculated by taking into account the effect of b on A_{33} and B_{33} . Based on Table 2, it can be easily concluded that WEC2 presents a well-tuned device for the specific installation site, since its T_{n3} for all b values examined is closer to the peak period ($T_p = 6.11$ s) of the most frequent sea state of the installation site (sea state No.4, Table 1).

Table 2 T_{n3} and b_{PTO} for WEC1 and WEC2

No. of WEC	$b = 0.5$ m		$b = 1.0$ m		$b = 4.0$ m	
	T_{n3} (s)	b_{PTO} (kNs/m)	T_{n3} (s)	b_{PTO} (kNs/m)	T_{n3} (s)	b_{PTO} (kNs/m)
WEC1	2.14	1.517	2.15	0.841	2.19	1.442
WEC2	5.90	46.725	5.87	46.849	5.74	35.819

4 RESULTS AND DISCUSSION

For the case of regular waves, Figure 2 shows the effect of b and β on $p(\omega)$ (Eq. 3) for WEC1 (Figure 2a) and WEC2 (Figure 2b). In the case of WEC1, b affects significantly $p(\omega)$. For both examined β values, largest peaks of $p(\omega)$ occur when WEC1 is installed far from the wall ($b = 4$ m). On the other hand, in the case of WEC2, the placement of the device close to the wall affects positively its power absorption, since the largest $p(\omega)$ peak values are observed for $b = 0.5$ m for both $\beta = 225^\circ$ and 270° . With regard to the effect of β on $p(\omega)$, for a given WEC and b value, the action of perpendicular incident waves ($\beta = 270^\circ$) leads to a decrease of $p(\omega)$ compared to $\beta = 225^\circ$, which is more intense in the case of WEC1. Moreover, for WEC1 it introduces a shift of $p(\omega)$ peaks at smaller ω values (for $b = 0.5$ m and 4 m). Finally, the results of Figure 2 clearly illustrate that by increasing the device's draft and radius (WEC2), the power absorption effectiveness of the WEC is greatly enhanced. All the above are in absolute accordance with the results related to RAO_3 (Figure 3).

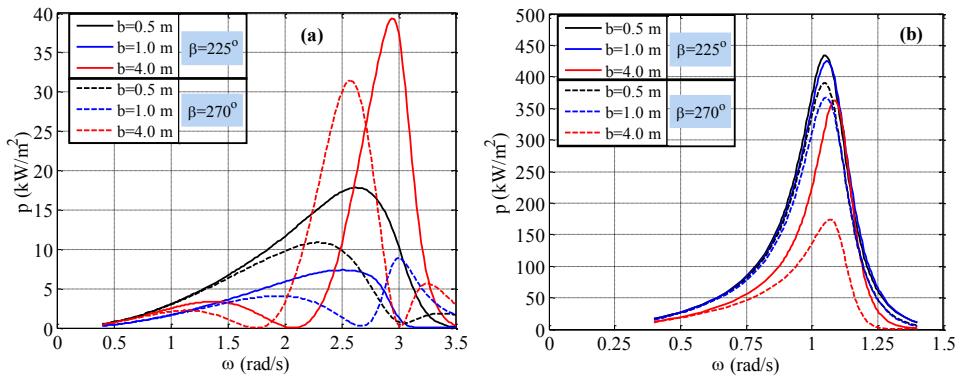


Figure 2 Effect of b and β on $p(\omega)$: a) WEC1, b) WEC2

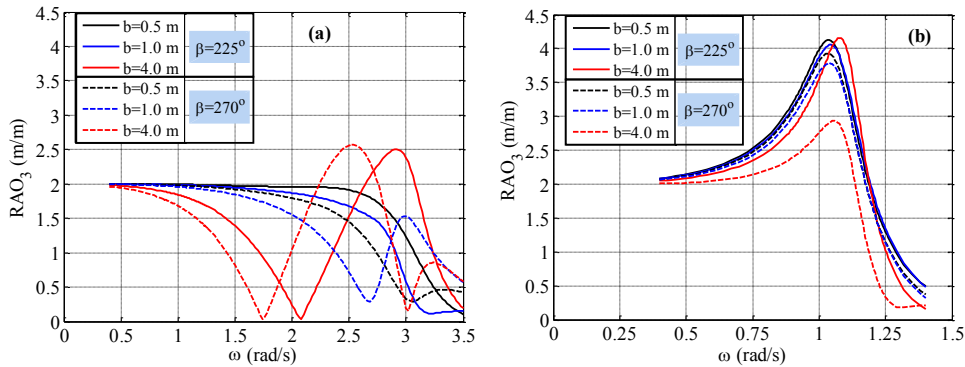


Figure 3 Effect of b and β on RAO_3 : a) WEC1, b) WEC2

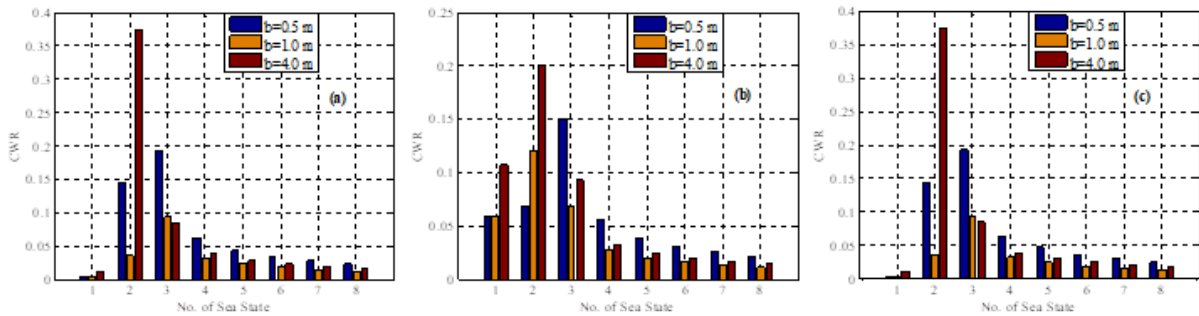


Figure 4 CWR of WEC1 for all b values examined and for: a) $\beta = 225^\circ$, b) $\beta = 270^\circ$, c) $\beta = 315^\circ$

In the case of irregular waves, the Capture Width Ratio (CWR) is used in order to assess the power absorption effectiveness of WEC1 and WEC2. CWR is defined as the ratio of the absorbed power (Eq.

4) to the product of the available power with the diameter, $2r$, of the WEC. Figures 4 - 5 show the CWR of WEC1 and WEC2 for the eight sea states of Table 1 and for the three examined b and β values. It is clear that WEC2 has a better power absorption ability, since it leads to larger CWR values for most of the examined sea states. For WEC1, the maximum CWR value (equal to 0.37) occurs for the sea state No. 2 and for $b = 4$ m (Figures 4a and 4c), while for WEC2, CWR obtains its maximum value (equal to 0.58) in the case of the site's most frequent sea state, i.e. sea state No. 4, for $b = 0.5$ m (Figures 5a and 5c).

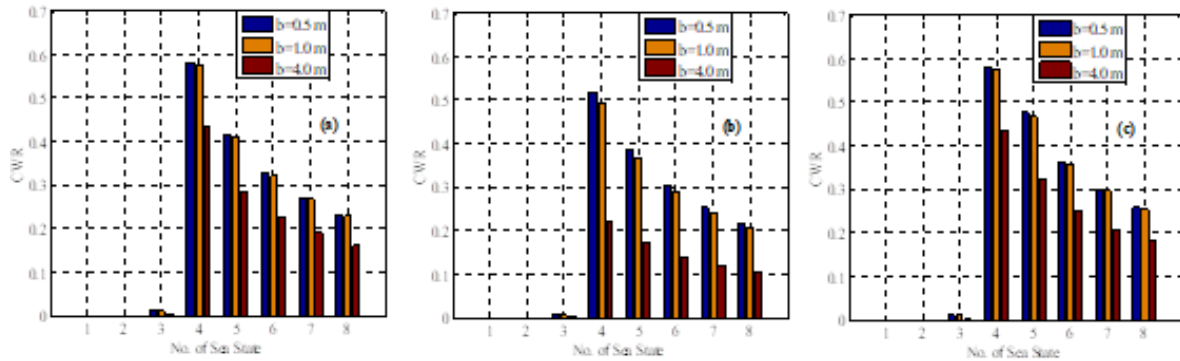


Figure 5 CWR of WEC2 for all b values examined and for: a) $\beta = 225^\circ$, b) $\beta = 270^\circ$, c) $\beta = 315^\circ$

5 CONCLUSIONS

In the present paper, the performance of a free-floating, heaving, cylindrical WEC placed in front of a bottom-mounted vertical wall is investigated in the frequency domain. Under the action of regular waves, the relevant results illustrate that the WEC's dimensions have a great effect on the WEC's response and, therefore, on its power absorption. Specifically, by increasing the draft and the radius of the device, the WEC's power absorption effectiveness is greatly enhanced. The placement of the deep draft cylinder (WEC2) close to the wall affects positively its power absorption, while the opposite holds true for WEC1. Moreover, for both WECs, maximum power absorption occurs under the action of oblique with respect to the wall waves. In the case of irregular waves, the deep draft floater (WEC2) shows a better annual power absorption effectiveness (525.5 kW per year compared to 15.1 kW for WEC1), since WEC2 is better tuned with respect to the characteristics of the site's most frequent sea state. Finally, for the specific installation site, the placement of WEC2 close to the wall affects positively its power absorption, since for $b = 0.5$ m CWR obtains its largest values, while the opposite holds true for WEC1, where the largest CWR values are observed for $b = 4.0$ m.

References

- Bergdahl L (2009) Comparison of measured shallow-water wave spectra with theoretical spectra. Paper presented at the 8th European Wave and Tidal Energy Conference, Uppsala.
- Det Norske Veritas – Germanischer Lloyds (DNV – GL) (2017) Environmental conditions and environmental loads. Recommended Practice DNVGL-RP-C205.
- Lee CH, Newman, JN (2005) Computation of wave effects using the panel method. In: Chakrabarti S (ed) Numerical models in fluid-structure interaction, WIT Press, Southampton, UK, p 211–251.
- Mavrakos SA, Katsaounis GM, Nielsen K, Lemonis G (2004) Numerical performance investigation of an array of heaving power converters in front of a vertical breakwater. Paper presented at the 14th International Offshore and Polar Engineering Conference, Toulon, France, 1:238–245.
- Mustapa MA, Yaakob OB, Ahmed YM, Rheem C-K, Koh KK, Adnan, FA (2017) Wave energy device and breakwater integration: A review. *Renew Sust Energ Rev* 77: 43–58. doi:10.1016/j.rser.2017.03.110.
- Schay J, Bhattacharjee J, Soares CG (2013) Numerical modelling of a heaving point absorber in front of a vertical wall. Paper presented at the 32nd International Conference on Ocean, Offshore and Arctic Engineering, Nantes, France, Paper No. OMAE2013-11491.

Hydrodynamic interactions by arrays of vertical axisymmetric bodies in front of a wall for wave energy converter applications

I. E. Anastasiou*, K. I. Chatjigeorgiou, D. Th. Tsaousis

School of Naval Architecture and Marine Engineering, National Technical University of Athens, Athens, 9
Heroon Polytechniou Ave, 15773 Zografos Campus, Greece

* Corresponding author: eiranasta@gmail.com

Abstract

The purpose of this study is to investigate the interactions of sea waves with arrays of vertical axisymmetric bodies, in front of a vertical wall. The circular (truncated) cylinders are conceived as wave energy converters for exploiting, through the heave forces, the wave energy transmitted to the solids. The wall is placed purposely to induce wave reflections technically with aim to amplify the wave potential that influences the solids yielding thus larger heaving motions. The main goal is to study possible alterations in the transfer functions of heaving motions and desirably the magnification of the productive interval of wave frequencies. The formulation of the problem is performed analytically using the matched eigenfunction expansion technique. The task is to develop an efficient, robust and fast solution methodology. The approach is accurate and complete in the sense that it does not account for reverse propagating waves which is typically used by the method of image bodies and assumes univocally that the wall is infinite. The obtained results show that indeed, the existence of the wall amplifies the magnitudes of the heave forces, while in the correct approach, does not double the values for zero frequency as for instance is done by the method of image bodies which by default assumes pure reflection of the waves by the infinite wall.

Keywords Hydrodynamics, Circular and Elliptical Cylinders, Wave Energy Converters, Addition Theorems.

1 INTRODUCTION

The hydrodynamic interactions developed between structures is of substantial importance for marine structures. A number of notable works that study hydrodynamic interactions with structures have been elaborated, such as Chatjigeorgiou and Mavrakos (2010), Chatjigeorgiou (2011), Chatjigeorgiou and Molin (2013), Chatjigeorgiou and Katsardi (2018), Chatjigeorgiou (2018), Chatjigeorgiou et al. (2019), Mavrakos et al. (2004), Siddorn and Eatock Taylor (2008) who tackled multiple bodies using analytical approaches. Cases of wall induced wave reflections were studied by Teng and Ning (2003) and Teng et al. (2009) who investigated the wave diffraction and radiation problem of a cylinder which is fixed on the bottom and is placed in front of a wall.

The present study extends past efforts including a vertical wall in front of an array of truncated cylinders. It develops a semi-analytical approach in an effort to investigate/examine the velocity potential generated by the superposition of the diffraction potential induced by the wall and by the truncated circular cylinders as well as the velocity potential due to the incoming wave. The wall is simulated as an elliptical cylinder, with a semi-minor axis equal to zero, fixed on the bottom and piercing the upper free surface. In the present investigation, arrays of circular truncated cylinders are placed in front of a vertical wall. Circular cylinders are preferred due to their simple geometry, the possibility to use the separable solutions of the Laplace equation, and mostly because they are dominant in numerous applications in the open ocean.

2 FORMULATION OF THE PROBLEM

2.1 *The boundary value problem*

The vertical wall is simulated as an elliptical cylinder with zero semi-minor axis and semi-major axis

equal to a . An elliptical coordinate system is used which is placed on the center of the wall. The transformation from elliptical to Cartesian coordinates is achieved through the equations $x = c \cosh u \cos v$ and $y = c \sinh u \sin v$, where u and v denote families of confocal ellipses and hyperbolae respectively, while c is the semi-focal distance which is equal to $c = \sqrt{a^2 - b^2}$. A local polar coordinate system is used for each cylinder, which is placed at the center of the cylinder. The transformation from polar to cartesian coordinates is achieved through $x = r_k \cos \theta_k$ and $y = r_k \sin \theta_k$.

The schematic of the problem considered herein is given in "Figure 1".

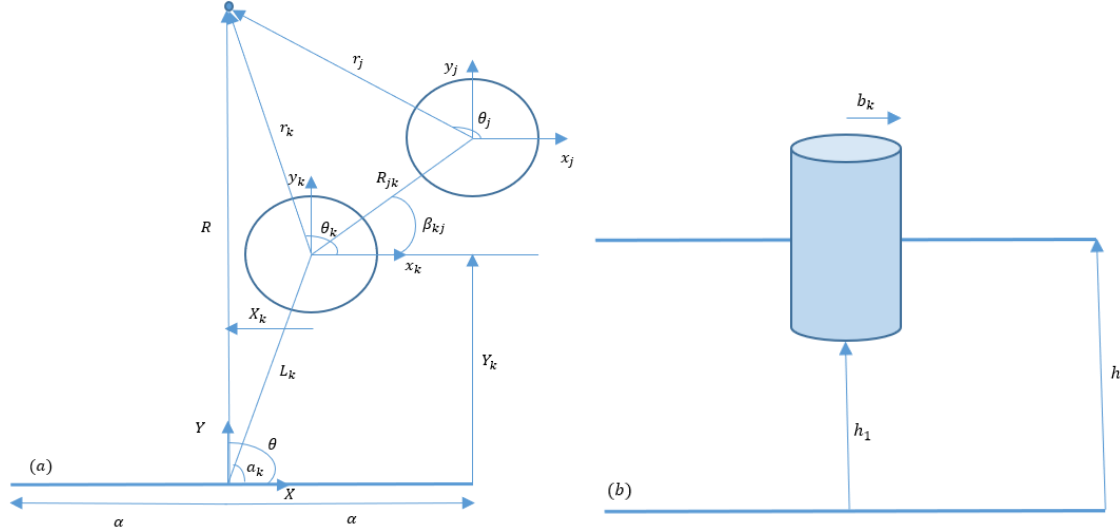


Figure 1 a) Top view, b) Side view

L_k is the distance between the center of the wall end the center of the cylinder k , α_k is the angle between the length L_k and the horizontal axis, b_k is the radius of the cylinder, $R_{jk} = R_{kj}$ is the distance between the center of two cylinders, β_{kj} is the angle between the length R_{jk} and the horizontal axis, h_{1k} is the distance between the flat bottom and the underneath area of the cylinder and h is the water depth.

We assume that the fluid is inviscid, incompressible and the fluid motion is irrotational. A regular wave with linear amplitude A and circular frequency ω is assumed as well, which propagates towards the arrays of the cylinders and the wall. All these assumptions allow as to introduce a linear velocity potential $\Phi(x, y, z, t)$, which can be written as:

$$\Phi(x, y, z, t) = Re[\varphi(x, y, z)e^{-i\omega t}] \quad (1)$$

The governing boundary value problem is expressed through the following equations:

$$\nabla^2 \varphi = 0, \quad \text{in } \Omega \quad (2)$$

$$-K\varphi + \varphi_z = 0, \quad \text{on } S_F, \quad z = h \quad (3)$$

$$\varphi_z = 0, \quad \text{in } \Omega, \quad z = 0 \quad (4)$$

$$\varphi_z = 0, \quad z = h_{1k}, \quad 0 \leq \theta_k \leq 2\pi, \quad 0 \leq r_k \leq b_k \quad (5)$$

$$\varphi_{r_k} = 0, \quad r = b_k, \quad 0 \leq \theta_k \leq 2\pi, \quad h_{1k} \leq z \leq h \quad (6)$$

$$\varphi_u = 0, \quad u \rightarrow 0, \quad 0 \leq z \leq h \quad (7)$$

where $K = \omega^2/g$, g is the gravitational acceleration, Ω is the liquid domain, which extends to infinity and S_F is the undisturbed free surface. "Eq. 2" is the Laplace equation "Eq. 3" is the free-surface boundary condition (dynamic and kinematic), "Eq.4" is the zero velocity condition which must be satisfied on the flat bottom, "Eq.5" is the zero velocity condition which should hold on the bottom surfaces of all cylinders, respectively and "Eqs.6-7" are the Neumann conditions on the wetted surface of the cylinders and the wall. The overall/total velocity potential that extends to the infinite domain (A) can be expressed as

$$\varphi_A = \varphi_I + \sum_{k=1}^N \varphi_D^{(k)} + \varphi_D^{(e)} \quad (8)$$

where φ_I denotes the incident wave, $\varphi_D^{(k)}$ is the diffraction caused by the k th cylinder and $\varphi_D^{(e)}$ is the diffraction caused by the wall. It is worth noting that the present boundary value problem can be solved only in the case where the total velocity potential is expressed with respect to a single coordinate system. The velocity potential(s) in the lower domain(s) below each cylinder is denoted by φ_B . The defined potentials must satisfy the following matching conditions

$$\frac{\partial \varphi_A}{\partial r_k} = \frac{\partial \varphi_B}{\partial r_k}, \quad r_k = b_k, \quad 0 \leq \theta_k \leq 2\pi, \quad 0 \leq z \leq h_{1k} \quad (9)$$

$$\varphi_A = \varphi_B, \quad r_k = b_k, \quad 0 \leq \theta_k \leq 2\pi, \quad 0 \leq z \leq h_{1k} \quad (10)$$

2.2 Exciting forces

The derivation of the velocity potentials allows the calculation of the hydrodynamic loading on the cylinders and the wall via direct pressure integration. The surge, sway and heave forced will be given by

$$F_x^{(k)} = -\rho g A b_k \int_{h_{1k}}^h \int_0^{2\pi} \varphi_A(b_k, \theta_k, z) \cos \theta_k d\theta_k dz \quad (11)$$

$$F_y^{(k)} = -\rho g A b_k \int_{h_{1k}}^h \int_0^{2\pi} \varphi_A(b_k, \theta_k, z) \sin \theta_k d\theta_k dz \quad (12)$$

$$F_z^{(k)} = \rho g A \int_0^{b_k} \int_0^{2\pi} \varphi_B(r_k, \theta_k, h_{1k}) r_k d\theta_k dr_k \quad (13)$$

2.3 Case Studies

The developed method is applied for an array of circular cylinders in front of a vertical wall. The array considered here consists of five circular cylinders arranged in a line. The radius of all the cylinders is equal to b and the length of the wall is equal to $6b$. This array is studied for two different cases in the first (case 1) "Figure 2" the distance between the cylinders is equal to $5b$ while in the second (case 2) "Figure 3" the distance is equal to $3b$. The cylinders are numbered from right to left.

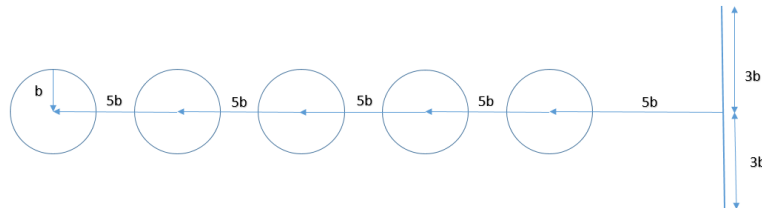


Figure 2 Case 1

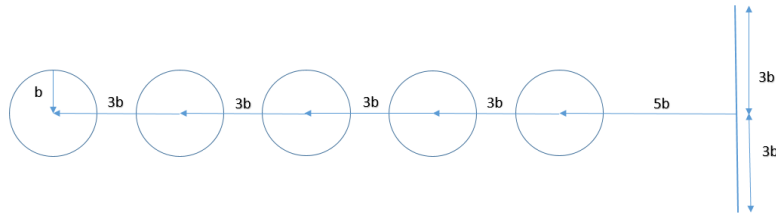


Figure 3 Case 2

3 RESULTS

Of major importance are the heave loads on the cylinders which are the mechanism for absorbing wave energy. Thus, only this type of forces will be presented. "Figures 4-6" depict the heave forces (normalized by $\rho g A b^2$), exerted on all cylinders assuming that the direction of the incoming wave 270 degrees. In each case, a wide range of wave frequencies has been taken into account. The results in "Figure 4a-5a" corresponds to the array which is depicted in "Figure 2" while the results in "Figure 5b-6b" corresponds to "Figure 3".

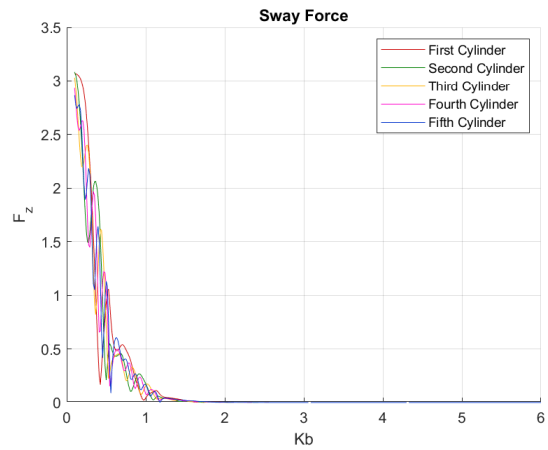
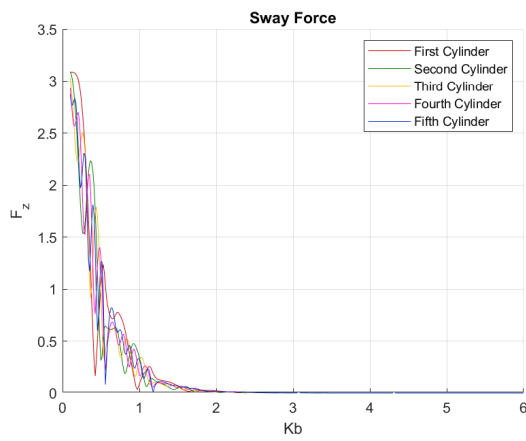


Figure 4 Heave forces on the cylinders case 1: a) $h_1/h = 0.5$, b) $h_1/h = 0.25$

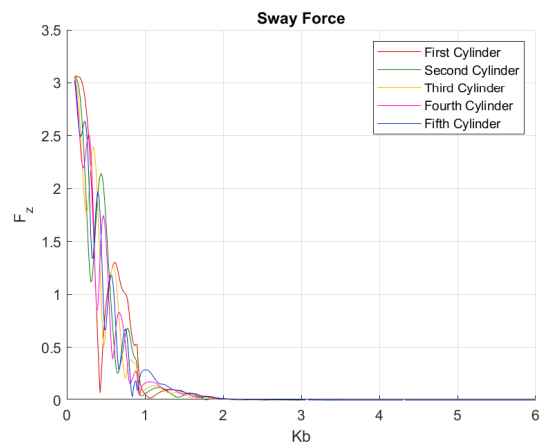
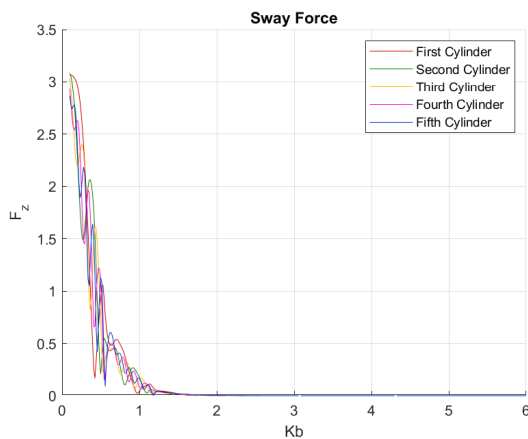


Figure 5 Heave forces on the cylinders: a) case 1 $h_1/h = 0.8$, b) case 2 $h_1/h = 0.5$.

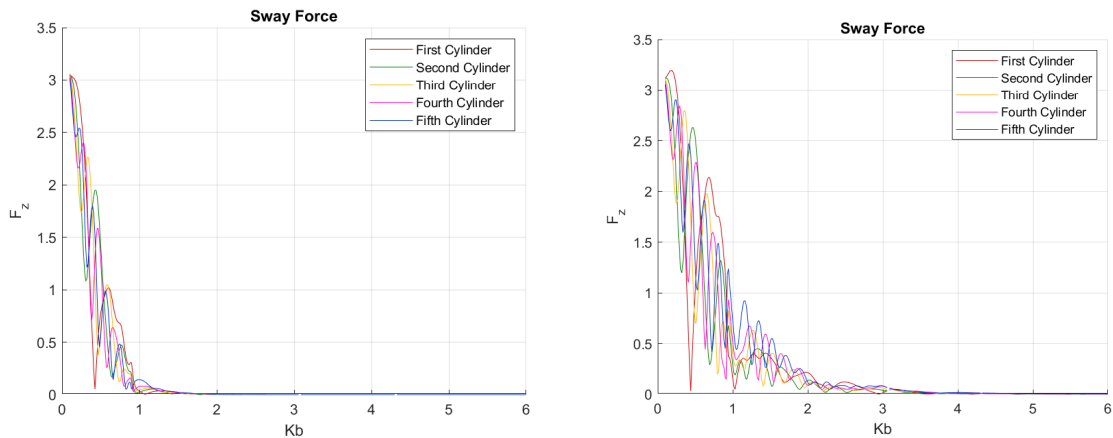


Figure 6 Heave forces on the cylinders case 2: a) $h_1/h = 0.25$, b) $h_1/h = 0.8$.

The results depicted in "Figures 4a-5a" demonstrate that the decrease of the depth increases the force in each cylinder. This conclusion is confirmed in "Figures 5b-6b". In particular while the distance between the cylinders is decreased the heave forces increases as well. Comparing "Figures 4a, 5b", "Figures 4b, 6a" and "Figures 5a, 6b" we may conclude that the decrease of the distance between the cylinders increases the heave force in each case.

4 CONCLUSIONS

The hydrodynamic diffraction problem by an array of circular cylinders in front of vertical wall was investigated. The ultimate task of the study is to design optimum wave energy converters of cylindrical shape. This is an ongoing work that will be followed by the investigation of additional configurations of WEC clusters.

References

- Chatjigeorgiou IK and Mavrakos SA (2010) An analytical approach for the solution of the hydrodynamic diffraction by arrays of elliptical cylinders, *Applied Ocean Research* 32, p 242-251.
- Chatjigeorgiou IK (2011) Three dimensional wave scattering by arrays of elliptical and circular cylinders, *Ocean Engineering* 38, p 1480-1494.
- Chatjigeorgiou IK and Molin B (2013) Third- order interactions, wave un-up and hydrodynamic loading on a vertical plate in an infinite wave field, *Applied Ocean Research* 41, p 57-64.
- Chatjigeorgiou IK and Katsardi V (2018) Hydrodynamics and near trapping effect in arrays of multiple elliptical cylinders in waves, *Ocean Engineering* 157, p 121-139.
- Chatjigeorgiou IK (2018) Water wave trapping in a long array of bottomless circular cylinders, *Wave Motion* 83, p 25-48.
- Chatjigeorgiou IK, Chatziioannou K and Mazarakos T (2019) Near trapped-modes in a long array of truncated circular cylinders, *Journal of Waterway, Port, Coastal and Ocean Engineering*, 145, 01018035.
- Mavrakos SA, Katsaounis GM, Nielsen K and Lemonis G (2004) Numerical performance investigation of an array of heaving power converters in front of a vertical breakwater, *Proceedings of the 14th International Offshore and Polar Engineering Conference*, Toulon, France, May 23-28.
- Siddorn P and Eatock Taylor R (2008) Diffraction and independent radiation by an array of floating cylinders, *Applied Ocean Research* 35, p 1289-1303.
- Teng B and Ning DZ (2003) Wave diffraction from a uniform cylinder in front of a vertical wall, *Ocean Engineering* 21, p 48-52.
- Teng B, Ning DZ and Zhang XT (2004) Wave radiation by a uniform cylinder in front of a vertical wall, *Ocean Engineering* 31, p 201-224.

Experimental investigation of the oscillating properties response of a three-legged jacket tower

V. Katsardi^{1*}, I. Santic², K. Chatziioannou¹, A. Koukouselis¹, E. Mistakidis¹, V. Tsoukala³, I.K. Chatjigeorgiou⁴

¹Department of Civil Engineering, University of Thessaly, Volos, Pedion Areos, 38334, Greece

²CNR-INM Italian Marine Technology Research Institute, Via di Vallerano, 139 - 00128 Roma, Italy

³School of Civil Engineering, National Technical University of Athens, Athens, Zografos, 15773, Greece

⁴School of Naval Architecture and Marine Engineering, National Technical University of Athens, Athens, Zografos, 15773, Greece

*Corresponding author: vkatsardi@civ.uth.gr

Abstract

The paper presents large scale laboratory measurements involving the response of a three-legged jacket structure representing the support structure of an offshore wind turbine. The full-scale structure was assumed to be installed in water depth ranging between 50-60m and in the laboratory scale the water depth was 3.5m. To simulate the flexibility of the foundation system and test the dynamic soil-wave-structure interaction, the jacket model was placed on top of a set of novel special devices (bearings), consisting of spring assemblies, allowing relatively small but realistic horizontal and vertical motions of the structure. The experimental data presented herein involve the oscillating properties response of the model subjected to ocean waves. Regular wave events are presented. It is shown that the structure moves as expected (and designed) in surge and pitch. The displacements were analogous to the wave steepness and peak displacements are evident near certain frequencies which indicate the occurrence of resonance or near resonance phenomena.

Keywords Three-legged jacket structure, Offshore wind energy, Large experimental scale.

1 INTRODUCTION

The current trend of the offshore industry for offshore renewables focuses towards the use of increased output wind turbines installed in large water depths using bottom founded or floating support systems (de Vries 2011; Musial and Ram 2010). Jacket substructures constitute an attractive solution, offering the required strength and stability to facilitate large output wind turbines and have been used in numerous offshore wind parks. In an attempt to minimize the construction costs of conventional four-legged jacket substructures, de Vries (2011) as well as Chew et al. (2013; 2014) investigated three-legged jackets as an alternative, showing that improvements in terms of their hydrodynamic performance and costs can be achieved. The present study concerns the experimental investigation of the oscillating properties of a three-legged jacket tower. The experimental study was conducted within the framework of MARINET-2 as a sequel of the work presented in MARINET and was realized in CNR-INM (former INSEAN) facilities in Rome.

2 METHODOLOGY

The present study concerns the experimental investigation of the oscillating properties of a three-legged jacket tower. A three-legged jacket support system, fabricated using a 1:18 scale-down factor, was examined under a wide range of steady/unsteady wave cases with characteristic wave steepness varying between 0.05 and 0.29. Experiments were conducted in a wave flume with length, width and depth equal to 220m, 9m and 3.5m respectively. Regular and random waves were generated by a mechanical wavemaker, situated at the end of the wave basin and were absorbed by an artificial sloping bay at the other end of the basin. Measurements were recorded with respect to surface elevation, wave run-up, peak displacements and acceleration measurements at the centroid of the assembly. Steady wave solutions were employed to investigate resonance phenomena and are presented herein.

2.1 The jacket configuration

The experimental setup outlined in the present study was based on a scaled-down model of such a structure. The geometric characteristics of the scaled-down model are presented in Figure 1(a). It has a triangular shape, tapering from a wide bottom section to a top smaller section, consisting of three columns, interconnected by means of bracings. The total height of the structure is 5.01m, while each side of the triangular shape has an axial length of 1.06m near the deck and an axial length of 1.75m at the bottom. The height of the jacket is 5.01m and the attachment of the pads increased this height to 5.32m. The three legs are interconnected by means of diagonal members. In total, five sets of diagonal members are arranged at each face along the height of the tower. The jacket was constructed by welding the steel tubular members. For the three columns, CHS219×5 tubular members were used, while for the bracings CHS114×5 ones. Finally, a 20mm thick plate was placed at the top of the jacket. The above configuration led to a structure with a total mass of approximately 1200kg. The scaling factor is not explicitly fixed, as the specific structure (in full scale) can be installed in various water depths. A rational scaling factor can be assumed to 1:18. Each side of the equilateral triangle at the bottom part of the model is 1.75m, which implies that in full scale the structure would occupy 430m² at the bottom.

2.2 Soil-structure interaction

In a previous project conducted within the context of the MaRINET EU program, the jacket was submerged in water in the long towing tank of the CNR-INM facilities in Rome and was subjected to various wave conditions. The results of this program have been published in Loukogeorgaki et al. (2016) and Chatjigeorgiou et al. (2018). Among the top priorities set for the present experimental program, which was funded by the MaRINET2 project, was to consider the flexibility of the foundation and test the dynamic soil-wave-structure interaction, when the structure is subjected to wave loads of different characteristics. For this reason, special devices were designed and constructed (bearings), consisting of spring assemblies, that were fastened at the baseplates of the columns, and, in turn, were attached at the bottom concrete slab of the basin, which simulate the flexibility of the foundation system.

Each bearing (Figure 1(b)) consists of a large rectangular plate [A], aimed to be fastened on the basin slab, on which two pairs of plates are perpendicularly welded. Plates [B] are used in order to hold the assembly of the vertical springs, while plates [C], [D] are used in order to hold the horizontal spring. Plates [B] have a horizontal longitudinal slot, in which two steel rods can move freely. The horizontal (resp. vertical) springs have an axial stiffness of 7.65kN/m (resp. 370kN/m). The vertical springs have an axial stiffness significantly higher than the horizontal springs, a typical situation in practical cases of pile foundations. It has to be emphasized here that the specific values of the axial stiffnesses used,

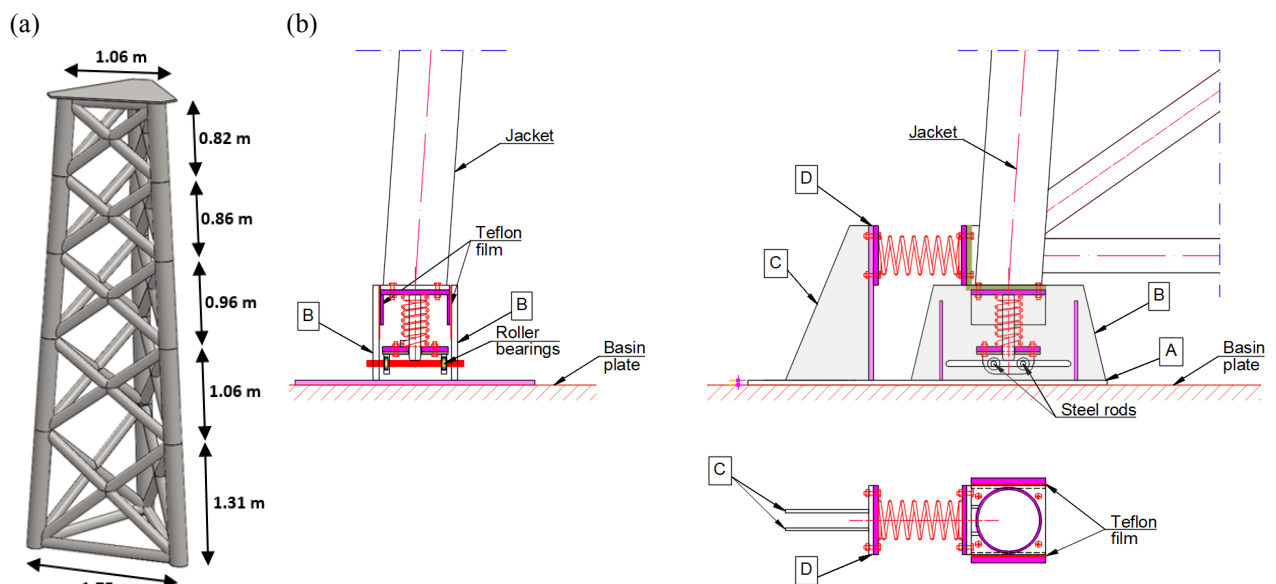


Figure 16 a) Jacket model, b) Bearing systems attached in each jacket leg

are not meant to simulate a real case of pile foundation, but rather to lead to a specific dominant period for the whole structural system, which was calculated to be 1.54s. This target for the dominant period was set, so that the wave periods causing resonance, to be within the capacity of the wave generator of the facility.

2.3 Instrumentation

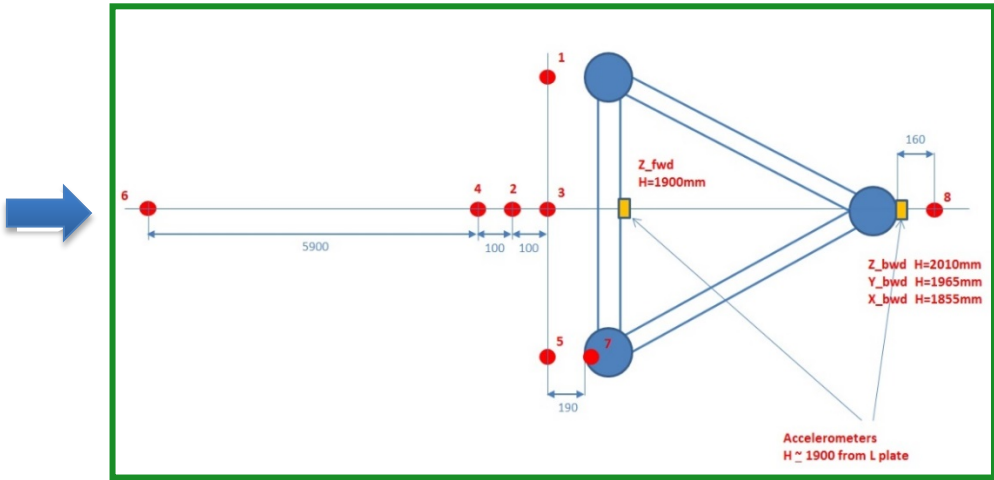
The model was oriented towards the wave maker as shown in Figure 22. The orientation of the model ensured the worst case of loading. Due to the inherent limitations of the experimental set-up in combination with the available measurement apparatus, the direct measurement of the induced hydrodynamic loading was an impossible task. Therefore, the quantities evaluated in this paper are (a) the accurate measurement of the wavefield, (b) the displacements at the of the structure’s top end.

With respect to (a), 9 wave gages were placed in the area of interest as shown in Figure 2. One of the wave gauges was placed in the far-field in order to measure the generated wave prior to any kind of interactions. An additional wave gauge was placed behind the structure, to identify the alterations of the wavefield due to the presence of the structure. In addition, six more wave gauges were placed near the front of the jacket, to allow the measurement of the surface elevation.

With regards to point (b), the time-history of the arising deformations was also measured during each trial. That was achieved with the use of a high accuracy, Krypton data acquisition device. The arising deformations were measured at the location of the plate, concerning all six-degrees of freedom, three for displacements and three for rotations.

3 RESULTS

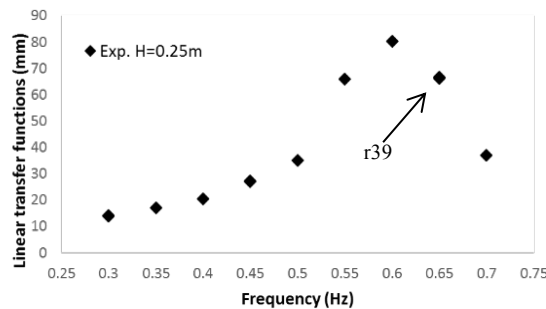
Both regular and long-crested irregular waves were tested; the paper focusing on the former. The laboratory measurements presented herein refer to a range of relatively small waves to the largest waves produced during the experimental sequel. Selected results are presented in **Error! Reference source not found.** In detail, the first column of **Error! Reference source not found.** presents the reference name of the experimental case addressed, with R referring to regular waves. The period T of the regular waves are presented in column 2. In the following columns (3-4) the measured wave heights H and respective wave steepness $kH/2$ are presented, for the positions corresponding to wave gauge 6 as shown in Figure 2 and represent the surface elevation, as it was derived by the wave-maker. The final two columns of **Error! Reference source not found.** present the response measurements associated with the dominant displacements (surge and pitch). The relatively small-wave cases, R-r14 and R-r28, which hit the jacket, are weakly nonlinear waves, while the rest of the cases are associated with highly nonlinear waves.



23. Figure 2 Schematic of the configuration

Table 1 Experimental measurements

Case	T (s)	Frequency (Hz)	H _{mo} (mm)	$\frac{kH_{mo}}{2}$	Max Surge (mm)	Max Pitch (deg)
R-r14	3.33	0.3	220	0.045	13.2	0.157
R-r28	2.00	0.5	300	0.151	60.4	0.657
R-r42	2.00	0.5	465	0.235	90.7	0.900
R-r39	1.54	0.65	250	0.213	68.1	0.755
R-r43	1.54	0.65	391	0.333	91.8	0.977
R-r27	1.43	0.7	200	0.197	44.1	0.492

**Figure 3** Linear transfer functions

The linear transfer functions obtained from the analysis of peak displacement measurements concerning regular wave tests with waveheight equal to 0.25m are shown in Figure 3. The maximum induced peak displacement is noticeably increased as the wave frequency approaches the value of 0.6Hz, indicating either the occurrence of resonance or near resonance phenomena or the increased forces due to the impact force caused by wave slamming. A similar trend is noted in the other tested cases. Indeed, R-r42 and R-r43 cases are associated with a large nonbreaking regular wave case and a breaking regular wave case respectively; the latter breaking on the jacket and not earlier in the wave basin. R-r43 has much larger wave steepness than R-r42 but both surge and pitch are of similar magnitude for both cases. This difference is also related with the additional wave-impact loads that are developed due to wave-slamming caused by wave breaking on the jacket (Wienke and Oumeraci 2005).

4 CONCLUSIONS

The paper presented laboratory measurements involving the response of a jacket structure properly scaled to represent (in full scale) an offshore wind turbine support structure. To simulate the flexibility of the foundation system and test the dynamic soil-wave-structure interaction, the jacket model is placed on top of a set of novel special devices (bearings), consisting of spring assemblies, allowing relatively small but realistic horizontal and vertical motions of the structure. The structure experienced the action of large regular waves. From the investigation of the measurements it is shown that the structure moves in surge and pitch, while the motions in the other degrees of freedom were, as expected (and designed), negligible. The displacements were analogous to the wave steepness. The focused events yielded larger displacements than regular waves of similar wave steepness. Nonlinear effects were evident. The occurrence of resonance or near resonance phenomena and/or the effect of impact forces is evident and the investigation of the irregular wave cases, where nonlinearity can become more important, is subject to future work.

Acknowledgements

This study was supported by the H2020 MaRINET-2 program (Marine Renewables Infrastructure Network for Emerging Energy Technologies) under the individual project VIHYDRO II and was realized in CNR-INM (former INSEAN) facilities in Rome. EREN Hellas S.A. additionally funded the project and VIO.DO.MI Constructions S.A. complimentary constructed the bearings.

References

- Chatjigeorgiou I-K, Chatziioannou K, Katsardi V, Koukouselis A, Mistakidis E (2018) Numerical and experimental investigation of the wave loading on a three-legged offshore wind turbine jacket platform. Paper presented at the 37th International Conference on Ocean, Offshore & Arctic Engineering. Paper No. 78416, Madrid, Spain.
- Chew, KH, Ng, EYK, Tai, K, Muskulus, M, Zwick, D (2014) Offshore Wind Turbine Jacket Substructure: A Comparison Study Between Four-Legged and Three-Legged Designs *Journal of Ocean and Wind Energy*, ISOPE 1:74-81
- Chew, KH, Ng, EYK, Tai, K, Muskulus, M, Zwick, D (2013) Structural Optimization and Parametric Study of Offshore Wind Turbine Jacket Substructure.
- Loukogeorgaki E, Lentsiou E-N, Chatjigeorgiou I-K (2016) Experimental Investigation of Slamming Loading on a Three-Legged Jacket Support Structure of Offshore Wind Turbines. Paper presented at the 26th International Conference on Offshore and Polar Engineering (ISOPE 2016), 192-198, Rhodes
- Musial, W, Ram, B (2010) Large-scale offshore wind power in the United States: Assessment of opportunities and barriers. Golden, US: National Renewable Energy Laboratory, p 1–221.
- de Vries, W (2011) Final Report WP 4.2: Support Structure Concepts for Deep Water Technical Report UpWind Deliverable D428, Delft University of Technology, Delft.
- Wienke J, Oumeraci H (2005) Breaking wave impact force on a vertical and inclined slender pile-theoretical and large-scale model investigations, *Coastal Engineering*, 52(5): 435-462.



SESSION 3 INPUT DATA FOR COASTAL STUDIES

UAS-SfM as a cost-effective tool for coastal monitoring and management

K. Lazogiannis¹, Emm. Vassilakis¹, S.E. Poulos¹, S. Kotsopoulos², J.D. Alexopoulos³, N. Alamanis², G. Papageorgiou²

¹Department of Geography & Climatology, Faculty of Geology & Geoenvironment, University of Athens, Panepistimioupolis, Zografou, 15784, Greece

²General Department, University of Thessaly, 41110, Larissa, Greece

³Department of Geophysics and Geothermy, Faculty of Geology and Geoenvironment, University of Athens, Panepistimioupolis, Zografou, 15784, Greece

*Corresponding author: klazog@geol.uoa.gr

Abstract

Coastal zone monitoring is essential in order to understand their evolution and incorporate sustainable coastal management practices. Frequent data collection is essential but often surveys can be costly and time-consuming. Several costly and time-consuming tools and techniques have been developed during the last few years for change detection and monitoring, allowing for both qualitative and quantitative analysis. In this study we present the ability of an off-the-shelf Unmanned Aerial Systems (UAS) coupled with Structure-from-Motion (SfM) photogrammetry to map and measure coastal features (e.g. shorelines). The UAS surveys taken place over three campaigns during Autumn 2017 (November), Spring 2018 (March) and Autumn 2018 (October) in Pinios river deltaic coast. The demonstrated UAS-SfM methodology produced remote sensing data with great spatial resolution which could be used to visually identify important parameters for coastal research and management at a fraction of the cost of other available techniques and. Even an off-the-shelf UAS is suitable for repeat surveys to assess spatial and temporal changes at small spatial extents and to better comprehend how these may be related with site-specific natural processes along the coast.

Keywords Coastal area Monitoring Management Remote sensing Structure from motion.

1 INTRODUCTION

Coastal zone monitoring of dynamic morphodynamical environments such as river deltas is essential in order to understand their evolution and incorporate sustainable coastal management practices. Frequent data collection is essential but often surveys can be costly and time-consuming. This often leads to increase the time lag between successive monitoring campaigns to reduce survey costs, with the consequence of fragmenting the data available for coastal zone management. In this study we present the ability of off-the-shelf Unmanned Aerial Systems (UAS) coupled with Structure-from-Motion (SfM) photogrammetry to map and measure coastal features (e.g. shorelines).

2 MATERIALS AND METHODS

2.1 Study Area

The study area is in Thessaly, an administrative region of Greece, on the western shore of the northwest Aegean Sea in the eastern Mediterranean Sea and the receiving basin is Thermaikos Gulf which extends from Thessaloniki bay to 200 m isobath (Figure 1). Annually, the deltaic coastline is mainly exposed to winds blowing from the north, northeast and east with a frequency of about 17%, 13% and 15% respectively. Additionally, waves have heights of <1 m and of >2 m with a frequency of 83.2 % and 4.82 % respectively (Athanasoulis and Skarsoulis 1992). From the dominant north direction, the fetch is about 105 km and the mean wave height is 0.6 m. Waves from the east have a fetch of 125 km and mean wave height of 0.9 m whereas, waves from the northeast have a reduced fetch of about 60 km and mean wave height of 0.8 m. The longest fetch is from southwest (275 km) but the waves originating from this direction are much less frequent (2.6 %). Hence, the Pinios delta is

exposed to long fetches available from N, NE, E and SW (Foutrakis et al. 2007) subjecting the deltaic coastline to a relatively monthly high wave attack of 70-1454 w/m² (Poulos et al., 2000). Surface currents are generally weak (<10 cm s⁻¹) (Karageorgis and Anagnostou 2001) and the mean tidal range is 19 cm (Tsimplis 1994). The socio-economic development in the deltaic plain is based on agriculture and tourism. Hence, the cultivated and urban areas have increased significantly over the recent decades and the main land use along the coastline is buildings (e.g. hotels, vacation residences). For the purposes of the study three segments of the deltaic coast were selected; Stomio, Alexandrini and Nea Mesagkala.

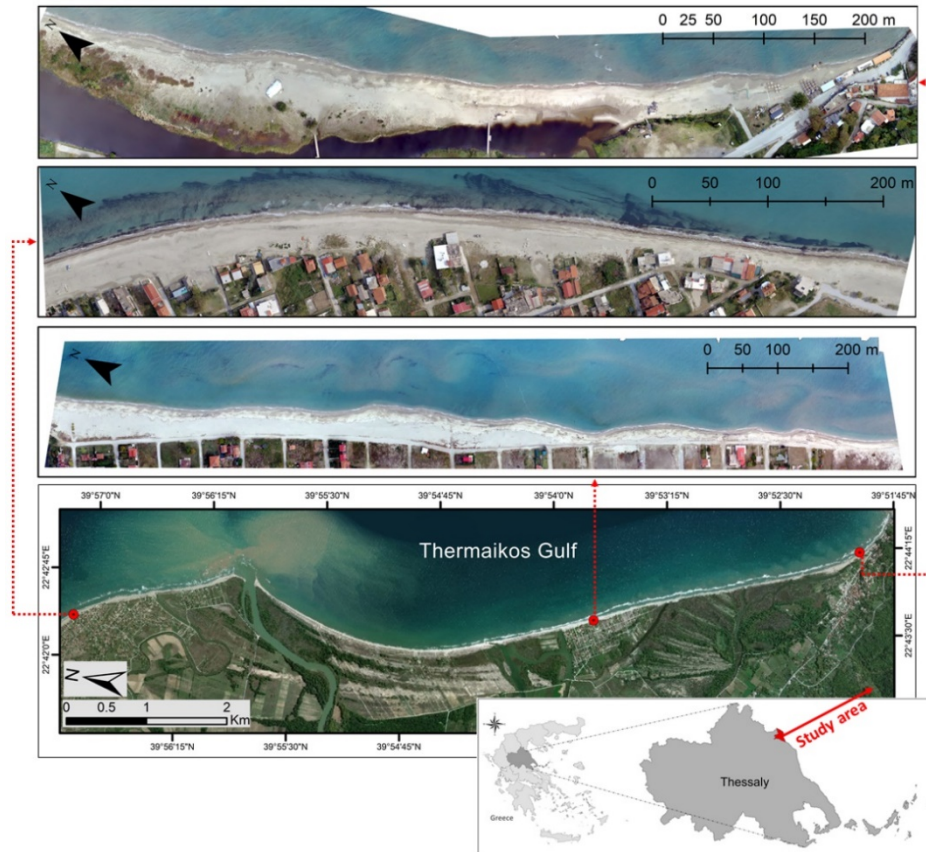


Figure 1 From bottom to top: Study area and UAS surveys in Alexandrini, Nea Mesagkala, and Stomio.

2.2 Methodology

2.2.1 UAS platform and field data collection

We deployed a Phantom 4 (P4) manufactured by DJI Inc. (Shenzhen, China); a popular quadcopter which has many features of interest for scientific applications. The integrated camera can acquire 12-megapixel still imagery and uses a wide-angle rectilinear lens and thus avoid the heavy distortions common with the fish-eye lenses employed in several older drone and camera models. For navigation and flight stabilization, the internal consumer-grade positioning system uses both the GPS and GLONASS systems, increasing the number of satellites used in the position determination. DJI's specifications report a positioning accuracy of ≈ 2.5 m; adequate especially for the horizontal axis the measurements of which are also used for the alignment of the images captured during the survey. These positions are automatically exported to the EXIF metadata for each image in WGS84 latitude and longitude thus providing a location stamp (geotag) for each image.

The high resolution natural colour aerial images of the three coastal areas were collected over three campaigns in Autumn 2017 (24/11/17), Spring 2018 (11/03/18) and Autumn 2018 (02/10/18). Skies were cloud free and wind speeds never exceeded P4's maximum wind speed resistance (10 m/s). Each fully automated survey was planned and executed with the freeware "Dronedeploy" mobile application which allows the user to define and check effortlessly on site a variety of flight and camera

capturing parameters (e.g. flight altitude and resolution, battery usage, front and side overlap etc.) before the image acquisition.

2.2.2 Structure-from-Motion

Visual-topographic point clouds and an orthomosaic were produced using SfM algorithms in Agisoft Metashape Professional software (Agisoft 2019). The SfM workflow to generate a point cloud includes photo alignment and tie point generation, camera optimization, and finally dense point cloud construction. Since fine topographic details were available, the workflow continued with meshing the original images. Texturing was also applied to the resulted mesh in a future step and a high quality orthophoto was generated (Figure 1).

2.2.3 Shoreline change monitoring

The most critical part of the methodology, in terms of shoreline change monitoring, is to identify with high accuracy the separation points between the waterbody and the land. To this purpose, the high quality orthophoto of each period was used (Figure 1). Due to very high density of pixels, the wet and dry areas were detected readily in the image, making the shoreline digitizing procedure an effortless task with very accurate results. Afterwards, the Digital Shoreline Analysis System v.4.3 (DSAS) was employed to estimate the seasonal shoreline changes. It is an extension of the ESRI ArcGIS v.10 software that computes rate-of-change statistics for a time series of shoreline vector data using a measurement baseline method. According to this method, the baseline is constructed by the user and serves as the starting point for all transects cast by the DSAS application. The measurement transects intersect each shoreline at the measurement points used to calculate rates of changes. The distances from the baseline to each intersection point along a transect are used to compute the selected statistics. For the purpose of this study an onshore baseline was constructed roughly parallel to the general trend of the coastline and transects were spaced at 5 m intervals. Although there are several methods for calculating the rate-of-change by DSAS, Net Shoreline Movement (NSM) method was chosen to analyze the shoreline changes. It is associated with the dates of only two shorelines and reports not a rate but the distance between the oldest and youngest shorelines for each transect (Thieler et al. 2009).

3 RESULTS AND DISCUSSION

3.1 *Nea Mesagkala*

This segment is located north of Pinios river mouth and is characterized by the expanding residential use of the beachfront over the past 30 years not within a coastal management framework. Also, during the summer season the beach is modified to create more space for recreational use. SCE analysis showed that the lowest maximum total change in shoreline movement is observed at Nea Mesagkala (13 m) among the three studied areas. In terms of NSM analysis, 78% of the shoreline has propagated from 11/2017 to 03/2018 (winter period) and 69% retreated from 03/2018 to 10/2018 (winter-summer) (Figure 2a and 2b). The same analysis for the period 11/2017-10/2018 reports that 77% of the shoreline has propagated (Figure 2c). Although SCE and NSM analysis reported insignificant net retreat during the monitoring period, this part of deltaic coast is the most vulnerable and susceptible to increases in wave runup, storms and inundation because of its physical attributes (e.g. gentle slope, small width, absence of dune system). As shown in Figure 3a at some parts of the stretch coastal buildings are affected by storms originating from the less frequent east and southeast waves during the year.

3.2 *Alexandrini*

This segment is located between the river mouth and Stomio and together with Nea Mesagkala is highly anthropized with many fixed structures along the beachfront. However, Alexandrini represents a more natural beach system than the Nea Mesagkala. DSAS analysis reported that maximum total change in shoreline movement in this part of deltaic coast is 19.3 m while the 67% and 62% of the shoreline retreated the periods 11/2017-03/2018 and 03/2018-10/2018 respectively. Even though, the above statistics suggest a risky and hazardous setting for coastal structures along the stretch, the undisrupted, in most cases, dune system, provide a buffer against extensive shoreline retreat and wave overtopping during storm events and provide a source of sand to replenish the beach during periods of

erosion a buffer against sea erosion and wave overtopping during storm events (Figure 3c).

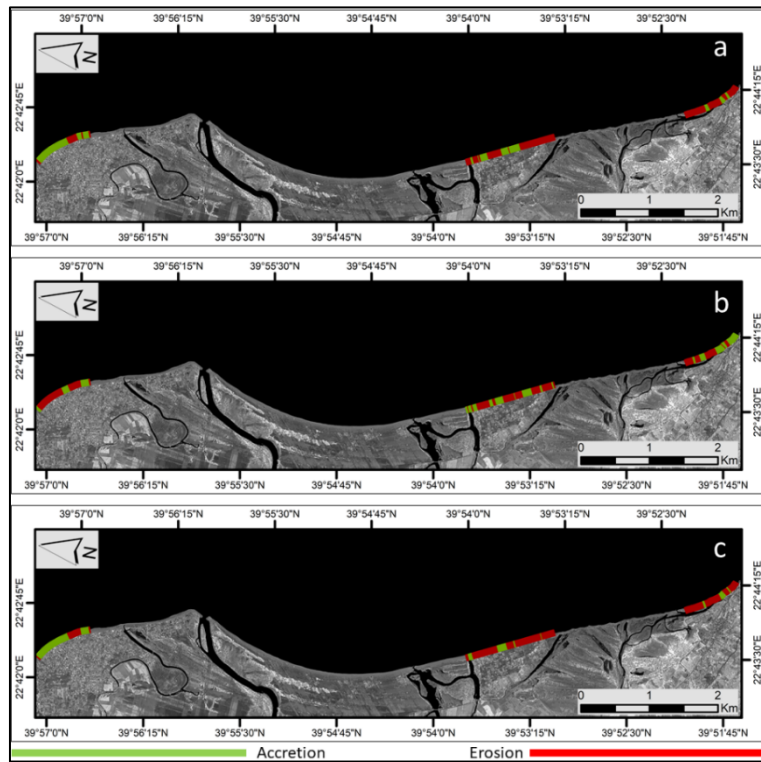


Figure 2 Results of NSM analysis during three periods: a) 11/2017–03/2018, b) 03/2018–10/2018 and c) 11/2017–10/2018.

3.3 Stomio

Stomio, positioned at the south edge of the deltaic coast, is not characterized by urbanization like the other two segments and can be considered as natural dynamic system controlled mainly by physical processes. It has the widest beach in the entire study area and hosts the mouth of an abandoned channel of Pinios river. Usually, during wet period the mouth is opened dividing the beach into two segments.



Figure 3 The potential of UAS surveys in coastal monitoring: a) old/contemporary wave runup level and disrupted dune at a part of Nea Mesagkala beach characterized by shoreline retreat during whole monitoring period, b) vegetated dunes and wave runup in Nea Mesagkala, c) beach cusps and eroded dune in Alexandrini

and d) beach cusps and winter vegetation in Stomio.

and providing additional sediment input. During the dry period the mouth is closed, and the beach is used for recreational and touristic purposes. Among the three studied segments, SCE analysis presented that the greatest maximum total change in shoreline movement for all available shoreline positions is observed at Stomio (34 m). However, the big beach width dissipates wave energy and consequently decreases the impact of storms. Like Alexandrini, exhibits almost identical trend through the monitoring period in terms of shoreline movement; 80%, 43% and 83% of the shoreline has retreated during the periods 11/2017-03/2018, 03/2018-10/2018 and 11/2017-10/2018 respectively.

It is worth noting that during the period 11/2017-03/2018 while in Nea Mesagkala most of the shoreline (78 %) has propagated in Alexandrini and Stomio most of the shoreline has retreated. Probably this difference was caused by flood incident occurred 15 days before the UAS survey. Nea Mesagkala beach being very close to the Pinios river mouth affected by the plume dispersion in a greater degree than the other two sites.

Finally, beach cusps, dunes and vegetated areas were detected and recorded easily at different sites and dates; their size and position could potentially provide valuable information about the state of the beach (accretion/erosion) and the related wave regime.

4 CONCLUSIONS

The use of UAS-SfM has enhanced the ability of monitoring coastal features. Thus, the extraction of the shoreline position was very precise (e.g. clearly visible berm, swash zone, beach step) and the resulted statistics characterized by very low uncertainty. UAS-SfM produces remote sensing data of great spatial resolution which could be used to visually identify important parameters for coastal research and management at a fraction of the cost of other available techniques and means (e.g. topographic surveys, airborne lidar and high-resolution satellite images). This method can serve as an important tool for coastal management because it is suitable for repeat surveys to assess spatial and temporal changes at small spatial extents and to better comprehend how these may be related with site-specific natural processes along the coast.

References

- Agisoft Metashape user manual: professional edition (v.1.5) https://www.agisoft.com/pdf/metashape-pro_1_5_en.pdf.
- Athanasoulis G.A. and Skarsoulis E.K. (1992) Wind and Wave Atlas of the Northeastern Mediterranean Sea. Hellenic Navy General Staff. Athens.
- Foutrakis P, Poulos S, Maroukian X, Livaditis G (2007) A study of the deltaic coast morphometry of River Pinios in relation to its hydro and sediment dynamics. Proceedings of the 11th Intern. Congr. Geol. Soc. Greece, Athens, vol. XXXX(4), 1522-1529.
- Karageorgis A.P. and Anagnostou C.L (2001) Particulate matter spatial-temporal distribution and associated sediment properties: Thermaikos Gulf and Sporades Basin, NW Aegean Sea. Continental Shelf Research 21, 2141-2153.
- Thieler E.R, Himmelstoss E.A, Zichichi J.L, Ergul Ayhan (2009) Digital shoreline analysis system (DSAS) version 4.3-An ArcGIS extension for calculating shoreline change: U.S. Geological Survey Open-File Report 2008-1278.
- Tsimplis, M.N, (1994) Tidal Oscillations in the Aegean and Ionian Seas. Estuarine, Coastal and Shelf Science, 39, 201-208.

Automated 2-D wave run-up detection from coastal video imagery. Examples from the islands of Santorini and Mykonos

A.E. Chatzipavlis*, V. Trygonis, A. Eleftheriou, O. Andreadis, I. Monioudi and A.F. Velegrakis

Department of Marine Sciences, University of the Aegean, University Hill, 81100, Mytilene, Greece

*Corresponding author: a.chatzipavlis@marine.aegean.gr

Abstract

In this contribution the results of an automated coastal feature, capable to detect the (2-D) wave run-up positions on specialized optical imagery of high spatio-temporal coverage are presented. The wave run-up detector was developed/used to record/monitor the positions of the swash maxima, in georectified coastal imagery obtained through a Beach Optical Monitoring System (BOMS). The automated procedure was tested on video imagery obtained from two highly touristic beaches (Kamari, Santorini and Kalo Livadi, Mykonos), during a highly energetic 3 and 2-month period for each beach respectively. In addition, a wave logger deployed offshore each beach provided hourly wave records, concurrent to the detected wave run-up positions. The detected wave run-up positions showed good agreement with the recorded wave forcing. The maximum wave run-up range for the examined beach sections was found to be at 37 m and 32 m from the swash minima in Kamari and Kalo Livadi beaches respectively. The study results suggest that the developed methodology can provide a fast, powerful and efficient beach monitoring tool, capable to provide high-frequency time series of wave run-up positions; and thus, accurately define the swash maxima (i.e. the “aigialos” line) of a beach. The latter is of extremely importance when it comes to proper beach spatial planning and coastal zone management scheme.

Keywords Wave run-up, Swash zone dynamics, Coastal video monitoring, Image processing

1 INTRODUCTION

Wave run-up, i.e., the time-varying position of the shoreward excursion of water on the beach, is an important beach dynamic feature. Its maximum excursion and height above the mean sea level form fundamental parameters of swash zone dynamics, the zone which probably is the section of highest interest for engineers, geologists and managers working on the coastal zone; being the most frequently accessed part of the beach, where morphological changes can be frequent. At the same time, wave run-up is a common hazard factor for beaches and barrier islands through overwash and an essential factor to be considered for the effective design of coastal works and beach nourishment projects, the prediction of storm surge and wave impacts and the planning of coastal management schemes (Vousdoulas 2014). Moreover, wave run-up is related to regulatory boundaries; the maximum recorded wave run-up at a beach (commonly defined as “aigialos” line in greek) forms the baseline from which a ‘setback’ zone should be defined and in which no further development shall be allowed, according to the Greek (Law 2971/2001) and European legislation (e.g. the ICZM Protocol to the Barcelona Convention (Art. 8(2)) and the 490 Directive 2014/52/EU). However, accurate records of wave run-up is at least hard (if not impossible) to retrieve with the classic mapping or/and image processing techniques. Repeated topographic leveling during and after storm events require dedicated human efforts under extreme conditions, while satellite images except their cost, are characterized by low temporal coverage. At the same time, the estimation of wave run-up is also a complicated task, as nearshore hydro-morphological changes are based on complex processes-response mechanisms driving the swash zone, operating at various spatio-temporal scales (Suanez et al. 2015). Coastal engineers commonly use empirical formulae to predict this crucial parameter, which have derived over previous parameterization efforts that suggest control by the nearshore seabed slope and the incident wave energy (e.g. Holman, 1986; Stockdon et al. 2006). Over the recent years, emphasis has been given to the development of image processing algorithms/techniques, capable to record/monitor with high accuracy specific coastal features of interest on specialized optical

datasets deriving from coastal video monitoring systems (e.g. Vousdoukas et al. 2010; Vousdoukas 2014; Velegrakis et al. 2016).

2 METHODOLOGY

An autonomous Beach Optical Monitoring System (BOMS - http://www.vousdoukas.com/index_video.html) was installed in two highly touristic beach systems of the Cycladic islands of Santorini (Kamari, an open beach of SE orientation) and Mykonos (Kalo Livadi, a typical “pocket” sandy beach) (Figure 1a-c)). The BOMS comprises of a station PC and 1 or more Vivotek IP8362 video cameras, set to obtain beach imagery (videos) with a sampling rate of 5 frames per second in burst mode (for 10 minutes at the beginning of each daylight hour). Images are corrected for lens distortion, geo-rectified and projected on real-world (UTM) coordinates using standard photogrammetric methods and Ground Control Points (GCPs), collected with a Differential GPS (Topcon Hipper RTK-DGPS). The geo-rectified and UTM-projected images of each hourly 10-min burst (3,000 snapshots/frames) are furthermore processed in order to generate high resolution time-stack images of the cross-shore position of the swash maxima (IMMAX images - Figure 1d-e)) amongst other optical coastal products (for details see Velegrakis et al. 2016). For the purpose of this study, IMMAX datasets for a highly energetic period (in terms of wave activity) for each beach have been extracted, covering 107 (16/12/2016 – 29/03/2017) and 61 (20/10/2014 – 19/12/2014) days for Kamari and Kalo Livadi beaches respectively. In addition, a pressure sensor/wave logger (RBR*Virtuoso*) deployed offshore each beach (at 9.1 and 9.3 m depth – Figure 1a) and 1c)), provided high frequency (4 Hz) wave parameters of zero-moment wave height (H_{m0}) and peak wave period (T_p) during the 10-min hourly bursts, concurrent to the optical datasets. However, in the case of Kamari beach due to video system downtime, continuous and concurrent morphodynamic and hydrodynamical information was not available for 14 days (21-24/01/2017 and 06-15/02 2017).

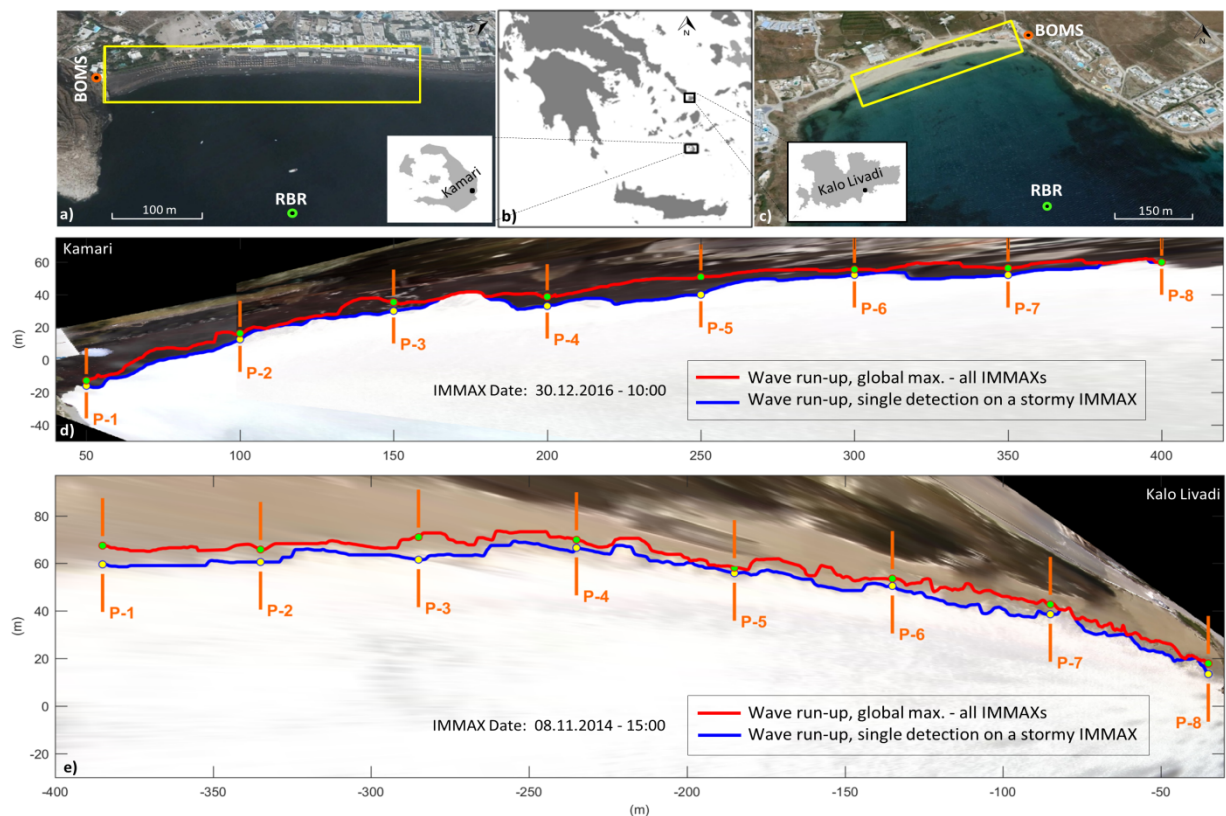


Figure 1 a)-c) Locations of Kamari and Kalo Livadi beaches showing also the locations of the BOMS, the deployed wave logger (RBR) and the monitored beach sections; d)-e) example of a single wave run-up detection on the plotted IMMAX image of a stormy hour (blue line), wave run-up global maxima (i.e. the “aigialos line” for the monitored period - red line) and the 8 selected cross-shore profiles for Kamari and Kalo Livadi beach respectively.

A fully-automated coastal feature detector was developed in order to record/monitor the wave run-up positions on each hourly IMMAX image. The detector is based on a very fast algorithm that uses a localized kernel that progressively grows along the IMMAX digital image, following the maximum backscatter intensity along the feature of interest (Chatzipavlis et al. 2018). In terms of record accuracy, this tends to decrease with the distance from the camera due to the increasing pixel footprint. Therefore, detections from the proximal beach stretch (350 m long) were considered in the analysis; in this area, the pixel footprint and the accuracy of detections are estimated at about 0.25 m. The wave run-up maxima of all single detections on the hourly IMMAX imagery (i.e. the “aigialos line” for the monitoring period of each beach) was estimated (depicted as red line in Figure 1d-e)). This is set as reference line in order to estimate the distance between the wave run-up maxima and the daily maximum single wave run-up detection. In this contribution, information is shown for 8 representative and equally spaced (with a 50 m distance between each other) cross-shore profiles (Figure 1d-e).

3 RESULTS

The wave run-up changes of the studied period were found to be significantly correlated with the wave climate recorded from the RBR wave loggers in both beaches, as expected. During periods of increased wave energy, the distance between the reference line (wave run-up global maxima) and the daily maxima recorded wave run-up is decreasing or even eliminated, meaning that wave run-up reaches its maxima point for the studied period (Figure 2a-d)). Interestingly, this distance elimination occurs at different time periods between the examined beach sections. In Kamari beach 5 out of the 8 examined cross-shore profiles reach their max. recorded wave run-up position on 30/12/2016 when wave heights of 1.8 m have been recorded. However, cross-shore profiles P-1, P-5 and P-7 reach their maxima recorded wave run-up at different dates when the recorded wave heights were of about 1.2 m (Figure 2a) and 2c)). Similar trend can be found in Kalo Livadi beach, where half of the examined beach sections (P-1, P-3, P-4 and P-6) reach their maxima recorded wave run-up point on 08/11/2014 when the highest wave has been recorded (1.7 m), whereas on 23/10/2014 with milder wave heights (1.3 m) the remainder cross-shore sections (P-2, P-5, P-7 and P-8) reach their limit wave run-up point (Figure 2b) and 2d)).

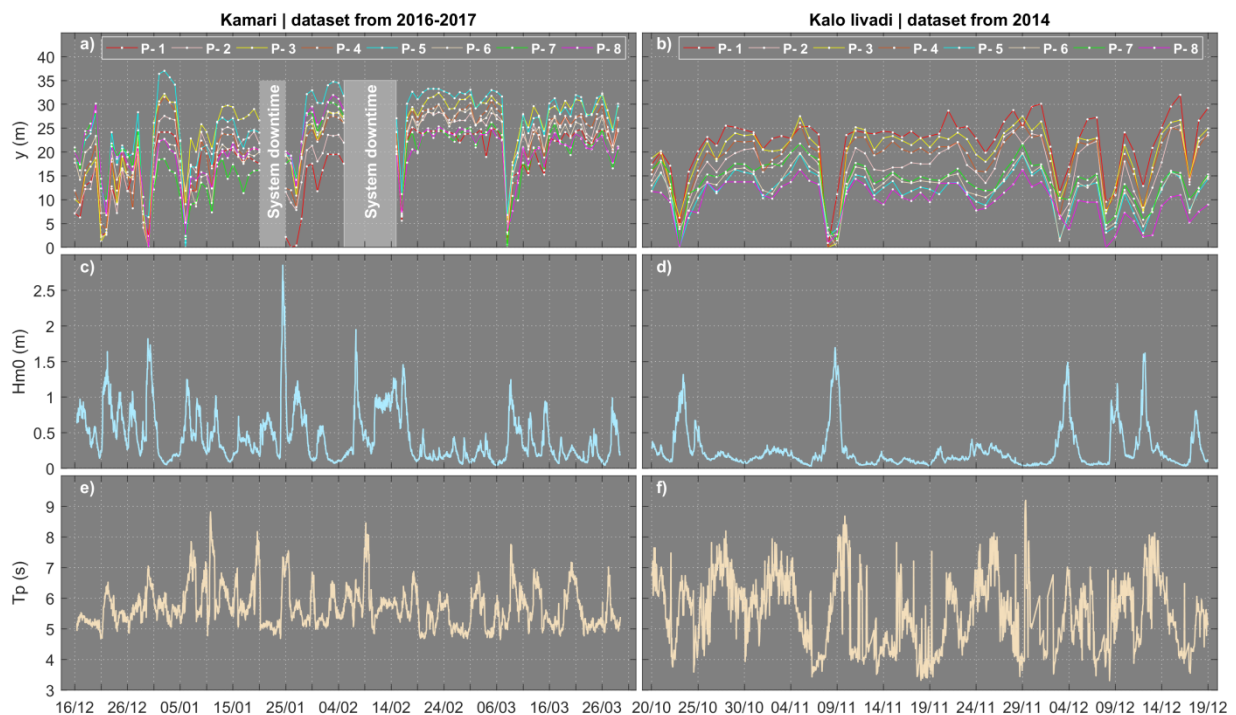


Figure 2 a)-b) Variability of the distance between the reference line (global max. wave run-up) and the daily maxima wave run-up at the 8 selected cross-shore profiles for Kamari and Kalo Livadi beach respectively; c-d) zero-moment wave height; and e)-f) peak wave period recorded from the wave logger (RBR) in Kamari and Kalo Livadi beaches respectively.

It is also evident that the 8 cross-shore profiles of each beach show different behavior regarding their wave run-up range (i.e. distance between the max. and min. wave run-up positions). In Kamari beach, the central section of the monitored beach stretch showed increased variability (wave run-up range > 30 m for P-3, P-4 and P-5). The highest range was found to be associated with P-5 (37m) while the lowest value was recorded at the most southwestern beach point (P-1, 24 m). In Kalo Livadi beach, the western section of the monitored beach stretch was found to be associated with increased wave run-up variability (> 24 m for P-1, P-2, P-3 and P-4), whereas the remainder beach sections are associated with wave run-up ranges < 24 m (P-5, P-6, P-7 and P-8). The highest wave run-up range is recorded for the westernmost cross-section (32 m, P-1) while the lowest value is recorded for the easternmost beach section (16 m, P-8).

4 CONCLUSIONS

The wave run-up positions at the examined cross-shore sections showed good agreement with the wave forcing records in both beaches. However, there are beach sections in both beaches where the wave run-up maxima didn't occur at the time of the highest recorded wave. This is attributed to the ever changing beach morphology (and especially the seabed slope), which controls the swash maxima excursion. In addition, most of the examined cross-shore beach sections were found to be areas of increased wave run-up variability, whereas some beach sections (P-1 located at the southwestern part of Kamari beach and P-8 at the easternmost edge of Kalo Livadi) showed lower variability. This is also attributed to the milder beach slopes, evident on these areas through previous topo-bathymetric surveys. The wave run-up maximum range was found to be at a distance of 37 m and 32 m from the swash minima of the monitoring period for Kamari and Kalo Livadi beaches respectively.

The study results suggest that the developed methodology can provide a fast, powerful and efficient beach monitoring tool, capable to provide high-frequency time series of wave run-up positions; and thus, accurately define the swash maxima limit (the "aigialos" line). The latter is of extremely importance when it comes to proper beach spatial planning, coastal engineering and coastal zone management scheme.

References

- Chatzipavlis A, Tsekouras GE, Trygonis V, Velegrakis AF, Tsimikas J, Rigos A, Hasiotis Th and Salmas C (2018) Modeling beach realignment using a neuro-fuzzy network optimized by a novel backtracking search algorithm. *Neural Computing and Applications*, 17 pp. doi: 10.1007/s00521-018-3809-2.
- Holman RA (1986) Extreme value statistics for wave run-up on a natural beach. *Coastal Engineering*, 9(6):527–544. doi: 10.1016/0378-3839(86)90002-5.
- Stockdon HF, Holman RA, Howd PA, Sallenger JAH (2006) Empirical parameterization of setup, swash, and runup. *Coastal Engineering* 53(7):573–588. doi: 10.1016/j.coastaleng.2005.12.005.
- Suarez S, Blaise E, Cancouet R, Floc'h F (2016). Empirical Parameterization of Wave Runup and Dune Erosion during Storm Conditions on a Natural Macrotidal Beach Serge. *Journal of Coastal Research*, 75:932-936. doi : 10.2112/SI75-187.1.
- Velegrakis AF, Trygonis V, Chatzipavlis AE, Karambas T, Vousedoukas MI, Ghionis G, Monioudi IN, Hasiotis T, Andreadis O, Psarros F (2016) Shoreline variability of an urban beach fronted by a beachrock reef from video imagery. *Natural Hazards* 83(1):201–222. doi: 10.1007/s11069-016-2415-9.
- Vousedoukas MI, Ferreira PM, Almeida LP, Ferreira O, Psaros F (2010) Coastal video monitoring system optimization using computational intelligence methods. Paper presented at the Maritime Rapid Environmental Assessment conference, Lerici, Italy, 18-22 October, 2010.
- Vousedoukas MI (2014) Observations of wave run-up and groundwater seepage line motions on a reflective-to-intermediate, meso-tidal beach. *Marine Geology*, 35:52-70. doi:10.1016/j.margeo.2014.02.005.

Trends in coastal erosion by combining satellite image analysis and copernicus wave data: Paggaion coastline, Northern Greece

K. Zachopoulos, N. Kokkos, M. Zoidou and G. Sylaios*

Laboratory of Ecological Engineering and Technology, Department of Environmental Engineering,
Democritus University of Thrace, Vas. Sofias 12, 67100 Xanthi, Greece

*Corresponding author: gsylaios@env.duth.gr

Abstract

Coastal zones are facing intensified natural and anthropogenic disturbances including sea level rise, coastal erosion and over-exploitation of resources. Coastal zone monitoring of these effects involves satellite-borne shoreline extraction and detection of change rates over time. Shoreline changes are directly related to waves, tides, winds, storms, extreme events, sea level change and human activities affecting the geomorphologic processes of the coast. The shoreline evolution along the study site (Paggaion Municipality coastline, Northern Greece) was examined and assessed blending satellite-borne shoreline changes with the incident wave power, acting in the area during the latest decade (2009 - 2018). The study focuses on two geographical sub-areas: the eastern site representing the highly touristic sand dunes zone (Ammolofi), and the western site of Kariani-Orfani coastal zone, where significant erosion is evident. Both areas were selected based on their high economic and aesthetic values and the potential vulnerability to coastal erosion and climate changes impact, as identified by previous studies.

Keywords Coastal processes; Shoreline evolution; Satellite image classification; DSAS; GIS analysis.

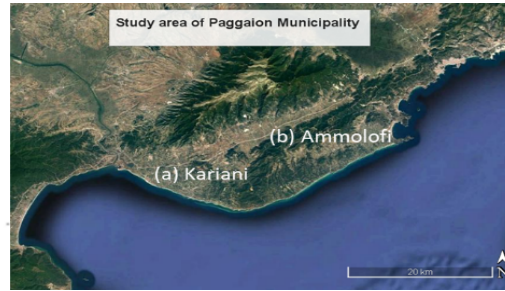
1 INTRODUCTION

The coastal zone is a very dynamic geomorphologic system where changes occur at diverse temporal and spatial scales (Mills et al. 2005), mostly related to erosion, as a result of natural and/or anthropogenic activities (Van Rijn 2011). Natural effects include shoreline interactions with incident waves, tides, storms, tectonic and physical processes and the sediment load transported from the watershed by rivers (Dolan et al. 1980). Coastal zone monitoring is an important task for national/regional development and environmental protection, in which the assessment of the state of historic shorelines is important (Rasuly et al., 2010).

Coastal authorities are faced with the increasingly complex task of balancing development and managing coastal risks. Integrated Coastal Zone Management (ICZM) provides a framework to resolve conflicts, mitigate impacts of short-/long-term uses and support strategies for sustainable coastal management (Anfuso et al., 2011). The present study is focused on the dynamics of shoreline movement in Paggaion Municipality, Northern Greece. The area was selected based on its high economic, archaeological and aesthetic values and the potential vulnerability to coastal erosion and their exposure to climate change impacts. The methodology carried out by examining and assessing the coastline erosion and accretion “hotspots” from the period 1986 to 2018, using lower and higher resolution historical satellite images. Furthermore, the incident wave power and wave angle acting in the coastal zone during the latest decade (2009 – 2018) was correlated to the erosion activity using higher resolution historical satellite images.

2 STUDY AREA

The study is focused on the southern shoreline of the Paggaion Municipality, Northern Greece (Figure 17). The total length of the shoreline is 36.3 km, covering the zone from Ofrinio to Ammolofi Beach. The study is focused on two geographical sub-areas: a) the eastern site, representing the highly-touristic sand dunes zone (Ammolofi), extending up to 50 m in width and approximately 20 km in length; and b) the western site of Orfani-Kariani coastal zone. Both areas have beach sediments composed of fine sand to very coarse sand (0.230 to 1.573 mm), separated by rocky peninsulas.



24. *Figure 17 Study area of Paggaion Municipality (Kariani (a) and Ammolofo (b) study sites)*

3 METHODOLOGY

3.1 Satellite Imagery

Eight historical satellite images were retrieved to cover the time period from 1986 to 2018 (Table 1). The historical image selection was mainly based on the correct geo-reference and on the image clarity from cloud cover. The monochromatic Near Infrared Band was selected for the image analysis and historic shoreline extraction.

The shoreline movement analysis was carried out into two different time periods, based on the spatial resolution of the examined satellite images: (a) satellite images from Landsat 4-5 TM during 1986 to 2009, with lower spatial resolution (pixel size of 30 m), retrieved from the Earth Explorer database of the United States Geological Survey Global Visualizer, and (b) satellite images from RapidEye and PlanetScope during 2009 to 2018, retrieved from Planet Explorer Beta, with higher spatial resolution of 5 m and 3.1 m, respectively.

25. *Table 2 Data products and its specifications*

Data Products	Resolution	Year of Image Acquisition	Source
Landsat 4-5 TM	30 m	20-04-1986	Earth Explorer, USGS
		29-07-1999	
		08-04-2005	
		15-08-2009	
RapidEye	5 m	23-06-2009	Planet Explorer Beta
		12-07-2012	
		18-07-2015	
PlanetScope	3.1 m	15-08-2018	

3.2 Coastline extraction from satellite images

The methodology employed in this study entailed the semi-automatic procedure of shoreline delineation, using a semi-automatic image classification technique. Historic satellite images were analyzed and their shorelines were extracted by applying the semi-automatic classification process, allowing the identification of materials in an image according to their spectral signature. For the classification process only the Near Infrared Band of the satellite images was used. The image was imported to Semi-Automatic Classification Plugin (SCP) for QGIS (Congedo, 2016) and we manually identified around 30 areas on each image by recognizing the two classes. The new raster file was classified by applying the minimum distance classification algorithm. The shoreline was extracted by vectorizing the classified raster image and applying a Gaussian filtering algorithm in order to smooth the polyline and receive a better fit to the coast.

3.3 Evaluation of the shoreline evolution

The shoreline analysis was performed in two time periods (1986 – 2009 and 2009 – 2018), based on the satellite image resolution. In order to evaluate the shoreline evolution, an analysis was carried out by the Digital Shoreline Analysis System (DSAS), provided by the USGS (Thieler et al., 2009). The DSAS procedure used transects positioned along the shoreline at distances of 20 m. The reference baseline required by the DSAS procedure was manually digitized and positioned offshore and parallel to the most recent shoreline (2018). A series of statistical indices was produced, such as the Net Shoreline Movement (NSM, meters) index, reporting the distance between the oldest and the earliest shorelines for each transect, the End Point Rate (EPR, m/y) calculated by dividing the distance of Net Shoreline Movement by the time elapsed between the oldest and the most recent shoreline, and finally, the Weighted Linear Regression (WLR, m/y), in which the weight w is a function of the variance of the measurement uncertainty (Genz et al., 2007):

$$w = 1/e^2 \quad (1)$$

where e is the shoreline uncertainty value. Using the data produced by the DSAS transects, a statistical analysis of the shoreline evolution along the study years was applied and various statistical parameters were calculated and analysed. The results were verified by applying two methodologies for outlier removal: the Interquartile Range (IQR) method and the method of extreme values removal (based on quantile distribution – 1%) to “clip” the data and remove the outliers. Both methods were applied in combination with an optical and empirical detection.

3.4 Wave Characteristics at the Breaker Zone and Incident Wave Energy Calculation

Historic offshore wave time-series data at fourteen data points, were retrieved from the reanalysis product of the Copernicus Marine Environmental Monitoring Service (CMEMS). Wave data were comprised of the daily time-series of the spectral significant wave height (H_{mo}), the zero up-crossing wave period (T_{02}) and the wave direction relative to the north (ϕ_o). These data, as open sea significant wave height (H_o), wave period (T) and open sea direction (ϕ_o) were imported into a simple wave-ray model to transform the offshore wave characteristics into the wave characteristics at the breaker zone. More precisely, a long list of parameters was estimated such as; a) the wavelength [m], b) the wave celerity [m/s], c) the wave group celerity [m/s], d) the breaker zone, e) the significant wave height [m], f) the breaker was computed, g) the shoaling coefficient, h) the refraction coefficient, i) the wave dispersion coefficients at offshore and breaker zones, j) the wave direction at the breaker zone, k) the longshore wave-induced current, V_{long} [m/s], l) the incident wave energy at the breaker zone [$J m^{-1} s^{-1}$], m) the longshore sediment transport on annual basis [$m^3 yr^{-1}$]. All parameters were produced following the equations described by the Coastal Engineering Manual (2008). Therefore, the estimated longshore sediment transport at segments of the coastline, over selected periods, will be correlated to the assessed shoreline retreat/advancement rates.

4 RESULTS

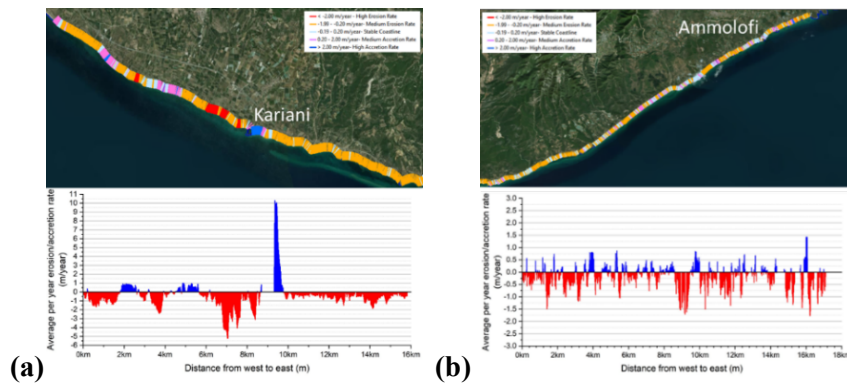
4.1 Erosion and Accretion Hotspots

Investigation of the shoreline status from 1986 to 2018 reveals that severe erosion is noticed along the Paggaiou Municipality coastline. The study was carried out in two steps: a) coarse shoreline analysis for the period 1986 to 2009, highlighting the erosion and accretion hotspots, and b) a more detailed investigation of shoreline change rates for the period 2009 to 2018, correlating the erosion results to the estimated incident wave power.

26. Table 3 Statistical parameters produced from DSAS for the two study areas; NSM (shoreline movement in m), WLR (erosion/accretion rate in m/y)

	Kariani 1986-2009		Ammolofi 1986-2009		Kariani 2009-2018		Ammolofi 2009-2018	
	NSM	WLR	NSM	WLR	NSM	WLR	NSM	WLR
Maximum accretion	34.37	1.33	26.90	1.37	97.72	10.83	21.06	2.27
Maximum erosion	-35.08	-1.47	-22.10	-1.03	-48.40	-5.37	-22.07	-2.28
Average erosion	-0.70	0.15	2.21	-0.10	-4.11	-0.53	-2.46	-0.25

The western coastal area covers the shoreline from Ofrinio to Kariani Beach. Several hotspots of erosion and accretion are observed along the western coastal zone for the time period 1986-2009, with average erosion rate of -0.10 m/y. High erosion rates are observed in the southern-east area of Kariani coastline (about -0.70 m/y) and in the zone located on the west side of the new port of Kariani (up to -1.47 m/y). On the other hand, the higher accretion rates are observed in the east side adjusted to the harbor with maximum shoreline movement of +34.37 m and accretion rate of +1.33 m/y. The eastern coastline of the study area covers the coastal zone from Loutra Eleftheron to Ammolofi Beach. The erosion activity in that area is significantly lower compared to the western coastal zone. More precisely, the average rate of total shoreline change is around -0.10 m/y, with maximum erosion rate of -1.03 m/y and maximum accretion rate of +1.37 m/y. The higher accretion rates are observed at the north-eastern site of Mirtofito beach, with maximum shoreline movement of +26.90 m from 1986 to 2009. On the contrary, the higher shoreline retreatment of -22.10 m is observed at the western region of Eleochori Beach.



27. Figure 18 Erosion and accretion rate (WLR) in (a) Kariani and (b) Ammolofi study areas for the time period 2009 to 2018

Additionally, a more detailed study of evaluating the shoreline movement at both study areas was carried out for the time period 2009 to 2018, using higher resolution satellite images. In Kariani study site, the average shoreline retreat of -4.11 m is estimated, corresponding to an average erosion rate of -0.75 m/y. The higher shoreline erosion is observed at the west of the Kariani Port, with maximum erosion rate -5.37 m/y and coastal retreat of -48.40 m. In Ammolofi study site the average erosion rate is significant lower (-0.25 m/y). The higher erosion rates occurred mostly at the western sandy beaches of this area (-1.70 m/y) and at the central sector of Mirtofito beach (-1.62 m/y) (Figure 18b).

4.2 Correlation between Copernicus wave data and the erosion trends from 2009 to 2018

The incident wave energy prevailing over the study area influences sediment budget according to wave height and wave direction, which determine accretion or erosion features. More precisely, the mean incident wave energy in Kariani ($239.93 \text{ J m}^{-1}\text{s}^{-1}$) is significantly higher than the wave energy in Ammolofi study site ($102.32 \text{ J m}^{-1}\text{s}^{-1}$). The period 2009 to 2012 was the most energetic period with average wave power of $251.07 \text{ J m}^{-1}\text{s}^{-1}$ in Kariani and $109.98 \text{ J m}^{-1}\text{s}^{-1}$ in Ammolofi Beach. In both areas, shoreline retreat of -2.97 m and -2.56 m is observed. Moreover, for both study areas, the time period where the lower wave energy occurs corresponds to the period that slight shoreline accretion is observed.

In Kariani the most frequent incident wave orientation is ESE and SE with wave heights up to 3.6 m and the mean incident wave energy is estimated $\sim 239.93 \text{ J m}^{-1}\text{s}^{-1}$. In that area the higher wave activity is observed in the south-eastern edge of Kariani shoreline, with estimated average incident wave energy of $260.24 \text{ J m}^{-1}\text{s}^{-1}$. At this beach segment the most significant shoreline movement of -2.10 m is observed in the same time period. Moreover, in Kariani the wave power and direction seem to affect the sediment transportation, moving from the south-eastern sandy beaches to the north-western coastal zone, thus confirming the DSAS results (Figure 18a). On the other hand, in the Ammolofi study area, the wave power appears significantly lower ($102.32 \text{ J m}^{-1}\text{s}^{-1}$) and the wave orientation is mostly from SSE and SE directions with wave heights up to 3.8 m. The wave crests reach the breaker zone at directions almost perpendicular to the shoreline, favoring cross-shore transport and the development of an extended sandy bar lowering the impact of erosion (-0.96 m). The higher erosion is observed at the eastern edge of Ammolofi beach, where the average incident wave energy is around $55 \text{ J m}^{-1}\text{s}^{-1}$ and the shoreline movement is approximately -1.20 m. The sandy dunes of Ammolofi are vulnerable to coastal erosion although lower wave activity occurs (Figure 18b). The coastal erosion recorded from 2009 to 2018 is correlated to the incident wave energy on the coast and to the size of the sediment. Sandy beaches with fine grain sediment are more vulnerable to coastal erosion under the impact of high wave power. Moreover, the incident wave angle affects the wave power required to sediment flushing from the beach and also to the sediment transportation. In Kariani the average incident wave angle is around 118 degrees and the waves propagate from ESE to SE directions. In Kariani higher wave energy is required to transport the sediments from the south east to the north west of the study area. In contrast, in Ammolofi beach the wave direction is almost perpendicular to the shoreline (around 162 degrees) and the waves propagate from SE to SSE directions. Although the erosion rates are relatively high, the wave power is significantly lower compared to Kariani.

28. Table 4 Parameters contributing to shoreline change at four indicative areas

Study Site	CMEMS points	Shoreline change (m)			Wave energy ($\text{Jm}^{-1} \text{s}^{-1}$)			Grain size (mm)		Wave angle (degrees)			Wave Orientation
		2009-2012	2012-2015	2015-2018	2009-2012	2012-2015	2015-2018			2009-2012	2012-2015	2015-2018	
Kariani	182239	-1.49	-1.64	1.55	295.81	276.45	250.71	0.485	Medium sand	118.11	118.21	118.98	ESE - SE
	182240	-2.40	-1.28	1.05	305.60	288.81	263.58	0.488	Medium sand	117.54	117.95	117.50	ESE - SE
Ammolofi	183437	-2.52	3.45	-3.74	74.29	60.79	72.16	0.230	Fine sand	160.76	161.71	155.65	SE - SSE
	183438	-3.01	2.58	-3.07	60.38	45.25	58.91	0.414	Medium sand	161.28	162.41	156.17	SE - SSE

29.

5 CONCLUSION

The assessment of shoreline change using satellite images reveals that the study area has experienced high rates of erosion and accretion along the coastline during 1986 – 2018. Processes of erosion increased due to anthropogenic activities and natural conditions, such as wind and wave action. The erosion in the study area is affected both from the incident wave energy, the direction of waves propagation and the sediment grain size. The higher erosion rates correspond to periods of increased incident wave energy from directions favoring the longshore sediment transport. On the other hand, the lowest erosion rates correspond to segments that the coastline presents a smoother profile with minor changes in orientation. The present study constitutes a successful effort to correlate the offshore wave data given from the Copernicus Marine Environmental system to coastal erosion rates produced by historic satellite images.

Acknowledgement

This work was funded by the European Union and national funds of the participating countries in the framework of the INTERREG Balkan-Mediterranean Program, Project HERMES: “A HarmonizEd fRamework to Mitigate coastal EroSion promoting ICZM protocol implementation”, Subsidy Contract BMP1/2.2/2546/2017.

References

- Anfuso G Pranzini E, Vitale G (2011) An integrated approach to coastal erosion problems in northern Tuscany (Italy): Littoral morphological evolution and cell distribution. *Geomorphology*, 129(3-4), 204-214.
- Congedo, L. (2016) Semi-automatic classification plugin documentation. Release, 4(0.1), 29.
- Dolan, R.O.B.E.R.T., Hayden, B. P., May, P., & May, S. (1980) The reliability of shoreline change measurements from aerial photographs. *Shore and beach*, 48(4), 22-29.
- Mills, J. P., Buckley, S. J., Mitchell, H. L., Clarke, P. J., & Edwards, S. J. (2005). A geomatics data integration technique for coastal change monitoring. *Earth Surface Processes and Landforms: The Journal of the British Geomorphological Research Group*, 30(6), 651-664.
- Rasuly, A., Naghdifar, R., & Rasoli, M. (2010) Monitoring of Caspian Sea coastline changes using object-oriented techniques. *Procedia Environmental Sciences*, 2, 416-426.
- Thieler, E. R., Himmelstoss, E. A., Zichichi, J. L., & Ergul, A. (2009) The Digital Shoreline Analysis System (DSAS) version 4.0-an ArcGIS extension for calculating shoreline change (No. 2008-1278). US Geological Survey.
- United States (2008) Coastal engineering manual. Washington, D.C.: U.S. Army Corps of Engineers.
- Van Rijn LC (2011) Coastal erosion and control. *Ocean & Coastal Management*, 54(12), 867-88.

BIM application to high-end public realm design on waterfront reclamation areas

Ch. Tzoumas

Project Manager at SALFO AND ASSOCIATES SA – Qatar Branch

*Corresponding author: ctzoumas@salfo.gr

Abstract

Building Information Modelling (BIM) services were applied to the design development of the project: “CP10B1 – Design & Construction of Lusail City Marina District Waterfront Promenades areas”, which was awarded to SALFO & Associates, SA. The Lusail City Development is located north of Doha within a 2,000 hectare site and its total resident, office and visitor population is expected to be approximately 450,000 people at its completion. Marina District promenades are designated for high end waterfront public realm areas with many distinctive amenities. The project was developed in areas that as a result of extended soil reclamation works. The main objective of the BIM implementation was to prevent uncoordinated design leading to missed milestones and deadlines, abortive design works and finally to budget overruns. The BIM model was divided into zones and further into design disciplines and sub-disciplines following the project’s work breakdown system. Elements in the BIM environment were modeled depending on the specified level of detail for each discipline and design stage, starting from LoD 200 for the Concept Design stage up to LoD 500 for the As-Built design stage. BIM Models were developed throughout all project phases, providing clash detection reports, Quantity Takeoffs and 4D Construction scheduling, allowing the Contractor to mitigate the project risks.

Keywords 3D BIM Model (Level of Detail), Clash free design, Time and Cost Monitoring & Control

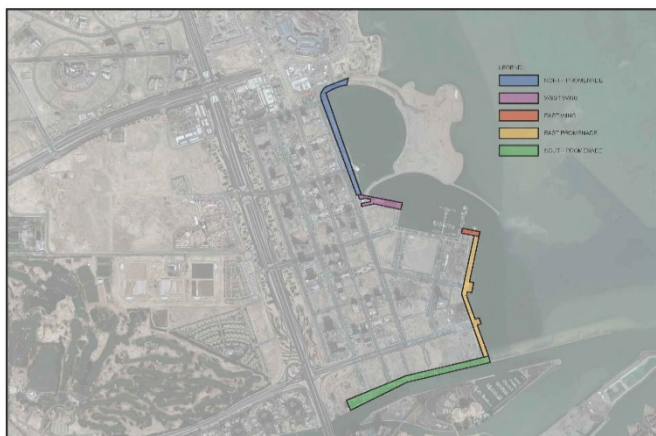
1 PROJECT DESCRIPTION

1.1 Project’s location

The ‘Lusail Development’ is located north of Doha within a 2,000 hectare site, which will comprise of residential housing for 200,000 residents, mixed-use retail, commercial centers, hotels and community facilities. The total resident, office and visitor population is expected to be roughly 450,000 people.

1.2 Project’s scope

The CP10B1 package, which is an integral part of the “Lusail Development” included the landscape and utilities design of the Marina District North Promenade, the South Marina West & East Wing, the East Promenade and the South Promenade, which cover an area of 130,000 sq. m. approximately. (See below map).



The landscape design included amenities such as interactive water-features with underground plant rooms, shade structures, kiosks, waterfront platforms, waterfront steps and ramps, whereas the infrastructure utilities include all the required services for the promenades landscape features and for the services connections to the adjacent projects, such as potable water, firefighting, district cooling, fuel line from fuel tanks to fuel dock, irrigation water (potable water or treated sewage effluent), foul sewage, surface water drainage, power and electrical network (11kV low voltage & extra low voltage), CCTV network, emergency access for fuel dock and VIP yacht facilities, gas, pneumatic waste collection system, public address and general alarm.

1.2 Existing Conditions

The project was developed within a very long (approx. 4 km) and very confined (approx. 30 m wide) corridor which resulted from extended soil reclamation works and was secured by either rip rap or quay walls, as reflected in the below section profiles.

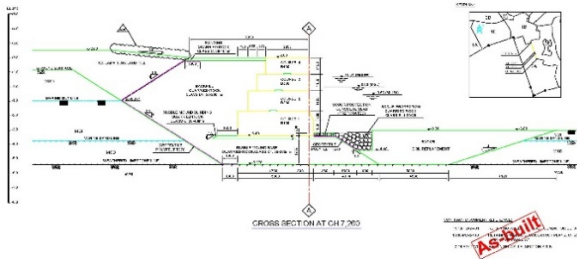


Figure 1 Section Profile at Quay Wall area

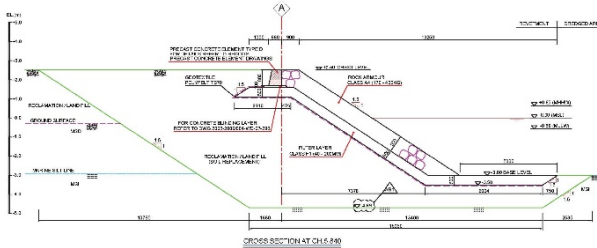


Figure 2 Section Profile at Rip rap area

The design scope had to take into consideration all the aforesaid existing conditions and especially the marine construction elements (e.g. geotextile, filter layer, rock armour) which had to remain intact and not to be disturbed by any drilled pile, or any casted foundation, or any excavated trench. Furthermore, within the project’s limit of works, there were existing utilities already being installed by previous construction packages.

2 BIM IMPLEMENTATION METHODOLOGY

The BIM methodology was utilised to develop a detailed BIM model early in the design stages, which was regularly updated with all design changes, and developed in more detail (Level of Detail) as necessary.

2.1 Objectives

The main objective of the BIM implementation and BIM use were to prevent uncoordinated design leading to missed milestones and deadlines, abortive design works and finally to budget overruns. The BIM model assisted in regular design auditing regarding the detection of uncoordinated details and their timely corrections, provided detailed quantity take-offs and 4D construction simulations showing the construction process, in order to compare the planned schedule with the actual construction progress.

2.2 Overall BIM Model Strategy

2.1.1 3D Model Breakdown Structure

The BIM model was divided into zones and further into design disciplines and sub-disciplines following the project’s work breakdown system (WBS) structure.

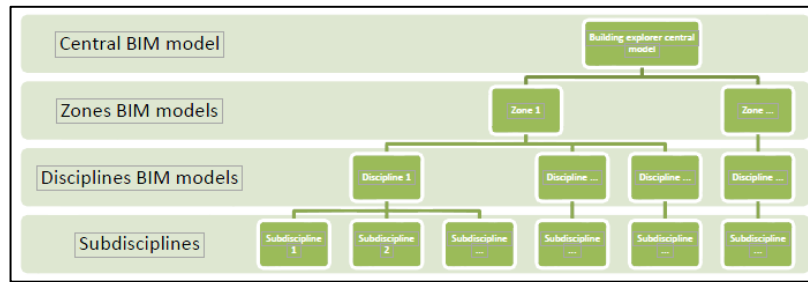


Figure 3 3D Model Breakdown Structure

Those work packages were merged into one unique, complex BIM model, using the Building Explorer BIM software platform, which allowed smooth work with a very large amount of BIM elements in one place, inter-disciplinary collaboration and simultaneous working on the same BIM model by different teams.

2.1.2 Level of Detail

Elements in the 3D BIM were modelled depending on the specified level of detail for each design element category and on the design stage. Starting with the Concept design model, the level of detail increased until concluding at the As-built stage from LOD 200 to LOD 500. The elements to be modelled and the specific LOD were determined at the beginning of each stage and varied from each design stage and each discipline, according to the purpose for which the BIM model was intended to be used.

Table 1 Disciplines Design Level of Detail

	3D BIM Model		
	Concept model	IFC Model	As-built model
	LOD	LOD	LOD
Landscape			
Wall	200	300	500
Slab	200	300	500
Furniture	200	300	500
Planting	200	300	500
Railing	200	300	500
Lighting fixtures	200	300	500
Structural works			
Wall	200	300	500
Slab	200	300	500
Beam	200	300	500
Column	200	300	500
Stair	200	300	500
Ramp	200	300	500
Generic model	200	200	
MEP works			
Pipe	200	300	500
Pipe fitting	200	300	500
Flex pipe	200	300	500
Conduit	200	300	500
Conduit fitting	200	300	500
Electrical equipment		200	500
Mechanical equipment		200	500
Pipe accessories		200	500
Security devices		200	500
Sprinklers		200	500

2.1.3 BIM Uses

The BIM Models were developed throughout all project phases, assisting with design coordination and clash detection in the early design phases. As the design progressed, Quantity Take-offs and 4D Construction scheduling were possible. During the construction phase, the BIM Model was utilised for monitoring, controlling and reporting the planned versus the actual progress. Finally, a detailed As-built Record BIM model was developed in order to depict project's as-built conditions and allow the end user to facilitate maintenance.

Table 2 BIM Uses

	BIM Use	Project Stage		
		Schematic Design Phase	Issue For Construction Phase	Construction Phase
1	Existing Conditions Modelling	x		
2	Design Authoring with BIM Modeling	x	x	
3	Design Coordination (Conflict Analysis)	x	x	
4	Model Element Scheduling (QTO generation)	x	x	
5	4D Construction Simulations	x	x	x
6	Progress Monitoring			x
7	As-built BIM Model			x

2.3 BIM Deliverables

2.3.1 BIM Execution Plan: A comprehensive document defining how all BIM deliverables were produced and delivered and determined the responsibilities of the on-site BIM team.

2.3.2 Building Information Models (Architectural, Structural, MPE Services, Landscape, Outdoor Utilities 3D BIM Modelling), 3D Virtual Building & Advanced 3D visualisations, developed at the designated Level of Detail according to Model Element Matrix

2.3.3 BIM Spatial Conflict Analysis and Design Inconsistencies (see 3 INCONSISTENCIES AND CONFLICT ANALYSIS): Clash Reports on monthly basis, including 2D drawings with marked area of clashes, 3D BIM model with highlighted conflicts, Screenshots, exported from the detailed 3D BIM model (See below Figure), showing clashes in design documentation, Reports with specified numbers of clashes within and between different trades, updates of BIM model after clashes were resolved, and final verification report.

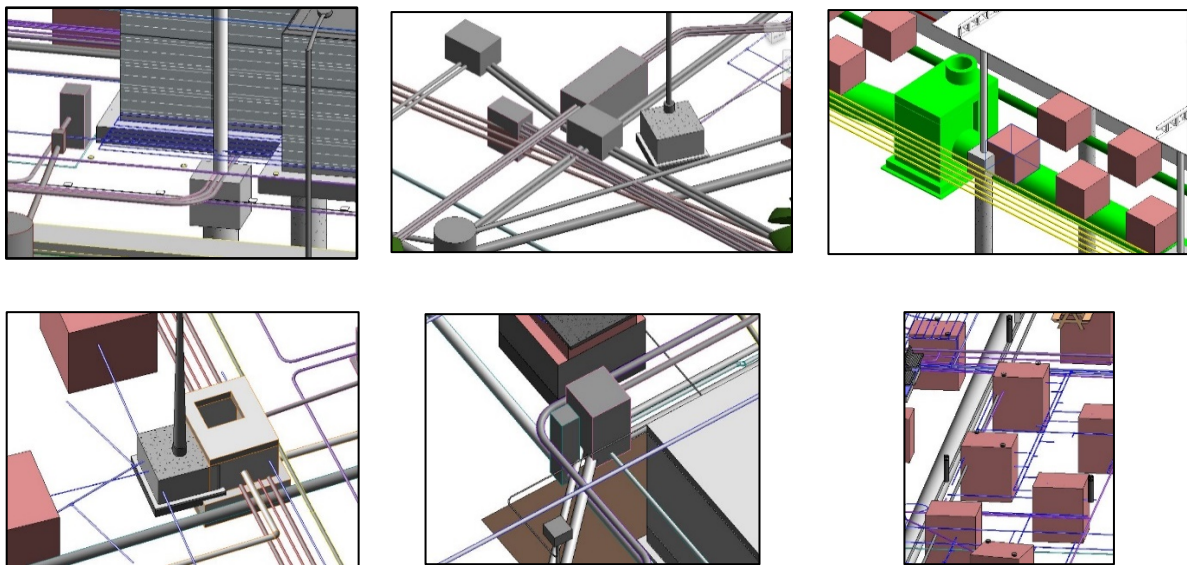


Figure 4 Clashes between several design elements (Tree pits, Foundations, Structures & Utilities pipes)

2.3.4 Design visualisations and presentation material including model screenshots, 3D walkthroughs and flyovers directly from the software.

2.3.5 2D BIM Drawings extracted from the BIM model to substantiate design deliverables preparation.

2.3.6 Quantity Take-off Analysis based on the Work Breakdown Structure, in order to support the design team to create the final Bill Of Quantities (BoQ) required for the project budgeting.

2.3.7 4D Schedule Planning & Linking the construction program with specified elements within the model in order to create 4D visualisation of the proposed construction schedule and help mitigate program delays

2.3.8 Progress Monitoring and Control by tracking construction progress, updating Construction Schedule with progress data, regenerating 4D simulations in order to monitor actual Construction Progress versus planned Construction Schedule

2.3.9 As-built BIM Record model by developing the final As-Built 3D BIM model during and after the construction phase, according to summarised data received from the construction site. The final As-built model was developed at the designated Level of Development 500 in accordance with LOD definition as per Client's requirements by collecting all relevant as-built documentation from the Contractor.

3 INCONSISTENCIES AND CONFLICT ANALYSIS

BIM Technology was used in order to develop a clash free design in terms of coordinating all the infrastructure underground disciplines, respecting the site constraints including the Rip Rap and Quay Wall construction elements and meeting the Client’s requirements to construct a prestigious high end public realm landscaping project. The 3D model for the main corridors and the concept landscape was developed in order to coordinate main routes of the required utilities, by ensuring that there were no clashes with underground hardscape and soft-scape elements. The procedure was implemented in coordination with the design experts, starting from the early phase of the design process by validating the tender inputs and elaborating them in the concept design development. The model was used to ensure proper distances between systems, as required by local regulations reflected in the table below and taking also into consideration the landscape structure foundations, e.g. light poles, benches and bike racks, etc along with all underground structures, such as manholes, chambers, irrigation tanks, fuel tank and control rooms, district cooling Energy Transfer System Room and water-feature plantrooms.

Table 3 Utilities clearances

Clash strategy	LV	11kV cables	ELV (Smart city, PA, WiFi, Media)	SSD/CCTV	Lighting	Earthing	PWC	Gas	District cooling	Fuel system	TSE	Irrigation	Main	Trees	Grass	Potable water	Storm drainage	Foul sewer	Fire fighting	Oil	Dewatering	Water features system	Tree pits	Plant rooms
LV																								
11kV cables																								
ELV (Smart city, PA, WiFi, Media)																								
SSD/CCTV																								
Lighting																								
Earthing																								
PWC																								
Gas																								
District cooling																								
Fuel system																								
TSE																								
Irrigation																								
- Main																								
- Trees																								
- Grass																								
Potable water																								
Storm drainage																								
Foul sewer																								
Fire fighting																								
Oil																								
Dewatering																								
Water features system																								
Tree pits																								
Plant rooms																								

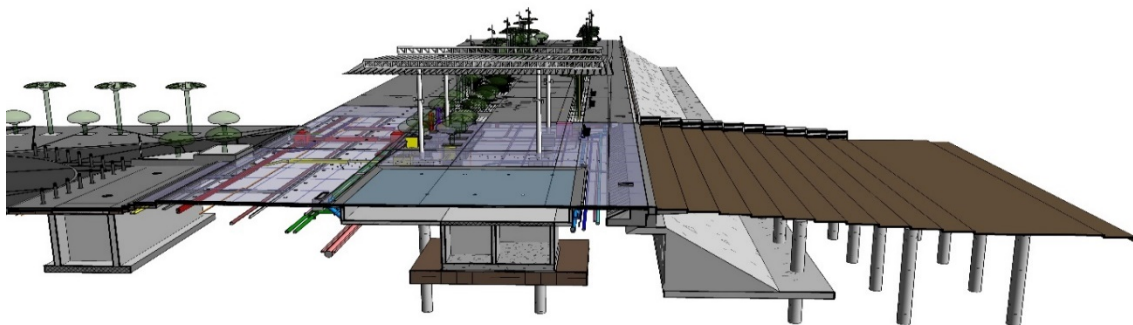
	Hard clash
	250mm clearance
	300mm clearance
	350mm clearance

These clearances apply to main routes of the systems

By carrying out this exercise, the design experts were able to locate initially the required services and as the design was evolving through the next design stages (Schematic – Detailed Design – Issued for Construction) constant clash analyses were performed in order to ensure that the design remains clash free.

4 CONCLUSION

BIM Modelling services contribution to the successful completion of CP10B1 project was especially significant, considering the confined available space, the tight time schedule, the amount of the in-scope utilities services and last but not least the Client’s particular demanding requirements.



Combination of Very High Resolution (VHR) satellite imagery and side scan data for low cost seagrass mapping

A. Tsokos¹, V. Tsoukala¹, C. Petropoulos², P. Sartampakos³, Emm. Vassilakis^{4*}

¹Department of Civil Engineering, National Technical University of Athens, Athens

²Lykofronos 6, Chalkida

³Nireas Engineering LTD, Skra 1-3, Kallithea

⁴Faculty of Geology and Geo-environment, National & Kapodistrian University of Athens, Athens

*Corresponding author: evasilak@geol.uoa.gr

Abstract

The use of techniques of two different origin were compared and combined aiming to map the seagrass meadows at shallow waters of South Evoikos Gulf, in central Greece. The high spatial and spectral resolution of WorldView-2 satellite images and its ability of water penetration, offers a positive approach for sea bottom mapping, in a relatively high resolution. In addition, the ground truth fieldwork survey with side scan data acquisition revealed that it was in impressively high agreement with the outcomes from the remote sensing data interpretation.

Keywords WorldView-2, South Evoikos Gulf, sea bottom classification.

1 INTRODUCTION

The use of Very High Resolution (VHR) satellite imagery at various applications is gaining more and more popularity due to the growing number of offered data and the increasing spectral properties. WorldView-2 is the first commercial VHR multi-spectral satellite providing imagery in eight different sensors having bands that range from the visible to near-infrared (0.40-1.04 μm). The integration of the “Coastal” band (0.40-0.45 μm) in the 8-band WorldView series of satellite imagery data, which was followed by the addition of the similar wavelength band 1 (0.43 - 0.45 μm) in the Landsat-8 Operational Land Imager (OLI), gave a great boost to applications related to shallow water depths. The fundamental principle underlying the methods used to study the sea bottom from remotely sensed imagery is that different wavelengths of the solar light penetrate the water body to different depths (Phinn et al. 2008).

The ability to accurately determine the seagrass at underwater regions is of great importance for the biodiversity of the submarine environment (Schmidt and Skidmore 2003). The use of certain spectral wavelength data tends to be the most cost-effective way of monitoring the marine habitats by mapping the sea bottom type along with several other jobs like modeling coastlines or even navigating through shallow aquatic areas by studying the bathymetry (Lyzeng 1978; Fornes et al. 2006).

2 DATA AND METHODS

The northern part of South Evoikos Gulf was chosen as a test site for this research work, due to its sea bottom morphology as shallow depths extend at a wide area and the frequent presence of *Posidonia oceanica* species (Figure 1).

WorldView-2 scene acquired on January 11, 2014 was used, after careful search at DigitalGlobe’s Image Finder quick look archives, as a number of conditions should have been fulfilled (Figure 2). Initially, the sea surface should have been calm enough and the solar angle should have been as much vertical as possible at the time of acquisition (Mean Sun Elevation 59.1°). Accordingly, the satellite sensors should also be in a relatively small angle across the nadir track (Off Nadir View Angle = 10.1°).



Figure 1 Field photograph of seagrass as seen from the beach



Figure 2 Index map of the area of interest at South Evoikos Gulf, between Mainland Greece and the island of Evia, comprised by two separate satellite images with natural color band combination. The VHR WorldView-2 image in the middle of the figure is in contrast with the medium resolution Landsat-8 OLI, which completes the map figure. The yellow rectangle delineates the study area represented in Figure 4

The dataset was pre-processed before ortho-rectification procedure (Deida and Sanna 2012), including pan-sharpening for increasing the spatial resolution by using the Hyperspherical Color sharpening algorithm (Padwick, et al, 2010), which is specially designed for the WorldView- 2 sensor multi-band data and seems to work efficiently also with other multispectral data containing at least 3 bands. According to the workflow of this algorithm the imagery data are transformed from native color space to hyperspherical color space, in order to replace the multispectral intensity component with an intensity matched version of the panchromatic band.

The satellite image processing part of the methodology was followed by the classification of the Coastal band. Supervised classification was used to cluster the pixels of the image into classes

corresponding to user-defined object/areas including the seagrass, based on training classes which consist of groups of pixels representing individual spectra (Phinn et al. 2008).

Several routes were carried out, with a vessel carrying side scan equipment, for mapping large areas of sea bottom, primarily for locating the presence of seagrass meadows (Figure 3). The collected data were registered and geo-rectified for constructing a map representing the seagrass distribution around the test site. The extensive seagrass deployments at the clayey sea bottom of the study area at Avlida, consists of *Cymodocea* along with *Cystoseira crinite* (at shallower areas closer to the coastline). Moreover, sparse developments of *Ulva Enteromorpha* and *Colpomenia* were also located during the fieldwork, which are indicators of organic pollution.

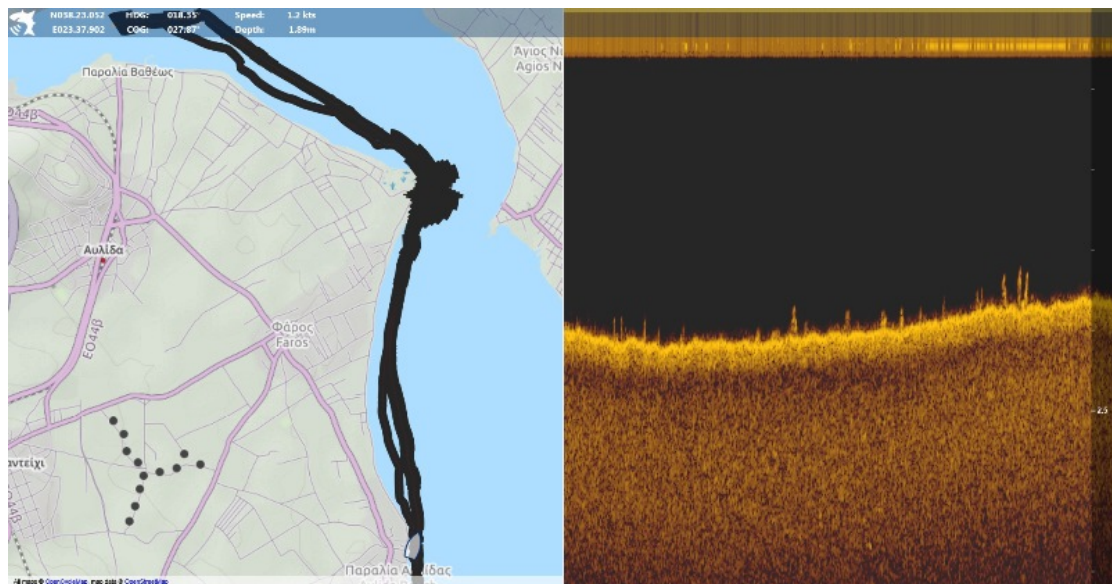


Figure 3 The vessel's routes are displayed at the map on the left and sample of the capture images is displayed at the right

3 RESULTS AND DISCUSSION

The classified images of the Coastal band appeared to have very accurate depictions of the shallow water regions covered by seagrass in the original radiance images, based on visual comparisons with the side scan data interpretation (Figure 4).

The spectral reflectance pattern as revealed by remote sensing spectral measurements shows subtle differences between various sea bottom coverages. The difference is quite evident between submerged seagrass and the other types of sediments.

The cost of providing a VHR satellite image is highly competitive comparing to a marine survey, especially when the pricey side scan equipment along with its maintenance is included in the investigation budget. On top of that the possibility of automating this technique for being efficient at large areas is quite promising. However, the possibility of coupling remote sensing techniques with other ancillary data such as side scanning, would be the best combination for obtaining even more reliable results.

Minor issues concerning the accurate geo-rectification of the satellite imagery can be overruled since a fair geographic placement of the datasets can be applied by using the geo-location information of the satellite, mentioned in the metadata files. Nevertheless, a serious objection could be the effective penetration depth of the Coastal band wavelength spectral radiance, which cannot exceed the 30 meters at clear and moderate turbid water bodies (Stumpf 2003), bearing in mind that several species of seagrass can be found at much deeper sea bottoms.

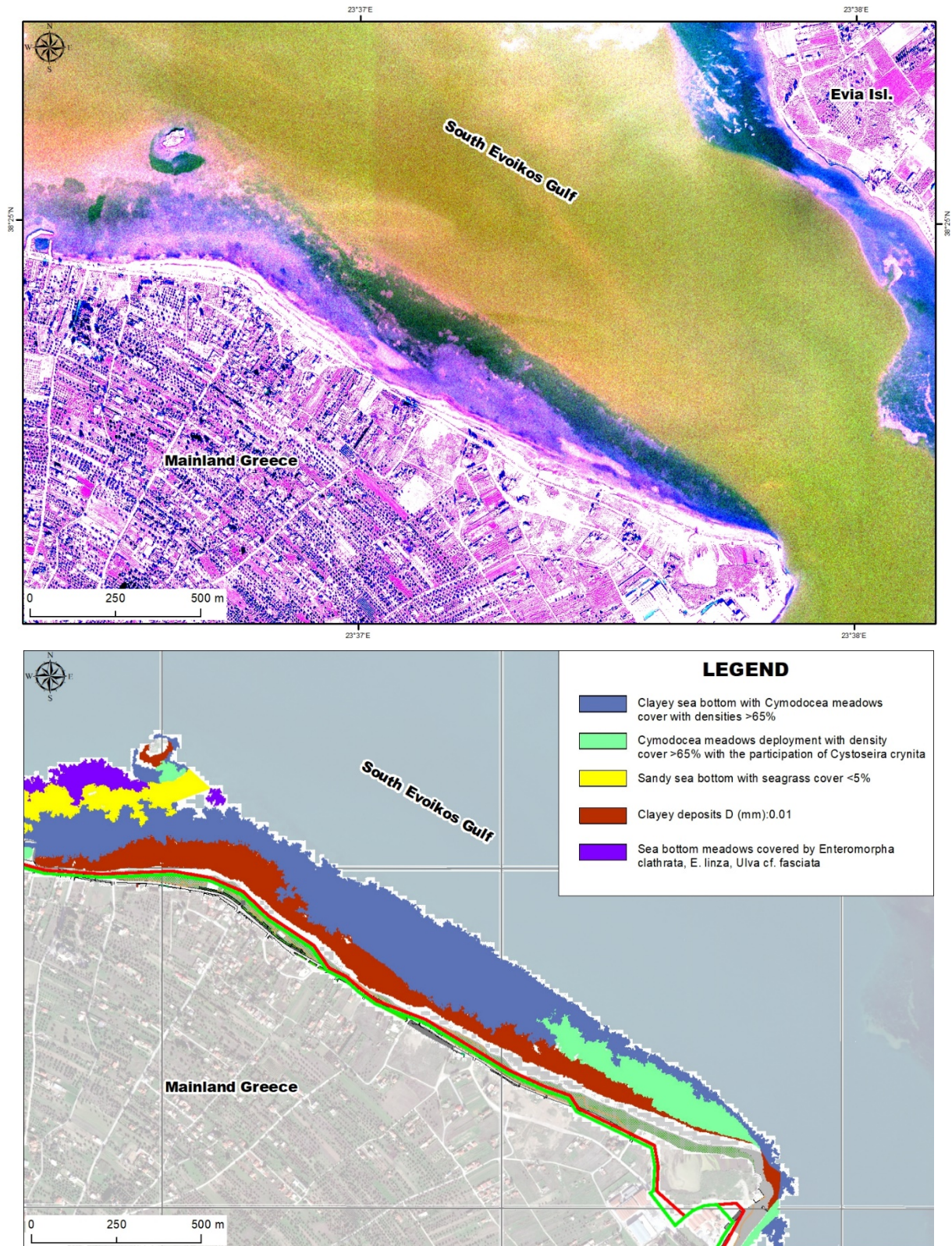


Figure 4 Processed pseudo color WorldView-2 satellite image of the area of interest (band combination 314/RGB), showing the seagrass development at the sea bottom between mainland Greece and Evia island (upper image). At the bottom image, the fieldwork seagrass mapping results are displayed

The additional spectral bands of the VHR images acquired by WorldView series of satellites, especially the use of red-edge, improved the separability of the different Aquatic Macrophyte species. Additionally, multi-band operations such as the Normalized Differential Vegetation Index (NDVI) using the new red-edge band yielded good result. Specifically, NDVI of red-edge (instead of

NearInfraRed1) to red showed better variability and separability of seagrass communities than the NDVI of using the classic NearInfraRed1 and red normalization ratio, even though higher values were obtained in the latter case. Other applied ratios were generated but didn't yield any use for the discrimination of seagrass.

The remote sensing spectral measurements added value to the use and interpretation of WorldView-2 images. The increased spatial resolution after the pan-sharpening procedure improved the visual interpretability to a great extent. More studies are required to prove the use of the additional bands for biomass estimation from satellite images and further to know about the vegetation carbon pool.

References

- Deidda M, Sanna G (2012) Pre-processing of high-resolution satellite images for sea bottom, Italian Journal of Remote Sensing, vol 44(1), pp. 83-95.
- Fornes G, Basterretxea A, Orfila A, Jordi A, Alvarez J (2006) Mapping *Posidonia oceanica* from IKONOS, Journal of Photogrammetry & Remote Sensing, vol 60, pp. 315–322.
- Lyzeng D (1978) Passive remote sensing techniques for mapping water depth and bottom features. Applied Optics, vol 17, pp. 379-383.
- Padwick C, Pacifici F, Smallwood S (2010) WorldView-2 pan-sharpening. In: ASPRS 2010 Annual Conference, San Diego, CA, USA.
- Phinn S, Roelfsema C, Dekker A, Brando V, Anstee J (2008) Mapping seagrass species, cover and biomass in shallow waters: An assessment of satellite multi-spectral and airborne hyper-spectral imaging systems in Moreton Bay (Australia), Remote Sensing of Environment, vol 112, pp. 3413–3425.
- Schmidt K, Skidmore A (2003) Spectral discrimination of vegetation types in a coastal wetland. Remote sensing of Environment vol 85, pp. 92 – 108.
- Stumpf R, Holderied K, Sinclair M (2003) Determination of water depth with high-resolution satellite imagery over variable bottom types, Limnology and Oceanography, vol 48(1), pp. 547-556.

Preliminary assessment of observing different regimes in the marine environment using SAR mode altimetry data

N. Flokos*, D. Delikaraoglou

National Technical University of Athens, Department of Surveying Engineering, 9 Iroon Polytechniou Str., Zografou Campus, 15780 Athens, Greece

*Corresponding author: flksnik@gmail.com, ddeli@mail.ntua.gr

Abstract

The Sentinel-3 constellation of Earth Observation satellites is designed to provide accurate and timely information to better manage the marine environment, and to understand and mitigate the effects of climate change by utilizing systematic measurements and products of sea-surface topography, sea-state and ecosystem characteristics over the open ocean and the regional and shelf seas. The aim of the paper is twofold: (a) to provide a brief overview of the types of new altimetry data available to users from the current Sentinel-3 satellites, and (b) to outline the new features, compared to the conventional radar altimeters, and the new capabilities provided by the Sentinel-3 SRAL (SAR mode) altimeters. The presentation will show representative results based on comparative analyses using previous (conventional) and current Sentinel-3 altimetry data, in an effort to identify critical data handling aspects (i.e. data access) and associated constraints (such as primary outputs, ground coverage, etc.) vis-à-vis typical user requirements for various marine applications, especially closer to the coastal areas where the SAR altimetry method is shown to be superior to conventional systems in terms of accuracy, spatial resolution of the observations etc.

Keywords Satellite altimetry, Sentinel-3 Mission, Marine observations, Sea Surface Topography.

1 SCOPE AND CAPABILITIES OF SATELLITE ALTIMETRY

In the 1970s, the satellite altimetry technique was initially designed to observe sea level by a combination of radar pulses used to measure the distance from the satellite to a reflecting (sea, lake or ice) surface, and positioning techniques allowing the precise location of the satellite on its orbit. These measurements yield a wealth of information about the state of the sea surface which, in turn, can be used for a wide range of marine applications – in particular, for mapping the global/regional ocean surface topography with sufficient accuracy to describe and study the marine environment, from the large-scale ocean circulation to the detailed observations of ocean mesoscale variability.

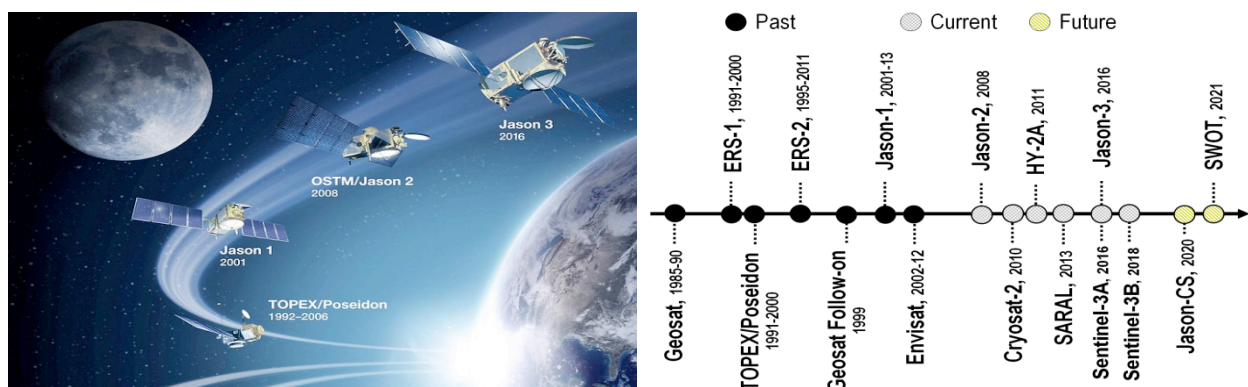


Figure 1 Past altimetry missions often used as reference (left)-Image credit NASA/JPL; Timeline of past, current, and planned missions (right)

Since 1992, a 20-year period of “continuous ocean surface measurements”, with the operation of TOPEX/Poseidon, Jason-1, -2, GFO and ENVISAT as the follow-on to the ERS-1 and -2 satellites, led to an explosive growth in ocean and climate studies made possible by a longer and more accurate time

series of sea surface measurements. In 2013, the launch of SARAL/AltiKa, marked the beginning of a series of new generation altimetry satellites with objectives geared towards the SWOT (Surface Water Ocean Topography) mission envisioned for 2021, and the Jason Continuity Service (Jason-CS/Sentinel 6) series of satellites planned for 2020 and 2025. The SWOT mission aims to make the first global survey of the Earth's surface water (of rivers, lakes and flooded zones) and to observe the fine details of the ocean surface topography (the ocean mesoscale and sub-mesoscale circulation), and to measure how terrestrial surface water bodies change over time (Morrow et al. 2018). It will all be done from a single satellite to be equipped with the latest altimetry concept technology: a Ku-band wide-swath interferometric altimeter (SIRAL), with multiple antennas, and capable of nadir, SAR, and InSAR mode measurements allowing better acquisition of measurements closer to the coastlines.

1.1 Saral/AltiKa and Sentinel-3 mission characteristics – New robust and stable altimetry technology advancements

Among the current altimetry satellites the SARAL and Sentinel-3 satellites provide the opportunity for systematic evaluation of the new capabilities of Ka- and Ku-band altimeters for fine resolution along-track applications, including for new coastal and inland water applications, which will also help further developments for the future Swot mission.

The SARAL (*Satellite with ARGos and ALtiKa*) mission is considered to be complementary to the Jason-2 mission and serving as a gap filler between the Envisat and the Sentinel-3 missions. SARAL's AltiKa altimeter is the first oceanographic altimeter working in the Ka-band (35.75 GHz) at a pulse repetition frequency of 4000 Hz, whereas conventional Ku-band altimeters operate at a pulse repetition frequency of 2000 Hz. Such a high radar signal frequency enables better observation of ice, rain, coastal zones, land masses (forests, etc.), and wave heights for coastal, inland waters and ice applications. Furthermore, the Ka-band (as compared to altimeters operating at Ku-band) is much less affected by the ionosphere, and has greater performance in terms of vertical resolution, time decorrelation of the radar echoes, spatial resolution and range noise. On the other hand, its main drawback is that Ka-band electromagnetic waves are sensitive to strong (>1.5 mm/h) rain rates which, nevertheless, only occur globally 10% of the time, and mostly in the Tropics.

The Sentinel-3 mission is dedicated to providing operational oceanographic services within the frame of the European Union's *Global Monitoring of Environment and Security* (GMES) programme. Using multiple state-of-the-art sensing instruments (such as the *Sea and Land Surface Temperature Radiometer/SLSTR*, the *Ocean and Land Colour Instrument/OLCI*, the *SAR Altimeter/SRAL*, and the *Microwave Radiometer/MWR*), two satellites are already in orbit (the Sentinel-3A and -3B available since 2016 and April 2018 respectively), and two more satellites are scheduled to be launched by 2021. Their sensors deliver high-quality measurements for determining the sea surface topography, significant wave height (SWH), sea-surface temperature and ocean-surface color parameters, all with dense global coverage.

The Sentinel-3 SRAL altimeter is a nadir-looking radar designed with many “dual-functionality” technical characteristics such as: dual frequency signals for sea surface measurements in the Ku-band (13.575 GHz, bandwidth = 350 MHz) and C-band (5.41 GHz, bandwidth = 320 MHz); dual radar modes, with the conventional altimeter pulse *Low Resolution Mode* (LRM), providing sea surface topography measurements approximately every 7 km, and the SAR mode for along-track *High Resolution Mode* (approximately every 300 m) composed of combined bursts of Ku- and C-band pulses (cf. Fig. 2); and dual, closed-loop (traditional) and open-loop tracking modes for better monitoring of the radar return pulses and the corresponding waveforms over rough surfaces. In addition, the SRAL altimeter is supported by a dual frequency (23.8/36.5 GHz) microwave radiometer measuring atmospheric humidity as supplementary information for added precision of the tropospheric path correction of the altimeter signal, as well as a DORIS (Doppler Orbitography and Radiopositioning) and a GNSS receiver, and a laser retroreflector for precise orbit positioning.

In order to address the differing user needs for various applications in both the online and offline domains, the Sentinel-3 altimetry data products are disseminated at various pre-processing levels (e.g. Product Level-1, -2, -3, -4); according to the surfaces covered by the data (e.g. WAT (water) or LAN (land)); and by geographical region (global or regional). There are also delivered with differing

turnaround (availability) timelines, as: *Near Real-Time* (NRT), *Short-Time-Critical* (STC) and *Non-Time-Critical* (NTC) products which are made available to the users within 3 and 48 hours and 1 month after acquisition, respectively. For many marine applications (e.g. ocean weather forecasts) the 48-hour turnaround of the STC products may still be considered as near real time.

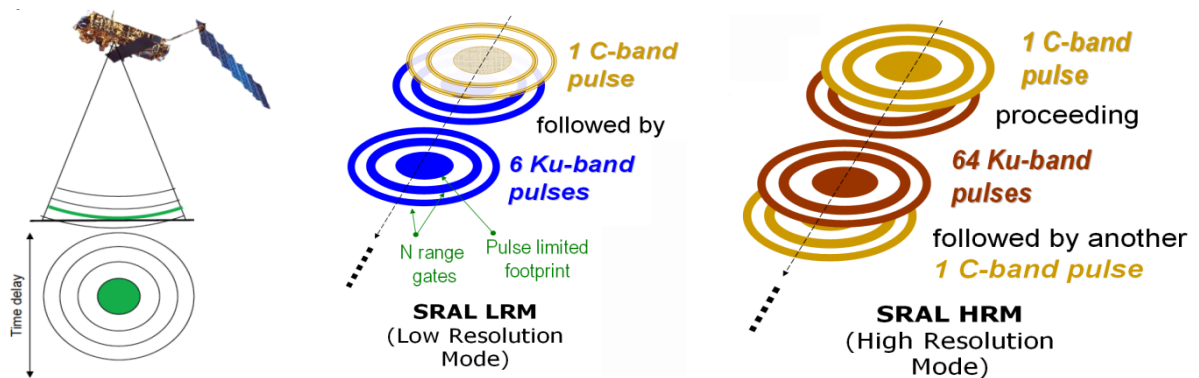


Figure 2 Schematics of conventional LRM altimetry (left), Patterns of radar pulses in SRAL’s LRM and HRM radar cycles respectively(middle and right)

2 USAGE OF SATELLITE ALTIMETRY IN COASTAL AREAS

Conventional satellite altimetry has had large success over the open ocean, the domain for which it was originally designed. In this endeavor, the unique combination of day/night and all weather operation, global coverage of high resolution sea state-related measurements along tracks of the sea surface with the possibility of revisiting the some marine locations regularly makes it possible to provide a detailed global picture of sea level and monitor its spatial-temporal changes routinely.

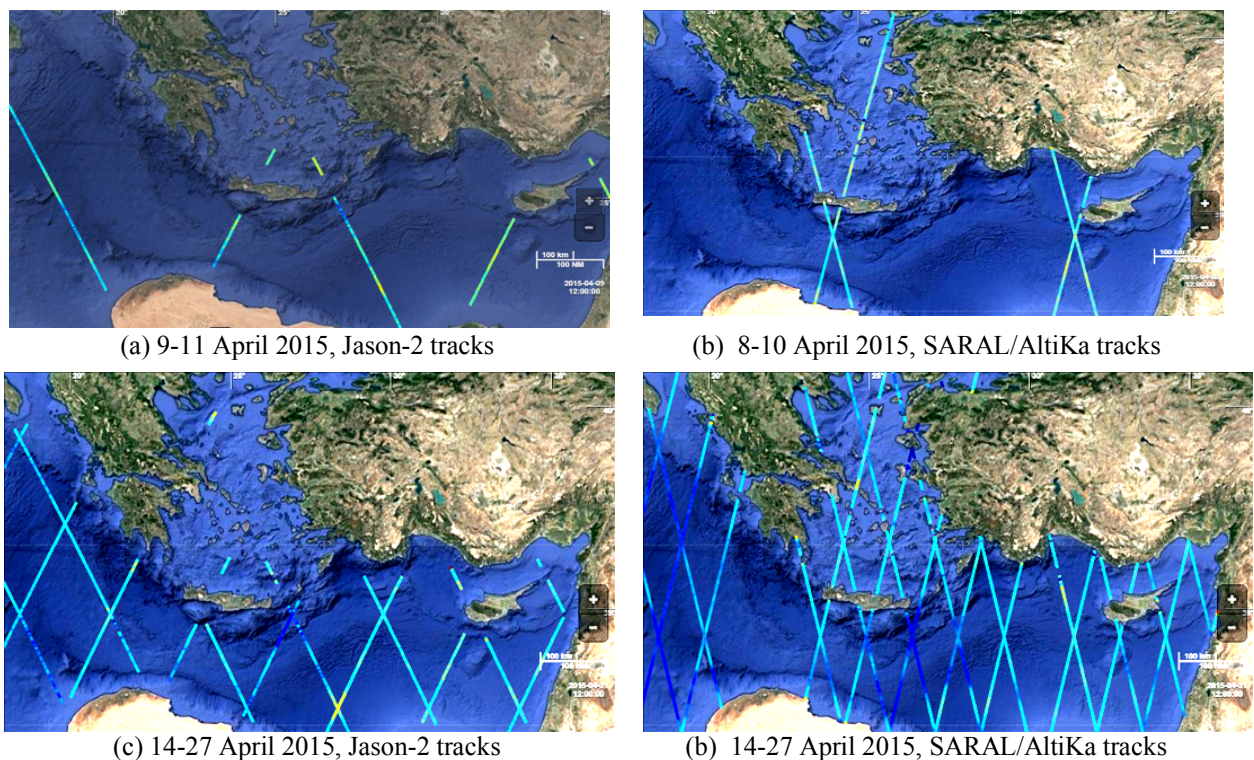


Figure 3 Altimetry data availability from the conventional vis-à-vis the new generation altimeters

On the other hand, the processing strategies used in analyzing altimetry data from the open ocean are not fully exploited to their full potential in getting sea level information in the coastal zones, i.e. in the domain that should be of interest to a broad range of marine data users that have an interest in using altimeter data from the coastal regions in their operational products or services.

From the viewpoint of altimetry data usage, coastal zones (usually within a few tens of kilometers from a coast) present a more complex environment where water conditions change all the time. In such areas, altimetry data from the conventional satellite missions are often discarded as exhibiting extreme noise levels making it difficult to interpret or model land contamination effects on the altimetric waveforms (Idris et al., 2014; Vignudelli, 2011). As a result, utilizing coastal altimetry data becomes a more complicated task mainly due to the intrinsic difficulties in performing a computationally intense ‘retracking’ of the observed waveforms and to correct the estimation of various critical geophysical parameters (i.e. sea level anomalies (SLA), significant wave height and wind speed). The practical implication is that for the purpose of retrieving SLAs near coastal zones, particular attention is also needed when applying the corrections of sea states (e.g. inverse barometer and sea state bias), oceanic signals and tides, and of the atmospheric effects on the radar signals (e.g. wet and dry tropospheric components, ionospheric delays, and high-frequency wind and pressure (barometric) response to atmospheric forcing which otherwise are less accurate due to high variability of the sea surface closer to the coasts).

Figure 3 illustrates the coverage and data availability constraining factors of the conventional LRM altimeters vis-à-vis the new capabilities made available with the newer generation SAR altimeters. In Fig. 3(a), the 3-day altimetry tracks of Jason-2 stop providing data when the satellite crosses over the Aegean islands. By contrast, as shown in Fig. 3(b), similar 3-day altimetry tracks of SARAL/AltiKa provide continuous data coverage over the same area. Respectively, Fig. 3(c) and 3(d) show analogous situations over a 2-week period, with the SARAL tracks providing good continuous spatial sampling over the Aegean region. Practically, this means that in order to provide homogeneous maps of sea level would require analysis and homogenization of the data from multiple altimeters typically on at least biweekly basis. Furthermore, together with the ground-tracks repeatability patterns and the dense spatial sampling achieved due to the orbital characteristics of the different satellites, it is now possible to acquire very accurate marine topography data over all types of surfaces (sea, coastal areas, sea ice, ice sheets, ice margins, and in-land waters). All these factors provide significant advantages in many marine applications gearing towards the management of the marine environment, e.g.: the support of coastal and offshore operations, the monitoring of wave propagation and the protection of the coastal zones against extreme environmental conditions, and the location of ‘hot spot areas’ suitable for deploying wind and wave systems for sustainable energy conversion and exploitation.

This improved performance of the SAR altimeters in coastal zones is largely due to the way both the time delay and the Doppler shift of the radar pulse echoes are recorded. Firstly, in a similar manner to the conventional pulse-limited LRM, the observed time delay indicates which annulus or ring of constant return signal strength (i.e., range gate) about the nadir point is contributing to the returned pulse energy. In addition, the measured Doppler shift gives the position fore or aft of the satellite flight direction, thus providing a much finer spatial resolution, nominally as narrow as 300 m in the along-track and 1.64 km in the across-track directions. A SAR altimeter thus provides multi-look viewing for each sub-satellite point; range correction then aligns these multiple records for a given point within a "waveform stack". An incoherent sum over all look directions gives a SAR waveform, which is sharper than an LRM waveform because of the finer footprint achieved through Doppler processing, and has a lower noise level due to the higher number of pulses averaged.

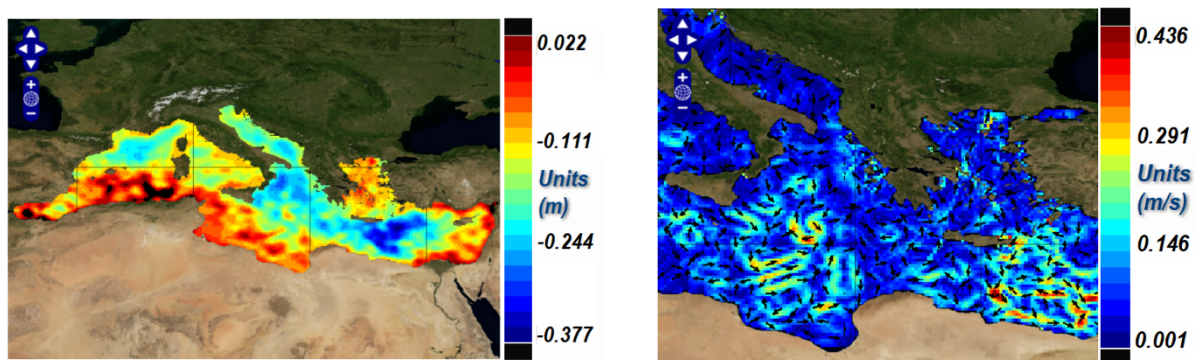


Figure 4 Regional patterns of observed sea level anomalies (left), and velocity field (right)

Overall, with the new SAR mode altimeters, combining data from several of the currently operational satellites gives a better space/time resolution (typically at scales of 50 km to 500 km and 10 days to 100 days respectively), and thus enable to observe nearly the full spectrum of the sea-level and ocean circulation variations. Typical examples are shown, in Fig. 4, where on the left is a map of regional patterns in sea level anomalies (in m), $SLA_N = SSH - MSS_N$, expressing the dynamic part of the SSH signal, for day 1/4/2019 from NRT data, as deduced from the combination of gridded, multi-mission altimetry sea surface heights with respect to a twenty-year mean sea surface ($MSS_{N=20}$) since 1993. Such maps enable local sea surface slopes to be estimated with high resolution ($1/4$ degree), as shown on the map in Fig. 4 (right) which, for the same day, depicts the geostrophic velocity field of the sea surface. Such maps are useful because the sea surface slopes relative to the geoid basically carry the information on the ocean surface circulation, and can be used for many applications, from the assimilation of altimetric data into operational ocean forecasting systems, to the study of eddy-mean interactions, the computation of volume transport, and the monitoring of ocean currents. Similarly, Fig. 5 (left) and Fig. 5 (right) depict respectively, the along-track variations and a composite map of the Absolute Dynamic Topography of the sea surface, as deduced from the combination of gridded, multi-mission-derived SLAs using the Mean Dynamic Topography (MDT), $MDT_N = MSS_N - geoid$, which is the temporal mean of the SSHs above the geoid, over a period of N years ($N=20$ in this case). That is: $ADT = SLA_N + MDT_N = SSH - MSS_N + MDT_N$.

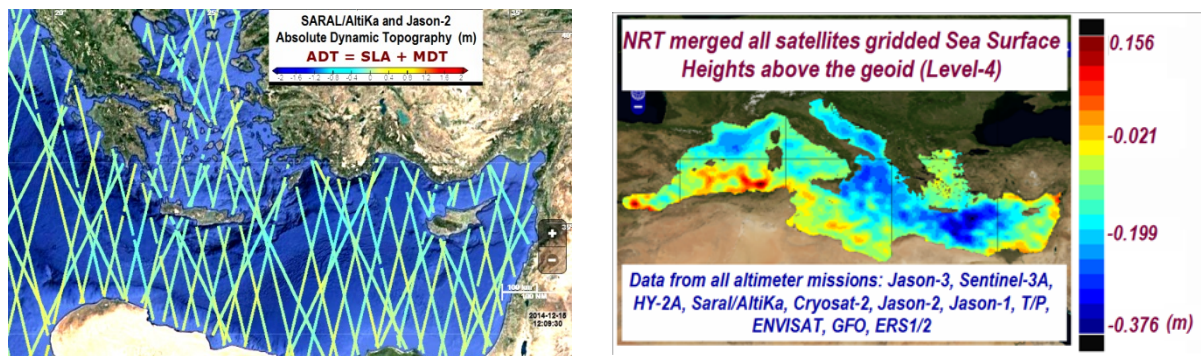


Figure 5 Multi-mission altimetry data availability enables to observe nearly the full spectrum of the sea-level and ocean circulation variations

3 SUMMARY

On the way to the future SWOT mission, the SARAL/AltiKa and Sentinel-3 satellites provide operational wide-swath high-quality altimetry measurements for open ocean, coastal and atmospheric applications requiring accurate information from sea and lake surface height, and significant wave height and surface wind speed, to sea ice height and thickness. Especially, near the coasts (and more so for inland waters) where the precision of conventional altimeters decreases, SAR altimetry measurements contain extremely useful information, allowing to get closer to the coasts or over continental water bodies with a better coverage and with good quality data.

References

- Idris NH, Deng X and Andersen OB (2014) The importance of coastal altimetry retracking and detiding: a case study around the Great Barrier Reef, Australia Int. Journal of Remote Sensing 35(5): p 1729-1740
- Morrow R, Blumstein D, and Dibarboure G (2018) Fine-scale altimetry and the future SWOT mission. In "New Frontiers in Operational Oceanography", E. Chassignet, A. Pascual, J. Tintoré, and J. Verron, Eds., GODAE OceanView, 191-226, doi:10.17125/gov2018.ch08
- Seitz BC, Mavrocordatos C, Rebhan H, Nieke J, Klein U, Borde F and Berruti B (2018) The Sentinel-3 mission overview. In 2010 IEEE International Geosciences and Remote Sensing Symposium, 25-30 July; DOI: 10.1109/IGARSS.2010.5650772
- Vignudelli S, Kostianoy AG, Cipollini P and Benveniste J (2011) Coastal altimetry (Berlin: Springer)

Nearshore wave energy potential estimation using Sentinel-3 data

M. Kaselimi*, N. Doulamis, D. Delikaraoglou

¹National Technical University of Athens, Department of Surveying Engineering,
9 Iroon Polytechniou Str., 15780 Zografou, Greece

*Corresponding author: mkaselimi@mail.ntua.gr

Abstract

The main purpose of this study was to evaluate and compare the wave energy potential between different locations of Eastern Mediterranean, and in particular Greece's marine areas, using available wave data provided by satellite altimetry missions. In particular, this study focuses on the use of Significant Wave Height (SWH) data Sentinel -3A and -3B new generation of altimetry satellites, along with respective data from previous altimetry missions, in order to make a renewed assessment of the wave energy concentrations in Greece's marine areas and to investigate near shore hot spots as prospective wave farm sites. We present recent results, for evaluating and comparing the levels of wave energy potential between different locations, using available altimetry-derived SWH data processed with statistical analysis tools and machine learning techniques.

Keywords Sentinel-3, Satellite altimetry, Significant wave height, Machine learning, K-means clustering, Wave energy potential.

1 INTRODUCTION

Nowadays, the imbalance between availability, demand, and production capacity of energy resources, coupled with the impacts of climate change and of fossil fuels-related ecological risks make the future energy resources planning, management, and decision-making a challenging process. The transition to cleaner energy resources, such as solar, wind and wave energy, has financial and environmental incentives. Greece, with its approximately 16.000 km of coastline, has high wind potential over the Aegean Sea that induces relatively moderate to strong, but constant wave activity, with an annual mean wave power projected at 4-11 kW/m. Furthermore, as strong reflection and diffraction phenomena of waves occur in this region, the exploitable wave energy potential of Greece is considered as the highest in the Mediterranean, estimating that it amounts to be about 5-9 TWh of electricity that can be generated annually (Delikaraoglou, 2006). Naturally, such levels of wave energy if appropriately harvested, could contribute significantly to the power needs of many of the islands in the Aegean Sea, especially the non-interconnected ones.

1.1 Preliminaries and Related Work

Wave energy farms, if suitably selected in locations with optimal wave conditions could be established offshore, near shore or even close to the coasts in some cases. Their exploitation requires three basic levels of decisions: (i) assessing the wave energy potential and detecting the most energetic coastal areas, (ii) selecting appropriate type of wave-energy-converters (WEC) and (iii) optimally distributing the captured wave energy to the power network.

A first coordinated attempt to quantitatively assess the offshore European wave energy potential was done, in the mid-1990s, using the third-generation wave analysis model (WAM) in the context of the European Wave Energy Atlas –WERATLAS Project. However, from both the systematic quality control of the WERATLAS data products and the prognostic capability studies of the underlying WAM model (Soukisian and Prospathopoulos, 2003) it has been shown that, in this area, the WERATLAS and WAM models tend to underestimate the significant wave heights (SWH) in a systematic way. Near shore areas are the preferred choice for possible wave energy park installations due to their proximity to other coastal engineering facilities. A conventional method for locating such “wave energy hot-spot areas” would be to deploy moored buoys so that to collect direct wave measurements at selected locations, but such an endeavor, in practice, provides very sparse data due to less mooring of buoys in vast areas, as well as that it often results with missing data and/or non-continuous coverage of data measurements within the area of interest. On the other hand, the task of detecting “wave energy hot-spots” can be done very effectively using satellite altimetry data from various past and currently operating missions which, among other geophysical parameters, provide valuable measurements of the *Significant Wave Height* (SWH) which relates closely to wave energy density potential. From SWH data, covering lengthy periods of time, the wave variability in various locations of interest can be

evaluated, consequently leading to safe conclusions regarding the wave energy potential in these regions. Altimetry satellites equipped with radar and/or laser altimeters provide wave and sea level observations that are long-term, accurate, and reliable and with consistent temporal and spatial coverage. However, with earlier altimetry satellites, using altimetry data close to the coasts posed considerable processing difficulties due to the increased levels of measurement noise in the altimetry waveforms from which the SWH parameter is derived. Since the launch of SARAL/AltiKa (in 2013) and the Sentinel-3A and -3B satellites (in 2/2016 and 4/2018 respectively), Synthetic Aperture Radar Altimeters (SRAL) have greatly improved our capability to correct the altimetry measurements especially in the wet tropospheric component, high-frequency atmospheric and oceanic signals and tides. Additionally, the Sentinel-3 SRAL instruments provide enhanced along track (azimuth) resolution of the order of 300 m, thus facilitating sea surface height measurements closer to coastal zones, areas covered with ice of different types, as well as inland lakes and rivers.

The main purpose of this paper is to provide an overview on the use of SWH data deriving from Sentinel-3A and -3B new generation of altimetry satellites along with SWH data from previous altimetry missions (Jason, Envisat and TOPEX/Poseidon), in order to make a renewed assessment of the wave energy concentrations in the marine areas of Greece and Cyprus and to investigate near shore hot spots as prospective wave farm sites.

2 FROM SWH TO WAVE ENERGY INDICATORS

Wind waves, or wind-generated waves, are wrinkles that occur on the surface of open waters due to air pressure variations and shear effects caused by the blowing wind. Enclosed seas such as the Mediterranean, the Baltic, and the Black Sea are considered almost free of tides and the wind is the main cause of the observed formation of waves on their surface. Assuming an ideal sinusoidal wave, its total (kinetic plus dynamic) energy is dependent on the length of the wave and the square of wave height and given by the following simple equation:

$$E = E_K + E_D = \frac{1}{2} \rho g a^2 \lambda = \frac{1}{8} \rho g H^2 \lambda \quad (1)$$

where $\rho=1025 \text{ kg/m}^3$ is the seawater density, $g=9.81 \text{ m/s}^2$ is the gravity acceleration, H and a are respectively the height and width of the wave (in m), and λ (also in m) is the length of the wave. An important indicator for assessing the wave energy potential is the energy density of waves (in J/m^2 or Wh/m^2) which is defined as the ratio of energy to the length of the wave:

$$E_{dens} = \bar{E} = \frac{E}{\lambda} = \frac{1}{8} \rho g H^2 \quad (2)$$

Energy density reflects the mean energy of the entire length of a wave, whereas wave power P is equal to the rate of work (i.e., the transfer or absorption of energy) being produced. It can be shown that, in deep water, where the water depth is larger than half the wavelength, the wave power transmitted by a wave front passing through a vertical plane perpendicular to the direction of motion of the wave is given by the so-called deep-water force relationship:

$$P = E_{dens} * c_g = \frac{\rho g^2 H^2 T}{32\pi} \quad (3)$$

Where c_g is the wave's group velocity (in m/s) and T (in s) is the period of the wave motion. Turning to random waves, the previous relationship can be expressed in terms of the so-called significant wave height (denoted, in the literature, as SWH or H_s or $H_{1/3}$) representing the average wave height (trough to crest) of the highest one-third of the waves observed, and based on the relationship:

$$H_s = \frac{(1/N)}{3} \sum_{i=1}^N H_i \quad (4)$$

where N is the number of waves in a sample ordered from highest to lowest. In practice, most wave-measuring devices estimate SWH from a wave spectrum, relating H_s to the zeroth-order moment (area) of the wave spectrum or spectral wave height H_{m0} and the square root of the average of the squares of all wave heights, symbolically H_{rms} , through the relationship $H_{1/3} \approx H_{m0} = \sqrt{2} H_{rms}$. Consequently, the deep-water force relationship can also be expressed as

$$P = \frac{\rho g^2 H_{rms}^2 T}{32\pi} = \frac{\rho g^2 H_{m0}^2 T}{64\pi} = \frac{\rho g^2 H_s^2 T}{64\pi} \cong 0.5 H_s^2 T \quad (5)$$

3 EXPERIMENTAL EVALUATION

3.1 Dataset description & Experimental setup

Satellite radar altimeters are designed to measure the return power of a radar pulse that is reflected off the ocean surface. They are unique in measuring directly the SWH from the different times of the radar pulse return from wave crests and troughs within the area illuminated by the radar beneath the satellite. A measured backscatter coefficient of these pulse returns is an indicator of the sea roughness which depends mainly on the wind speed. The strength of the return radar pulse depends on the SWHs sampled within the reflection area (footprint) of the pulse.

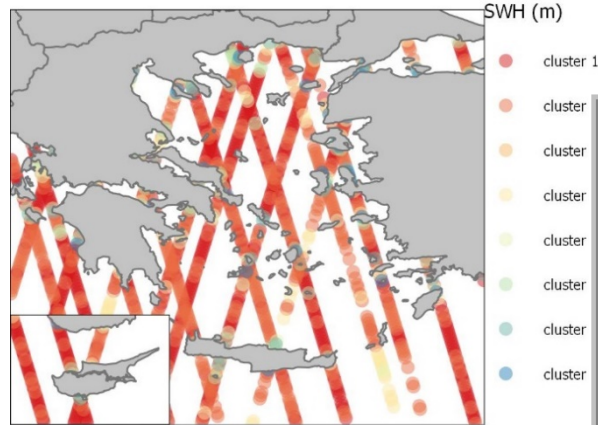


Table 1 Table along track SWH (m) 1-Hz for between 15/02/2019 and 28/02/2019

	H_c (m)	Centroid	Minimum	Maximum
cluster 1	0.08	0.00	0.66	
cluster 2	1.24	0.66	1.80	
cluster 3	2.37	1.80	3.10	
cluster 4	3.84	3.10	4.79	
cluster 5	5.75	4.79	7.06	
cluster 6	8.38	7.06	10.26	
cluster 7	12.15	10.26	14.67	
cluster 8	17.16	14.67	19.85	

Figure 19 Map showing along track SWH (m) 1-Hz for C band between 15/02/2019 and 28/02/2019

French AVISO Service provides altimeter-derived daily SWH data in the form of multi-satellite (Jason-1, Jason-2 and Envisat) timeseries at $1^\circ \times 1^\circ$ grid points per day. This sparse space-time data frame (i.e. grid) lacks accuracy and continuity considering its data inadequate for various applications. However, due to its multi-mission character, this dataset extends over a large time span, this is suitable for climate research related applications (Kaselim, 2015). By contrast, Sentinels' satellites products have high spatiotemporal resolution, but so far, we have limited duration of data since the Sentinel-3A and -3B satellites were launched on February 2016 and April 2018 respectively. The twin satellites are equipped with SRAL (Synthetic Aperture Radar Altimeter), which is a dual-frequency (C-band and Ku-band) instrument for determining the two-way delay of the radar echo from the Earth's surface with a precision better than a nanosecond. For this initial study, we have processed *SRAL Level 2 Marine Products* (Roy, 2018), which contain useful sea surface topography information over the open ocean, the coastal zones, sea-ice regions and inland lake and river water surfaces. The measurements over the coastal areas and over part of the land within a certain distance from the coastline are contained both in the land and marine products to ensure the analysis of transition and meaningful continuity of segments. Figure 1 shows clustered SWH values along the satellite's track between the time period 15/02/2019 to 28/02/2019. Cluster analysis offers a useful way to organize and represent complex data sets. In particular, k-means clustering (Wu, 2012), as a practical and convenient clustering algorithm, aims to partition n observations into k clusters, such that each observation is assigned to the cluster it is most similar to (with the cluster centroid serving as a prototype of the cluster). It is a classical approach that can be implemented in many ways and for various distance metrics. The main drawback is that the number of clusters should be known a priori. The optimal number of clusters is determined to be equal to 8. Table 1 shows the centroid of each cluster, along with minimum and maximum SWH values per cluster. Based on Sentinel's 3 altimetry-derived SWH data, various statistical measures related to the temporal (monthly and seasonal) and/or spatial variations of significant wave heights and wave power were obtained, in order to detect locations of interest. Figure 1 shows that the majority of the SWH values is between 0 and 5m (clusters 1, 2, 3, 4). Most of the extreme high values (i.e. clusters 6, 7, 8) are close to the shore in coastal areas. Therefore, the noted SWH values in these clusters indicate, on one hand, the Sentinel's SRAL indeed has the capability to provide measurements near and on the land surface, but also point to the fact that one still needs to perform a more careful editing of the altimetry data so that to eliminate land measurements which would be of no immediate interest to such a wave study.

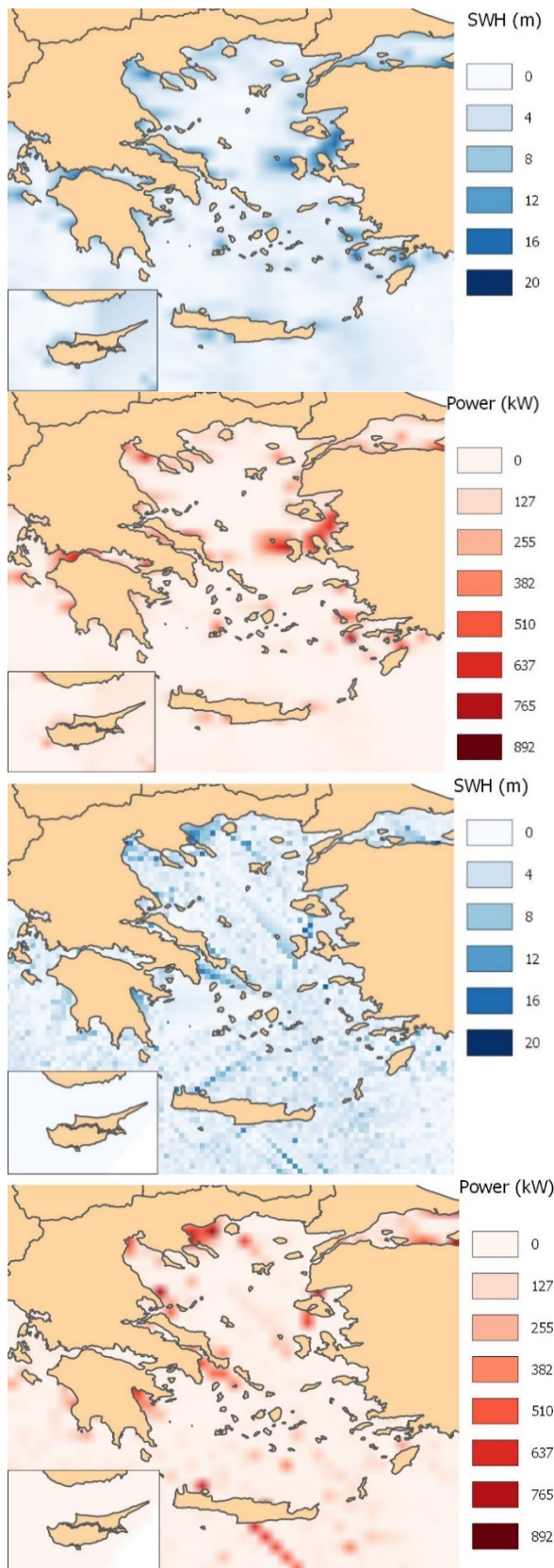


Figure 20 Maps showing SWH (m) 1-Hz (above left) and 20-Hz (down left) for C band and power (kW) 1-Hz (above right) and 20-Hz (down right) for C band, between 15/02/2019 and 28/02/2019

Figure 2 shows the SWH and wave power maps that are constructed using tracks between the time period 15/02/2019 and 28/02/2019. The maps were obtained using altimetry wave data from the C

band, in two rates (1 and 20 Hz). We observe that the higher the rate, the better the accuracy. The most energetic areas are located south in Crete, in Lesvos and in the coasts of Peloponnese. It is worth mentioning that these areas were also ‘designated’ as energetic areas in an earlier detailed study by Kaselimi (2018) using SWH data from conventional altimeters (e.g. Jason-1, -2 and Envisat). Table 2 shows statistical metrics for the areas that considered as areas with the most intense conditions.

4 CONCLUSION

From the current analysis of limited amount of SWH data derived from Sentinel’s altimeter radar measurements and measurements derived from earlier multi-mission altimeter satellites, it is confirmed that the Eastern Mediterranean has significant exploitable wave energy potential, especially within the maritime regions of southwestern Aegean and the western and southern sea areas of Cyprus. These areas display the highest levels of the Mediterranean, while having favorable low annual variability, but also stable, as well as small exposure to extreme sea state conditions that can lead to weak performance.

Such exploitation of wave energy potential, albeit at smaller levels than those, for instance, along the Atlantic coast or the northern European seas, could meet a significant proportion of the energy needs of the many islands in this region. Evidently, the areas examined in this study offer a clear example that given time and with the right governmental support, wave energy can progress along the innovation chain towards commercial viability and easier adaptation to large power grids. Therefore, as a next step, it would be prudent to initiate further efforts leading towards practical demonstration of innovative, cost efficient and environmentally benign offshore renewable energy conversion platforms for wave energy resources in these areas.

Table 2. Descriptive statistics obtained for altimetry-derived SWH for locations of interest exhibiting high and low wave conditions

H _s (m)	Gavdos	Kithira	Koufonisia	Skopelos	Lesvos	Limnos	Pafos
Days	1935	1911	1929	1925	1877	1885	1906
Mean	1.10	1.06	1,07	0.86	0.83	0.83	0.98
St Dev	0.56	0.55	0,54	0.49	0.51	0.52	0.57
Min	0.14	0.12	0.09	0.01	0.00	0.00	0.03
Q1	0.70	0.66	0.69	0.50	0.48	0.46	0.56
Median	0.97	0.94	0.94	0.75	0.71	0.71	0.84
Q3	1,40	1.34	1.33	1.10	1.07	1.08	1.24
Max	3.87	3.96	3.54	3.47	4.05	3.95	4.24
% H _s >1m)	48	45	46	30	29	29	30

Acknowledgements

This research is implemented through IKY scholarships programme financed by the action titled “Reinforcement of Human Research Potential through Doctoral Research”, in the framework of the Operational Programme “Human Resources Development Program, Education and Lifelong Learning” of the National Strategic Reference Framework (NSRF) 2014 - 2020.

References

- Delikaraoglou D and S Delikaraoglou (2012) The contribution of geodetic altimeter satellites in mapping the Greek area: a feasibility study for the exploitation of the wave energy (in Greek). GEOGRAFIES 19, pp. 70-88. Available at: http://geographies.gr/wp-content/uploads/2013/05/GEO19-070-088_new.pdf.
- Kaselimi M (2015) An analysis of multi-mission satellite altimeter data for estimating the prospects of wave energy potential in Eastern Mediterranean (in Greek). Diploma Thesis, Department of Surveying Engineering, National Technical University of Athens. Available at: <http://publications-list.org/php/publist.php?u=maria.kaselimi&t=85#refid85>. Book chapter.
- Kaselimi M Delikaraoglou D (2018) “Estimating the Prospects of Wave Energy Potential in Eastern Mediterranean using Multi-mission Satellite Altimeter Data,” 2018, pp. 221–238. Online document

- Soukissian TH, Prospathopoulos AM, (2003) Implementation of the 3rd Generation Wave Model WAM-Cycle 4 in Aegean Sea (in Greek). Tech. Chron. Sci. J., IV, No 1-2. pp. 7-19.
- Le Roy Y, Deschaux-Beaume M, Mavrocordatos C, Aguirre M, Heliere F (2018) SRAL SAR Radar Altimeter for Sentinel-3 mission. In 2007 IEEE International Geoscience and Remote Sensing Symposium, Barcelona, Spain, 23-28 July. DOI: 10.1109/IGARSS.2007.4422769.
- Wu J, Advances in K-means Clustering: A Data Mining Thinking. Berlin Heidelberg: Springer-Verlag, 2012.

A	Pag	F	Pag
Afentoulis V.	5 v1, 91 v2, 243 v2	Fakiris E.	47 v1, 231 v2
Aggelerou P.	53 v1	Ferentinos G.	47 v1
Alamanis N.	135 v1, 37 v2	Flokos N.	163 v1
Alexandrakis G.	29 v2, 217 v2	Fotia M.	123 v2
Alexopoulos J.	135 v1 37 v2	Fourniotis N.Th.	335 v2
Anagnostou Ch.	11 v2, 255 v2	Frangomanolaki G.	105 v1, 217 v2
Anastasiou I.E.	121 v1, 305 v2	Frantzis C.	299 v2
Andreadis O.	141 v1		
Androulidakis Y.	5 v1, 11 v1	G	Pag
Apergis S.	63 v1	Galani K.	147 v2
Asariotis R.	211 v2	Galiatsatou P.	153 v2, 169 v2
		Georgiou G.C.	103 v2
B	Pag	Georgiou N.	47 v1 , 231 v2
Baltikas V.	5 v1, 11 v1,17 v1	Giannakidou Ch.	17 v2
Bardey P.	243 v2	Gianni A.	329 v2
Benoit M.	91 v2	Giantsi Th.	341 v2
Biliani I.	141 v2	Gouloumis S.	261 v2
Biniskos P.	89 v1, 93 v1	Grigoriadis D.G.E.	299 v2
Boile M.	99 v1		
Boutatis A.	89 v1, 93v1, 43 v2, 237 v2	H	Pag
Bujac D.	349 v2	Horsch G.M.	335 v2
C	Pag	I	Pag
Carevic D.	349 v2	Ieridis V.	261 v2
Chalastani V.I.	49 v2		
Chalmoukis I.	85 v2	J	Pag
Charchousi D.	55 v2	Jacovou Cha.	DMPCO-068
Charisi E.	311 v2		
Chatjigeorgiou K.I	121 v1, 127 v1, 305 v2, 311 v2	K	Pag
Chatzigiagou Chr.	261 v2	Kalogirou M.	53 v1
Chatziioannou K.	127 v1	Kalpyri M.	93 v1, 43 v2
Chatzipavlis A.E.	141 v1	Kampanis N.	29 v2, 217 v2
Chondros M.	5 v1, 17 v1, 23 v1, 29 v1, 43 v2, 181 v2, 237 v2, 269 v2	Kampolis K	63 v1
Chouliaras I.	37 v2	Kapopoulos Ch.	111 v2
Christodoulou D.	47 v1, 231 v2	Kapsimalis V.	255 v2
Christou A.	261 v2	Karagiannis N.	97 v2
Christou M.	281 v2	Karambas TH.	5 v1, 11 v1, 17 v1, 23 v1, 67 v2, 97 v2, 269 v2, 275 v2, 293 v2
Coccossis H.	7 v2		
		Karathanasi F.	111 v2
D	Pag	Karditsa A.	41 v1
Delikaraoglou D.	163 v1 169 v1	Karmpadakis I.	281 v2
Diakoulaki D.	17 v2	Kaselimi M.	169 v1
Dimas A.	79 v2, 85 v2, 129 v2,	Kasidoni M.	361 v2
Dimas X.	47 v1, 231 v2	Katsardi V.	127 v1, 311 v2
Doulakis I	61 v2	Kazakis I.	275 v2
Doulamis N.	169 v1	Kikaki A.	11 v2
Drimonas Ch.	37 v 2	Klonaris G.	5 v1 73 v2
		Kokkinos D.	143 v2, 169 v2
E	Pag	Kokkos N.	145 v1
Eleftheriou A.	141 v1	Kontos Y.	5 v1 11-15 17-21
Emmanouilidou	M.5 v1	Kotsopoulos S.	135 v1
Evelpidou N.	255 v2	Koukouselis A.	127 v1
		Koumparakis G.	23 v2

Kousoulos S.	249 v2	Papadimitriou A.	5 v1, 23 v1, 29 v1, 91 v2, 269 v2
Koutitas C.	97 v2	Papadopolis-Dezorzis A.	99 v1
Koutsikopoulos C.	231 v2	Papadopoulou M.P.	55 v2
Koutsourelakis I.G.	53 v1, 249 v2	Papageorgiou G.	135 v1, 37 v2
Krebs H.	207 v2 223 v2	Papatheodorou G.	47 v1, 231 v2
Krestenitis Y.	11 v1, 169 v2	Perogiannaki S.	105 v1, 217 v2
Kypraiou E.	201 v2, 237 v2	Petrakis S.	29 v2
L	Pag	Petropoulos A.	255 v2
Lazogiannis K.	135 v1, 37 v2	Petropoulos C.	157 v1, 11 v2
Leftheriotis G.	79 v2, 335v2	Petsa D.	77 v1, 83 v1
Lirintzakis S.	105 v1, 217 v2	Polte D.	57-61
Litinaki Chr.	105 v1, 217 v2	Poulos S.E.	41 v1 135 v1
Loizides M.I.	77v1, 83 v1	Prinos P.	143 v2, 169 v2 187 v2
Loizidou M.	361 v2	Pritsivelis A.	35 v1
Loizidou X.I.	77 v1, 83 v1	R	Pag
Loncar G.	349 v2	Raffourt C.	243 v2
Loukogeorgaki E.	109 v1, 115 v1	Ralli P.	71-75
M	Pag	Rempis N.	29 v2
Makatounis P.E.	323 v2	Repousis E.	135 v2
Makris Ch.	5 v1, 11v1, 153 v2, 169 v2	Rogan I.	43 v2
Malliouri D.	129 v2, 163 v2	Rompogianakis D.	217 v2
Manetos P.	DMPCO-253	Rouchotas E.	53-56
Manoglou S.	361 v2	S	Pag
Martzikos N.	187 v2	Samaras A.G.	293 v2
Mavraeidopoulos A.K.	195 v2	Santic I.	127 v1
Mavrakos S.A.	175 v2	Sartampakos P.	35 v1, 41v1,157v1
Mavroudis O.	355 v2	Sifakis N.	355 v2
Melissas D.	5 v2	Sismani G.	109 v1
Memos C.	5 v1, 23 v1, 29 v1, 17 v2, 73 v2, 129 v2, 135 v2, 163 v2, 181 v2, 187 v2, 269 v2	Sklia M.	287 v2
Metallinos A.	5 v1, 23 v1, 29 v1, 181 v2, 269 v2	Solomonidis C.	89 v1, 93 v1, 43 v2, 237 v2
Michailides C.	103 v2, 117 v2	Sophianopoulos D.S.	317 v2
Milozis E.	37 v2	Soukissian T.	129 v2 175 v2
Mistakidis E.	127 v1	Spanaki E.	115-119
Monioudi I.	141 v1,211 v2	Spekker H.	207 v2, 223 v2
N	Pag	Spiliopoulos G.	5v1
Nikolaou A.	211 v2	Spiridakis M.	105 v1
Ntina M.I.	317 v2	Spyropoulos K.	35 v1
O	Pag	Stamou A.	323 v2
Orthodoxou D.L.	77 v1, 83 v1	Stylogiannis N.	361v2
P	Pag	Swan C.	281 v2
Panagopoulos N.	249 v2	Sylaios G.	145-149
Panas A.	71 v1	T	Pag
Pantazi V.S.	317 v2	Theofanis S.	99-103
Pantouvakis J.P.	71 v1	Toumazis A.	93-97 237 v2
Papadakis E.	217 v2	Trygonis V.	141-144
		Tsaousis D.Th.	121 v1, 305 v2
		Tsekos H.	249 v2
		Tselentis B.	367 v2
		Tsiaras A-Ch.	67 v2

Tsiatsiou L.	323 v2
Tsiplostefanakis M.	105 v1, 217 v2
Tsokos A.	157 v1
Tsoukala V.	5 v1, 49 v2, 127 v1, 157 v1, 55 v2, 91 v2, 129 v2, 181 v2, 187 v2
Tsoutsos Th.	355 v2
Tzoumas Chr.	151-155

V	Pag
Valsamidis A.	103 v2
Vassilakis Emm.	135 v1, 157 v1, 37 v2
Velegrakis A.F.	141 v1, 211 v2
Vousdoukas M.I.	211 v2

Z	Pag
Zacharias I.	329 v2
Zachopoulos K.	145 v1
Zissis D.	5 v1
Zoidou M.	145 v1



DMPCO 2019

Laboratory of Harbour Works, National Technical University of Athens

Iroon Polytechniou Str. 5, GR 15780, Athens, Greece

Phone: + 30 210 7722367, 210 7722374 | Fax: + 30 210 7722368

Email: registration@dmpco.gr | lhw@cental.ntua.gr

www.dmpco.gr



KEFI S.A.
TICKETS • TRAVEL • INCENTIVES
CONFERENCES • EXHIBITIONS

PCO | KEFI S.A. | 267, Kifissias Ave., 145 61 Kifissia, Greece | tel.: (+30) 210 62 32 710 | fax: (+30) 210 62 30 789 | email: info@kefitours.gr | www.kefitours.gr